N°d'ordre NNT : 2017LYSEI061

THESE de DOCTORAT DE L'UNIVERSITE DE LYON
opérée au sein de
INSA LYON

Ecole Doctorale N° ED162
MEGA

Spécialité de doctorat : Mécanique

Soutenue publiquement le 02/06/2017, par :
Sandrine Nicole Marie Laruelle

Etude du comportement thermique d'un motoréducteur
Study of the thermal behavior of a gear unit

Devant le jury composé de :

Fabre, Agnès	Docteur HDR	ENSAM	Présidente
Bouyer, Jean	Docteur HDR	UNIVERSITE DE POITIERS	Rapporteur
Changenet, Christophe	Docteur HDR	ECAM LYON	Directeur de thèse
Koechlin, Samuel	Ingénieur	MOTEURS LEROY SOMER	Examinateur
Maré, Jean-Charles	Professeur	INSA TOULOUSE	Rapporteur
Ville, Fabrice	Professeur	INSA LYON	Directeur de thèse

Département FEDORA – INSA Lyon - Ecoles Doctorales – Quinquennal 2016-2020

SIGLE	ECOLE DOCTORALE	NOM ET COORDONNEES DU RESPONSABLE
CHIMIE	**CHIMIE DE LYON** **http://www.edchimie-lyon.fr** Sec : Renée EL MELHEM Bat Blaise Pascal 3e etage secretariat@edchimie-lyon.fr Insa : R. GOURDON	M. Stéphane DANIELE Institut de Recherches sur la Catalyse et l'Environnement de Lyon IRCELYON-UMR 5256 Équipe CDFA 2 avenue Albert Einstein 69626 Villeurbanne cedex directeur@edchimie-lyon.fr
E.E.A.	**ELECTRONIQUE, ELECTROTECHNIQUE, AUTOMATIQUE** **http://edeea.ec-lyon.fr** Sec : M.C. HAVGOUDOUKIAN Ecole-doctorale.eea@ec-lyon.fr	M. Gérard SCORLETTI Ecole Centrale de Lyon 36 avenue Guy de Collongue 69134 ECULLY Tél : 04.72.18 60.97 Fax : 04 78 43 37 17 Gerard.scorletti@ec-lyon.fr
E2M2	**EVOLUTION, ECOSYSTEME, MICROBIOLOGIE, MODELISATION** **http://e2m2.universite-lyon.fr** Sec : Sylvie ROBERJOT Bât Atrium - UCB Lyon 1 04.72.44.83.62 Insa : H. CHARLES secretariat.e2m2@univ-lyon.fr	M. Fabrice CORDEY CNRS UMR 5276 Lab. de géologie de Lyon Université Claude Bernard Lyon 1 Bât Géode 2 rue Raphaël Dubois 69622 VILLEURBANNE Cédex Tél : 06.07.53.89.13 cordey@ univ-lyon1.fr
EDISS	**INTERDISCIPLINAIRE SCIENCES-SANTE** **http://www.ediss-lyon.fr** Sec : Sylvie ROBERJOT Bât Atrium - UCB Lyon 1 04.72.44.83.62 Insa : M. LAGARDE secretariat.ediss@univ-lyon1.fr	Mme Emmanuelle CANET-SOULAS INSERM U1060, CarMeN lab, Univ. Lyon 1 Bâtiment IMBL 11 avenue Jean Capelle INSA de Lyon 696621 Villeurbanne Tél : 04.72.68.49.09 Fax :04 72 68 49 16 Emmanuelle.canet@univ-lyon1.fr
INFOMATHS	**INFORMATIQUE ET MATHEMATIQUES** **http://infomaths.univ-lyon1.fr** Sec : Renée EL MELHEM Bat Blaise Pascal, 3e étage Tél : 04.72. 43. 80. 46 Fax : 04.72.43.16.87 infomaths@univ-lyon1.fr	M. Luca ZAMBONI Bâtiment Braconnier 43 Boulevard du 11 novembre 1918 69622 VILLEURBANNE Cedex Tél :04 26 23 45 52 zamboni@maths.univ-lyon1.fr
Matériaux	**MATERIAUX DE LYON** **http://ed34.universite-lyon.fr** Sec : Marion COMBE Tél:04-72-43-71-70 –Fax : 87.12 Bat. Direction ed.materiaux@insa-lyon.fr	M. Jean-Yves BUFFIERE INSA de Lyon MATEIS Bâtiment Saint Exupéry 7 avenue Jean Capelle 69621 VILLEURBANNE Cedex Tél : 04.72.43 71.70 Fax 04 72 43 85 28 Ed.materiaux@insa-lyon.fr
MEGA	**MECANIQUE, ENERGETIQUE, GENIE CIVIL, ACOUSTIQUE** **http://mega.universite-lyon.fr** Sec : Marion COMBE Tél:04-72-43-71-70 –Fax : 87.12 Bat. Direction mega@insa-lyon.fr	M. Philippe BOISSE INSA de Lyon Laboratoire LAMCOS Bâtiment Jacquard 25 bis avenue Jean Capelle 69621 VILLEURBANNE Cedex Tél : 04.72 .43.71.70 Fax : 04 72 43 72 37 Philippe.boisse@insa-lyon.fr
ScSo	**ScSo*** **http://recherche.univ-lyon2.fr/scso/** Sec : Viviane POLSINELLI Brigitte DUBOIS Insa : J.Y. TOUSSAINT Tél : 04 78 69 72 76 viviane.polsinelli@univ-lyon2.fr	M. Christian MONTES Université Lyon 2 86 rue Pasteur 69365 LYON Cedex 07 Christian.montes@univ-lyon2.fr

*ScSo : Histoire, Géographie, Aménagement, Urbanisme, Archéologie, Science politique, Sociologie, Anthropologie

Remerciements

Je tiens à remercier Fabrice VILLE et Christophe CHANGENET pour leur confiance dans la réalisation de cette thèse. Je remercie également Samuel KOECHLIN pour le sujet qu'il m'a proposé au sein de MOTEURS LEROY SOMER.

Cette thèse est le résultat de la collaboration entre le laboratoire de Mécanique des Contacts et des Structures (LaMCoS) de l'INSA de Lyon, le laboratoire d'Energétique et de Mécanique de l'ECAM de Lyon (LabECAM) et le service Recherche et Développement de MOTEURS LEROY SOMER.

Cette collaboration a lieu dans le cadre d'une Convention Industrielle de Formation par la Recherche (CIFRE) par l'Agence Nationale pour la Recherche et la Technologie (ANRT).

Je tiens à remercier Benoît VINCENT et Pascal CARRIOT pour leur accueil au sein du bureau d'études de Rabion. Je suis très reconnaissante envers Pascal PONT et Loïc VIGIER pour avoir été mes interlocuteurs privilégiés au sein du bureau d'étude, ainsi que Sébastien MOREAU qui m'a aidé pour la réalisation des essais sur le réducteur à échelle 1. Je tiens également à remercier sans les citer toutes, les personnes qui m'ont aidées ou accueillies à Angoulême.

Je remercie également mes amis et mes collègues avec qui j'ai pu échanger au cours de ces trois dernières années.

Je dédie cette thèse à ma famille et à mon amour.

Table of contents

List of figures

Abstract

Environmental concern leads to improvements in both efficiency and power density of electrical motors. For compact transmissions, thermal issues can become critical: the surface available for thermal exchange with the environment is reduced, minimizing the possibility to cool down the elements. To ensure the system reliability, the operating temperature for each operating condition must not exceed the required maximum oil temperature. In order to evaluate its thermal behavior, the whole system should be therefore evaluated in terms of power losses and heat transfer.

This PhD proposes a thermal model of an existing oil bath lubricated gear unit with spiral bevel gears. The thermal model uses the thermal network method, which needs an accurate prediction of power losses of the different elements and heat transfer between them. A review of the existing methods is presented. Since the churning losses of spiral bevel gears has never been fully characterized, specific tests have been done on a dedicated test bench. The last part of this work suggests possible improvements on the gearbox design.

Key words: thermal network method, spiral bevel gears, churning, power losses, heat transfers

Résumé

La diminution de l'impact environnemental des moteurs électriques conduit à des améliorations du rendement et de la compacité. Puisque la taille de la transmission est réduite, des problèmes d'échauffements peuvent apparaître car la surface d'échange avec l'environnement est fortement réduite, diminuant les possibilités de refroidissement. L'ensemble du système doit être caractérisé en termes de pertes de puissance et de capacité de transfert thermique pour déterminer si la température maximale en fonctionnement correspond aux exigences de fiabilité tout au long de la durée de vie du système.

Cette thèse propose un modèle thermique d'une transmission avec des engrenages spiraux coniques, lubrifiée par bain d'huile. Le modèle thermique utilise la méthode des réseaux thermiques. Par conséquent, une estimation précise des pertes et des transferts thermiques entre les différents éléments est nécessaire. Une revue des méthodes existantes est présentée, indiquant que les pertes par barbotage des engrenages spiraux coniques ne sont pas totalement maîtrisées, entraînant la conduite d'une série d'essais sur un banc d'essai dédié. Cette étude se conclue sur l'application du modèle à la transmission ainsi que la proposition de points d'améliorations.

Mots clés : méthode des réseaux thermiques, engrenages spiraux coniques, barbotage, pertes, transfert thermique

1. Introduction

La capacité thermique est devenue un critère limitant dans le cadre de l'augmentation de la compacité des systèmes. La chaleur générée par les pertes du système doit donc être évacuée à travers des surfaces d'échange réduites. L'équilibre entre les pertes et la chaleur transférée à l'environnement définit la température maximale rencontrée dans le réducteur. La modélisation complète d'une transmission est encore un sujet de recherche pour la modélisation des pertes et du comportement thermique à cause de la complexité des phénomènes représentés et de la taille du problème.

Les pertes sont habituellement classées en deux catégories, comme présenté par Höhn et al. [54], ou encore par Martins et al. [82]:

- Les pertes sans charges qui ne dépendent pas de la charge appliquée au système, ceci inclut les pertes par barbotage, pertes hydrodynamiques dans les roulements ou le frottement aux joints.
- Les pertes dépendantes de la charge qui sont dues aux éléments chargés en contact comme les engrenages ou les roulements.

L'objectif est de fournir un modèle qui soit adapté aux besoins en termes de recherche et de conception, ce qui signifie que le modèle doit être assez précis pour donner des valeurs significatives pour les pertes et les températures du système. Différentes méthodologies de modélisation thermique existent. Après avoir considéré les forces et les faiblesses des différentes méthodes, la méthode la plus adaptée est retenue et détaillée.

2. Modèle thermique

2.1. Différentes méthodes

Le choix entre les différentes méthodes est un compromis entre le temps de calcul nécessaire et la précision du modèle. Trois niveaux de discrétisation sont possibles : le système est supposé isotherme, les éléments de la transmission sont supposés isothermes ou l'ensemble de la transmission est discrétisé.

La méthode la plus globale suppose l'ensemble de la transmission comme isotherme. Cela signifie que le temps de résolution nécessaire est limité cependant les détails des résultats sont également limités puisqu'une seule température est déterminée. Les rapports techniques ISO/TR 14179-1 [1] et ISO/TR 14179-2 [2], ou encore Höhn et al. [54] ont étudié l'augmentation de température du bain d'huile dans une transmission mécanique. La température obtenue est un équilibre entre les pertes et les échanges avec l'environnement, par exemple les travaux de Winter et

Michaelis sur le banc FZG [115]. Höhn *et al.* [54] et Terauchi *et al.* [109] ont pris en compte l'évolution de la température avec le temps dans leur modèle. Le modèle isotherme permet d'obtenir un premier ordre de grandeur de la température d'huile, cependant il n'est pas assez précis pour prédire le rendement de la transmission puisque les points chauds ne sont pas mis en évidence, comme présenté par Changenet *et al.* pour une boîte à six vitesses [22]. Ces points chauds peuvent causer des changements dans les propriétés du lubrifiant qui doivent être capturées pour obtenir un modèle représentatif du comportement thermique de la transmission. Même si cette méthodologie ne fournit pas un haut niveau de détail sur le comportement à l'intérieur de la transmission, Henriot [53] donne un critère évaluant la capacité du carter à évacuer la chaleur par rapport à celle générée dans la transmission.

La seconde approche est associée à la méthode des réseaux thermiques [51] [22] [38]. Le système est discrétisé en plusieurs éléments isothermes, chacun représenté par un nœud dans le modèle. Ils sont reliés entre eux par des résistances thermiques à la manière d'un réseau électrique. Les équivalences entre les réseaux thermiques et électriques sont les suivantes :

- Le courant électrique I est associé au flux de chaleur Q entre deux nœuds
- La différence de potentiel U est liée à la différence de température entre deux nœuds
- La résistance électrique R est liée à la résistance thermique R_{th}, qui relie les nœuds entre eux.

Cela se résume à :

$$Q = \frac{\Delta T}{R_{th}}$$

Equation 1

Les réseaux thermiques sont efficaces avec moins d'une centaine de nœuds, par exemple Coe *et al.* [27] [28], ou plus d'une centaine de nœuds dans le cas d'études plus fines de Jan et Norman [60] ou Manin [77].

La troisième méthode décrit le comportement de l'ensemble du système et des gradients entre ses éléments internes. Il s'agit de la méthode la plus fine et permet une discrétisation en temps et en espace. Cependant cette méthode requiert un temps de calcul important du fait de l'échelle locale de discrétisation qui nécessite un maillage fin. Les échanges convectifs [63] restent la partie la plus complexe des modèles thermiques : ce phénomène n'est pas évident à résoudre à cause des nombreuses instabilités dans les écoulements du fluide qui doivent être résolues par des méthodes CFD [90]. Les simulations CFD ajoutent une complexité supplémentaire puisqu'elles sont les conditions limites du calcul par éléments finis. Cette méthode se limite à une partie de la transmission pour réduire le temps de calcul nécessaire.

Des couplages entre les réseaux thermiques et les éléments finis sont possibles pour obtenir différents niveaux de raffinement pour le modèle thermique de la transmission, par exemple [97], [98], [78] ou [77].

La méthode retenue est celle des réseaux thermiques [22]. Cette méthode est adaptée car elle permet une discrétisation en temps et en espace. L'efficacité de la méthode des réseaux thermiques a été mise en évidence par De Gevigney et al. [38] pour le banc FZG : cette méthode combine un faible temps de résolution tout en donnant des niveaux de température précis pour les pignons. Le phénomène de barbotage est simulé efficacement pour les différents régimes observés [21]. La résolution de l'équation des réseaux thermiques et la sélection des nœuds intéressants est l'objet de la partie suivante.

2.2. La méthode des réseaux thermiques

Les réseaux thermiques sont traduits par l'équation d'équilibre statique I.1. A partir de cette expression statique, une évolution avec le temps peut être traduite à l'aide de la première loi de la thermodynamique appliquée à chacun des nœuds (i) du réseau :

$$\frac{dT_i}{dt} = \frac{1}{m_i C_i}\left[Q_i - \sum_{j=1\,\&\,j\neq i}^{n} \frac{(T_i - T_j)}{R_{th,ij}}\right]$$

Equation 2

La température est imposée pour les nœuds qui sont associés à des conditions limites. Pour ces nœuds, Q_i représente la chaleur évacuée et leur énergie interne ne varie pas avec le temps.

A partir de l'équation de la conservation de l'énergie, les réseaux thermiques peuvent s'exprimer sous forme matricielle [19] :

$$[C]\{T'\} = \{Q\} - [S]\{T\}$$

Equation 3

Ce système d'équations est résolu sous la forme de blocs de matrices. Les températures des nœuds limites sont connues alors que les pertes évacuées sont inconnues, tandis que les pertes peuvent être calculées pour les autres nœuds et que leurs températures sont inconnues. Le système s'exprime alors ainsi :

$$\begin{bmatrix} C_{un} \\ C_k \end{bmatrix} \begin{vmatrix} T'_k \\ T'_{un} \end{vmatrix} = \left\{ \begin{vmatrix} Q_{un} \\ 0 \end{vmatrix} + \begin{vmatrix} 0 \\ Q_k \end{vmatrix} \right\} - \begin{bmatrix} S1 & S2 \\ S3 & S4 \end{bmatrix} \left\{ \begin{vmatrix} T_k \\ 0 \end{vmatrix} + \begin{vmatrix} 0 \\ T_{un} \end{vmatrix} \right\}$$

Equation 4

Les indices $_k$ et $_{un}$ concernent respectivement les valeurs connues et inconnues.

Les températures sont calculées grâce à la résolution de l'équation suivante :

$$C_k T'_{un} = Q_k - S3T_k - S4T_{un}$$

Equation 5

L'algorithme de résolution est la méthode prédicteur-correcteur d'Adams, qui est utilisée dans la fonction de résolution ode23t dans le logiciel MatLab® (plus de détails dans [19]). Après avoir calculé les températures inconnues, les pertes transférées à l'environnement sont calculées en tenant compte que $C_{un} T'_k = 0$ pour les nœuds limites, l'équation suivante est donc utilisée :

$$Q_{un} = S2T_{un} + S1T_k$$

Equation 6

Dans le cas permanent, l'équation se simplifie car la dérivée des températures en fonction du temps est nulle :

$$\begin{bmatrix} S1 & S2 \\ S3 & S4 \end{bmatrix} \left\{ \begin{vmatrix} T_k \\ 0 \end{vmatrix} + \begin{vmatrix} 0 \\ T_{un} \end{vmatrix} \right\} = \left\{ \begin{vmatrix} Q_{un} \\ 0 \end{vmatrix} + \begin{vmatrix} 0 \\ Q_k \end{vmatrix} \right\}$$

Equation 7

Le lubrifiant peut avoir une grande influence sur le comportement thermique de la transmission. Cependant les caractéristiques du lubrifiant sont fortement dépendantes de la température, ce qui signifie qu'une évolution des températures influence les caractéristiques du lubrifiant qui impacte les pertes. Plusieurs pas de temps sont nécessaires pour prendre en compte un changement des propriétés du lubrifiant et tendre vers la solution stabilisée. La prise en compte de l'influence de la température sur les propriétés du lubrifiant est détaillée dans l'annexe B.

2.3. Description du réducteur

L'étude se focalise plus particulièrement sur les réducteurs avec renvoi d'angle à 90°C entre l'entrée et la sortie. Les réducteurs étudiés sont parmi les plus grandes tailles produites par Moteurs Leroy Somer en France : le couple de sortie est compris entre 4000Nm et 23000Nm, pour des vitesses de rotation de l'ordre de la centaine de tours par minutes en sortie. Ils sont utilisés dans les applications de l'industrie minière, les grues, les convoyeurs…

Le réducteur est produit et vendu avec ou sans système de refroidissement supplémentaire en fonction des conditions opératoires. Le réducteur peut être fixé par un bras de levier ou par les fixations situées à la base du réducteur. Le cas le plus général d'application est retenu : le réducteur est placé en position verticale, les fixations vers le bas, le niveau d'huile est le niveau standard pour cette position (environ 5L).

Le réducteur comporte trois étages de réduction (voir Figure 1) : l'engrenage d'entrée est hélicoïdal, ensuite un engrenage spiro-conique permet le renvoi d'angle et l'engrenage de sortie est hélicoïdal également.

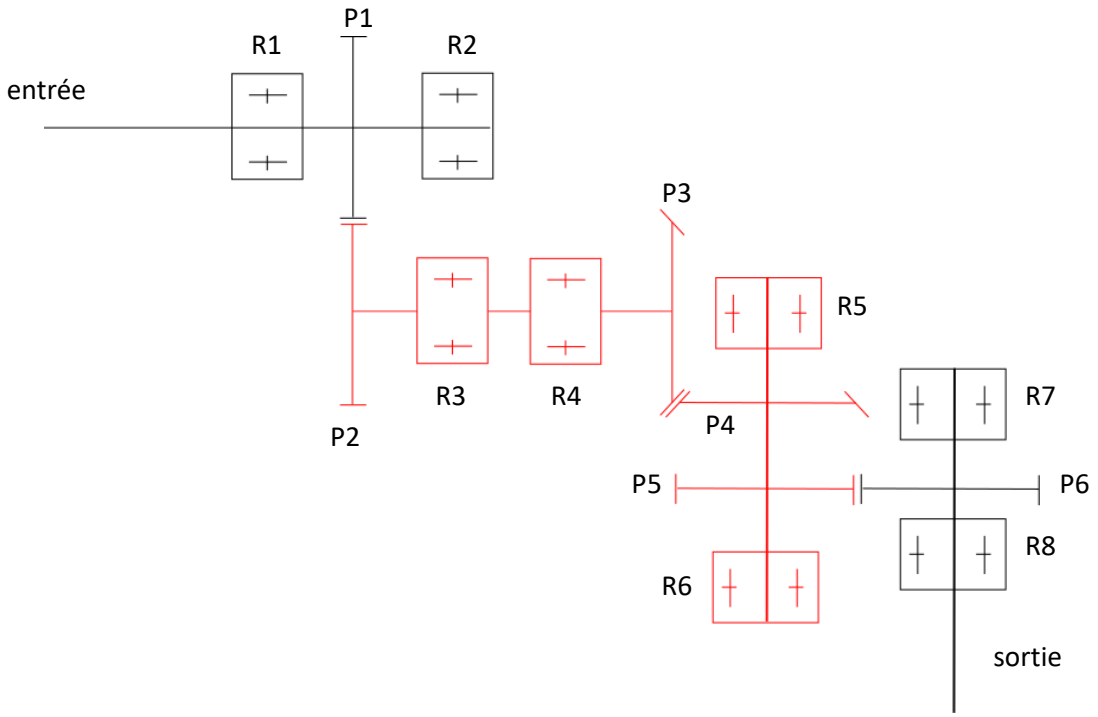

Figure 1 : schéma cinématique des éléments de la transmission – les éléments immergés représentés en rouge

La liste des éléments internes au réducteur est donnée dans la Table 1.

Table 1 : éléments de la transmission dans le schéma cinématique

Numéro	Eléments
R1 à R8	Roulements
P1 et P2	Pignons cylindriques (entrée)
P3 et P4	Pignons spiro-coniques
P5 et P6	Pignons cylindriques (sortie)

2.4. Réseau thermique du réducteur

L'objectif du modèle est d'estimer la température de masse des éléments tournants critiques comme les pignons, les roulements ou les arbres, avec une description de la distribution des températures dans le carter. La chaleur échangée entre le fluide et les éléments baignant dans l'huile

(roulements, pignons, arbres) est évaluée en utilisant des résistances thermiques de convection. L'air à l'intérieur du carter échange par convection avec l'arbre et la roue de sortie, et les roulements associés sont situés dans la partie supérieure du carter. Les éléments en contact échangent de la chaleur par conduction dans le matériau, cependant une résistance adaptée, dite de « striction », traduit la conduction à travers des surfaces de contact réduites entre les dentures qui diffuse la chaleur vers les massifs des pignons.

Une résistance thermique définit le transfert thermique entre deux nœuds du réseau thermique. Trois types de transfert thermique sont différentiables concernant le calcul des résistances thermiques : la conduction, la convection et le rayonnement.

Les descriptions des résistances sont détaillées dans l'annexe A.

2.5. Pertes de puissance

2.5.1. Engrènement des engrenages droit et hélicoïdal

Le coefficient de frottement est supposé constant tout au long de la ligne de contact. Les pertes sont exprimées selon la formule suivante [18] [86] [91] [52], H_v variant suivant les formules :

$$Q = P \times f \times H_v$$

Equation 8

La formule de Velex et Ville [112] concernant le paramètre H_v permet de considérer les améliorations apportées par une modification de profil.

2.5.2. Engrènement des engrenages spiro-coniques

Les engrenages spiro-coniques ont été moins étudiés que les engrenages cylindriques. Deux méthodes sont disponibles : l'approximation de Tredgold (annexe C) ou une étude locale du contact [117] [6]. L'approximation de Tredgold est basée sur la projection de la géométrie conique sur un plan. Buckingham [18] fournit des formules pour calcul des rendements des engrenages spiro-coniques (voir annexe C).

L'objectif est d'avoir un modèle utilisable dans des phases de conception. La formule de Buckingham est bien adaptée car le temps nécessaire et le nombre d'informations requis sont beaucoup plus limités que dans le cas d'une étude locale.

2.5.3. Détermination du coefficient de frottement dans les engrènements

Aucune formule disponible dans la littérature n'est la réponse parfaite au problème, puisque les informations dont nous disposons concernant le matériau et le lubrifiant sont limitées. De plus, aucun élément ne permet de choisir entre les différentes formulations et les résultats sont significativement différents entre eux. Par conséquent le coefficient de frottement est choisi constant par défaut. Des tests sous charge de la transmission permettront d'étudier l'impact de cette valeur sur le comportement de la transmission.

2.5.4. Roulements

Deux méthodes sont disponibles pour déterminer les pertes des roulements : une approche locale ou une approche globale. L'approche locale [100] décrit le comportement interne des éléments à l'intérieur du roulement. Cette méthode nécessite un grand nombre de données, par conséquent, la seconde semble la plus adaptée car elle ne nécessite que des données disponibles dans les catalogues constructeur. Cette seconde méthode est la plus adaptée dans le cadre de cette étude.

Deux modèles sont disponibles concernant l'approche globale : le modèle de Palmgren, décrit par Harris [51], ou le modèle SKF [106]. Des comparaisons ont été effectuées [20] [42] [43] [44] [102] [3] et l'un ou l'autre de ces modèles donne de meilleurs résultats en fonction du roulement considéré et des conditions opératoires. Cependant, Harris donne systématiquement de meilleurs résultats pour les cas sans charge car SKF considère les pertes nulles lorsque le roulement tourne sans chargement appliqué. De plus, la formule de SKF diverge lorsque la vitesse augmente, par exemple dans le cas de butées. De plus, la formule de Harris présente des résultats nettement meilleurs lorsque le paramètre f0, qui prend en compte l'influence de l'immersion, est adapté en fonction d'un essai de référence.

Les formules de SKF et Harris nécessitent de fixer expérimentalement certains paramètres pour corréler le comportement des roulements [3]. Puisque les deux formulations nécessitent des valeurs expérimentales, les tests en charge sont utilisés pour déterminer le coefficient de frottement dans les engrènements et les essais sans charge sont utilisés pour déterminer les paramètres des roulements. Sachant que la formule de SKF est moins performante pour ce type de tests, la formule de Harris est retenue pour la suite de l'étude.

2.5.5. Joints

ISO/TR 14 179-2 [2] présente une formule pour calculer les pertes dues aux joints qui est la même que celle de SIMRIT [105] :

$$Q = 7.69 \times 10^{-6} \times d_{shaft}^{2} \times N$$

Equation 9

Cette formule est donnée dans le cas d'un joint comportant une seule lèvre. Il convient de multiplier le résultat par le nombre de lèvre si nécessaire.

2.5.6. Barbotage

Concernant les pertes par barbotage des engrenages cylindriques, Changenet et al. [23] [21] ont développé un modèle basé sur une analyse dimensionnelle. Cette formulation donne de bons résultats pour une large gamme d'engrenages cylindriques, de lubrifiant et de vitesses de rotation. La perte par barbotage se définit comme suit :

$$P = \frac{\rho \omega^3 S_m R_p^3 C_m}{2}$$

Equation 10

Les détails du calcul sont présentés dans l'annexe D. La détermination du paramètre C_m est donnée dans l'annexe G pour différentes conditions opératoires.

Pour les engrenages spiro-coniques, les formules ne sont pas les mêmes que pour les engrenages cylindriques. Plusieurs formulations sont disponibles dans la littérature. Deux rapports techniques [1] [2] suggèrent que les pertes par barbotage sont quantifiables en considérant la dimension du cylindre enveloppant le pignon ou la roue conique respectivement. Pour les engrenages hypoïdes, dont la géométrie se rapproche des engrenages spiro-coniques, Kolekar et al. [67], dont les travaux ont été poursuivis par Jeon [62], proposent des formulations à partir d'une analyse dimensionnelle (voir annexe G pour plus de détails).

Cependant, ces formulations donnent des résultats très différents entre elles (jusqu'à 10°C d'écart pour la température du bain d'huile) sans qu'il soit possible de privilégier l'une ou l'autre des solutions. Pour cette raison, des essais sont réalisés sur des pignons coniques afin d'évaluer les différentes formules en fonction des résultats expérimentaux.

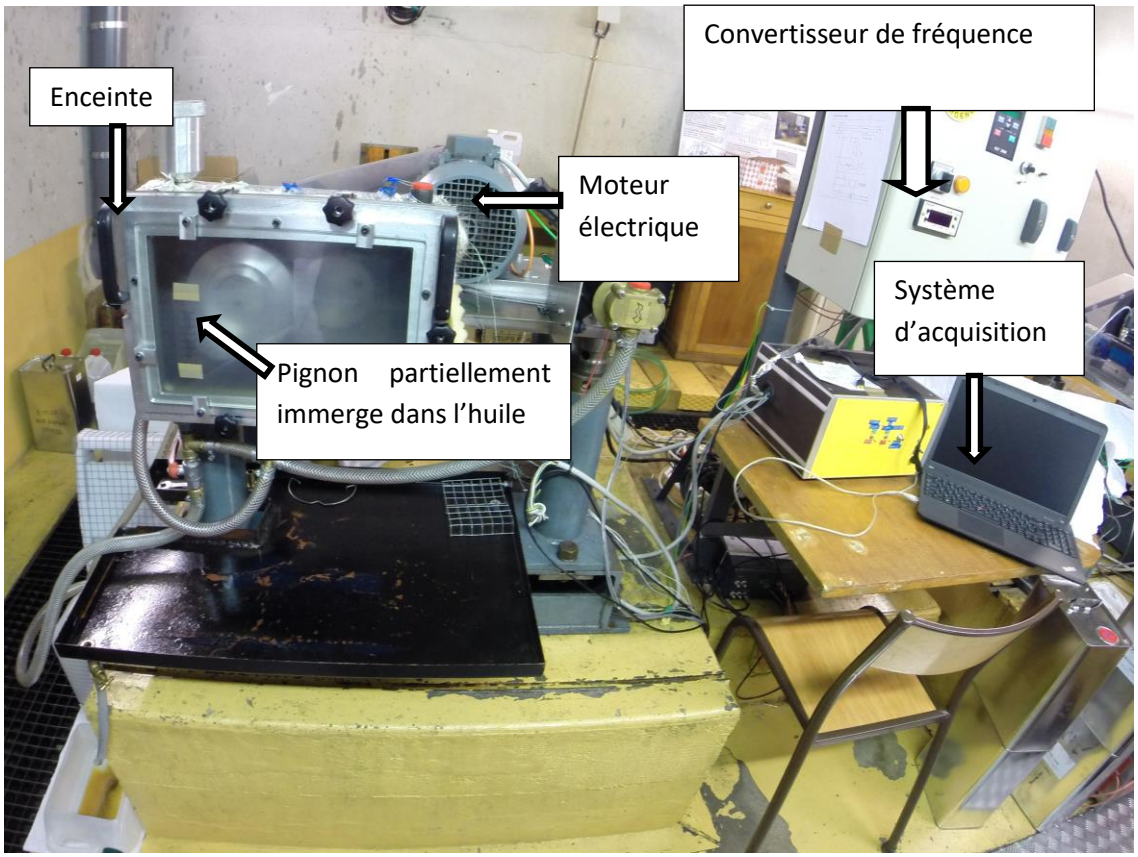

Figure 2: banc d'essai

Dans le cas des engrenages spiro-coniques, l'expression de la perte due au barbotage est la même que celle donnée (équation 10) pour les engrenages cylindriques. Par contre, l'expression du paramètre Cm est modifiée (équation 11 et 12) :

Si $Re > 25\,000$,

$$Cm = 0{,}15\, Fr^{-0{,}6} \left(\frac{h}{R_O}\right)^{0{,}4} \left(\frac{V_0}{{R_O}^3}\right)^{0{,}1}$$

Equation 11

Si $Re \leq 18\,000$

$$Cm = 2{,}3\, Re^{-0{,}25} Fr^{-0{,}6} \left(\frac{h}{R_O}\right)^{0{,}7} \left(\frac{V_0}{{R_O}^3}\right)^{0{,}1}$$

Equation 12

L'erreur moyenne est inférieure à 15%, sauf pour quelques points où la viscosité est faible (moins de 20cSt) ou haute (supérieure à 400cSt). En effet, une faible viscosité conduit à des instabilités importantes dans le bain d'huile. Une viscosité élevée induit une variation importante de la viscosité lorsque le pignon tourne dans le bain d'huile et réchauffe le bain.

Il est important de noter que la forme de l'enceinte joue un rôle sur les pertes par barbotage et explique la difficulté de proposer une formulation unique.

3. Validation et application du modèle à un réducteur industriel

Tout d'abord, un essai en refroidissement est utilisé pour valider les échanges thermiques avec l'environnement du réducteur. Puis, le modèle est comparé à des résultats expérimentaux réalisés à vide : le réducteur est entraîné en rotation sans charge. Ces essais permettent de valider la sélection du f0 et le comportement du modèle à vide.

Ensuite, des essais sous charge sont réalisés à l'aide du banc d'essais présenté Figure 3. Les résultats sont comparés avec les calculs pour différentes conditions opératoires.

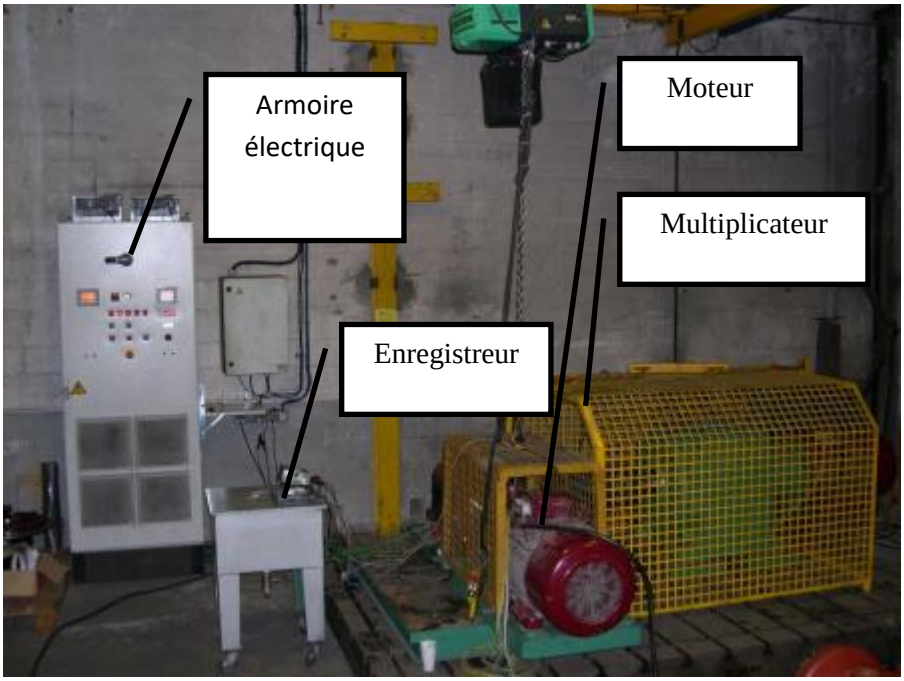

Figure 3 : banc d'essai sur le réducteur

Après cette phase de validation, le modèle est utilisé pour tester les différentes pistes qui peuvent influencer le comportement thermique d'un réducteur. Cette étude permet de quantifier l'efficacité des différentes solutions : un calcul entre le coût et le gain de chaque solution permet ensuite de déterminer la solution optimale.

3.1. Modification des échanges avec l'environnement

Plusieurs éléments permettent de modifier l'échange avec l'environnement, soit avec l'air ambiant soit avec le support.

Pour augmenter l'échange avec l'air ambiant, il faut modifier la quantité d'énergie transférée par une augmentation de la vitesse de l'air ambiant ou de la surface d'échange. La vitesse de l'air est augmentée par l'ajout de ventilation supplémentaire (ventilateur). L'ajout d'ailettes sur le carter permet d'augmenter de manière significative la surface d'échange avec l'air, ce qui augmente le transfert de chaleur.

Un support peut également augmenter la capacité du système : en échangeant par conduction avec un support massif, une partie de la chaleur est dissipée dans le support.

Dans ces cas, les pertes sont peu impactées tandis que les températures sont fortement réduites.

3.2. Modification de l'échange à l'intérieur du réducteur

Pour modifier les échanges à l'intérieur du réducteur, il faut modifier la géométrie interne ou modifier les échanges convectifs entre le fluide interne et les éléments solides. Le plus simple est de modifier les échanges convectifs en modifiant le niveau du bain d'huile : cette solution modifie le niveau des pertes par barbotage en plus de modifier les échanges. Un minimum peut être fixé pour garantir la lubrification et un niveau trop faible conduit à une augmentation des températures par manque d'échange même si les pertes sont diminuées. Un maximum est observé car les pertes augmentent même si l'augmentation des températures est limitée. Le niveau utilisé actuellement pour le bain d'huile est le niveau optimal en tenant compte des deux considérations précédentes.

Une piste de modification concernant la géométrie interne se situe au niveau des corrections de dentures à apporter. L'influence se situe principalement sur une réduction des pertes au niveau des engrènements, ce qui a pour conséquence de réduire globalement les températures.

3.3. Changement de lubrifiant

Un changement de lubrifiant impacte la viscosité mais plus généralement l'ensemble des propriétés du lubrifiant. Une réduction de viscosité réduit les pertes, donc les températures. Cependant, il est à noter qu'une amélioration du comportement en frottement est plus influente qu'une simple réduction de la viscosité.

Le choix du lubrifiant est donc complexe et seuls des essais pour un couple lubrifiant – matériau permettent de trancher entre plusieurs lubrifiant, bien que des tendances de comportement soient données dans le rapport technique 14179-2 [2].

4. Conclusion et perspectives

L'objectif de cette étude est de fournir un programme robuste, efficace et rapide pour permettre une description précise et fiable du comportement thermique d'un réducteur. Le programme doit être utilisable dans des phases de développement ou pour estimer le comportement d'un réducteur existant. Il doit fournir les températures des différentes parties de la transmission et le niveau de pertes pour chaque condition de fonctionnement. Le modèle numérique ne doit nécessiter que des informations disponibles dans une phase de conception pour aider les ingénieurs dans ses choix de conception.

Le premier chapitre décrit la méthode des réseaux thermiques et pointe les raisons de choisir cette méthode. L'utilisation des résistances thermiques et de nœuds est détaillée pour représenter le comportement du réducteur discrétisé en éléments isothermes. Les sources d'incertitudes sont pointées concernant les pertes par barbotage des engrenages spiro-coniques.

Le second chapitre se concentre sur les pertes par barbotage des engrenages spiro-coniques. Plusieurs méthodes sont disponibles et la comparaison des méthodes entre elles ne permet pas de choisir de manière concluante. Les différences entre les méthodes ne permettent pas de les considérer comme équivalentes entre elles. Des essais sont conduits pour déterminer les pertes associées au barbotage des engrenages spiro-coniques. Au moyen d'une analyse dimensionnelle, une formule est proposée pour modéliser le comportement observé, puisqu'aucune des formules de la littérature ne semble représenter correctement les résultats expérimentaux.

La comparaison entre des résultats expérimentaux et théoriques du réducteur est présentée dans le troisième chapitre. Des essais en refroidissement, sans charge et chargés sont utilisés pour valider le modèle pour différentes conditions opératoires. Deux paramètres, décrivant le niveau de ventilation et le comportement des roulements sans charge, sont déterminées expérimentalement et validées sur les essais non exploités lors de leur détermination.

Le coefficient de frottement entre les engrenages spiro-coniques est obtenu par des mesures expérimentales des pertes et des températures (ingénierie inverse). Une modification du coefficient de frottement a une forte influence sur les pertes et les températures du réducteur.

Cette thèse fournit un modèle qui donne des indications concernant les choix de conception. Plusieurs éléments peuvent influencer l'échange avec l'environnement ou l'échange à l'intérieur du réducteur. Il est également possible d'évaluer l'influence d'un changement de lubrifiant. Cette étude montre l'impact de chacune des modifications suggérée, donnant au concepteur des indications pour faire le meilleur choix concernant la contrainte performance – coût.

Pour poursuivre les travaux de cette thèse, certains aspects peuvent être développés dans de futurs travaux. Plusieurs phénomènes influencent les pertes dans un réducteur et les températures stabilisées.

Tout d'abord, la précharge des roulements influence les pertes : la précharge doit être réduite au maximum tout en permettant de conserver suffisamment de rigidité pour garantir un engrènement correct. La précharge impacte indirectement le rendement des engrenages : cette influence n'est pas considérée dans cette étude car cette relation est non-linéaire et complexe à utiliser sans avoir une idée de la géométrie fine des engrenages.

Ensuite, les pertes des engrènements spiro-coniques sont étudiées grâce à l'approximation de Tredgold avec des engrenages virtuels équivalents. Des études 3D représentent le comportement de l'engrènement spiro-coniques par des études détaillées de Jbili et al. [61] ou Teixeira-Alves [108]. Cela nécessite plus de temps de calcul : ces méthodes sont à utiliser plutôt dans des phases de validation plutôt que dans des phases de conception.

Une manière de réduire les pertes est de réduire les frottements dans un réducteur : un changement de lubrifiant influence le coefficient de frottement. Cette solution est souvent un moyen efficace et peu coûteux pour diminuer le frottement dans les transmissions. Ce modèle permet un changement de viscosité ou de densité, cependant l'introduction d'une loi de frottement associée à un couple lubrifiant-matériau peut être une amélioration du modèle existant.

Au lieu de chercher à réduire les pertes pour diminuer les températures des éléments du système, il est possible de favoriser les échanges thermiques avec l'environnement. Mettre en place différentes géométries d'ailettes est une solution intéressante pour des développements ultérieurs du modèle existant.

Le modèle actuel peut être encore amélioré en intégrant les différents développements précédents.

Nomenclature

A	Area	[m²]
Ag	Arrangement constant	[-]
a	Thermal diffusivity	[m²/s]
b	face width	[m]
b_{tooth}	Tooth width	[m]
C	Heat capacity	[J/kg.°K]
C1	Geometrical and operating conditions factors	[-]
C2	Geometrical and operating conditions factors	[-]
C_m	Dimensionless torque	[-]
C_{sp}	Splash oil factor	[-]
C_w	Parameter accounting for bearing geometry	[-]
c	Absorption coefficient depending on X-ray energy and material	[-]
d_m	Mean diameter	[m]
d_{shaft}	Shaft diameter	[m]
e	Thickness	[m]
F	Radiation shape factor	[-]
F_n	Normal load	[N]
F_{nu}	Normal load per unit length	[N/m]
F_{radial}	Radial load	[N]
f	Friction coefficient	[-]
fa	friction coefficient in approach path of contact	[-]
fr	Friction coefficient in recess path of contact	[-]
f_g	Gear dip factor	[-]

f_{sl}	Sliding friction coefficient	[-]
f_t	Parameter associated with the oil level	[-]
f_0	Parameter accounting for bearing and lubrication type	[-]
f_1	Parameter accounting for equivalent static load and base static load, and bearing type	[-]
G_{rr}	Parameter accounting for load, dimensions and bearing type	[-]
G_{sl}	Parameter accounting for load, dimensions and bearing type	[-]
g	Gravitational acceleration	[m²/s]
g_α	Recess lengths of the path of contact	[m]
g_f	Approach lengths of the path of contact	[m]
H_{tooth}	Tooth height	[m]
H_v	Geometric factor	[-]
h	Gear immersion depth	[m]
h_{conv}	Convective exchange coefficient	[W/m².°K]
h_{Fair}	Exchange coefficient	[W/m^3.°K]
I	Intensity	[A]
K_w	Parameter accounting for bearing geometry	[-]
K_{roll}	Parameter accounting for bearing geometry	[-]
k	Thermal conductivity	[W/m.°K]
L	Characteristic dimension	[m]
l_h	Half width of the contact between two teeth	[m]
M_0	Load independent torque	[N.m]
M_1	Load dependent torque	[N.m]
M_{drag}	Drag torque linked with the lubrication mode	[N.m]
M_{rr}	Torque caused by rolling	[N.m]
M_{sl}	Torque caused by sliding	[N.m]
M_{total}	Total torque of a bearing	[N.m]

m	Mass of an element	[kg]
N	Rotational speed	[RPM]
n	Number of nodes	[-]
P	Power	[W]
P_{sides}	Power loss associated with the faces of the gear	[kW]
P_{tooth}	Power loss associated with the tooth surfaces	[kW]
P_1	Combination of axial and radial load on the bearing	[N]
p	Perimeter	[m]
p_{bt}	Transverse base pitch	[m]
Q	Heat generated per unit of time	[W]
Q_m	Mass flow	[kg/s]
q_x	Heat flux along the x direction	[W/m²]
R	Radius	[m]
R_b	Base radius	[m]
R_p	Pitch radius	[m]
R_s	Parameter associated with the oil level	[-]
R_{th}	Thermal resistance	[°C/W]
Ra	Mean roughness	[µm]
Ra_r	Mean roughness of the tooth side of the pinion and the wheel	[µm]
R_f	Roughness factor	[-]
r	Radius	[m]
r_c	Equivalent curvature radius at the pitch diameter	[m]
S	Surface of exchange	[m²]
S_a	Apparent contact area	[m²]
S_m	Immersed area	[m²]
T	Temperature of an element	[°K]

T_H	Churning torque	[Nm]
t	Time	[s]
u	Reduction ratio	[-]
U	Rolling speed	[m/s]
V	Speed	[m/s]
V_M	Parameter associated with the oil level	[-]
V_0	Oil volume	[m^3]
V_s	Sliding speed	[m/s]
V_t	Peripheral speed	[m/s]
$V_{shaft/seal}$	Relative speed between the shaft and the seal	[m/s]
X_L	Coefficient associated with the oil type	[-]
X	Distance along the flow	[m]
Z	Number of teeth	[-]

Dimensionless number

Gr	Grashof number	[-]
Nu	Nusselt number	[-]
Pr	Prandtl number	[-]
Re	Reynolds number	[-]

Greek letters

Γ	Dimensionless extent of profile modification	[-]
Δ_m	Average normal approach with respect to rigid body positions	[m]
ΔT	Temperature difference	[°K]
Λ	Dimensionless loss factor	[-]

Y	Dimensionless tip relief amplitude	[-]
α	Pressure angle	[rad]
α_n	Normal pressure angle	[rad]
α_p	Apparent pressure angle	[rad]
α_t	Transverse contact angle	[rad]
β	Helix angle at pitch radius	[rad]
β_b	Base helix angle	[rad]
β_f	Coefficient of thermal expansion of a fluid	[K^{-1}]
δ	Width	[m]
γ_p, γ_g	Half top angle of the pinion/gear	[rad]
γ_i	Constant coefficients	[-]
ε	Emissivity (dependent on material)	[-]
ε_α	Transverse contact ratio	[-]
η	Efficiency	[-]
θ	Centrifugal projection angle	[rad]
K_0	Position of the rolling without sliding point along the path of contact	[-]
μ	Dynamic viscosity	[Pa.s]
ν	Kinematic viscosity	[m^2/s]
ρ	Density	[kg/m^3]
σ	Stefan-Boltzmann constant	[$W/m^2.K^4$]
χ	Thermal effusivity	[$N/m^{1/2}.°C$]
ϕ_a	Arc of approach	[rad]
ϕ_r	Arc of recess	[rad]
φ_{ish}	Inlet shear heating reduction factor	[-]
φ_{rs}	Kinematic replenishment/starvation reduction factor	[-]
ω	Rotational speed	[rad/s]

Subscripts and exponents

in	Inner
k	For known values
o	Outer
un	For unknown values
v	Virtual

Matrix and Vectors

[MC]	Matrix of thermal inertia
[S]	Matrix obtained from the thermal resistances $R_{th,ij}$
{T'}	Vector of derivative of temperature as a function of time
{T}	Vector of temperature
{Q}	vector of heat generated (positive value) or evacuated (negative value) at each node

Introduction

Nowadays a global awareness points out the necessity to diminish the pressure of human activity on the environment. It means reducing both the needs of material and energy consumption. It means increasing the efficiency of systems and reducing their weight for the same power consumption. Moreover standards push towards this direction too. This tendency induces both research on alternatives to fossil energy and efficiency improvement.

Transmissions driven by electrical motors follow this evolution and standards become more and more stringent on the efficiency of systems. Electrical motors have become more compact and efficient for the past few years. Mechanical transmissions have followed this trend. However this evolution is now showing limits of such reduction of size: keeping the same power transmitted through a reduced system means to increase the temperature. Power losses are still to be evacuated to the environment to ensure a reasonable temperature of the system, so thermal problem should not be neglected. Thermal issues appear as a dimensioning criterion due to the reduction of the available surface allowing thermal transfer to the environment. It diminishes the capacity to cool down the system.

High temperatures in a system are a real problem since they lead to premature failure of the system, (due to limited thermal endurance of the transmission elements like oil, seals…), and to safety concerns.

Limiting the number of tests required to ensure the wanted behavior of the system means that the behavior of the transmission should be represented accurately: efficiency, thermal behavior, impact of environmental conditions…

This PhD is focused on the gear unit localized after the electrical motor and ensuring the speed reduction.

A model representing the thermal behavior of the gear unit should provide missing information on the internal behavior and the thermal transfer to the environment. The gear unit studied belongs to the bigger sizes of reducers produced by Moteurs Leroy Somer in France, where the output torque is above 4000Nm and lower than 23000Nm, for around a hundred RPM, focusing on reducers with a 90° angle between input and output shaft axes. They are used in transmissions for mining industry, cranes, conveyors… They encounter various operating conditions: high or low ambient temperatures, wet environment, dust, windy or enclosed environment, intermittent or continuous work for weeks, flexible or rigid supports… All these various conditions should be considered when dealing with defining the specifications of the product: the mechanics and thermal behaviors should both respect defined range. As for mechanical resistance, where the critical parts should be identified, the thermal limit is determined both by oil bath temperature and hot spots, which should be identified. Hot spot could only be noted on a detailed analysis of the system either with finite elements or thermal network with an appropriate refinement.

The power loss represents around 5% of the power input, which is high, from hundreds to thousands of watts, even if the loss is low in percentage of power. This is an efficiency level commonly encountered for a three gearing pair transmission. However, even if constant effort is

made on reducing power losses, the power losses will still exist and increase temperature through the transmission. Providing efficient and reliable products means to ensure that either the temperatures of the different parts are compatible with the expected operating conditions and product life, or an extra cooling system should be adapted to ensure the former condition to be respected. The second solution is often a problem, meaning extra maintenance, extra cost and a bigger volume. This solution is often the easiest way to solve a thermal problem; however it is not the easy way to produce neither appreciated by the client who should consider extra maintenance and extra space to install the system. Working on a solution without extra cooler means a great understanding of the gearbox thermal behavior: all the hot spots must be identified, and all the requested operating conditions must be complied with.

Understanding the thermal behavior of existing transmissions allows specifying the operating conditions that meet thermal requirements, defining a confidence range of operating conditions. It allows to provide reliable products for the conditions, or to better define the cooling system if it is still needed. Furthermore, experience is important; however trial-and-error is not the best way to find neither the optimum solution nor the fastest. Thermal model allows also modeling future transmission and accounting for thermal constraints since the development stage. The objective is to provide reliable products, and low delay between the design and the production steps, reducing the trials by analytical simulations.

The first part of this PhD presents the thermal model of a gearbox with its various components. The computation of power losses and thermal transfer is detailed. However it shows some weak points in the computation of churning losses, in particular when considering spiral bevel gears churning losses estimation.

The second part is focused on the modeling of spiral bevel gears churning losses. Series of tests with various geometries and oil types point out several flow regimes in the oil bath.

Then the third part presents the validation of the model through a comparison with the experiments realized on the whole gear unit. The sensitivity of the model to external parameters is tested: several parameters may vary from an experiment to another and each of these parameters influences at a different level the response of the model.

Chapter 1

Context

1. Introduction

Power density of gear units has greatly increased in the past few years, meaning their thermal behavior is becoming a design criterion since the heat generated by the power losses in the transmission should be evacuated through reduced exchange areas. The equilibrium between the power losses of the gear unit and the heat transferred to the environment defines the maximal temperature encountered in the gear unit. The power losses of 5% is a rough estimation of the power losses of the gear unit, the thermal behavior modelling of the gear unit requires more accurate models of the power losses. All power losses which are dissipated by the gear unit (churning losses, friction in contacts…) heat up the gear unit. Designers need accurate methods to define the thermal limit of gear units as a function of operating conditions and their environment. The efficiency of transmission has been studied for many years now, and thermal models theory also exists. However, a complete transmission modeling in terms of power losses and thermal behavior is still a research subject because of the problem size and the complex phenomena which occur.

All the power losses encountered in an oil bath lubricated gear unit are usually classified into two categories, as presented in Höhn et al. [54] work, or more recently by Martins et al. [82]:

- The no-load losses which do not depend on the applied load of the system. Churning losses, hydrodynamics losses in bearings or friction in seals can be associated with this category.
- The load dependent losses which are linked with the loaded contacting parts of the transmission such as gears or bearings.

From the determination of power losses, several methods can be used to study the thermal behavior of an enclosed gear drive: global methodology or thermal mapping of the transmission. Global methodology is an isothermal approach which allows estimating the mean temperature of the oil, considering the temperature of the whole transmission is equal to the oil temperature. Concerning the thermal mapping of an enclosed gear drive, two main methods are used: the finite elements and the thermal networks. Their objectives are not quite similar and their limits too. First, the finite element method discretizes the whole system in a meshed domain, compute theoretical solution for each node. It requires a huge amount of calculus depending on the problem size and complexity. Then the thermal network method isolates each node from another with thermal resistance, based on the same methodology as an electrical network [56]. Each node corresponds to an isothermal area, which can represent few parts of the system, an isolated component or a part of a component, depending of the needed level of complexity or detail of the system. This method is faster than finite element since less nodes have to be computed, however thermal gradients through pieces could only be acquired through a whole discretization of the system. It means that the thermal networks reason on a one dimension heat flow model instead of the finite element that represents heat flow through two dimensions or three dimensions models.

The objective here is to provide a model which corresponds to research and design needs, which means accurate enough to provide significant values in terms of power losses and temperatures of the system. As different methodologies deal with thermal models of a mechanical transmission, they are presented in the following section. From the observation of strengths and weaknesses of the various methods available, the most adapted should be kept. From this choice, the power losses and the heat-exchanges with the environment estimation are presented with respect to the chosen methodology.

2. Thermal model

2.1. Various methods

From standards to finite elements method, a wide variety of approaches are available. This choice between the different methods is the consequence of two constraints: the computational time required versus the accuracy of the model. Three levels of discretization are available: the transmission is supposed isothermal, the elements of the transmission are supposed isothermal or the whole transmission is discretized.

The most global method assumes the whole transmission as isothermal. It means that computational time required is low but the details in the results are reduced too since only one temperature is determined. Technical reports ISO/TR 14179-1 [1] and ISO/TR 14179-2 [2] or Höhn et al. [54] study the global increase of temperature of the oil bath in a mechanical transmission. It provides a temperature based on the equilibrium between power losses and heat transferred to the environment, as presented in a study of Winter and Michaelis on the FZG test rig [115]. Höhn *et al.* [54] and Terauchi *et al.* [109] accounted for the evolution of temperature with time in their model. The isothermal method allows having a first order of magnitude of the oil temperature; however it is not accurate enough to predict the efficiency of the transmission since localized hot spots are not identified as shown by Changenet et al. on a six speed gearbox [22]. These hot spots may be responsible of change in the lubricant properties that should be captured to obtain a representative thermal behavior of the transmission. Even if this methodology does not provide a high detail on the internal thermal behavior of the transmission, Henriot [53] provides a criterion evaluating the capacity of the housing to evacuate heat with respect to the heat generated in the transmission.

The second approach is associated with the thermal network method [51] [22] [38]. The system is discretized in several isothermal elements, each one represented by a node of the model. They are linked by thermal resistances to each other like an electrical network. Electrical and thermal network could be linked through equivalence in their notations:

- The electric current I is associated to a heat flux Q between two nodes,
- The potential difference U is linked to the temperature ΔT difference between two nodes,

- The electrical resistance R is related to the thermal resistance R_{th}, which links nodes between each other.

This could be resumed as:

$$Q = \frac{\Delta T}{R_{th}}$$

Equation 13

From the early work of Blok in 1970 on thermal network, Roulet [101] and Iritani [58] use empirical results as boundary conditions in terms of power losses, to define the temperature of the system. Roulet [101] also studies the stability of the thermal network as the fluid properties evolve which induces changes in the power losses level. Changenet [22] defines power losses thanks to analytical formulas, producing a generic model.

Thermal network could be used in case of analysis of a whole transmission or only of a part of a transmission, for example isolated bearings in studies of Pouly [100] or Harris [51]. Moreover a study on the thermal behavior of a FZG[1] test rig from Durand de Gevigney et al. [38] shows that thermal network provides accurate temperatures of fixed (housing, oil bath for example) and rotating (gear bulk) elements with less than 10°C of discrepancy, which is an efficient alternative to FEM models. Coe [26] and Kleckner and Dyba [66] use the thermal networks to study the different operating and lubrication conditions.

Thermal networks are efficient with less than a hundred nodes, for example Coe *et al.* [27] [28], or more than a hundred nodes in more refined studies of Jan and Norman [60] or Manin [77].

The modelization hypothesis of the thermal model is influenced by how the power losses are computed and inserted in the thermal model. Indeed the bearing discretization is dependent on how the power losses are computed: for example, if the bearing power loss is computed globally, the bearing is considered as a unique node since the heat gradient between internal and external ring is not expressed in the power loss computation.

The third method describes the whole behavior of all the elements and their internal gradient too. It is the finest method allowing both time and space discretization. However it is a time consuming method due to the local scale model which requires a fine mesh and induces an important computational time. For example, the temperature concentration near the contacting surface of two gears in mesh is studied by Handschuh [48] [49] thanks to a FEM model. Considering FEM models to represent the behavior of mechanical transmission, the most complex part of the model is the convection exchange simulation [63]. It is still a research topic since the phenomenon is

[1] FZG stands for "Forschungsstelle für Zähnräder und Getriebebau der Technischen Universität München": it is a back to back test rig designed to evaluate scuffing and wear of gears.

not easy to solve numerically because of the multiple instabilities in the fluid flow which should be solved through CFD simulation [90]. CFD simulation adds a new complexity, since CFD simulation is a boundary condition of the FEM resolution [63]. Some hypotheses are possible to reduce the complexity of the resolution, like cyclic solution in case of rotation of gears [118]. Further work is also done by Concli et al. concerning the reduction of computational time required by CFD simulation [30] and present studies on power losses through computation of the fluid behavior [31] [29].

This method is often limited to a part of a mechanical transmission due to the computational time required. For example, the mesh area is studied as an angular sector of the gear [96] [39] or [111]. If the study is not limited to a study in one plane, 3D studies should be realized like for spiral bevel gears [50] [49]. Other elements of the transmission are studied as isolated elements like the bearings for example the formulas from NASA [26] [28]. Other elements of the transmission have been studied locally like seals [17] or housing [63] [57].

It is also possible to combine the thermal network method with a FEM model to account for different level of refinement in the thermal model of the transmission. For example, Pinel *et al.* [97] or Pirvics [98] propose a local study of the bearing and a thermal network for the shafts and housing. Manin et al. [78] [77] also proposes a model of a transmission using both thermal network for the housing and FEM simulation for the internal elements.

The thermal method chosen in this study is the thermal network method [22]. To study the thermal behavior of a whole gear unit, this method is well adapted since it allows time evolving models while limiting the space discretization to the nodes. Moreover the objective is to obtain the bulk temperatures of the elements of the gear unit, with insight of the local power losses and temperature distribution. The first need is the oil bath temperature which is critical for the life of the gear unit, but the understanding of thermal problems requires much information than the isothermal model. The thermal network efficiency is shown in the article of De Gevigney et al. [38], in the case of the FZG test rig: the low computational time required is observed while giving accurate temperature level of the pinions. The complex phenomenon of dip lubricated gears can be efficiently simulated for different operating conditions by the thermal networks, accounting for the various regimes observed [21].The resolution of the thermal network equation and selection of interesting nodes in the model is the topic of the following parts.

2.2. Thermal network method

Thermal network could be resumed by a static equilibrium equation 13. From this static expression, a time dependent evolution could be expressed thanks to the first law of thermodynamics. It is applied on each node (i) of the network:

$$\frac{dT_i}{dt} = \frac{1}{m_i C_i}\left[Q_i - \sum_{j=1\,\&\,j\neq i}^{n} \frac{(T_i - T_j)}{R_{th,ij}}\right]$$

Equation 14

With:

- $\frac{dT_i}{dt}$ derivative of temperature versus time [K/s]
- m_i mass of element i [kg]
- C_i heat capacity of element i [J/kg.K]
- Q_i power losses introduced at i node [W]
- T_i temperature at node i node [K]
- $R_{th,ij}$ thermal resistance between the nodes i and j [K/W]
- n number of nodes in the thermal network

The temperature is imposed for the nodes which are associated with boundary conditions. For these nodes, Q_i represents an evacuated heat flow, and their internal energy does not vary with time.

From the equation of energy conservation, the thermal network could be resumed to a matrix system, as proposed by Changenet [19]:

$$[MC]\{T\} = \{Q\} - [S]\{T\}$$

Equation 15

With:

- [MC]: a matrix of thermal inertia
- {T'}: a vector of derivative of temperature as a function of time
- {Q}: a vector of heat generated (positive value) or evacuated (negative value) at each node
- [S]: a matrix obtained from the thermal resistances $R_{th,ij}$
- {T}: a vector of temperature

The system is solved through block resolution: the [S] matrix is divided in 4 blocks from S1 to S4.

It should be noted that the temperature is known for the boundary nodes, for example the ambient air, and the power evacuated is unknown. On the contrary, the power losses could be computed for the other nodes, for example the gears or bearings, and their temperature are unknown.

The system is expressed as:

$$\begin{bmatrix} MC_{un} \\ MC_k \end{bmatrix} \begin{vmatrix} T'_k \\ T'_{un} \end{vmatrix} = \left\{ \begin{vmatrix} Q_{un} \\ 0 \end{vmatrix} + \begin{vmatrix} 0 \\ Q_k \end{vmatrix} \right\} - \begin{bmatrix} S1 & S2 \\ S3 & S4 \end{bmatrix} \left\{ \begin{vmatrix} T_k \\ 0 \end{vmatrix} + \begin{vmatrix} 0 \\ T_{un} \end{vmatrix} \right\}$$

Equation 16

Where the subscripts mean:

- $_k$ for known values
- $_{un}$ for unknown values

The temperatures are computed through the resolution of the following equation:

$$MC_k T'_{un} = Q_k - S3T_k - S4T_{un}$$

Equation 17

The algorithm used to solve this Cauchy equation is Adams Predictor-Corrector method, which is used in the ode23t solver in MatLab® (further details in [19]). Different methods were tested in past studies (Runge-Kutta, Dormand-Prince…), this solver has been chosen since it allows both stability and fast convergence. The thermal network is adapted to the gear unit from existing algorithm previously established from other studies on thermal network method.

After computing all unknown temperatures, the power transferred to the environment through boundary nodes is calculated. Since for boundary conditions $MC_k T'_{un} = 0$, then the following equation is used:

$$Q_{un} = S2T_{un} + S1T_k$$

Equation 18

The algorithm to solve the time dependent equation is reported on Figure 4.

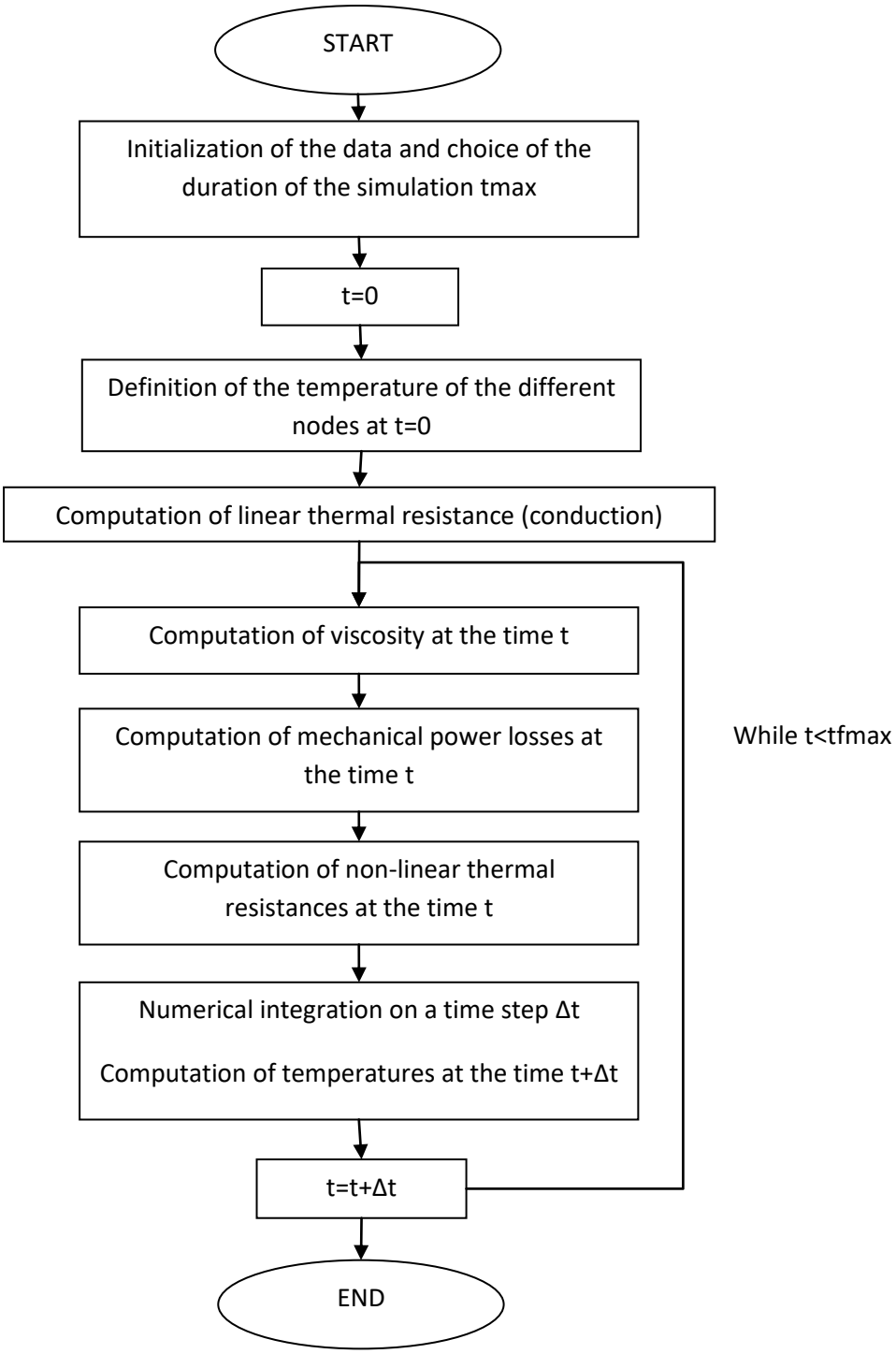

Figure 4: algorithm for time dependent system of equation

In case of steady state, the derivative of temperature as a function of time is null and the system of equation is simplified:

$$\begin{bmatrix} S1 & S2 \\ S3 & S4 \end{bmatrix} \left\{ \begin{vmatrix} T_k \\ 0 \end{vmatrix} + \begin{vmatrix} 0 \\ T_{un} \end{vmatrix} \right\} = \left\{ \begin{vmatrix} Q_{un} \\ 0 \end{vmatrix} + \begin{vmatrix} 0 \\ Q_k \end{vmatrix} \right\}$$

Equation 19

The algorithm to solve the steady state system is reported on Figure 5.

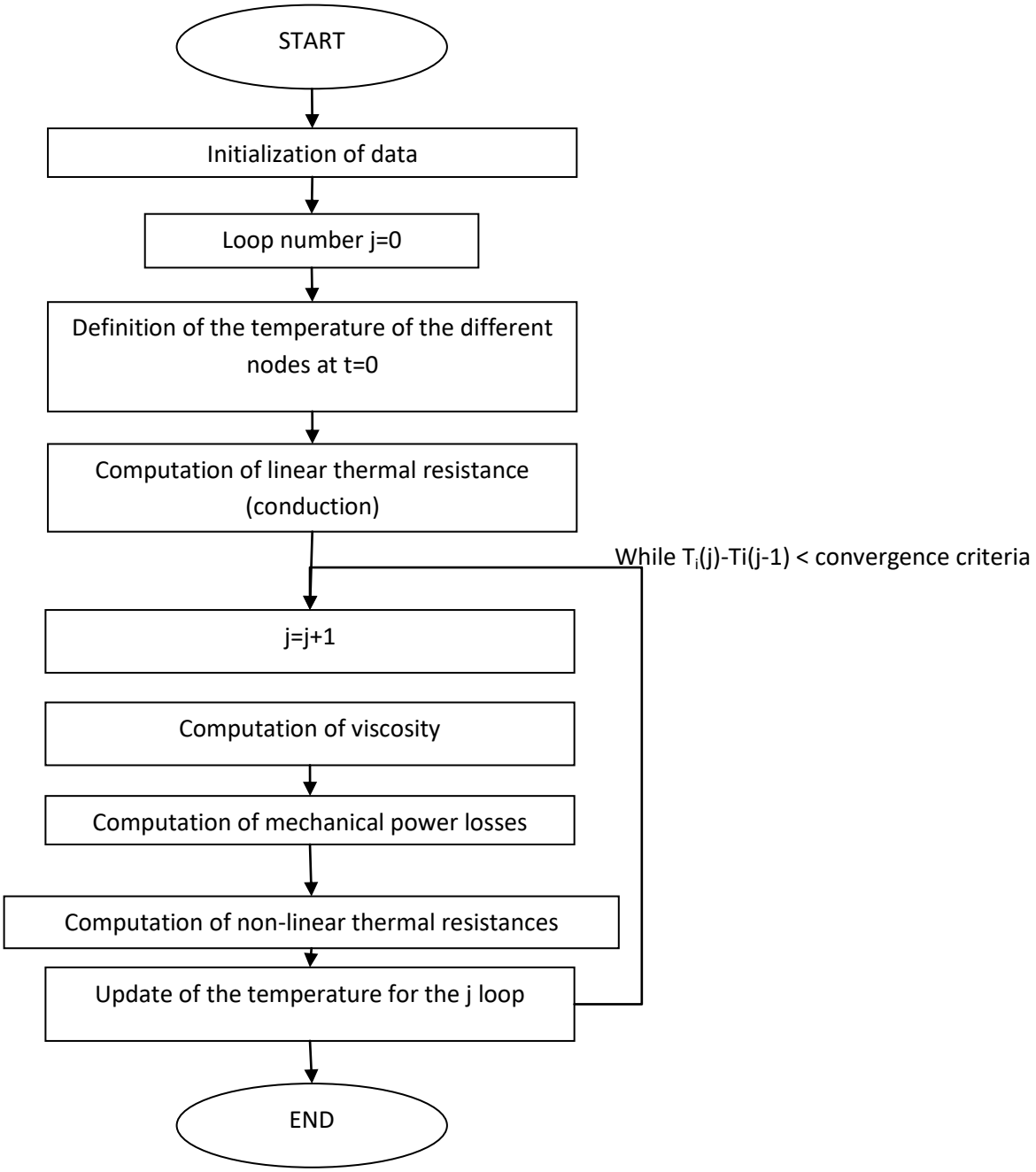

Figure 5: algorithm for the steady state system of equation

Due to the double function of lubricant that consists in lubricating and evacuating the heat generated, its characteristics have a high influence on the behavior of the transmission. However the lubricant characteristics are temperature dependent, which means that modification in temperatures modifies lubricant characteristics which impacts power losses, power losses that generate the temperature elevation. The system is complex and should account for the impact of temperature variation on the lubricant characteristics. It should also account of the impact of evolution of lubricant characteristics on power losses. There is a strong coupling between power losses, temperatures and lubricant characteristics. Several time steps are necessary to account for the change in lubricant properties and tend toward a stabilized temperature and power losses solution: several iterative steps are needed to account for variation induced by a temperature change.

The detailed methodology to account for the influence of temperature on the lubricant characteristics is detailed in appendix B.

2.3. Description of the gear unit

Focusing on reducers with a 90° angle between input and output shafts, the gear unit under consideration belongs to the bigger size of reducers produced by Moteurs Leroy Somer in France: the output torque is above 4000Nm and lower than 23000Nm, for a rotational speed around a hundred RPM. They are used in transmissions for mineral industry, cranes, conveyors…

The studied gear drive is produced and sold with or without extra cooler depending on operating conditions. It has to be fixed through an arm level or through fixations at the bottom of the housing. The more general case of application is retained for defining the thermal network: the reducer is vertical, its fixation is located at the bottom, the oil level is the standard one for this position (around 5 liters) allowing the gears at the bottom to dip in oil. For the tests necessities, two bearings were used to support the input gears, since the input shaft was long and linked to a torque-meter. This configuration is a little different from the general one which is shown on Figure 6: here, the first gear is mounted directly on the shaft of the motor to diminish the volume occupied by the motor and gear unit.

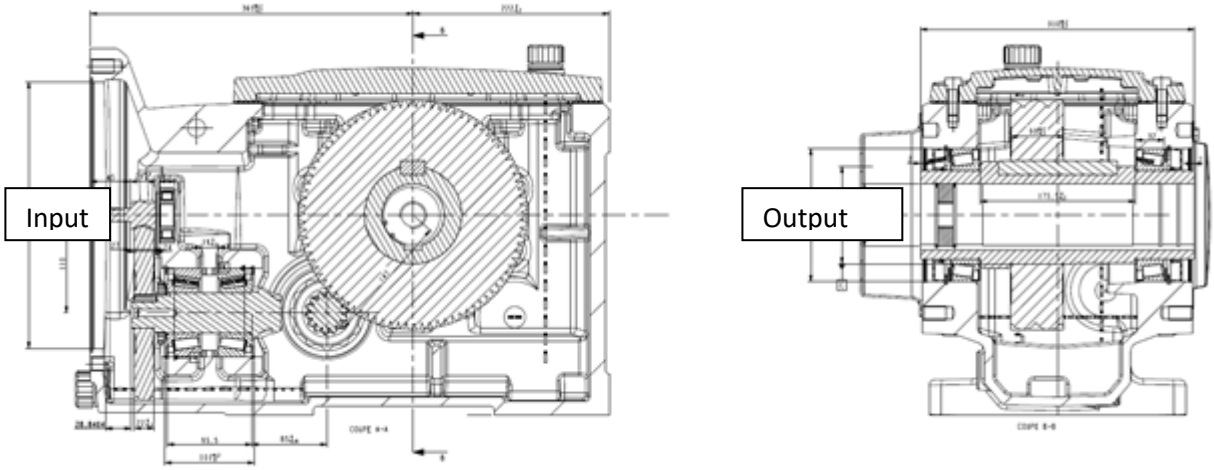

Figure 6: sketches of the gear unit – industry configuration

The gear unit is a three stage gear unit: from the input with a cylindrical gearing meshing, through the spiral bevel gear mesh to the cylindrical output mesh, as shown on Figure 7. The position of the bearings and the submerged elements are represented too.

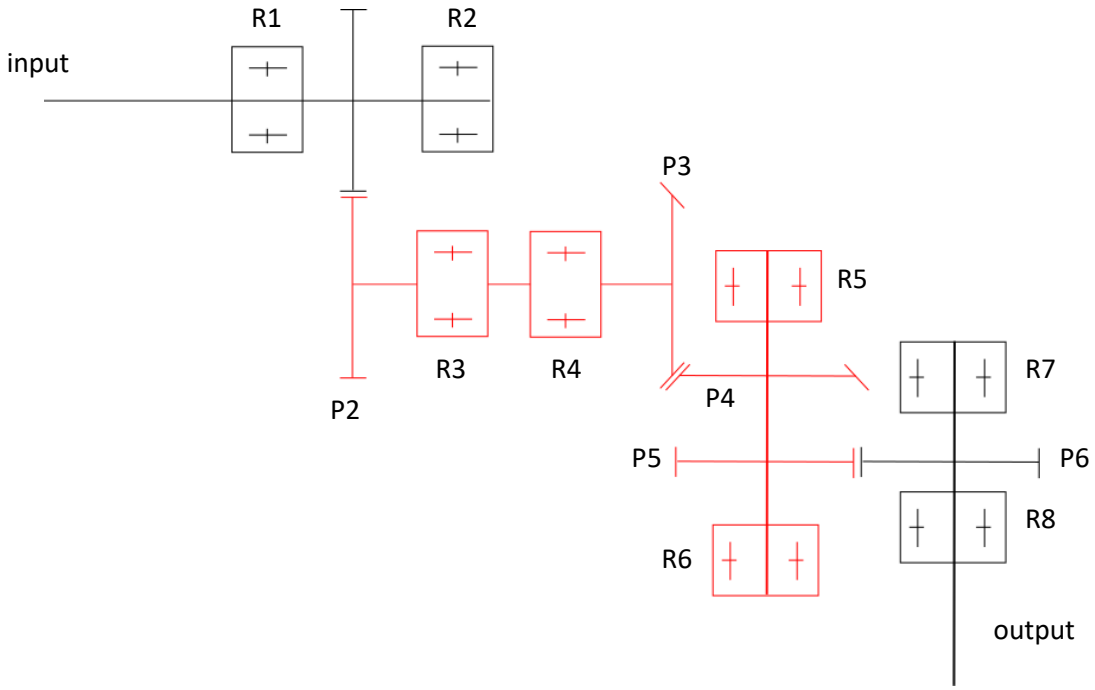

Figure 7: kinematic scheme - position of the bearings and dipping elements (red colored)

The list of elements and their dimensions are reported in Table 2.

Table 2 : elements descriptions

Reference in Figure 7	Element	Type	External diameter (and internal diameter in case of bearings) [mm]	Width [mm]
P1	Input Pinion	Cylindrical gear	96	29
P2	Input wheel	Cylindrical gear	133	22
P3	Intermediate pinion	Spiral bevel gear	57	34
P4	Intermediate wheel	Spiral bevel gear	157	51
P5	Output pinion	Cylindrical gear	49	87
P6	Output wheel	Cylindrical gear	258	60
R1	Input bearing (left)	Radial ball bearing	120 (55)	29
R2	Input bearing (right)	Cylindrical roller bearings	62 (25)	17
R3 and R4	Bearings of the conical pinion (x2)	Tapered roller bearings	100 (45)	36
R5 and R6	Bearings of the output pinion (x2)	Tapered roller bearings	100 (45)	36
R7 and R8	Bearings of the output wheel (x2)	Spherical roller bearings	150 (85)	36

The gear unit operates between 1000 RPM and 3000 RPM and the input torque is below 180 Nm. The reduction ratio is 28. In the following, the input speed and input torque are given to refer to operating conditions.

2.4. Thermal network of the gear unit

2.4.1. Thermal network of the gear unit

The thermal network of the gear unit is represented as an electrical scheme with nodes and resistances. The nodes correspond to isothermal elements. The resistances are placed between nodes which are thermally linked.

From the Figure 7, the thermal network is defined after identifying the main elements and the exchange surfaces: the description of the nodes is listed in Table 3.

In the case where the gear unit only exchanges heat with the ambient air and the bottom contact area is considered insulated, the thermal network is presented in Figure 8. In this figure, the ambient air, the air inside the casing, the housing, the shafts, the bearings, the gears and the oil are identified each by a color to show the main elements of the network. The thermal resistances which are taken into account are given in the Table 4. The objective of this model is to estimate the bulk temperature of the critical rotating parts like pinions, bearings or shafts, with a description of the temperature distribution in the housing. In this purpose, the heat exchange between the fluid and the elements dipping in the oil bath (bearings, gears, shafts) is quantified by using thermal resistances of convection. The air inside the housing also exchanges heat by convection with the output shaft and the output wheel and the associated bearings located in the upper part of the casing. The elements in contact exchange heat through conduction in the material, however an adapted resistance is considered in the case of contact in the meshing area: the “striction” resistance describes the conduction through the reduced area of contact of the meshing teeth to diffuse the heat through the bulk of the pinions.

Table 3: description and number associated to the thermal model nodes

Nodes	Description
1	Ambient air
2	Bottom of the housing
3	Top of the housing
4	Housing cover
5	Housing – area of the motor side bearing
6	Housing – area of the output side bearing
7	Oil bath
8	Air inside the housing
9	Bearing R1
10	Bearing R2
11	Bearing R3
12	Bearing R4

Nodes	Description
13	Bearing R5
14	Bearing R6
15	Bearing R7
16	Bearing R8
17	Input shaft
18	Output shaft
19	Input pinion P1
20	Input wheel P2
21	Intermediate pinion P3
22	Intermediate wheel P4
23	Output pinion P5
24	Output wheel P6
25	Input meshing
26	Second meshing
27	Output meshing

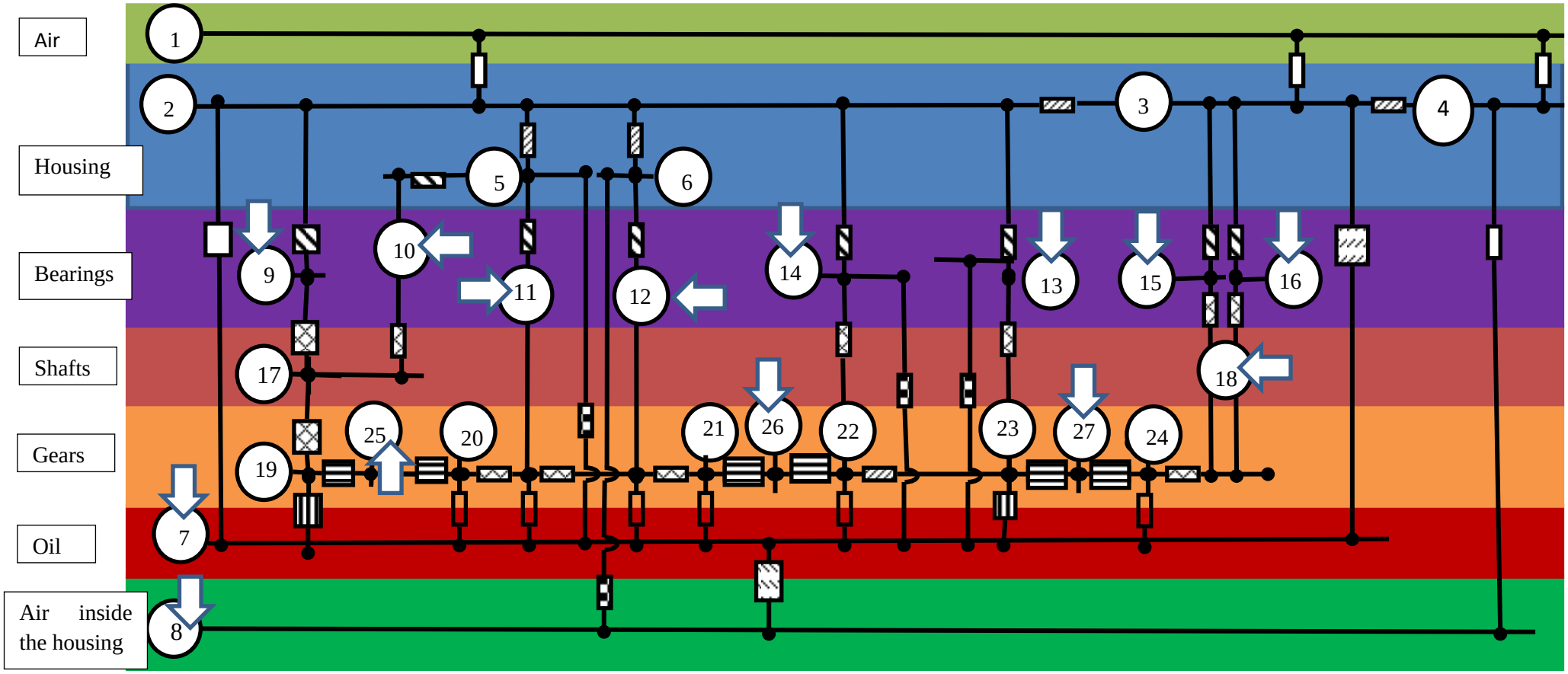

Figure 8: scheme of the thermal network of the gear unit

Table 4: description of symbols used to represent thermal resistances

Symbols	Description of resistances
	Resistance of convection
	Radial conduction
	Axial conduction
	Radial and axial conduction
	Projected oil resistance
	Resistance of the mesh area
	Resistance between air inside the housing and oil
	Streaming of the oil against the wall of the housing

The main assumption when dealing with thermal network is that each node is considered as isothermal, which means that an appropriate refinement has to be chosen to represent a significant temperature difference. In this study, a compromise between the number of nodes and the refinement of the gear unit is done, since the model should be used at a design stage. The objective is to elaborate a model that should not require too much information while providing values that should be accurate at +/-10°C. To this end the thermal network presented is chosen as a good comprise. To insert the computed losses due to the different sources of dissipation, the following method is used.

The bearing losses are applied to the node which refers to the associated bearing.

The power losses due to teeth friction are computed for each gear pair and injected to the corresponding meshing node. The heat repartition between the meshing gears is automatically determined through the thermal resistances of striction.

The churning losses generated by immersed gears are summed up and injected to the node which represents the oil sump. The same methodology is used when considering windage losses. This source of dissipation is injected to the node associated with the air inside the housing.

The losses due to a seal are injected to the node associated with the shaft on which the seal is rubbing.

White arrows are used in Figure 8 to symbolize power losses in the thermal network.

2.4.2. Thermal resistances

Thermal resistance defines the heat transfer between two nodes of the thermal network. Three kinds of heat transfer are differentiated concerning the computing of thermal resistance: conduction, convection and radiation.

Conduction is the heat transfer through a unique media from the high-temperature region to the low-temperature region. The conduction phenomenon is described by the Fourier's law which gives the heat-transfer rate per unit area:

$$q = -k\frac{dT}{dx}$$

Equation 20

To illustrate the way to compute the thermal resistance, equation (I.9) is used in the case of a plane wall heated on one side. If one considers a wall with a width e, an area S and a thermal conductivity k, the link between the heat flow and the temperature difference is given by:

$$Q = \frac{kS}{e}\Delta T$$

Equation 21

The thermal resistance of conduction is then identified as:

$$R_{th} = \frac{e}{kS}$$

Equation 22

The convection resistance is used to quantify heat-transfer between a fluid and a solid. The Newton's law describes convection and requires a convection coefficient (h_{conv}):

$$Q = h_{conv} \times S \times \Delta T$$

Equation 23

The thermal resistance of convection is:

$$R_{th} = \frac{1}{h_{conv} \times S}$$

Equation 24

The convection coefficient is defined through the Nusselt number, which is the ratio of convective to conductive heat transfer across the boundary layer within a fluid, where L is a characteristic dimension of the solid exchanging through convection with the fluid:

$$Nu = \frac{h_{conv} L}{k}$$

Equation 25

Nusselt number is estimated differently for natural or forced convection. In case of natural convection, Nusselt number is expressed as a function of Grashof and Prandtl numbers. In case of forced convection, Nusselt number depends on Reynolds and Prandtl numbers.

The radiation resistance is defined by quantifying the heat transfer by thermal radiation through space between bodies. Considering a gray body, which means that its emissivity is independent of wave length, Stefan-Boltzmann law defines the emissive power:

$$Q = S\sigma\varepsilon T^4$$

Equation 26

With:

- Q: power radiated from a body [W]
- ε: emissivity dependent on material, value in range 0 to 1,
- σ: Stefan-Boltzmann constant = $5.67.10^{-8}$ [$W/m^2.K^4$]
- T: temperature [K]

Considering two solids (1 and 2), separated by a non-absorbent medium, the power transferred by radiation between these bodies is given by:

$$Q = \frac{\sigma(T_1^4 - T_2^4)}{\frac{1-\varepsilon_1}{\varepsilon_1 S_1} + \frac{1}{S_1 F_{12}} + \frac{1-\varepsilon_2}{\varepsilon_2 S_2}}$$

Equation 27

$$Q = \frac{\sigma(T_1^2 + T_2^2)(T_1 + T_2)}{\frac{1-\varepsilon_1}{\varepsilon_1 S_1} + \frac{1}{S_1 F_{12}} + \frac{1-\varepsilon_2}{\varepsilon_2 S_2}} \Delta T$$

Equation 28

With:

- F_{12}: radiation shape factor between 1 and 2
- S_1: radiating surface of solid 1 [m²]
- S_2: radiating surface of solid 2 [m²]

The radiation resistance is then deduced:

$$R_{th} = \frac{\frac{1-\varepsilon_1}{\varepsilon_1 S_1} + \frac{1}{S_1 F_{12}} + \frac{1-\varepsilon_2}{\varepsilon_2 S_2}}{\sigma(T_1^2 + T_2^2)(T_1 + T_2)}$$

Equation 29

The detailed description of each resistance used in the thermal network is given in appendix A.

Once the thermal resistances are defined, the power losses have to be quantified to obtain the temperature distribution within the gear unit. To do that, analytical formulas are used to estimate each source of dissipation. Relationships proposed in literature are listed in the following sections of the manuscript.

3. Power losses of the meshing gears

3.1. Spur and helical gears

Meshing power losses have to be considered with care, since they are one of the most important parts of the total power losses in loaded transmissions.

The applied torque through the meshing teeth leads to power losses because of the loaded contact of moving elements. The pressure and relative movement in the contact generate power losses all along the path of contact. Several models are available from the literature to estimate these power losses. A formulation proposed by Loewenthal et al. [7] divides this source of dissipation into rolling and sliding losses and sums up the two components to obtain the mesh power losses.

Further studies use the hypothesis that the friction coefficient is constant along the path of contact and suggest simplified formulas. Buckingham [18], Meritt [86], Niemann and Winter [91], Henriot [52] or Velex and Ville [112] propose similar relationships.

The power loss is expressed as follows:

$$Q = PfH_v$$

Equation 30

With:

- P is the power transmitted [W]
- f is the mean friction coefficient along the path of contact
- H_v is a geometric factor

Each of the above-mentioned studies provides a specific equation to calculate H_v. Some examples are presented in the following part. For example, Buckingham expresses H_v as follows:

$$H_v = (1 + \mathrm{u})\frac{\pi}{Z_1}\frac{1}{\cos(\beta_b)}\varepsilon_\alpha(2\kappa_0^2 - 2\kappa_0 + 1)$$

Equation 31

With:

- u is the reduction ratio and equals Z1/Z2 with Z1<Z2
- Z1 is the number of teeth of pinion
- Z2 is the number of teeth of the wheel
- β_b is the base helix angle [rad]
- ε_α is the transverse contact ratio
- κ_0 is the position of the rolling without sliding point along the path of contact

Niemann suggests a different expression of H_v:

$$H_v = (1 + u)\frac{\pi}{Z_1}\frac{1}{\cos(\beta_b)}\varepsilon_\alpha\left(\frac{1}{\varepsilon_\alpha} - 1 + (2\kappa_0^2 - 2\kappa_0 + 1)\varepsilon_\alpha\right)$$

Equation 32

Henriot proposes another formula for H_v:

$$H_v = \left(\frac{1}{R_{p1}} + \frac{1}{R_{p2}}\right)\frac{g_f^2 + g_a^2}{2(g_f + g_a)\cos(\alpha_t)}$$

Equation 33

With:

- R_{p1} and R_{p2} are pitch radii of the pinion and the wheel [m]
- g_f and g_a are approach and recess lengths of the path of contact [m]
- α_t is transverse contact angle [rad]

None of these relationships accounts for the tooth profile modification. Some material at tip or root of the tooth can be removed to decrease the contact pressure in these areas where the sliding speed is high: this modification in the tooth shape improves operating conditions in the mesh, as studied by Ghribi [46] or Diab et al. [36].

A study of Velex and Ville [112] provides a formula of H_v that can consider the improvement in the dynamic behavior of a gear pair in case of tooth profile modifications, as illustrated on Figure 9 which represent the tooth profile modification with respect to the ideal tooth profile.

$$H_v = (1+u)\frac{\pi}{Z_1}\frac{1}{\cos(\beta_b)}\varepsilon_\alpha \Lambda$$

Equation 34

And:

$$\Lambda = \frac{1 - 2\kappa_0 + 2\kappa_0^2 - \Upsilon\Gamma\left(1 - \frac{2\Gamma}{3}\right)}{1 - \Upsilon\Gamma - f\left(\frac{\tan(\alpha_p)(2\kappa_0 - 1) - \varepsilon_\alpha\frac{\pi}{Z_1}(2\kappa_0^2 - 2\kappa_0 + 1 - \Upsilon\Gamma\left(1 - \frac{2\Gamma}{3}\right)}{\cos(\beta_b)}\right)}$$

Equation 35

Where:

- Y is the dimensionless tip relief amplitude [ ]
- Γ is the dimensionless extent of profile modification [ ]
- p_{bt} is the transverse base pitch [m]
- Δ_m is the average tooth deflection for unmodified profile [m]

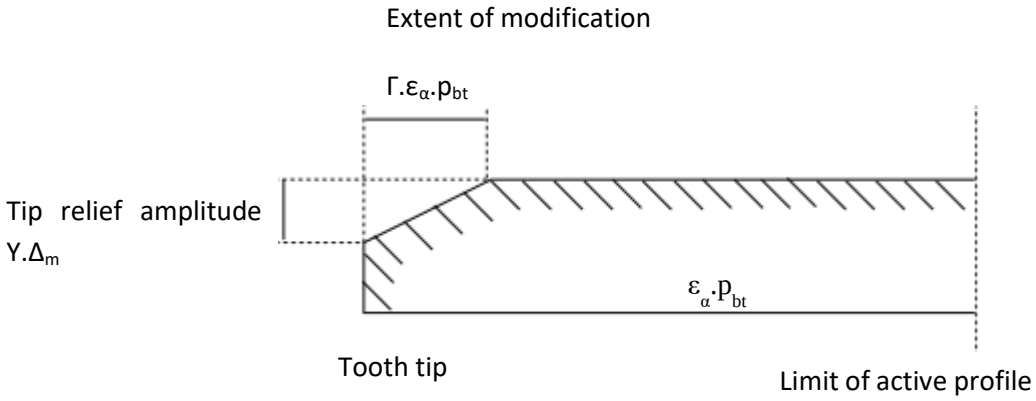

Figure 9: tooth modification diagram projected on the base plane (MAAG diagram)

The above-mentioned relationships give similar results for tooth without profile modification [112]. As the formula proposed by Velex and Ville [112] is the only one which can take into account this parameter, it will be used in the thermal network model.

3.2. Spiral bevel gears

Efficiency of bevel gears has been much less studied than spur and helical gears. Two methodologies are available: geometrical approximation of Tredgold or providing a local contact model.

Tredgold approximation is based on a projection of the conical geometry of the gear in a plane. This projection determines the equivalent virtual cylindrical gears dimensions. From this geometrical approximation (see Figure 10), Buckingham [18] provides formulas to compute efficiency of bevel gears.

Buckingham proposes the following efficiency formula for spiral bevel gears when considering the friction losses, further details in appendix C:

$$\eta = 1 - \left(\frac{\cos(\alpha)}{\cos(\alpha n)\cos(\beta)}\right)\left[\frac{1+\left(\frac{1}{u}\right)}{(\phi a1 + \phi r1)\cos(\beta)}\right]\left(\frac{fa}{2}\phi a1^2 + \frac{fr}{2}\phi r1^2\right)$$

Equation 36

With:

- u is the reduction ratio [ ]
- ϕa is the arc of approach [rad]

- ϕr is the arc of recess [rad]
- Rb is the equivalent base radius [m]
- α is the pressure angle [rad]
- β is the helix angle at the pitch radius [rad]
- fa and fr are respectively the friction coefficient in the approach and recess path of contact [ ]
- α_n is the normal contact angle [rad]

This formula needs to determine the virtual geometry of associated cylindrical gears obtained on the projection plane. The parameters determination is detailed in appendix C. On Figure 10, the spiral bevel pinion (in green) and gear (in blue) have respectively their radii Rp and Rg projected to get equivalent radii Rvp and Rvg of virtual cylindrical gears.

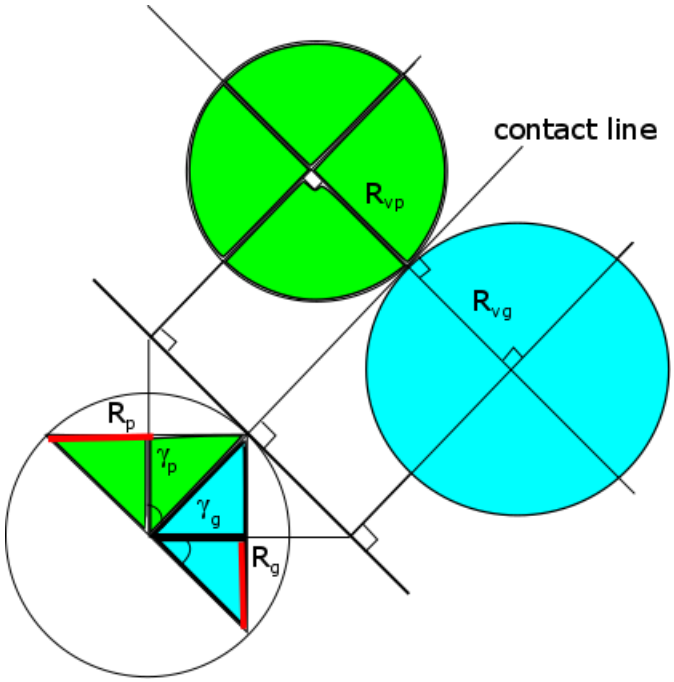

Figure 10: Tredgold approximation scheme

The second method consists in modeling the real contact geometry of the gears. A contact analysis model, including an elasto-hydrodynamic (EHL) based friction coefficient formula and a mechanical efficiency model, is presented by Xu and Kahraman [117]. Spiral bevel gears were also studied by Alves et al. [6] providing a quasi-static and a lumped parameter dynamic model. This method requires a lot of information concerning the rack design and the cutting conditions.

The study should provide a model which should be used in a design stage. Moreover no information is available on the actual real geometry, and then an analytical approach should be kept.

Buckingham method seems well adapted since the computational time required is low and the number of parameters required is much limited than of the one associated with a local refined model.

3.3. Friction coefficient determination

As pointed out by Pleguezuelos *et al.* [99], or Marques *et al.* [81], the friction coefficient has to be determined accurately since it is really influent on the computed frictional losses.

The friction coefficient is defined as the ratio of the tangential to the normal effort. In case of a lubricated contact, as for mechanical transmissions, three lubrication regimes are isolated as shown on Figure 11:

- The boundary regime leads to much contact between the two surfaces because the lubricant film thickness is not enough to separate the bodies. The friction coefficient is almost constant. Lubricant additives and surface roughness have much effect on the friction coefficient level.
- The mixed lubrication regime consists in few contacts between the two surfaces: it is a transition between the boundary and the full film regime. It is a very sensitive regime, where slight modifications in the operating conditions can greatly influence the friction coefficient.
- In the full film regime, there is no contact between the surfaces which are separated by a lubricant film: the friction coefficient is linked only to the lubricant properties.

In Figure 11, the friction coefficient is shown to evolve with the ratio of the gap height to the root mean square roughness of the surface h/Rms.

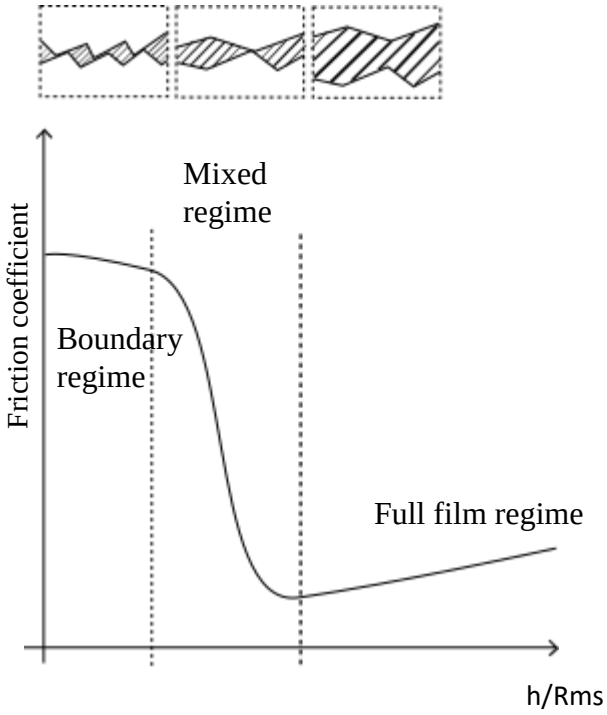

Figure 11: Stribeck curve: friction coefficient evolution as a function of gap height to root mean square roughness ratio

Since some lubricant properties are difficult to obtain (for example the piezo-viscosity) and complex to relate with the friction coefficient, the friction phenomenon is complex to model. From this observation, analytical friction coefficients formulas are often based on experiments. For example, the material, lubricant characteristics or surface roughness lead to various operating conditions and various lubrication regimes which are hard to define precisely over the whole contact area. Several formulas are available concerning the mean friction coefficient as the ones proposed by Kuzmin [69], Misharin [88], O'Donoghue and Cameron [93] or Kelley and Lemanski [65]. As an example, Benedict and Kelley [13] have established a formula based on numerous tests:

$$f = 0.0127 \times log_{10}\left(\frac{291205.8 \times 10^{-7}}{\frac{\rho \upsilon V_s U^2}{F_{nu}}}\right)$$

Equation 37

Where :

- ρ is the lubricant density [kg/m^3]
- ν is the kinematic viscosity [m²/s]
- Vs is the sliding velocity [m/s]
- U is the rolling velocity [m/s]

- Fnu is the normal unity load [N/m]

This friction coefficient formula is valid for high slide to roll ratio -SRR which is the ratio between the sliding speed and the rolling speed in a contact- (above 40%) [36]. The friction coefficient for a couple of a lubricant and a material is obtained from traction curve with twin-disc machine [35]: a typical traction curve is shown on Figure 12. A traction curve is composed of three parts: a linear part where the friction coefficient increases as the SRR increases, then a non-linear part where the friction coefficient increases slower and finally a thermal part where thermal effects tend to reduce the friction coefficient.

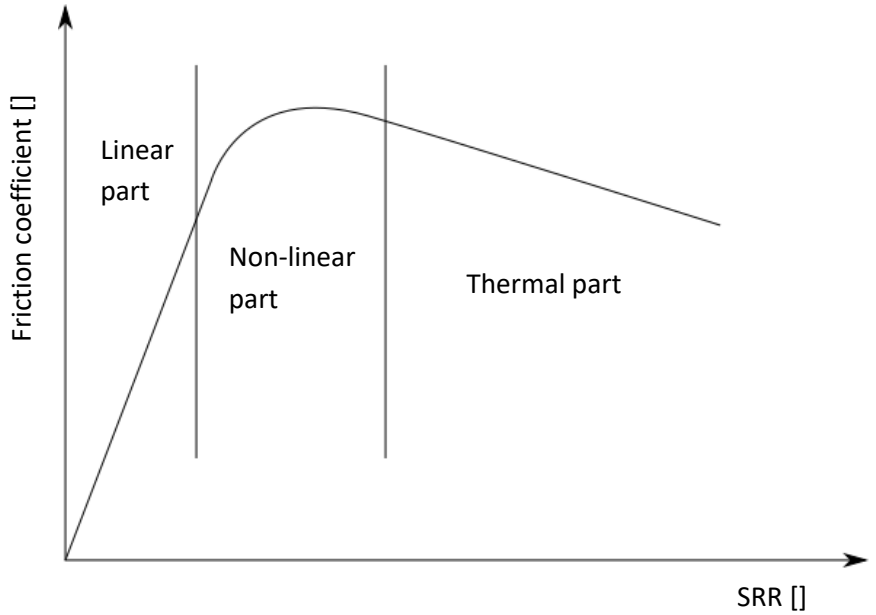

Figure 12: typical traction curve shape obtained from twin-disc machine

Data from an experimental twin-disc traction curve show a different trend compared with Benedict-Kelley or Kelley-Lemanski: experiments show a low value of the friction coefficient at low slide to roll ratio and an increase with the SRR. Instead of such behavior, the logarithmic formulation leads to high values of the friction coefficient at low SRR, and it tends towards zero as the SRR becomes higher (see Figure 13 [35]). Such differences between theoretical and experimental data could lead in the end to over 30% discrepancy between calculated and measured power losses, as shown by Diab et al. [36].

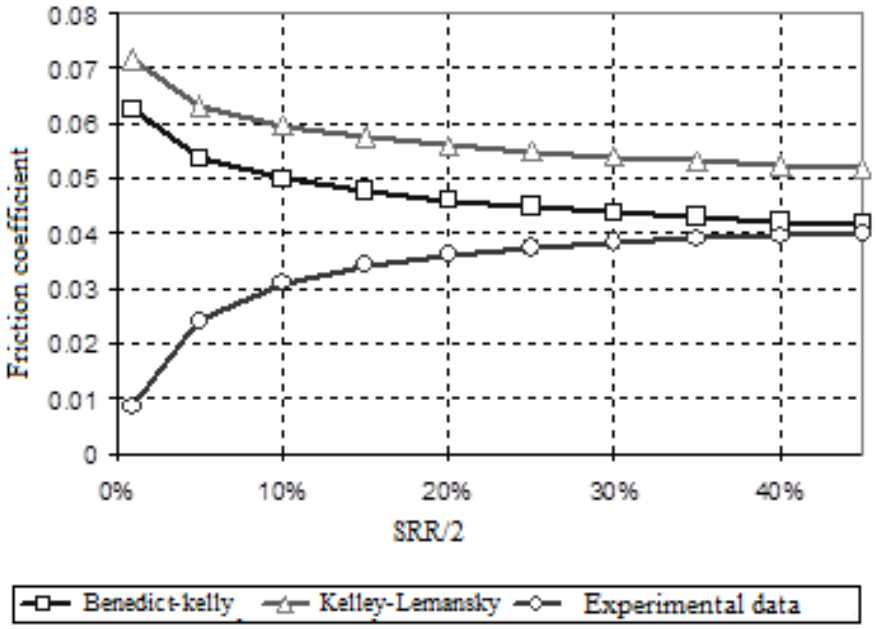

Figure 13: comparison of few friction coefficient formulas from literature [35]

The technical report 14179-2 [2] proposes another formula to provide a law for friction coefficient valid over wider range of operating conditions.

$$f = 0.048 \times \left(\frac{F_n/b_{tooth}}{r_c \times U \times 10^6}\right)^{0.2} (\mu \times 10^3)^{-0.05} Ra_r^{0.25} X_L$$

Equation 38

With:

- X_L is a coefficient associated with the oil type
- r_c is the equivalent curvature radius at the pitch diameter [m]
- b_{tooth} is the tooth width [m]
- μ is the dynamic viscosity of the lubricant [Pa.s]
- Ra_r is the mean roughness of the tooth side of the pinion and the wheel [µm]
- F_n is the normal load [N]
- U is the mean resultant sum velocity in the contact area [m/s]

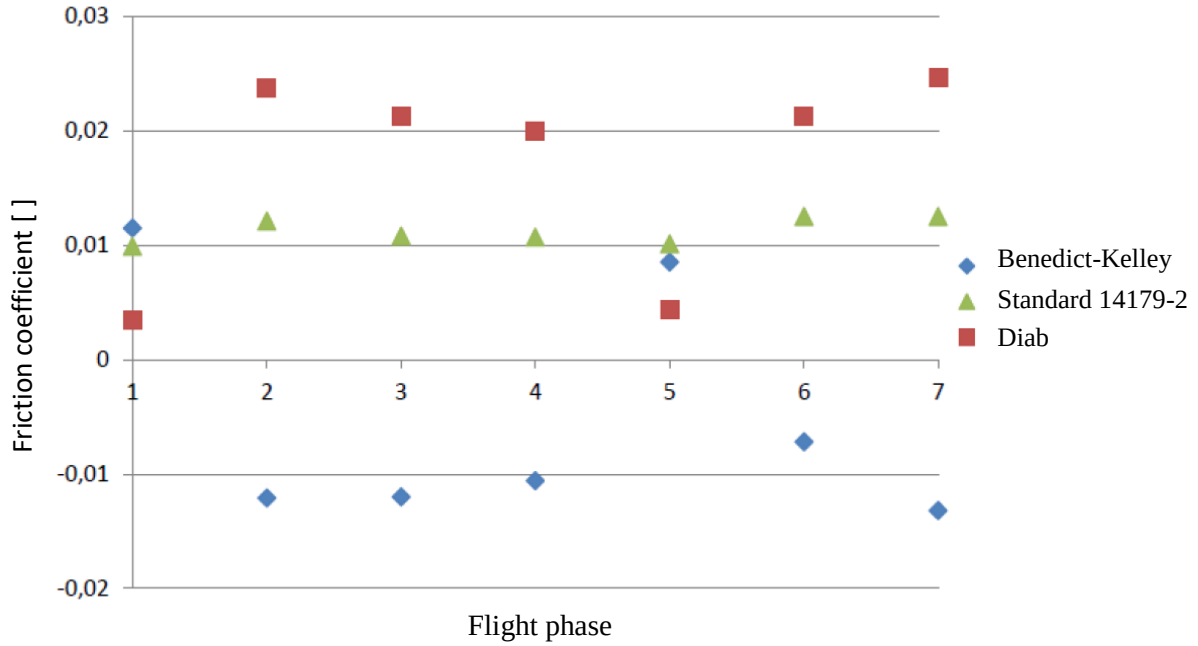

Figure 14: friction coefficient in function of the flight phase for 3 different formulas [59]

Figure 14, based on results from Durand de Gevigney [59], shows the comparison of several methodologies to determine the friction coefficient: for different flight phases, which means different operating conditions (speed, load and temperature), none of the formulas represents the experimental results measured by Diab [35]. From this observation, further interest is focused on work available in the literature to improve the friction coefficient estimation.

Another possibility is to determine the instantaneous friction coefficient, like in Matsumoto [83] or Diab [35] studies. Based on experimental tests resulting in friction curves, parameters are extracted to determine the analytical formula that represents experimental behavior. For example, Diab uses this method in his study, basing his work on Greenwood-Tripp [47] and Mikic [87] theories. This method requires specific tests on a twin-discs machine available at LaMCoS laboratory [113] with the chosen oil and material. However the contact conditions should be reproduced in the tests. In the case of cylindrical gears, great care is taken to reproduce the roughness profile and orientation with respect to the sliding direction. In the case of bevel gear, such tests are not possible since the contact conditions are not well reproduced thanks to contacting discs. Actually, the influence of the roughness and the contact geometry is not reproduced in such tests since the longitudinal and transverse speed and pressure evolution is not easy to reproduce. Some studies use EHL simulations to model small contact areas [117] [68] but still need experimental data to validate results for full model simulation [64].

To conclude, all formulas show weaknesses at some point. Moreover, in a development stage, experimental measurements are not possible since the surface features are not perfectly known.

In the objective to provide a model used in development stage, none of the previous formulas appears as the perfect response to our problem. In the following parts of this study, the friction coefficient will be set at a mean constant value, it is a strong approximation but without further elements, it is a reasonable choice to limit maximum error and define a default value. In general case of contacting cylindrical gears, a value between 0.01 and 0.09 is observed for a lubricated metal to metal contact, so a value of 0.05 is selected in the following as the default friction coefficient value in gears. In chapter 3, further work is done concerning the friction coefficient definition. Tests are performed under load on the studied mechanical transmission to correlate the friction coefficient value thanks to reverse engineering and the impact of a change in the friction coefficient is observed.

4. Bearing frictional losses

Bearings power losses may represent an important part of the total power losses in a gear unit. Bearing losses are linked with several phenomena: friction in the contact area between rotating parts and friction generated by lubricant drag.

Two methods can be used to determine bearing power losses: a local or a global approach. The local approach describes precisely the behavior of the elements in the bearing. However, it requires a great amount of data, like a fine description of the bearing internal geometry. Pouly [100] used this method to describe the thermal behavior of aeronautical bearing.

The second method consists in a global approach. Geometrical parameters used in this approach can be found in bearings manufacturer's catalogs. Because of the limited number of parameters which are necessary, the second method is chosen in this study.

When considering global approach, two models are currently used: Palmgren model or current SKF model. The Palmgren model is the older and is described by Harris [51]. The friction torque of a bearing is expressed as a sum of a load independent torque (M_0) and a load dependent one (M_1):

$$M_{total} = M_0 + M_1$$

Equation 39

Where:

If $vN > 2 \times 10^{-3} \frac{m^2}{s.\min}$

$$M_0 = 10^3 f_0 (v \times N)^{\frac{2}{3}} (d_m)^3$$

Equation 40

If $vN < 2 \times 10^{-3} \frac{m^2}{s.\min}$

$$M_0 = 16 \times f_0 (d_m)^3$$

Equation 41

And

$$M_1 = f_1 \times P_1^{a'} \times d_m^{b'}$$

Equation 42

With:

- f_0 is a parameter depending on the bearing and lubrication types
- v is the kinematic viscosity of the lubricant [m²/s]
- f_1 is a parameter depending on the equivalent and base static loads and the bearing type
- P_1 is a combination of the axial and radial loads [N]
- a' and b' are correction factor depending on the bearing characteristics
- d_m is the mean diameter of the bearing [m]
- N is the rotational speed of the bearing [RPM]

This model is still widely used and it is the model chosen by technical report ISO 14179 part I [1] and II [2], which is focused on the estimation of the power losses in a gear unit. In this model, the independent load torque is much more significant for high speed or high lubricant viscosity. Parameters f_0, f_1, a' and b' are coefficients available in manufacturers catalogs. They are based on experimental tests which do not cover the very high speed domain, but the commonly encountered range of speed.

SKF [106] proposes in 2004 a new relationship to quantify bearing losses. This model is based on a numerical tool developed by SKF, from which analytical formulas are extracted. The model is based on the sum of three torques: the first corresponds to the rolling frictional moment, the second to the sliding frictional moment, and the third to moment of drag losses or churning.

$$M_{total} = \varphi_{ish} \varphi_{rs} M_{rr} + M_{sl} + M_{drag}$$

Equation 43

With:

- M_{total} is the total resisting torque of the bearing [N.m]
- φ_{ish} is the inlet shear heating reduction factor
- φ_{rs} is the kinematic replenishment/starvation reduction factor
- M_{rr} is the rolling frictional torque [N.m]
- M_{sl} is the sliding frictional torque [N.m]
- M_{drag} is the drag torque associated to the lubrication mode [N.m]

The rolling friction torque impact on the total torque losses is corrected thanks to two parameters φ_{ish} and φ_{rs} detailed in appendix F.

The rolling frictional torque is:

$$M_{rr} = G_{rr}(\nu \times 10^6 \times N)^{0.6}$$

Equation 44

The sliding frictional torque is:

$$M_{sl} = G_{sl} f_{sl}$$

Equation 45

G_{rr} and G_{sl} depend on operating conditions (load, rotational speed) and on bearing geometrical parameters; f_{sl} is the sliding friction coefficient (see appendix F).

The drag torque can be determined as follows:

- For the ball bearing:

$$M_{drag} = 10^3\left(0.4 \times V_M \times K_Z \times (d_m \times 10^3)^5 \times N^2 + 1.093 \times 10^{-7} \times N^2 \times (d_m \times 10^3)^3 \times \frac{N \times (d_m \times 10^3)^3 \times f_t}{\nu \times 10^6}^{1.379} \times R_S\right)$$

Equation 46

- For the roller bearings:

$$M_{drag} = 10^3(0.4 \times V_M \times K_{roll} \times C_W \times B \times (d_m \times 10^3)^4 \times N^2 + 1.093 \times 10^{-7} \times N^2 \times (d_m \times 10^3)^3 \times \frac{N \times (d_m \times 10^3)^3 \times f_t^{1.379}}{\nu \times 10^6} \times R_S)$$

Equation 47

C_w, K_Z and K_{roll} are parameters which depend on the bearing geometry. f_t, R_s and V_M are associated with the influence of the oil level. The speed and the immersion of the bearing have a great influence on the drag power losses.

The drag formula was elaborated for a bearing dipping in an oil bath, in case of jet lubrication, SKF suggests using the previous formula with an oil level at half the diameter of the lowest rolling element.

In a study conducted by Changenet [20], some comparisons are presented between theoretical results obtained by using the above-mentioned models and different experimental data: Fernandes et al. for low speed tests [42] [43] [44], Schuller et al. for high speed [102] or CETIM [3] for no load tests. This study underlines that one model or the other can give the best results depending on the bearing considered and the operating conditions. However, Harris gives better results in the case of no load tests, since SKF formula provides no losses when the bearing is rotating without an applied load (see Figure 15). The SKF formula may also diverge as the speed increases, as shown on Figure 16 in the case of thrust roller bearings. It is observed that the SKF model overestimates when the peripheral speed exceeds the million of meter per second, which is much larger than the speeds encountered in this PhD.

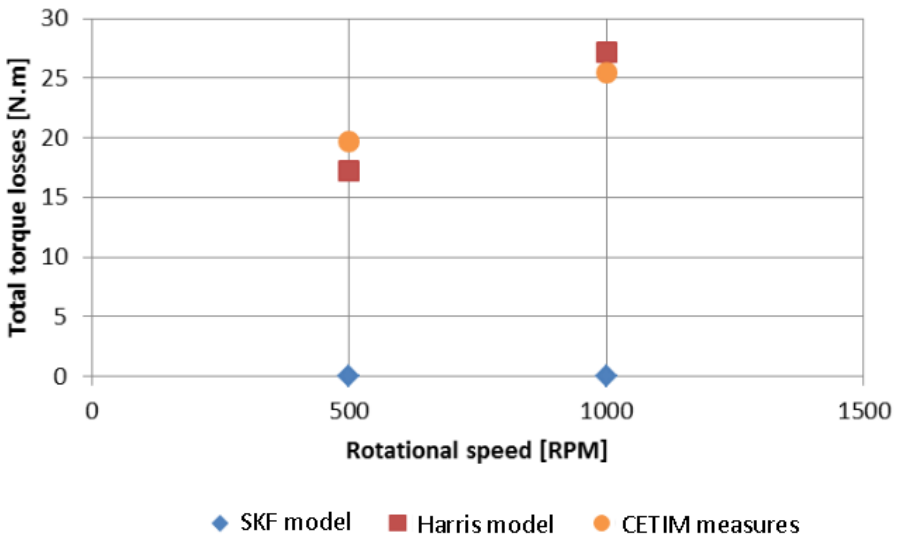

Figure 15: no load test on spherical roller bearing [3]

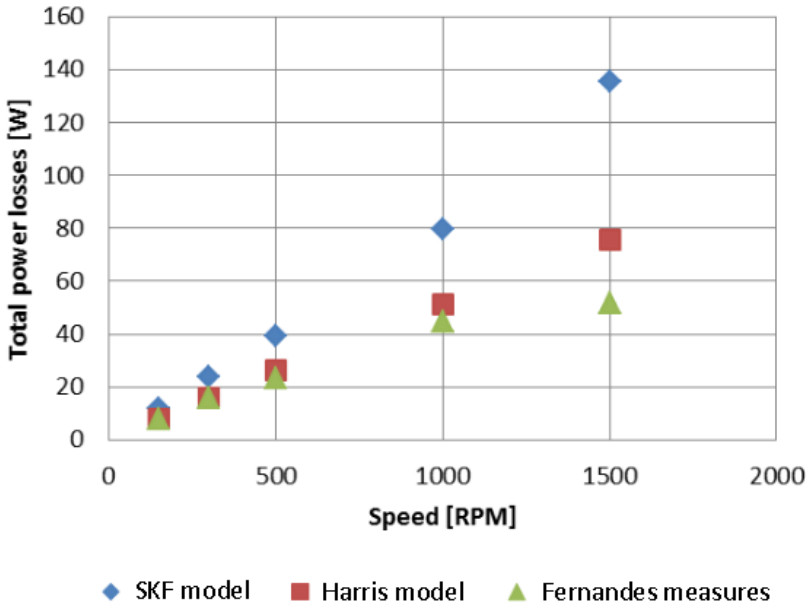

Figure 16: Fernandes measures on thrust roller bearings compared with SKF model and Harris model – mineral lubricant [45]

Moreover the results of Harris formula could be greatly improved when f_0, parameter accounting for the immersion level, is adapted from a reference test measurement.

It is important to note that both SKF and Harris formulas need experiments to fit correctly the value of some parameters, for example the f_0 parameter: it is pointed out in the CETIM technical report [3] concerning improvement of Harris formula and in Fernandes et al. [44] concerning the SKF formula. Since both models need experimental value, load tests will be used as a priority to determine the friction coefficient in meshing gear teeth. Some no load tests have to be used to determine the bearings parameters. As SKF relationship is less efficient that Harris for these operating conditions, the latter is retained in this study. Two elements are determinant in choosing Harris' model: its ability to reproduce the no load losses of a bearing and the possibility to improve the results when the f_0 coefficient is validated by experimental measurements.

5. Seal losses

The focus is here on sealing between moving parts, since sealing between motionless parts does not generate power losses.

When considering sealing between parts in motion, seals exist with and without mechanical contact. In case of no mechanical contact, for example labyrinth seals, power losses are linked to fluid shearing in the seal, which is low enough to be neglected [106]. However, for seal in contact

with rotating part, the power loss generated is the result of friction losses in the contact between the seal and the rotating part. In the studied transmission, radial lip seals are used. In that case, the power loss generated Q is product function of the relative speed between the shaft and the seal with the radial load and the friction coefficient between the seal and the shaft:

$$Q = F_{radial} \times f \times V_{shaft/seal}$$

Equation 48

Where:

- Q is the power loss [W]
- F_{radial} is the load applied [N]
- f is the friction coefficient []
- $V_{shaft/seal}$, is the relative speed between the shaft and the seal

Commonly, the relative speed between the shaft and the seal is equal to:

$$V_{shaft/seal} = \omega \frac{d_{shaft}}{2}$$

Equation 49

Where:

- ω is the rotational speed [rad/s]
- d_{shaft} is the shaft diameter [m]

Even if the analytical expression is simple, the friction coefficient and the normal load to consider are complex to define since these two parameters are linked with the seal shape, materials in contact, operating conditions…

Standards propose several methods to compute power losses due to seals. ISO/TR 14 179-2 [2] presents an expression which is the same than SIMRIT formulation [105]. Seal power losses in SIMRIT formulation only depend on shaft diameter and rotational speed:

$$Q = 7.69 \times (d_{shaft} \times 10^3)^2 \times N$$

Equation 50

This formula is given in the case of a seal with one lip in contact with the shaft. If there are several lips, the power losses are multiplied by the number of lips of the seal.

In this study, the rotational speed of the transmission is low (hundreds of RPM at the most) and the shafts have a diameter below 200mm. In this case, equation 50 leads to power losses smaller than 10W. This value has to be compared with the hundreds of watts which are usually measured for power losses in such transmissions. This comparison underlines that the approximation made to estimate seal power losses does not have a sufficient influence to need more accurate developments.

6. Churning losses

In the case of a dip lubricated mechanical transmission, power losses are generated when the rotating elements are passing through the oil sump. Power losses associated with this lubrication process are caused by different phenomena: the oil trapping in the mesh area, the windage losses and the churning losses of the dipping elements.

The trapping of fluid in the mesh has been studied by Ariura et al. [8], Akin et al. [5]. Mauz [84] also proposes a model of the power losses. Windage in gear has been the subject of experimental measurements based on experimental and theoretical results of various studies [33] [37] [55] [80]. Some models separate churning power losses into the different sources [104], but in most of the case, experimental based formulas include in their expression all kind of power losses without separating the relative influence of the different sources, for example [21] [76] [62].

The studies concerning power losses of rotating elements have begun with studies on discs completely immersed in a fluid [32] [79] [107]. From these studies, several flow regimes are observed as a function of operating conditions. These approaches are of little importance in the case of gear churning since only few mechanical transmissions have fully immersed elements. From this observation, two methods are used to determine the churning losses in the case of cylindrical gears: experimental measurements or analytical models. Experimental measurements are used to define extrapolated churning laws like Boness [16], Lauster and Boos [72], Terekhov et al. [110] or Höhn et al. [54]. An analytical model based on fluid mechanics was provided in Seetharaman and Kahraman study [103]. These different approaches can lead to significant deviations on power losses calculations.

In an effort to investigate the various fluid flow regimes generated by a pinion running partly immersed in an oil sump and the corresponding churning power losses, Changenet et al. [23] [21] have developed new relationships based on dimensional analysis. They give good results for a wide range of cylindrical gears, lubricants and rotational speed. The churning torque is defined as:

$$T_{churning} = \frac{\rho \omega^2 S_m R_p^3 C_m}{2}$$

Equation 51

With:

- ρ is the lubricant density [kg/m^3]
- ω is the rotational speed of the pinion [rad/s]
- S_m is the immersed area of the pinion [m²]
- R_p is the pitch radius of the pinion [m]
- C_m is a dimensionless drag torque

The immersed area of the pinion is decomposed into the lateral surface area and the teeth surface area. The details of the computation of the immersed areas are explained in appendix D. Further details are given in appendix G concerning the determination of C_m for different operating conditions.

As far as the churning losses of spiral bevel gears are concerned, the above-mentioned formulas cannot be used since this source of dissipation is quite different from churning losses of cylindrical gears.

Technical reports suggest that churning losses may be quantified by considering the dimensions on the large end of bevel gears. Two different expressions exist: one is given in ISO/TR 14179-1 [1] and the other in ISO/TR 14179-2 [2].

ISO/TR 14179-1 divides churning losses into a source of dissipation associated with the faces of the gear (P_{sides}) and into another source associated with the tooth surfaces (P_{tooth}):

$$P_{sides} = \frac{1.474 \times f_g \times \nu \times N^3 \times D^{5.7}}{A_g \times 10^{26}}$$

Equation 52

$$P_{tooth} = \frac{7.37.f_g.\nu.N^3.D^{4.7}.b.\left(\frac{R_f}{\sqrt{\tan(\beta)}}\right)}{A_g.10^{26}}$$

Equation 53

Where:

- P_{sides} and P_{tooth} are power losses [kW]
- f_g is the gear dip factor ($0 \leq f_g \leq 1$)
- R_f is the roughness factor
- D is the outside diameter of the element [mm]
- A_g is the arrangement constant
- b is the total face width [mm]
- β is the generated helix angle [°] (if $\beta < 10°$ then consider $\beta = 10°$)

ISO/TR 14179-2 gives a different expression for the churning losses:

$$T_H = C_{sp}.C_1.e^{C_2\left(\frac{V_t}{10}\right)}$$

Equation 54

Where:

- V_t is the peripheral speed [m/s]
- T_H is the churning torque [Nm]
- C_{sp} is the splash oil factor
- $C1$ and $C2$ are geometrical and operating conditions factors

Concerning hypoid gears, Kolekar et al. [67] proposes another formula to estimate churning losses. This formula is derived from the work of Changenet and Velex on cylindrical gears [23] and based on experiments performed on a hypoid axle. Further work was done by Jeon [62] and a dedicated test rig was designed to study churning of hypoid gears. This study includes a dimensional analysis on these measurements to propose a formula for hypoid gears churning:

$$P = \frac{1}{2}\rho_{lub}.\omega^3.R_p^2.b.S_m.C_m$$

Equation 55

-

Where:

- ρ_{lub} is the lubricant density [kg/m^3]
- ω is the rotational speed [rad/s]
- R_p is the pitch radius [m]
- b is the gear width [m]
- S_m is the submerged surface of the gear [m²]
- C_m is the dimensionless parameter accounting for specific gear geometry

Appendix G gives further details on the previous formulas concerning churning losses of spiral bevel gears.

In order to investigate the influence of the method used to quantify churning losses of spiral bevel gears, they were compared for a no loaded operating condition of the studied gear unit: a input speed of 3000 RPM and a typical oil level. The studied gear unit has a reduction ratio of 28. To this purpose, the three above-mentioned formulas were used by turns in the thermal network model integrated in the theoretical model programmed in the context of the PhD. The results are given in Figure 17. The distribution of the different sources of power losses is presented on Figure 18 for ISO/TR 14179-1, ISO/TR 14179-2 and Jeon PhD formula. To perform these calculations, the input torque is imposed at 3Nm (below 2% of the nominal torque) to avoid a trivial solution.

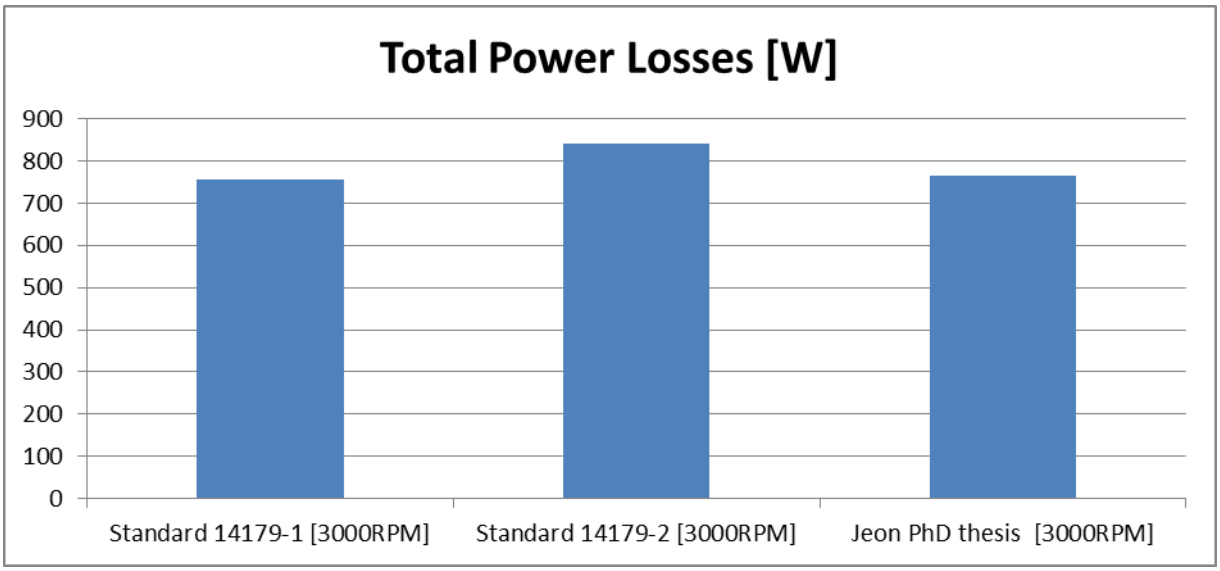

Figure 17: total power losses for various churning formula from 14179-1, 14179-2 and Jeon PhD thesis

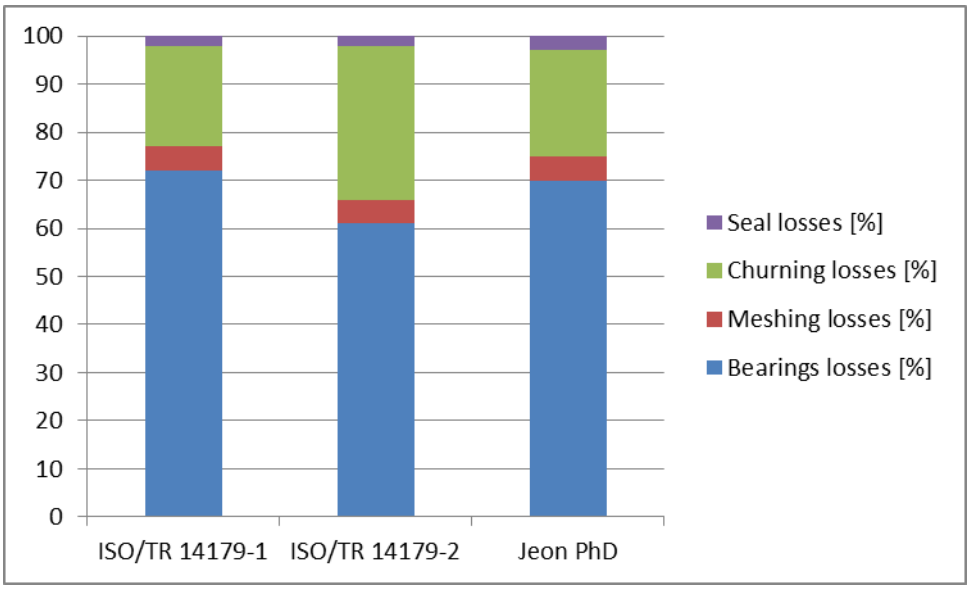

Figure 18: power losses distribution at 3000 RPM accounting for various formulas concerning churning behavior

The repartitions of power losses from ISO/TR 14179-1 and Jeon PhD thesis appear to be similar. However ISO/TR 14179-2 gives different results. The variation in the churning power loss changes power loss level. Then it influences the temperature level and changes power loss repartition since power loss and temperatures are strongly coupled. The whole behavior of the transmission is changed since the initial change in churning loss level leads to a different power loss and temperature distribution because of the strong coupling between power loosses and temperatures. Each law is considered separately as the churning loss formula in the programmed model leads to a difference up to 10°C for the oil sump temperature when comparing the temperature variation for all nodes. This kind of difference is not negligible. Further work is required concerning churning losses of spiral bevel gears.

It is important to keep in mind that the bearing losses coefficient f_0 (Equation 40 and 41) has to be experimentally correlated thanks to a no load test, as explained in chapter I-4. This approach is suitable if other sources of uncertainties are eliminated. With such level of uncertainties concerning churning losses, it is not possible to define the behavior of the bearings in a no load test. This conclusion underlines the necessity to deal in depth with churning losses of spiral bevel gears, which is the topic of the next chapter.

7. Conclusion

In this chapter, the method used to simulate the thermal behavior of a gear unit has been chosen: the thermal network method. This approach is well adapted to determine hot spots in an enclosed gear drive and can give results in transient or steady state contrary to the isothermal method. The low computational time required and the limited number of input data demonstrates that this methodology is well adapted at a design stage, contrary to the finite element method.

In a thermal model, the heat transfer between parts and the power losses generated by the components have to be quantified. The heat transfer determination has been presented. The different sources of dissipation come from the meshing of gear teeth, the bearings, churning of rotating parts and seals: the literature available on the topic has been presented.

From this state of art, it appears that very little experimental data concerning churning losses generated by bevel gears are available in literature. The published literature contains few calculation methods to quantify this source of dissipation but they may give widely different results and have a significant influence on the global thermal behavior. The thermal behavior is greatly influenced by the strong coupling between the power losses and the temperatures. It means that a change in the power loss level results in a change in temperatures distribution, which modifies the power losses repartition. In order to resolve the discrepancy between the different formulas available, one of the aims of the next chapter is to provide a number of simple experiments to determine the churning loss of a single spiral bevel gear.

Chapter 2
Churning behavior of spiral bevel gears

1. Introduction

The objective of this chapter is to reduce uncertainties concerning churning losses estimation. Actually discrepancies are observed concerning churning losses results for bevel gears considering the model available in technical report 14179-1 [1], technical report 14179-2 [2] and Jeon formula [62]. As presented in chapter I, these discrepancies are high enough to modify the power losses repartition in the gear unit and its thermal behavior.

To determine the validity of the above-mentioned methods to compute churning losses on bevel gears, some tests have been conducted on a specific test rig located at ECAM laboratory. The results of this study are presented in the following sections.

2. Presentation of the churning test rig

A precise description of the test rig shown in Figure 19 and Figure 20 is available in [21]; only the main features are exposed here. The author performed the experimental tests on spiral bevel gears in the context of this PhD on the test rig available at ECAM Lyon without requiring modification of the test rig (List of tests in appendix E).

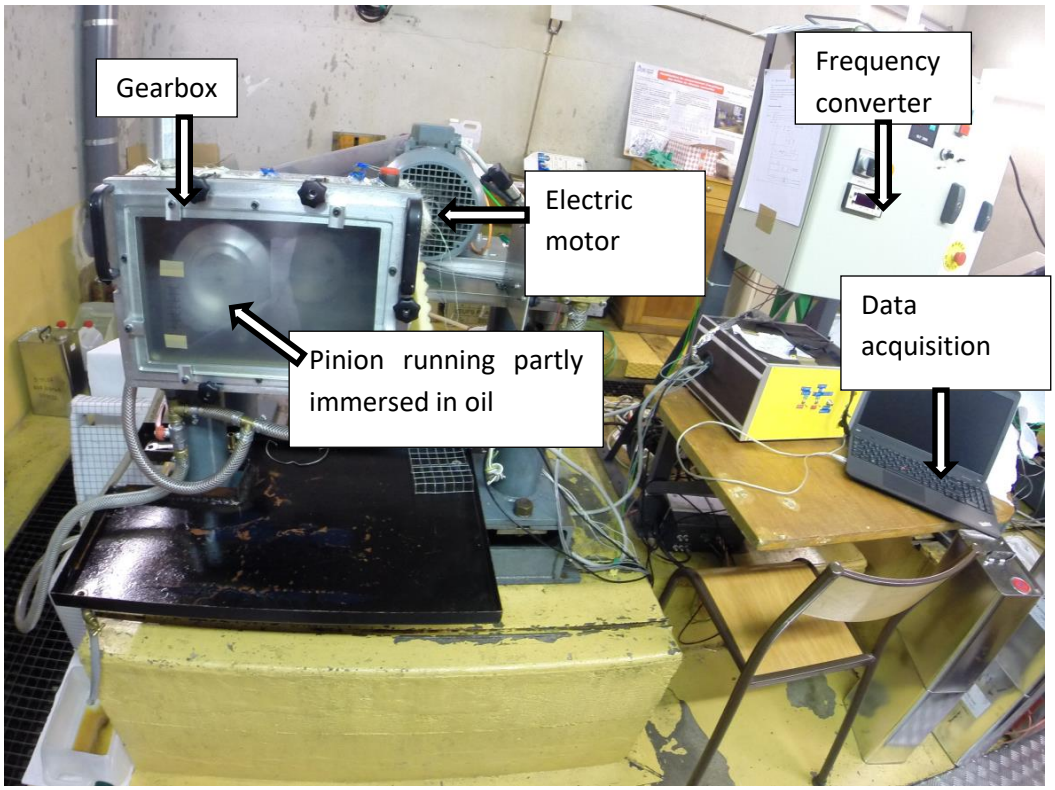

Figure 19: churning test rig

The test rig allows measuring the lubricant temperature and the churning torque of an isolated gear or of a couple of gears as detailed in Figure 20. The internal dimensions of the housing are 380 x 260 x 100 mm^3, large enough to minimize the enclosure effects with an enclosure volume significantly larger than the submerged elements volume. The gear is driven in rotation by an electric motor. The torque is directly measured by a strain-gauged, temperature compensated, contactless sensor (FGP-CD1140) with an accuracy of ±0.002 Nm, a scale range of 2Nm, a sensitivity shift of 0.009 %/°C, and a zero shift of 0.0004 Nm/ °C in the 5–45°C temperature range. The pinion is supported by two ball bearings. In order to eliminate bearing loss contributions, the bearing drag torque has been experimentally determined as a function of speed by removing the gear from the test rig. For example, it has been found that a pair of bearings generates a drag torque of 0.045 Nm at 7000 RPM. Such a value is significant compared to the accuracy of the torque sensor. The churning behavior can be measured for a gear pair or a unique pinion, mounted on the torque sensor shaft while the other gear location remains empty. Here the churning behavior of an isolated gear is studied, so only one gear is mounted on the test rig.

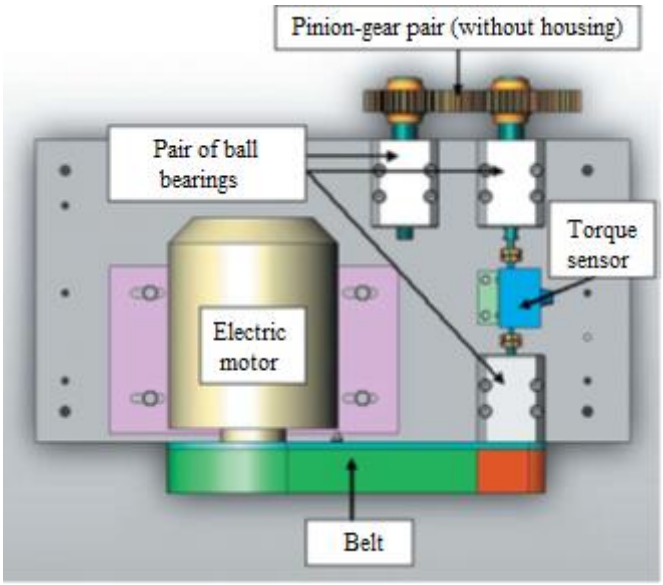

Figure 20: description scheme of the test rig

A pulse counter in the torque sensor ensures the speed measurement. The oil sump is a housing with a parallelepiped rectangle shape with a Plexiglas face which allows to observe the flow around the gears. The oil level can be modified. The oil bath temperature is controlled and measured by thermocouples of type K. Several heating covers are installed on the external faces of the housing: they allow heating up the oil bath. The maximum deviation between two repetitions of the same test is equal to 5% of the measured churning torque value.

Four bevel gear geometries are available for the tests. The geometry is selected from existing gear unit from different sizes and different reductions available at Moteurs Leroy Somer. Geometrical dimensions are given in Table 5. Several parameters are varied between geometries to allow studying their respective influence.

Table 5: gears data

	gear 1	gear 2	gear 3	gear 4	cone 1	cone 2
External diameter [mm]	157	130	188	154	157	160
Number of teeth [ ]	41	37	41	37	0	0
Face angle [°]	72,4	58,1	72,4	58,1	72,4	58,1
Module [mm]	2,6	2,4	3,1	2,9	/	/
Face width [mm]	27	24,5	32	27,5	27	24,5
Width [mm]	22	27	30	30	22	27
Pressure angle [°]	20	20	20	20	/	/
Mean spiral angle [°]	35	35	35	35	/	/
Hand of spiral	left	left	left	left	/	/

Two different macro-geometries were tested (Figure 21). One shape consists in a high face angle and a narrow width, the other has a smaller face angle and a larger width. In order to study the influence of tooth geometry on churning losses, it can be noted that two smooth cones have also been manufactured (Table 5).

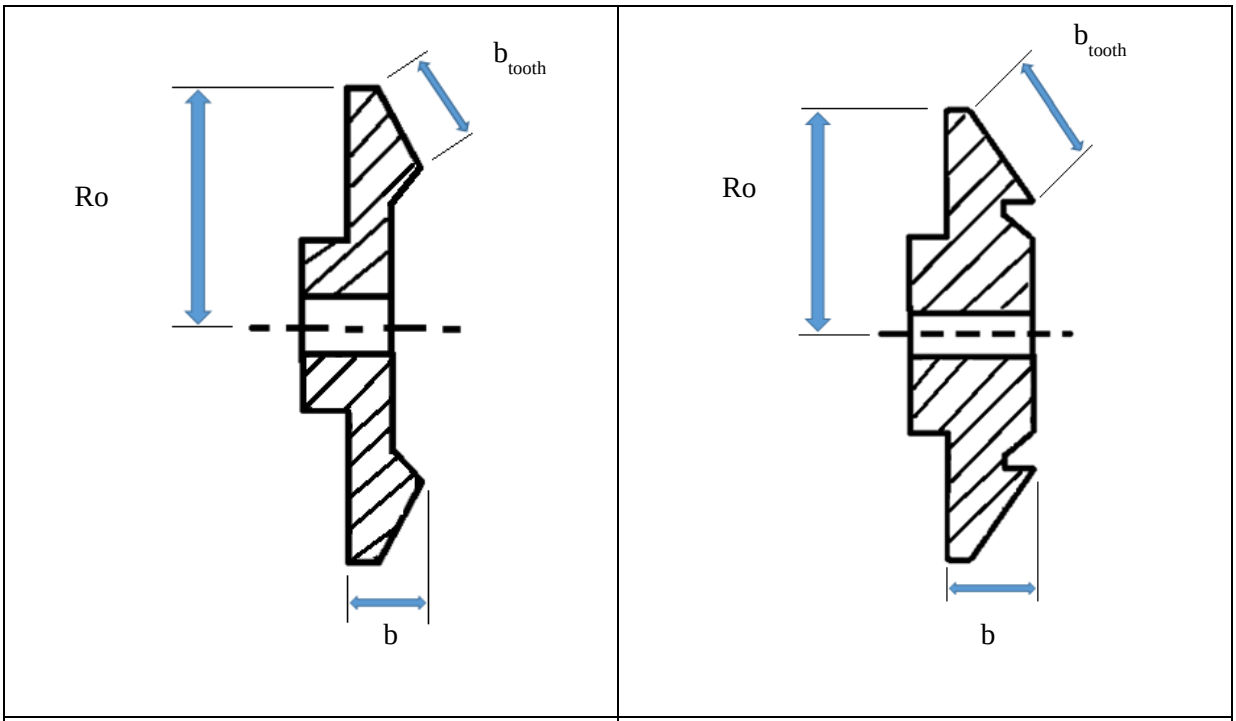

Gears 1 and 3 | Gears 2 and 4

Figure 21: typical gear geometries

As far as lubricants are concerned, four different oils were used. Their characteristics are resumed in the Table 6.

Table 6: oil data

Oil name	Oil A	Oil B	Oil C	Oil D
Kinematic viscosity @40°C	220 cSt	35 cSt	45,1 cSt	120 cSt
Kinematic viscosity @100°C	19 cSt	7,5 cSt	7,7 cSt	16 cSt
Density @15°C	895 kg/m3	870 kg/m3	885 kg/m3	860 kg/m3
Oil type	Mineral	Mineral	Mineral	Synthetic

As shown by Leprince *et al.* [74], oil aeration, which is defined as the volumetric fraction of air in the lubricant, has a negligible influence on the churning power losses when it is less than approximately 10%. With the same methodology as the one used in the above-mentioned publication on cylindrical gears, aeration measurements with the Air-X apparatus [34] have confirmed this observation for this study on spiral bevel gears in the tested domain.

The DSI Company has developed “Air-X”, an instrument for on-line monitoring of lubricant aeration in mechanical systems such as engines or gearboxes [75]. The operating principle of “Air-X” is based on low energy X-rays transmission. The amount of absorbed X-rays, which are emitted by a source, depends on various parameters such as their energy, the thickness and the density of the crossed material, and its composition (Figure 22).

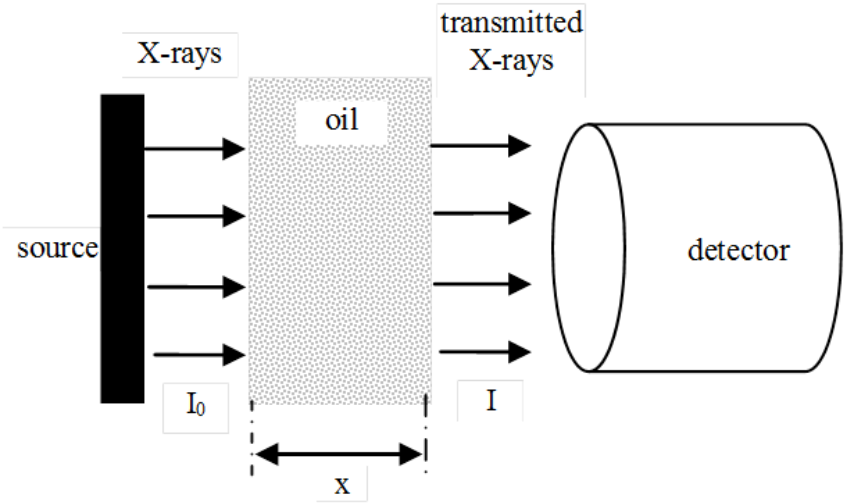

Figure 22: measurement principle

The transmitted intensity I of an X-ray beam is given by the following relationship:

$$I = I_0 \times e^{-c.x.\rho}$$

Equation 56

Where:

- I_0 is the intensity of the source beam [A]
- c is the absorption coefficient depending on X-ray energy and material
- x is the thickness of the oil bath crossed by radiation [m]
- ρ is the the aerated oil density [kg/m^3]

If A represents the fraction, by volume, of air in aerated oil, the density of this mixture is given by [92]. Then knowing the air ρ_{air} and oil ρ_{oil} density, the aeration A is obtained.

$$\rho = \rho_{oil}(1 - A) + \rho_{air}A$$

Equation 57

The lubricant density decreases when the concentration of air increases. The thickness of the oil crossed by radiation is constant, so the transmitted intensity from an X-ray source through a lubricant can be related to the percentage of air in this lubricant (accuracy 0.2% of the full scale which is 100% of air in the lubricant). Since the density measurement should be accurately determined, the law of variation of the lubricant density with temperature is experimentally determined.

The X-ray source is placed into the oil bath and the detector is mounted on the housing frame of the churning test rig outside of the gearbox. This detector is connected to a data acquisition system and a control PC with dedicated acquisition boards (Figure 23).

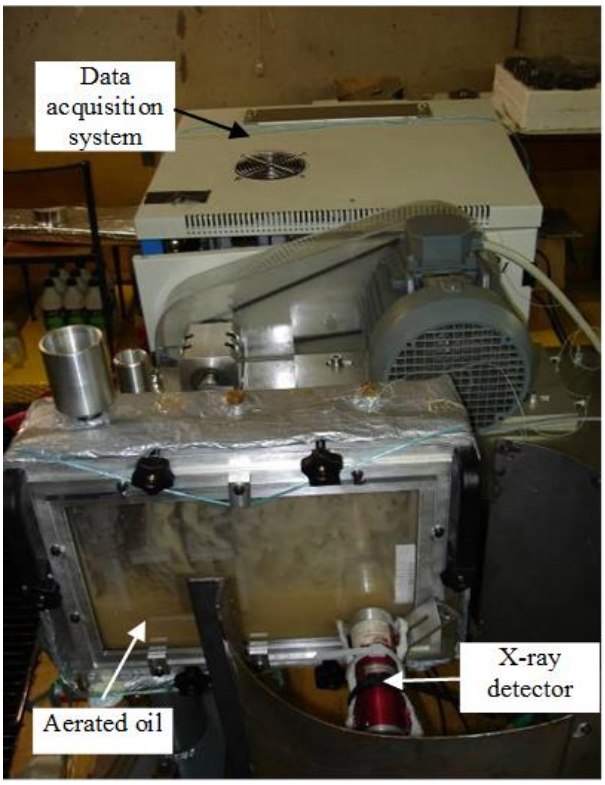

Figure 23: view on the churning test rig with "Air-X" unit

The aeration in the lubricant is smaller than 7% on the tested domain. A measure at 3000 RPM from 25°C to 70°C is shown in Figure 24: it confirms that aeration is negligible for the studied experimental domain.

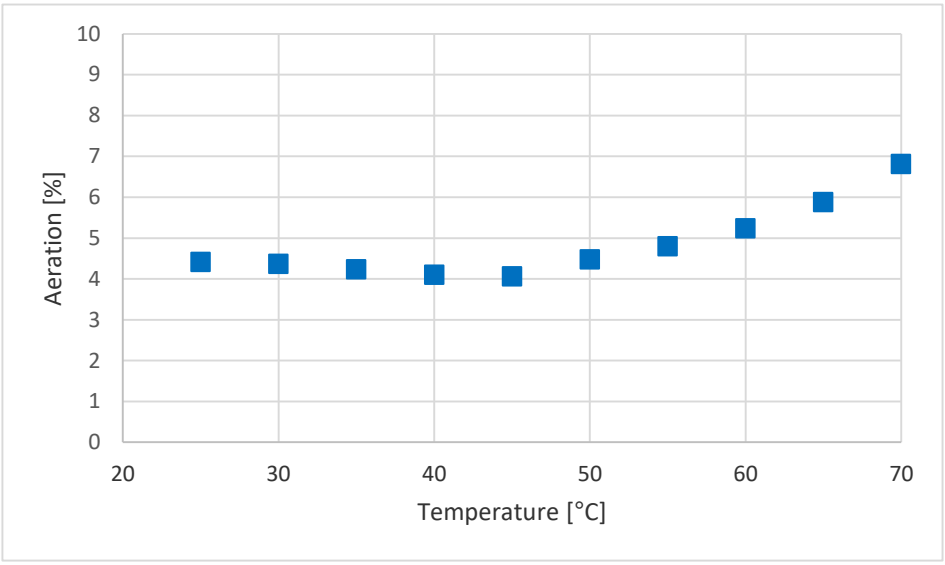

Figure 24: aeration measurements with Air-X apparatus at 3000 RPM, gear 1, oil B

3. Results

Experiments [70] were performed for different operating conditions (oil properties -viscosity and density-, rotational speed, gear immersion level) and different spiral bevel gear geometries (diameter, width, face width, face angle, tooth number, module). The objective is comparing experimental measurements with analytical formulas available for hypoid gears from Jeon by observing experimental trends.

The experiments are chosen and realized with respect to full factorial design: several levels are chosen for each of the operating conditions parameters and measurements are conducted for each of the different operating conditions obtained. It allows limiting the influence of measurements errors since numerous tests are conducted. Even if the total number could have been reduced through a fractional factorial design, some uncertainties concerning the influence of one or several parameters could have appeared and measurements errors would have had a greater influence on the results analysis.

The relative immersion of the gear in an oil bath is considered when studying the operating conditions in churning losses. Figure 25 shows how the immersion depth h is defined. The angle θ is represented as the immersion angle on Figure 25 and the radius of the gear R is reported. The relative immersion level is defined as the ratio of the immersion depth h and the radius of the gear R.

Operating conditions of the churning tests are defined through the oil chosen, the relative immersion of the gear, the rotational speed of the gear and the oil bath temperature. The oil temperature is the same for all elements inside the housing since the measurements are made in the steady state conditions so that the temperature of all the elements of the housing is the same as the oil temperature. Here, only churning loss comparisons are needed since the oil temperature is an operating condition.

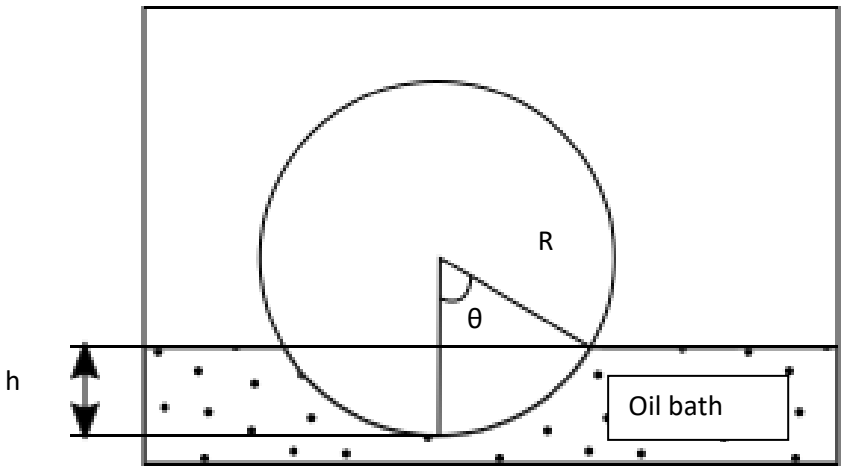

Figure 25: gear partially immersed in oil

Measurements for different spiral bevel gears as a function of their relative immersion depth are shown in Figure 26. It clearly appears that this parameter is a 1st order influent one on churning losses. Moreover the churning losses are observed to increase with the external diameter of the gear. The relative immersion is a dynamic measured oil level, it varies between the different geometries since the oil bath is filled at stillstand and the evolution of the dynamic level is slightly different for each geometry.

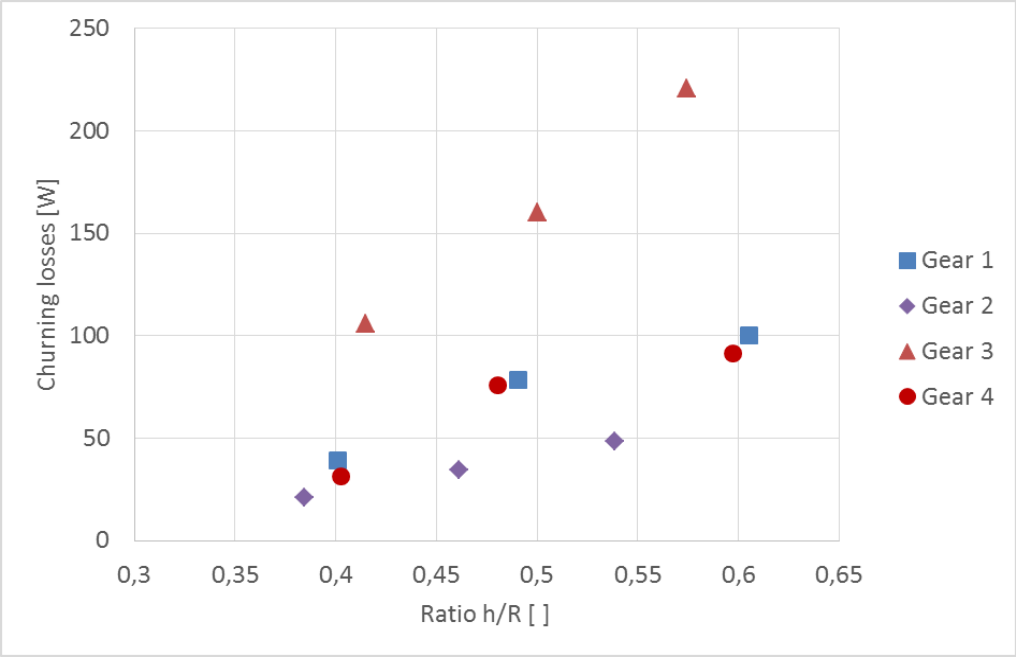

Figure 26: influence of immersion on churning losses (oil C, 2000 RPM - 40°C)

Considering rotational speed, it can be noticed that the losses are proportional to $N^{1.7}$ (see Figure 27; a similar relative immersion depth of approximatively 0.5 was used for the tested gears).

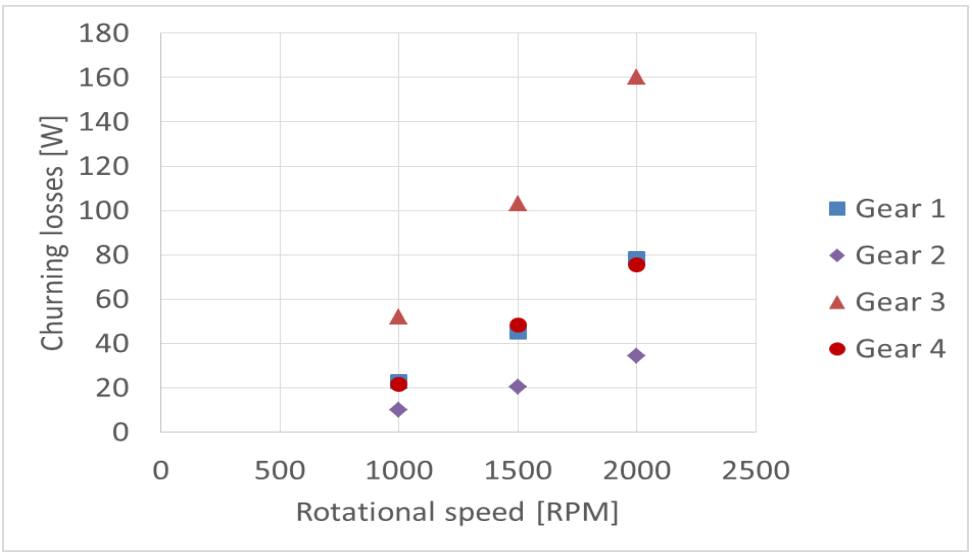

Figure 27: effect of rotational speed on churning losses (oil C, 40°C)

For higher rotational speeds, a drag torque decrease is observed, as presented on Figure 28 and noticed by Jeon [62]. Two types of regime were observed between 1000 to 4000 RPM: (i) for the first regime, the oil is projected and the torque increases with speed; (ii), for the second one, which corresponds to higher rotational speeds, the torque decreases. The second regime can be interpreted as follows: centrifugal effects generated by the rotating gears become significant and reduce the immersion depth, which leads to a decrease in churning drag torque. This phenomenon is also observed for a smooth cone. The present study is focused on the first regime where the churning torque increases with speed.

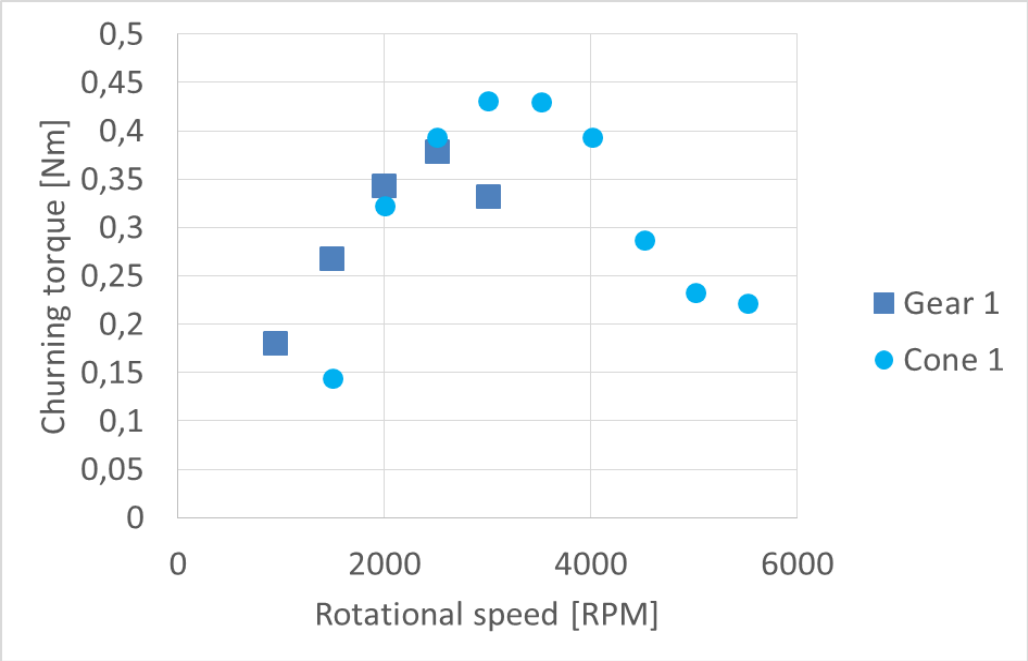

Figure 28: different regimes (oil B - h/Ro=0.5 - 50°C)

To further investigate the influence of spiral bevel gear geometry more tests were performed. Figure 26 and Figure 27 show that gears 1 and 4 have the same behavior. These gears have a similar external diameter (roughly equals to 160mm) but present different tooth geometries (number of teeth, face width, face angle…). On Figure 28, cone 1 and gear 1 have also a similar behavior.

In order to investigate more deeply the influence of parameters related to geometry, some tests were performed with cone 2. It has a similar diameter than cone 1, but different face angle and width. Figure 29 shows that its behavior is close to cone 1 and gear 1. It can be deduced from these experiments that the external diameter appears as the main geometrical parameter, whereas the tooth influence can be neglected for the tested conditions. As shown on Figure 26, the diameter is observed to be highly influent and the influence of tooth geometry is limited since gear 1 and 4 give similar results.

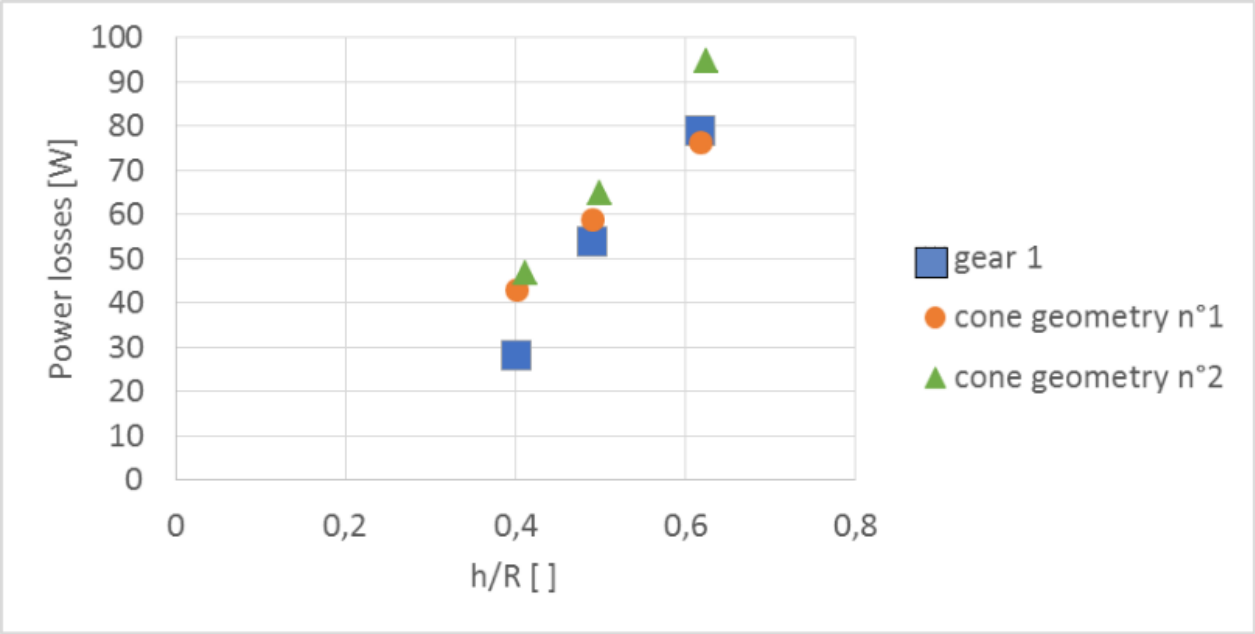

Figure 29: power losses for gear 1 and cones (oil D; 1500 RPM; 40°C)

Looking at the oil properties, Figure 30 presents churning losses generated by gear #3 versus oil viscosity for constant rotational speed and immersion depth. In order to analyze the influence of viscosity, the oil sump is heated using heating covers. Two flow regimes clearly emerge: for high values of viscosity, the churning torque decreases as viscosity is reduced whereas it remains constant for lower viscosity values. This behavior has already been pointed out by Changenet et al. [21] for cylindrical gears.

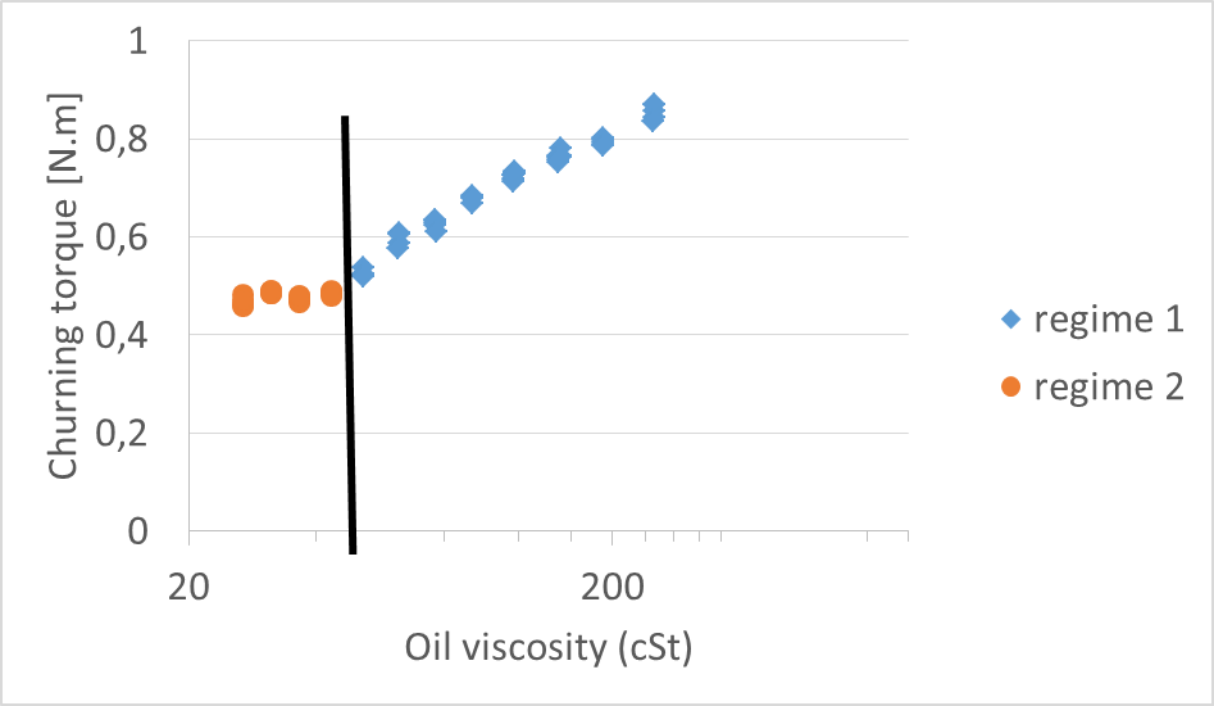

Figure 30: flow regimes (gear #3 - h/Ro=0.6 – 1000 RPM)

As the published literature contains few calculation methods to estimate churning losses of bevel gears, some comparisons of the measured power loss with those predicted from the existing relationships have been done. As an example, Figure 31 presents churning losses generated by gear #3 as a function of speed. This figure highlights that power losses calculated with ISO/TR 14179-1 overestimate the measured ones. Indeed, according to this calculation method, the losses are proportional to N^3 which is not in accordance with experiments (proportional to $N^{1.7}$). Because of this discrepancy ISO/TR 14179-1 is disregarded in the following analyses. In contrast, the churning loss level given by ISO/TR 14179-2 and Jeon formula are closer from experimental results, even if up to 15% discrepancy is observed on Figure 31.

Another comparison, associated with the influence of oil properties, is given in

Figure 32. As it has been underlined, two flow regimes clearly emerge from measurements whereas calculation methods are based on single regime: the churning torque always decreases with viscosity according to Jeon's approach and it remains constant by using the relationships of ISO/TR 14179-2.

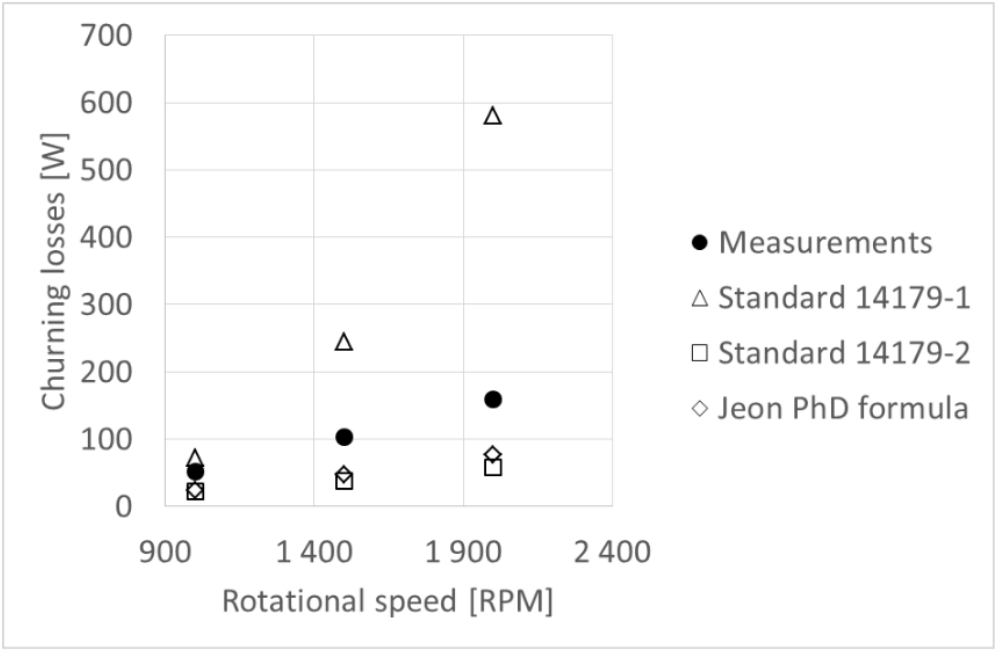

Figure 31 : influence of speed on measured and calculated churning losses (gear 3 – oil C – 40°C – h/R=0.5)

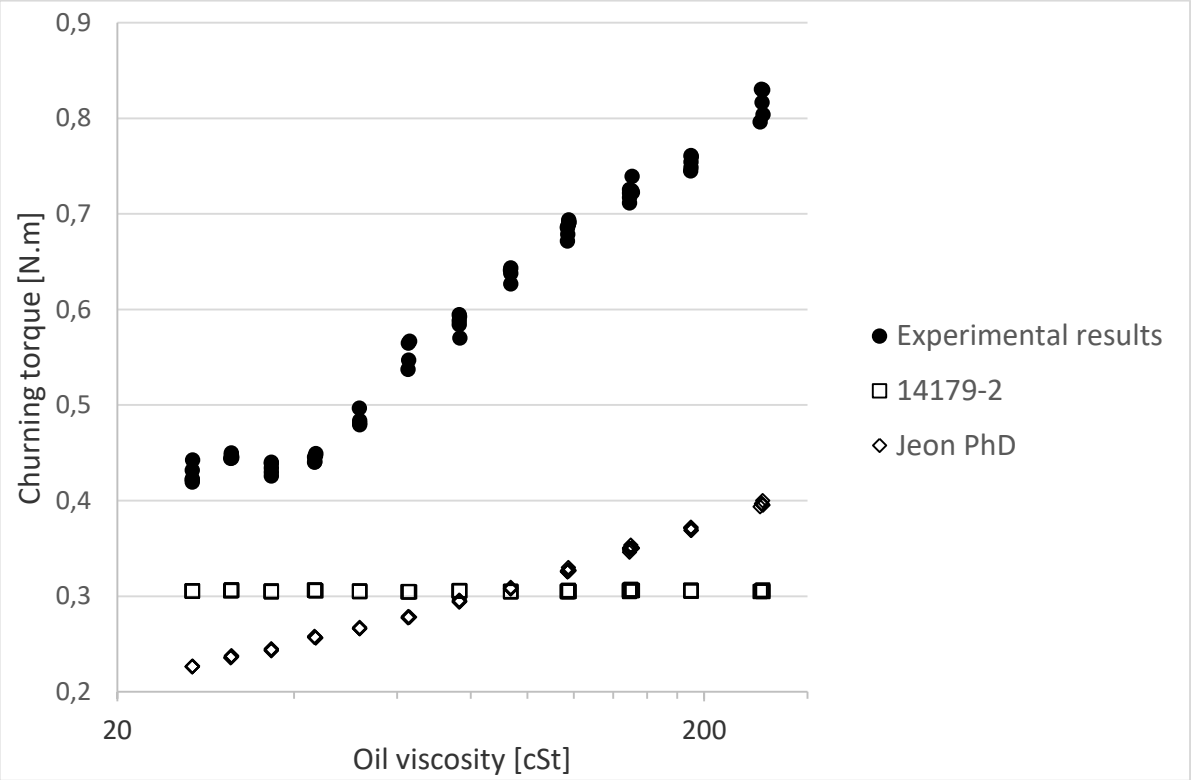

Figure 32: influence of oil properties on measured and calculated churning losses (gear 3 – oil D – h/R=0.6 – 1000 RPM)

Formulas available in literature do not represent the churning behavior observed experimentally. Further analysis is required to find an analytical expression to represent the experimental behavior observed.

4. Results analysis

As spiral bevel gears macro-geometry is close to hypoid ones, the methodology used by Jeon [62] on hypoid gears was considered to analyze experimental data [71]. Churning power losses are given by [62]:

$$P = \frac{1}{2}\rho\omega^3 {R_o}^2 b S_m C_m$$

Equation 58

Where:

- R_o is the outer radius on the large end of the bevel gear (see Figure 21) [m]

- b is the width [m]
- S_m is the submerged area [m²]
- C_m is the dimensionless drag torque:

$$C_m = 2.186 \left(\frac{h}{R_0}\right)^{0.147} \left(\frac{V_0}{R_0^3}\right)^{-0.198} Re^{-0.25} Fr^{-0.53}$$

Equation 59

Where:

- h is the gear immersion depth [m]
- V_0 is the oil volume [m^3]
- Re is the Reynolds number
- Fr is the Froude number

As experimental results have underlined that tooth geometry has a negligible influence on churning losses, the submerged area S_m is quantified by modifying the cylindrical gear formula provided by Changenet et al. [21] and by only taking into account the equivalent envelope geometry of a spiral bevel gear. The detailed S_m computation is presented in appendix D. The analytical formula of S_m concurs with Jeon's work on hypoid gears since the retained geometry is only related to the gear envelope dimensions. The geometry of the spiral bevel gears tested is constrained by existing geometries used on gear units of different sizes.

Then equation (58) can be used to determine the experimental dimensionless churning torques from measurements. A typical series of results is presented in

Figure **33**. As gear #1 and #4 do not have identical values of C_m but similar diameters, it can be deduced from dimensional analysis [89] that parameters associated with tooth geometry (module, tooth face width…) have also to be taken into account to determine C_m which is not in accordance with equation (59). A dimensional analysis is conducted in order to provide influential parameters on the churning behavior of spiral bevel gears. Different operating conditions are tested in order to explore a wide operating range.

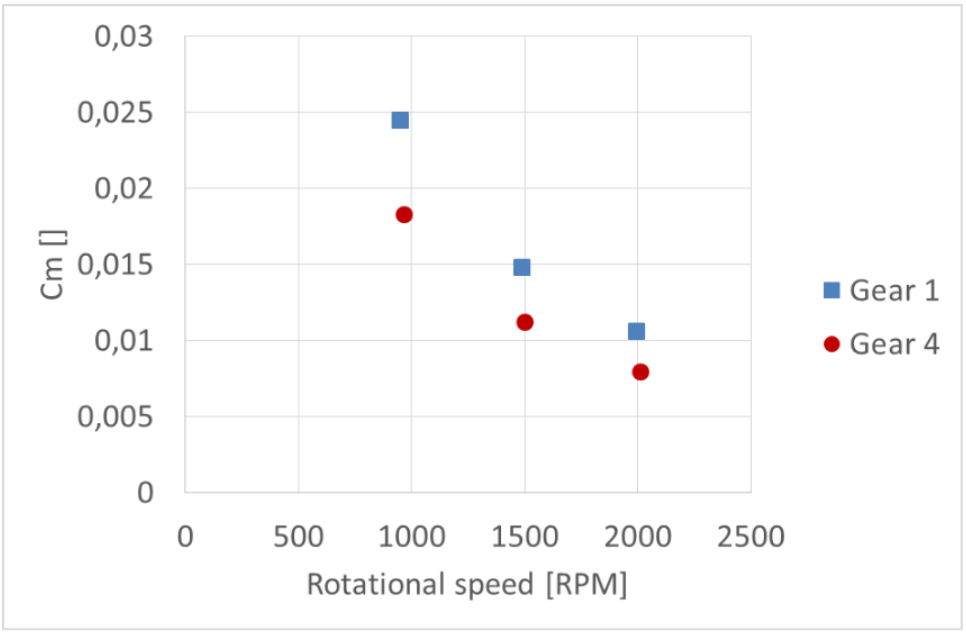

Figure 33: C_m for gears 1 and 4 according to equation II.1 (oil B, 70°C, hh/R_0=0.5)

As the experiments show that the outer radius is a first order influent parameter, it is proposed to change equation (60) as follows:

$$P = \frac{1}{2}\rho\omega^3 {R_o}^3 S_m C_m$$

Equation 60

Figure 34 demonstrates that this new relationship leads to identical dimensionless drag torque for gears #1 and #4. It implies that the tooth geometry parameters have not to be taken into account anymore in Dimensional Analysis. Nevertheless influential parameters identified in equation (59) can be kept for a further analysis.

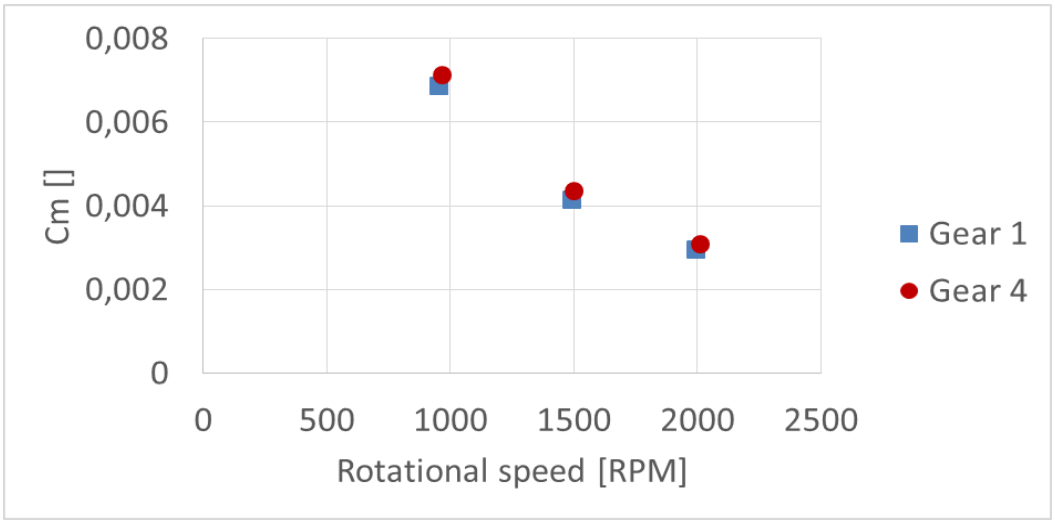

Figure 34: C_m for gears 1 and 4 according to equation II.3 (oil B, 70°C, h/R_0=0.5)

The following list of potentially influential parameters is then extracted:

- Operating data such as immersion level, rotational speed, gravity
- Lubricant data such as viscosity, density, oil sump volume
- Gear geometrical data such as external radius

So the churning loss P is expressed as:

$$P = f(h, \omega, g, \upsilon, \rho, V_0, R_O)$$

Equation 61

These seven parameters are expressed in terms of three fundamental unities: mass, length and time. From the Buckingham π theorem [89], four dimensionless numbers can be constituted. Main parameters retained are angular velocity, density and external radius, then four dimensionless number could be formed with the remaining parameters:

- Π_1 corresponds to the relative immersion of the pinion:

$$\Pi_1 = \frac{h}{R_O}$$

Equation 62

- Π_2 corresponds to the Reynolds number:

$$\Pi_2 = \frac{\nu}{\omega R_O^2} = \frac{1}{Re}$$

Equation 63

- Π_3 corresponds to the Froude number:

$$\Pi_3 = \frac{g}{\omega^2 R_O} = \frac{1}{Fr}$$

Equation 64

- Π_4 corresponds to the oil volume influence:

$$\Pi_4 = \frac{V_0}{R_0^3}$$

Equation 65

Then a dimensionless churning torque can be expressed as:

$$C_m = \gamma_1 Re^{\gamma_2} Fr^{\gamma_3} \left(\frac{h}{R_0}\right)^{\gamma_4} \left(\frac{V_0}{R_0^3}\right)^{\gamma_5}$$

Equation 66

Where γ_1 to γ_5 are constant coefficients which are adjusted from experimental results.

In the following, one parameter is changed at a time in order to isolate its influence independently of other parameters. Once a parameter is studied, its influence is substracted from the analysis of the remaining parameters.

Figure 35 presents dimensionless torque Cm for two different gears (#1 and #3) and two oils (A and D) according to the Reynolds number. On this figure, the temperature is varied to modify the relative influence of the inertia forces over the viscous forces in the fluid, which results in Reynolds number evolution. The two flow regimes that have been pointed out previously clearly appear on this figure. A transition between the two flow regimes is observed for a Reynolds number around 20000. For the regime bellow the transition, γ2 equals -0.25 (in agreement with Jeon's formula) whereas for higher Reynolds number, γ_2 is zero. For this last regime, it means that viscous forces become negligible.

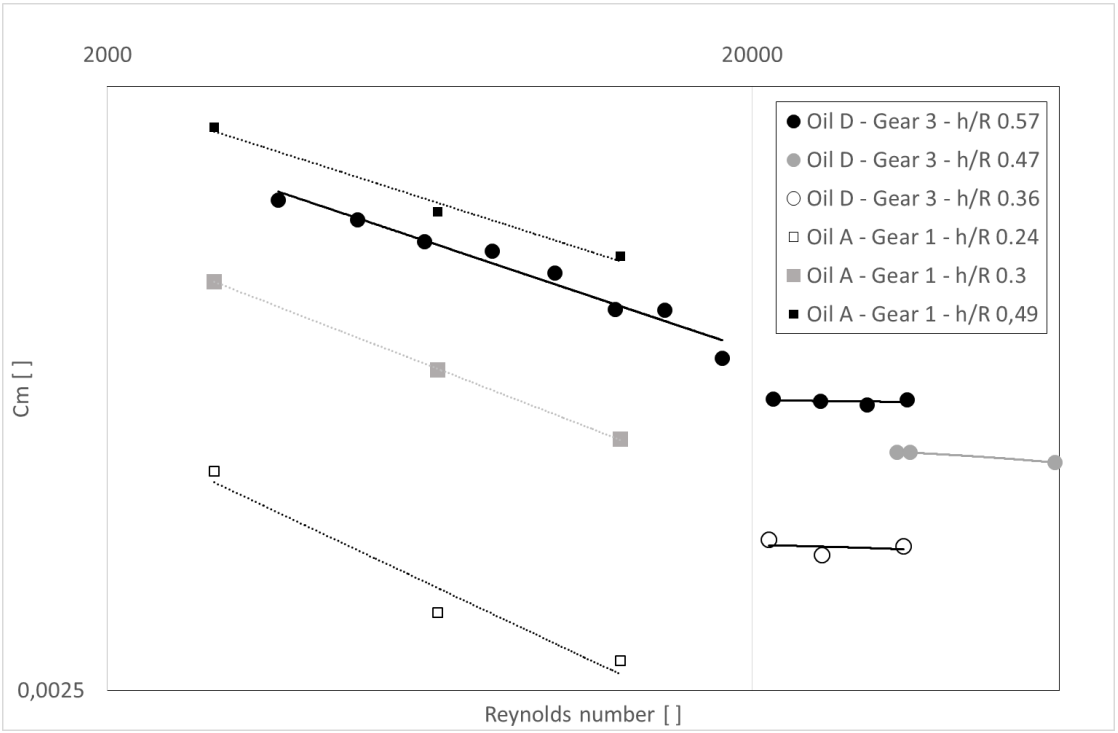

Figure 35: two flow regimes of churning depending on Reynolds number

Concerning the Froude number, its influence can be isolated through tests where only the rotational speed varies as the ones given in Figure 27. It has to be noted that the Reynolds influence has been eliminated (see equation 67).

$$\gamma_3 = \frac{\ln\left(\frac{Cm_1}{Cm_2}\left(\frac{Re_1}{Re_2}\right)^{\gamma_2}\right)}{\ln\left(\frac{Fr_1}{Fr_2}\right)}$$

Equation 67

The constant γ_3 can then be deduced. A value of -0.53 is found which is identical to Jeon's formula.

Then the objective is to provide a dimensionless ratio to isolate the immersion level influence. As far as influence of gear immersion is concerned, equation (68) is used to determine the following ratio according to the relative immersion depth (h/Ro). It allows isolating the influence of gear immersion independently of the volume of the oil bath which varies also with the gear immersion. The following ratio allows isolating the immersion level influence and determining its influence on churning losses:

$$\frac{C_m}{Re^{-0.25}\,Fr^{-0.53}\left(\frac{V_0}{R_0^3}\right)^{-0.198}}$$

Equation 68

After isolating the previous ratio, it allows comparing the experimental results sensitivity to the immersion level with Jeon's relationship for example. On Figure 36, this ratio (68) is calculated in two different ways: either using experimental data for C_m or using Jeon's relationship (59). After comparing experimental data with jeon's formula, experimental results show more sensitiveness to the relative immersion depth.

It should be noted that Jeon PhD does not provide much information on the experimental operating conditions and gear geometry. The diameter of the gears is given. The axial and radial clearances between the gears and the housing are given too. However no more information is available from Jeon PhD on the oil or on the detailed geometry of the gears tested.

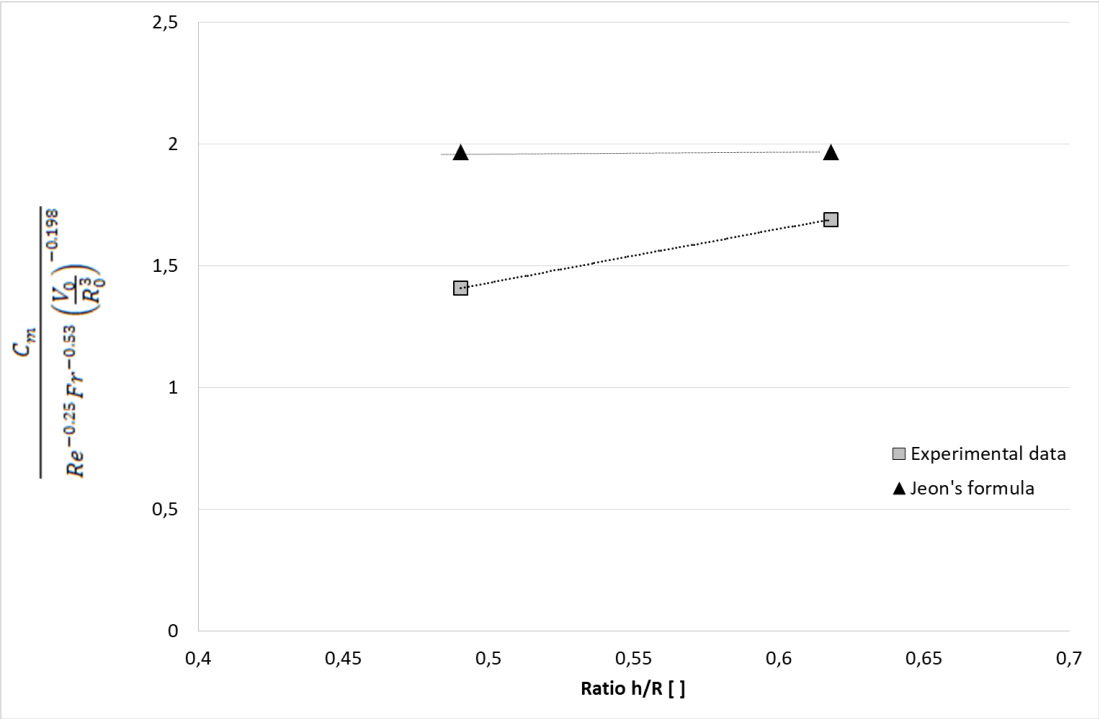

Figure 36: h/Ro influence (gear 1, 2000 RPM, oil D, 40°C)

Looking at the general geometry of the casing in the Jeon's experiments (Figure 37) and in the present study (Figure 38) it can be noticed that the gears do not generate a similar oil flow probably due to enclosure effect. The axle housing presents a circular shape around the crown gear, contrary to this study where a parallelepiped defines the oil sump. Moreover the enclosure volume (6.6 dm^3) is significantly larger than the gear dimension (R^3=3.5 dm^3).

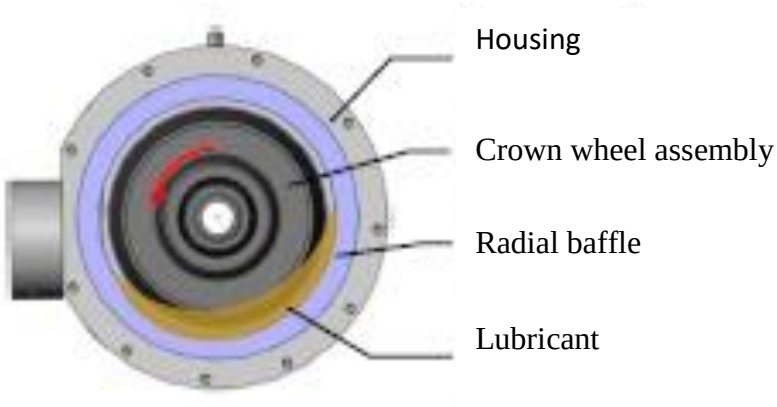

Figure 37: Jeon test rig, oil behavior during tests [62]

Figure 38: oil behavior in LabECAM test rig (oil A, 3000 RPM, 70°C)

In order to investigate this assumption, complementary tests were conducted with deflector around the bevel gear (Figure 39).

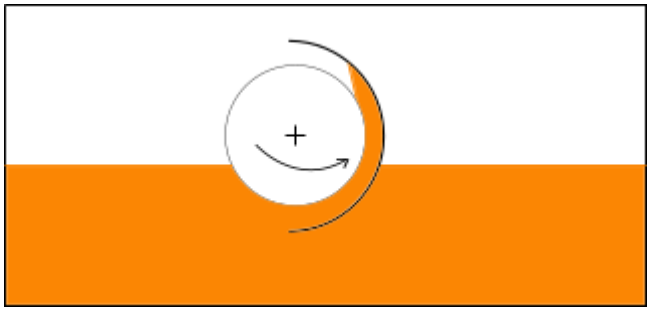

Figure 39: position of the deflector and direction of rotation of the gear

These tests (with and without a deflector) are reported on Figure 40 and show the impact of the housing on the dimensionless drag torque: adding a deflector modifies considerably the evolution of dimensionless torque according to the relative immersion. This is consistent with the observation mentioned previously.

From this observation, an adapted formula should be proposed to account for the previous observation. Parameters γ_1, γ_4 and γ_5 have to be defined accordingly.

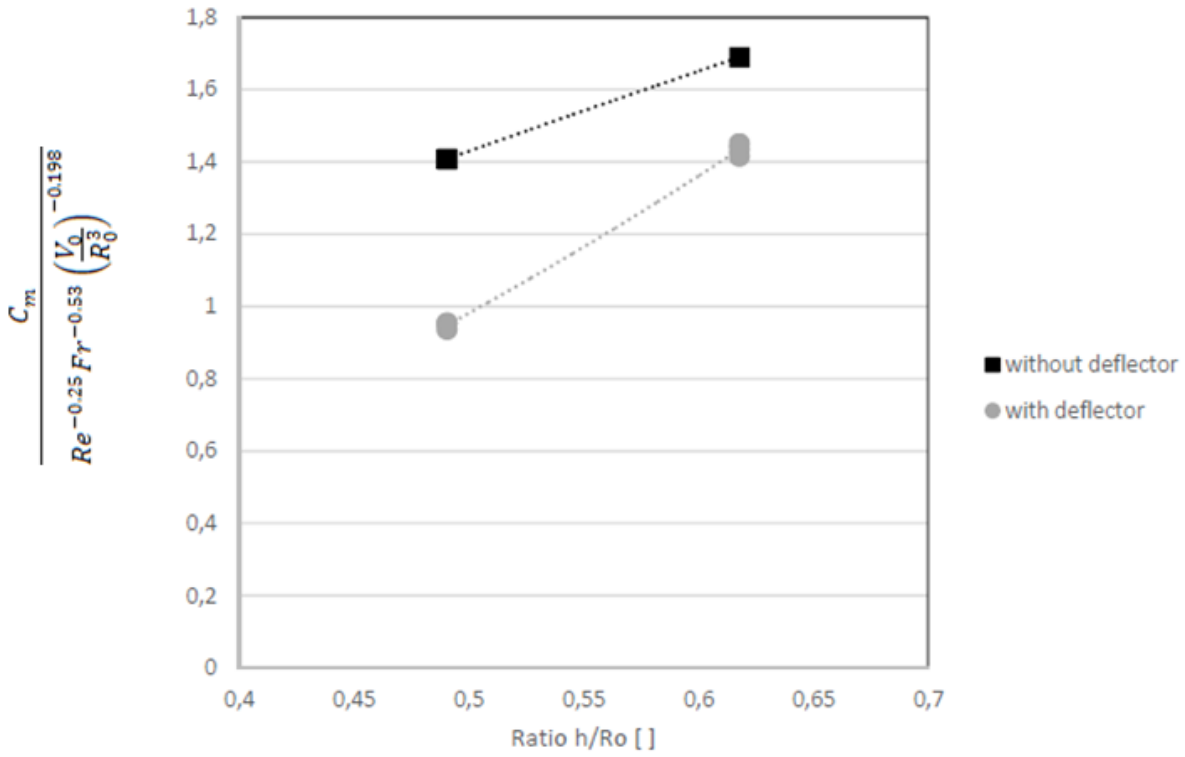

Figure 40: housing influence (gear 1, 2000 RPM, oil D, 40°C)

Since Jeon's formula provides some discrepancies with the measurements on the ECAM test rig, the enclosure effect is not negligible in Jeon study contrary to the tests conducted on ECAM test rig. However, the oil enclosure in the case of the studied gear unit is closer from the ECAM test rig than from Jeon's one. It means that further studies concerning the Cm formula should be done to account for the modified churning behavior in the case of a parallelepiped enclosure. It is observed that the complex behaviors observed are not resumed in a unique formula.

5. Proposed formula for churning of spiral bevel gears

Parameters γ_4 and γ_5 are defined by eliminating successively the influence of the other parameters. γ_5 is found equal to the value given in Jeon PhD then γ_4 describes the immersion influence. Finally, γ_1 is the coefficient which minimizes the gap between experimental and theoretical values. This leads eventually to two formulas describing the churning behavior of the experimental gears, for a validity domain from 1000 RPM to 2000 RPM, viscosity from 400cSt to 7cSt for an oil volume of approximately 3.5 dm^3, diameters from 130mm to 190mm, and an immersion level h/R_0 from 0.4 to 0.6. The maximum speed range is chosen since it is the maximum speed encountered in the gear dipping tin the oil bath, and the churning losses are much reduced under 1000 RPM.

If $Re > 25\,000$,

$$Cm = 0{,}15\, Fr^{-0{,}6} \left(\frac{h}{R_O}\right)^{0{,}4} \left(\frac{V_0}{{R_O}^3}\right)^{0{,}1}$$

Equation 69

If $Re \leq 18\,000$

$$Cm = 2{,}3\, Re^{-0{,}25} Fr^{-0{,}6} \left(\frac{h}{R_O}\right)^{0{,}7} \left(\frac{V_0}{{R_O}^3}\right)^{0{,}1}$$

Equation 70

For 18 000<Re<25 000, linear interpolation between the two formulas is used.

The dimensionless drag torque Cm (equation 60) obtained by the model is close to the Cm obtained through the experiments, as shown in Figure 41 for oil A and Figure 43 for oil B (refer to appendix E for results of oils C and D). The churning losses expression used is also verified as a good expression to represent experiments in Figure 42 or Figure 44. The root mean square error is less than 15%. Low viscosity leads to instabilities in the oil bath. High viscosity leads to high variation of viscosity as the gear rotates and heats the oil bath.

The relative immersion level is not exactly the same for all tests since level is set at standstill and the dynamic level evolves differently in function of the different gear geometry.

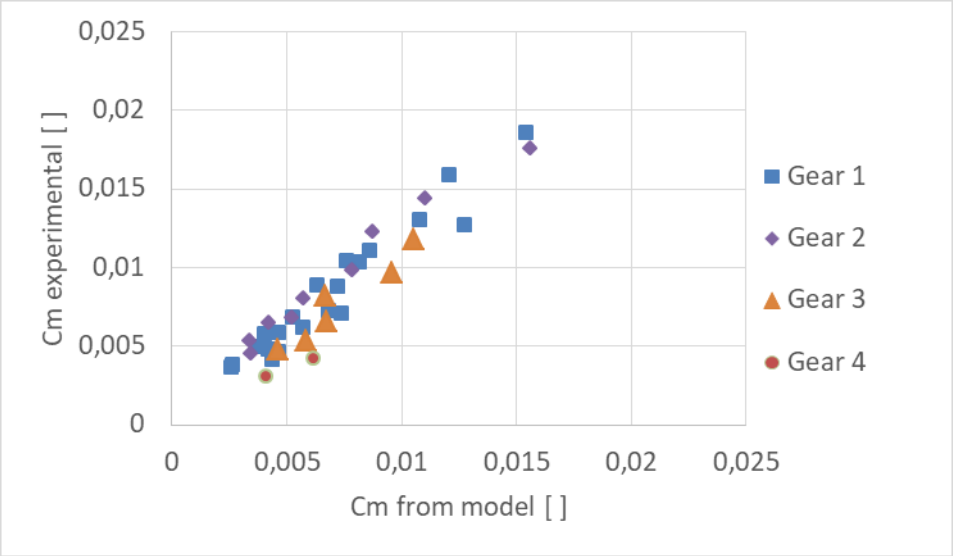

Figure 41: comparison between experimental Cm and theoretical (Oil A)

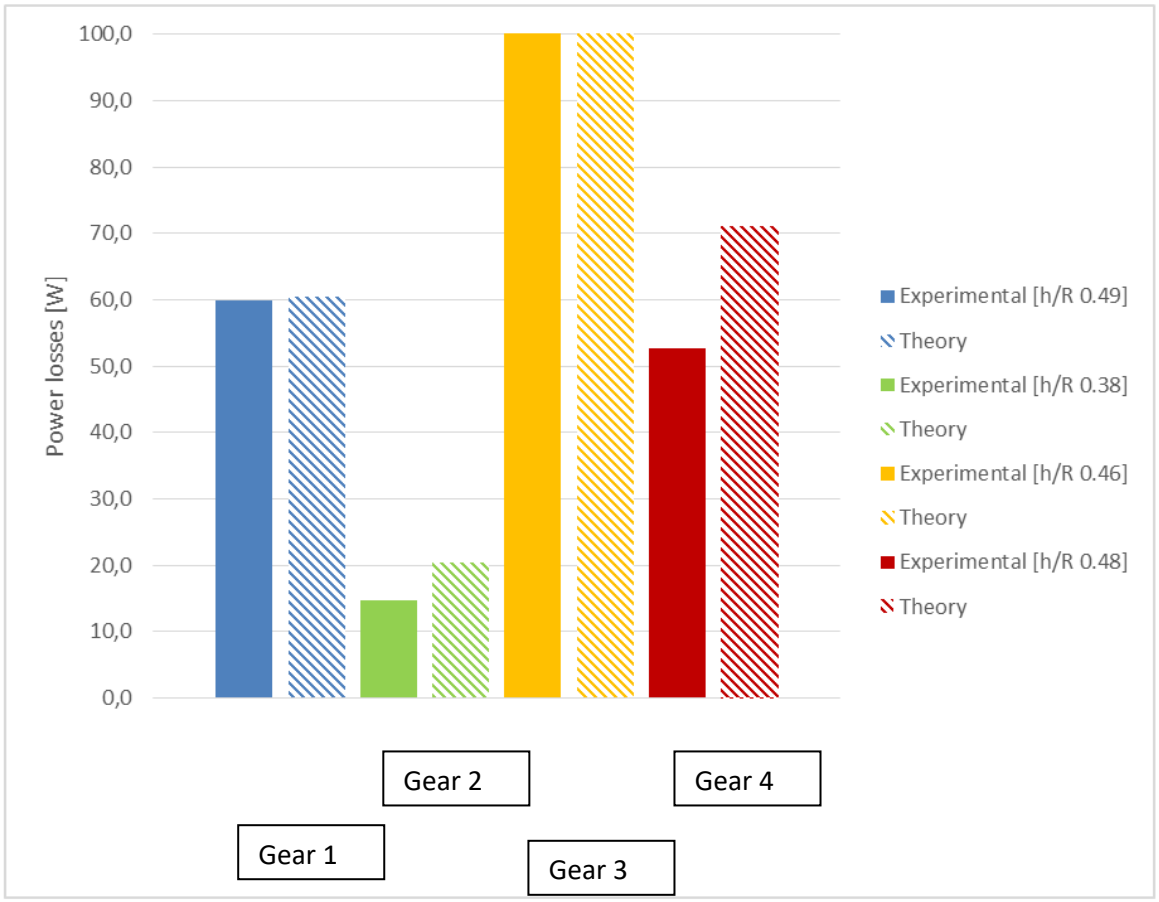

Figure 42: churning losses of the four gears at 40°C and 1000 RPM (oil A), experimental VS model

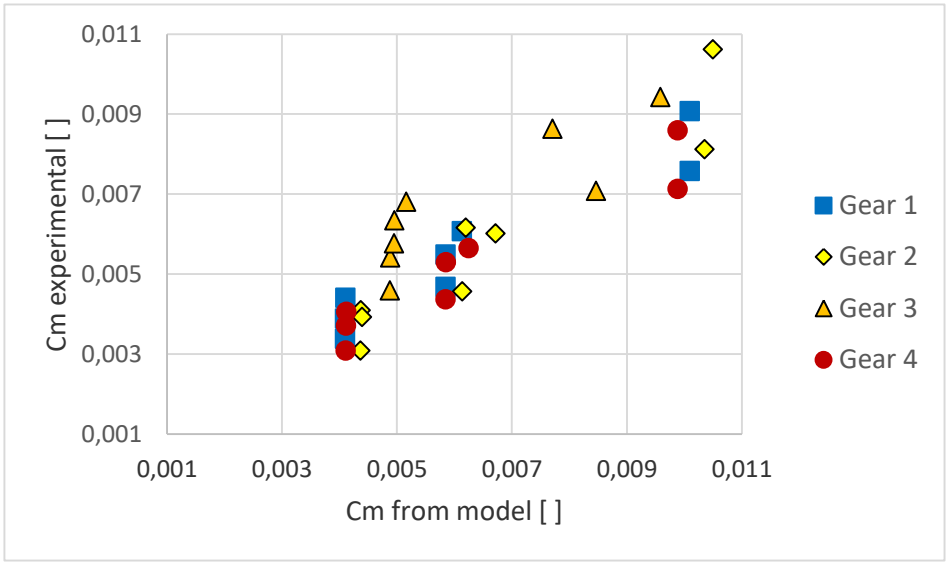

Figure 43: comparison between experimental Cm and theoretical (Oil B)

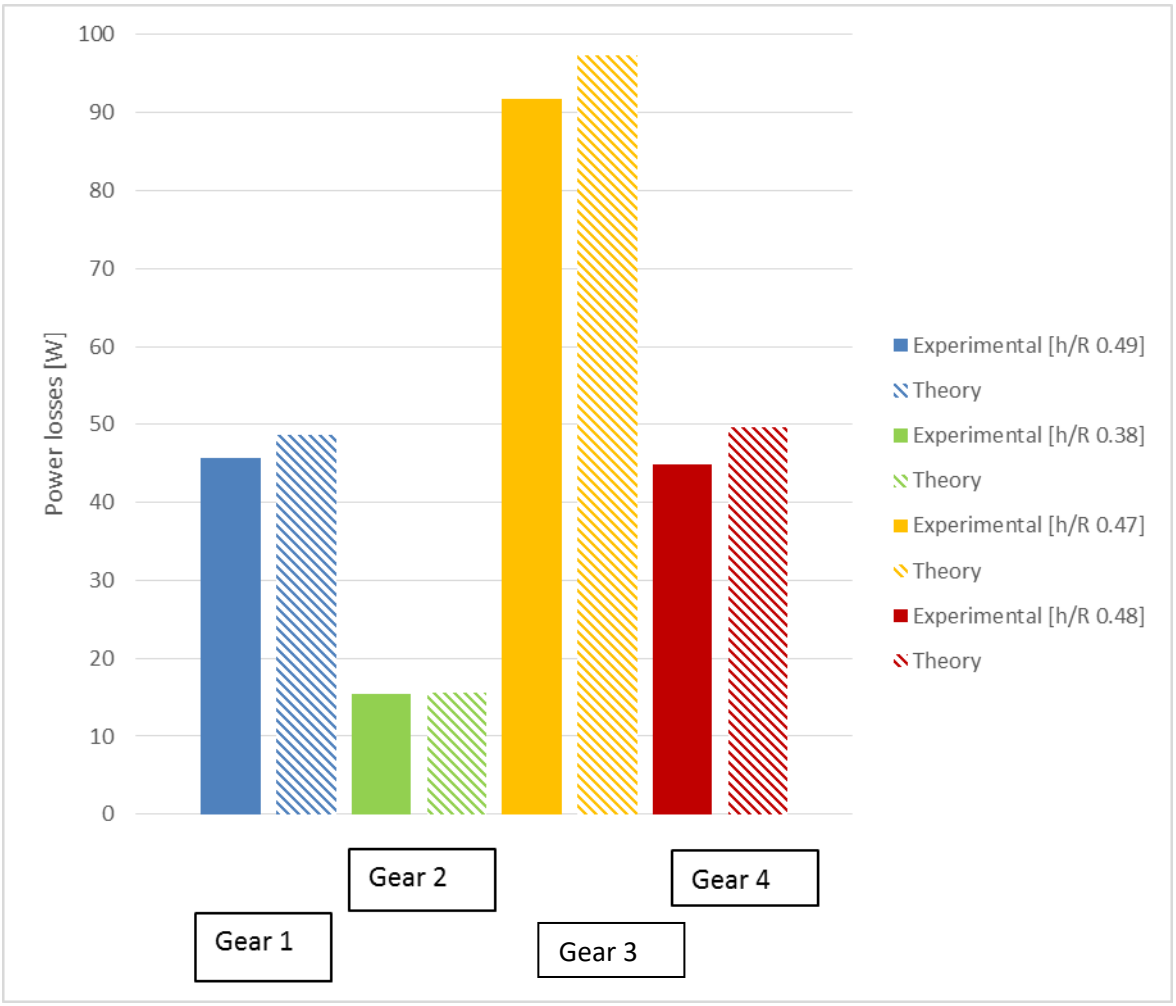

Figure 44: churning losses of the four gears at 50°C and 1500 RPM (oil B), experimental VS model

6. Conclusion

In the previous chapter, important discrepancies in the churning losses evaluation are observed concerning bevel gears. In chapter 1, the churning power losses is shown to have a significant influence on the temperature distribution within the geared transmission and on the power losses repartition, this source of dissipation is further studied in chapter 2.

In order to determine if formulas from technical report 14179-1, technical report 14179-2 and Jeon PhD work are valid for spiral bevel gears, experimental tests were performed on a specific test rig available at the ECAM Laboratory in Lyon. Both the operating conditions, oil types and gears geometries were modified to analyze the impact of these parameters on churning losses.

Technical report 14179-1 has shown weaknesses in reproducing the rotational speed influence observed in experiments. These discrepancies are large enough to discard this formula

from this study. Technical report 14179-2 is discarded since it fails to reproduce the viscosity impact on the churning losses since viscosity is not considered in its expression.

Jeon PhD consists in a specific study of churning losses of hypoid gears. From the comparison between experiments and Jeon's formula, some observations were noted:

- The envelope of the hypoid or spiral bevel gear is the volume to consider in the submerged area. The tooth geometry has not to be known.

- The dimensionless expression of the churning loss is revised considering experimental observation on the gear geometry influence in the case of large enclosure compared to the gear size. The enclosure is shown to influence the flow inside the enclosure which leads to the difference in the formula proposed in this chapter and Jeon work concerning the same flow regime. Moreover the dimensionless expression of the churning torque is proposed in a new formulation accounting for the Pi theorem applied on experimental data.

- Several flow regimes are observed depending on Reynolds number. Jeon notices only one flow, since its experiments cover a reduced range of Reynolds values compared to this study

From this study, the uncertainties concerning churning losses are reduced and it is now possible to characterize the behavior of the gear unit. The next chapter concerns no-load and loaded tests on the transmission to define its behavior. Two main parameters needs to be further studied: the no-load coefficient f_0 of the bearings (equation 40 and 41) and the friction coefficient in gears contact which are the two remaining unknowns concerning their evaluation. The chapter 3 is focused on this problematic. No-load tests allow to validate the heat-transfer between the gear unit and its surrounding environment and to characterize the no-load coefficient f_0 of the bearings, which is the remaining parameter to define on this transmission. Loaded tests are used to study the friction coefficient in the gear mesh through reverse engineering and also validate the model under various operating conditions.

Chapter 3

Application to an industrial gear unit

1. Introduction

In the first chapter, the context and methods chosen for the study have been presented. The second chapter has focused on churning losses estimation to reduce uncertainties. In this last chapter, the model, which has been programmed in MatLab by the author (not detailed for condidentiality constraints), is applied to an industrial gear unit.

The model allows conducting a coupled analysis on the power losses and temperature distribution in the gear unit. A comparison can be performed between experimental measurements of the thermal behavior of the gear unit and the thermal behavior simulated through the thermal behavior which has been programmed. This comparison allows testing different assumptions concerning power losses calculation or thermal exchanges. Indeed, few parameters are not precisely defined to calculate power losses and have to be adjusted. Nevertheless, for each considered assumption, the sum of the calculated power losses, which are injected into the thermal network, has to be equal to the measured power loss. Then for each simulation, the measured temperatures are compared with the experimental ones. If the numerical temperatures are not similar to the measured ones, the hypothesis is not validated. An accurate power losses distribution is obtained once the simulated thermal behavior is similar to experimental results obtained on the gear unit.

In this chapter, experiments are done with the complete system in order to determine the remaining parameters of the system. Cooling tests are conducted to validate the model concerning the heat exchange with the environment. The no-load experiments are conducted under ambient ventilation. Experiments without load allow studying the no load losses of the bearing and extracting the f0 parameter, which should be experimentally evaluated. The preload influence in the bearing supporting the spiral bevel pinion is computed too, since a hot spot are observed near this area on the transmission under operation. By default, tests are conducted with an anticlockwise rotation of the input shaft, unless otherwise indicated.

Additionally, loaded tests have been conducted to study the tooth friction coefficient. In loaded tests, the power losses related with the bearing load are lower than those of the gears. The latter can therefore be properly characterized. The motor has its own fan mounted on the motor shaft: the rotational speed of the fan is the one of the motor. The system is under forced ventilation in loaded cases.

Finally, elements influencing the thermal behavior of the gear unit are studied with respect to the transmission efficiency. Design modifications are suggested to improve the thermal behavior of the gear unit.

The tests rig were designed by the designer at Moteurs Leroy Somer accounting for the constraints the author formulated, tests were conducted by the test team. The author managed the design of experiments and the analysis of results in the context of the PhD.

2. No load tests on the gear unit

2.1. Description of the test rig for no load test

The test rig for no load tests consists of an electrical motor linked to the gear unit (Figure 45). The motor is monitored to control its speed, its coil temperature and electrical energy consumption. The gear unit is equipped with thermocouples to follow the temperature evolution of its internal elements (bearings for example). Tests are conducted under ambient ventilation (no fan on the motor) and the supporting plate is insulated to avoid heat exchanges through the supporting plate.

The measures of the no-load tests are realized in two steps, since the torques involved are very low (few Nm). It means that a torque sensor is not accurate enough to measure the no-load power losses.

First, the no-load measurements are conducted on the gear unit: a motor is linked to the gear unit and a voltage is imposed to the motor to make it runs at its nominal speed. The output shaft of the gear unit is not connected. A tachometer is used to measure the motor speed. To avoid uncertainties, no speed variator is used, moreover power losses measurement are more accurate near the nominal speed: it requires the use of the associated motor for each speed. Three motor were used: one for each speed to improve the reading of the power loss thanks to better speed measurement and stability. A voltage is imposed to the motor: the rotational speed, energy consumption and coil temperature are noted for each test.

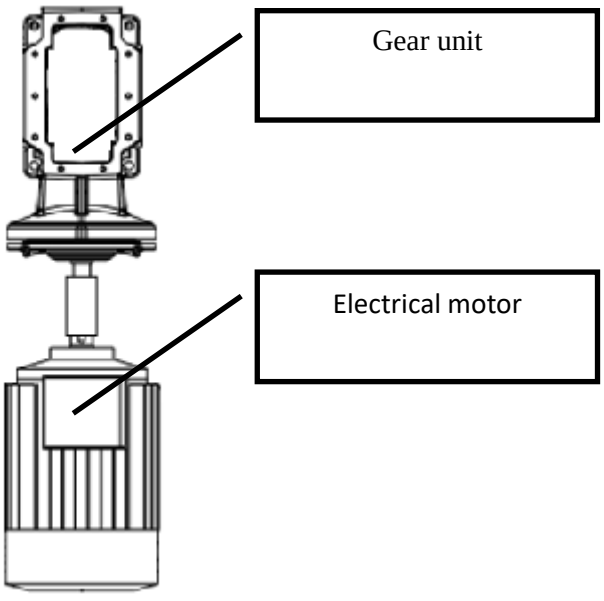

Figure 45: test rig for the no load tests (top view)

Then the second step is a precise identification of the motor characteristics which is required to determine accurately the no load losses of the transmission, which is about tens of Nm. The link

between the motor speed and its power losses is used to define the motor characteristics. The bench with Foucault current (see Figure 46) is used to measure the power losses associated with the speed at a given coil temperature. The motor is linked to a rotating disk, which undergoes Foucault current imposed by a jaw under voltage. The jaw is linked to a mass and moves under the induced resisting force resulting from the rotation of the disk under Foucault currents, the little movement around the jaw axis allows displaying the resisting torque. The Foucault currents appear in conductive bulk, either by variating the magnetic flux crossing the medium either by displacing the bulk through a magnetic flux. The resisting torque equals the power output at the imposed speed and coil temperature.

The power output equals the resisting torque imposed by the no-load losses of the gear unit in the step one. The measures are repeated of each of the operating conditions in step one to define the output power of the motor in all conditions. It means that the power loss of the gear unit is known after completing the second step for the three speeds tested.

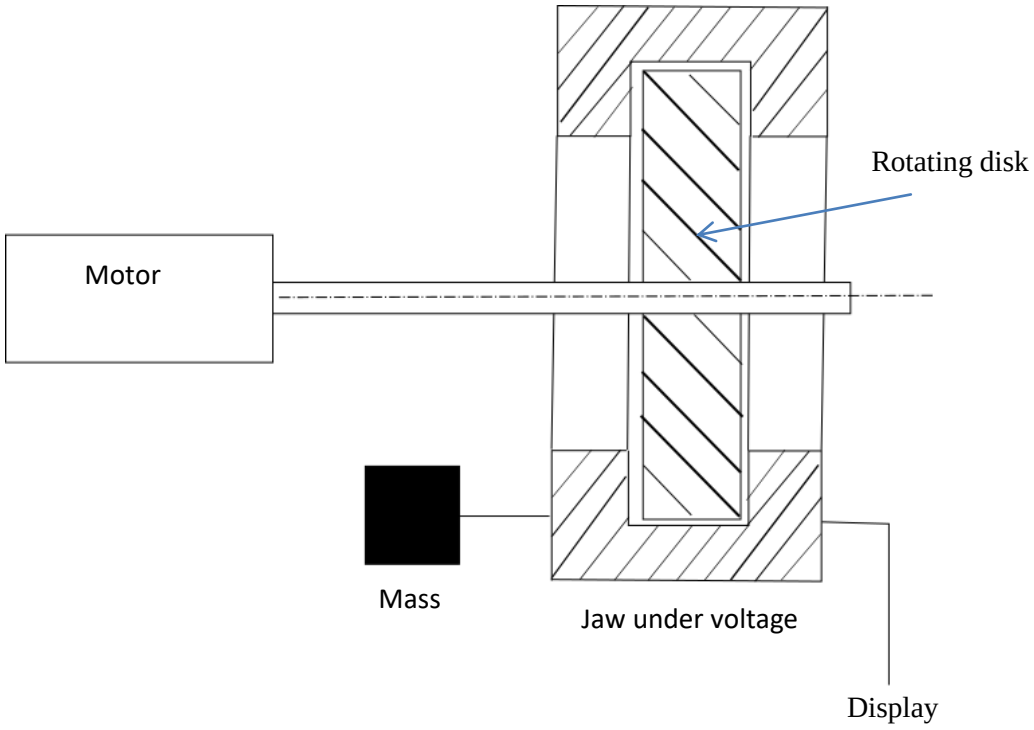

Figure 46: bench with Foucault current between the jaw and the rotating disk

Several thermocouples were placed at different positions in the gear unit, see the red dots reported Figure 47. Thermocouples are placed on the housing, on the external ring of bearings and in the oil bath.

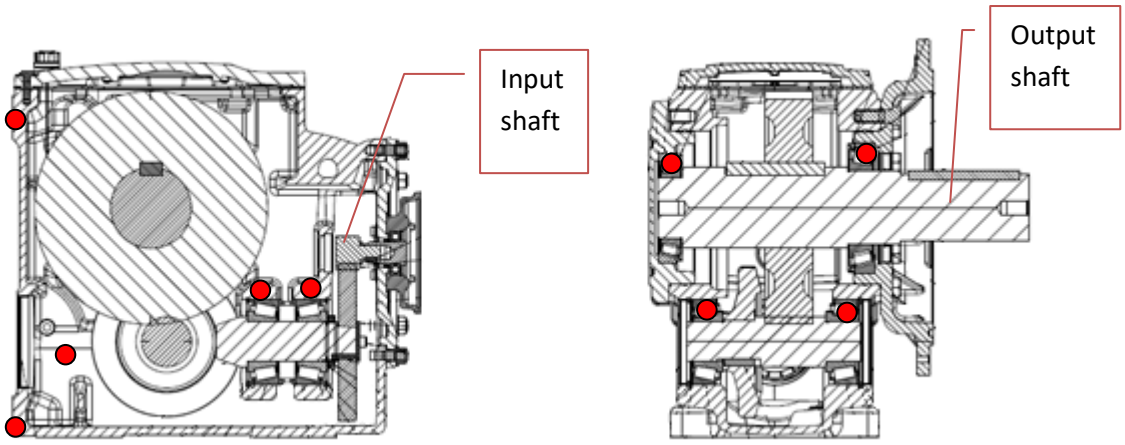

Figure 47: positions of thermocouple

The test rig elements are described in **Table 7**.

Table 7: no load test rig characteristics

	N°	Brand	Reference	Accuracy	Range	Comments
Tachometer	84111	BREMI	BRI5046	+/- 0.1 RPM		
Bench with Foucault current	-	Zöllner	Bench 10Nm	Reading uncertainty = +/- 0.1Nm	0 à 10 Nm	Resolution 0.2 Nm Direct reading of the torque value
Thermocouple			Type T and K	+/- 1.5°C on measuring range (0°C-100°C)		
Recorder	84389	GRAPHTEC	GL450	Thermocouple type K ±(0.05 % of reading +1.0 °C)	-100 °C ≦ T ≦ 1370 °C	
				Thermocouple type T ±(0.1 % of reading +0.5 °C)	-100 °C ≦ T ≦ 400 °C	
Motor	Reference	Shaft Height	Power	Voltage	Frequency	Ventilation
			kW	V	Hz	
2 Poles	LS	100	3	230-400	50	No fan
4 Poles	LS	100	2,2	230-400	50	No fan
6 Poles	LSES	100	3	400-690	50	No fan

2.2. Validation of the heat-transfer model with the environment – no load test rig

The transmission behavior during cooling tests is used to validate the calculation of heat-transfer between the gear unit and the environment. Ambient ventilation is considered and the motor does not rotate. The reducer is placed on the no-load test rig in the test area and its behavior during cooling down is monitored thanks to thermocouples, after a heating phase where the system heated itself under operation for several hours.

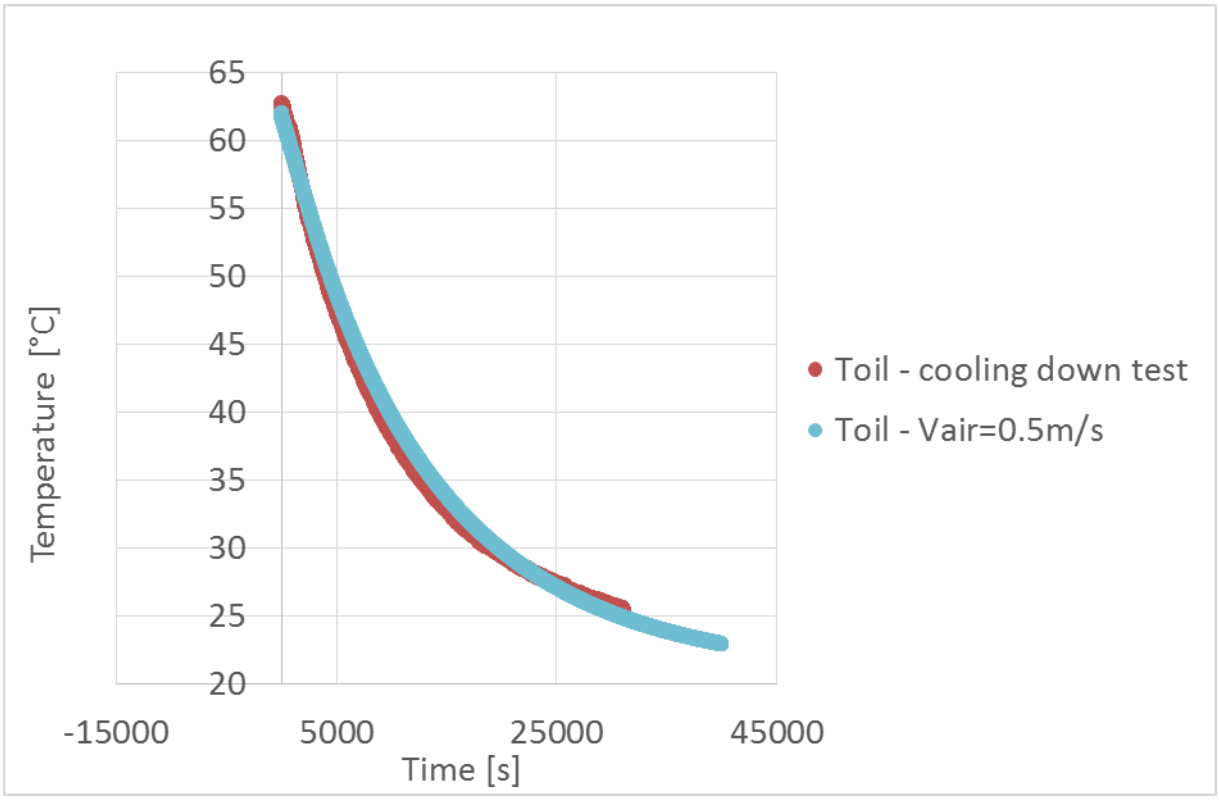

Figure 48: no load test configuration – cooling down test – 5.75L

Figure 48 shows the temperature evolution of the oil bath as a function of time for experimental measure in cooling down test and the theoretical model results. In the test area, an anemometer was used to measure ambient ventilation: a value under 0.5m/s is obtained (0.3m/s is obtained but it is lower than the recommended measure range). This value is in accordance with the measuring range and the simulated value obtained.

From these observations, the model represents well the behavior of the transmission since the temperature derivative is reproduced. Since the theoretical thermal behavior is in accordance with experimental results, the thermal model is valid concerning the exchange with the external environment, for example the ambient air.

2.3. Validation of the no load model

The behavior of the model under cooling down conditions being checked, the model is considered under a heating phase for no-load condition.

Tests are conducted varying the speed of the motor: 1000 RPM, 1500 RPM and 3000 RPM. Two tests with different oil levels are used to define the f0 evolution (equation 40 and 41) , see Figure 49 and Figure 50. The f0 parameter accounts for no-load losses of bearings and is influenced by the immersion level of the bearings. The exchange level with the external environment is estimated from cooling down tests. Neglecting the thermal resistance of conduction and convection with the oil, the power losses and the temperature difference between the oil and the air are linked by the thermal resistance estimated based on cooling down tests. It defines a theoretical line that is plotted on the Figure 49 and Figure 50.

The measures at 1000 RPM and 1500 RPM are valid since the previous proportionality is respected. However the 3000 RPM shows a difference with respect to measures at 1000 RPM and 1500 RPM, only the results at these two speeds are considered in the following.

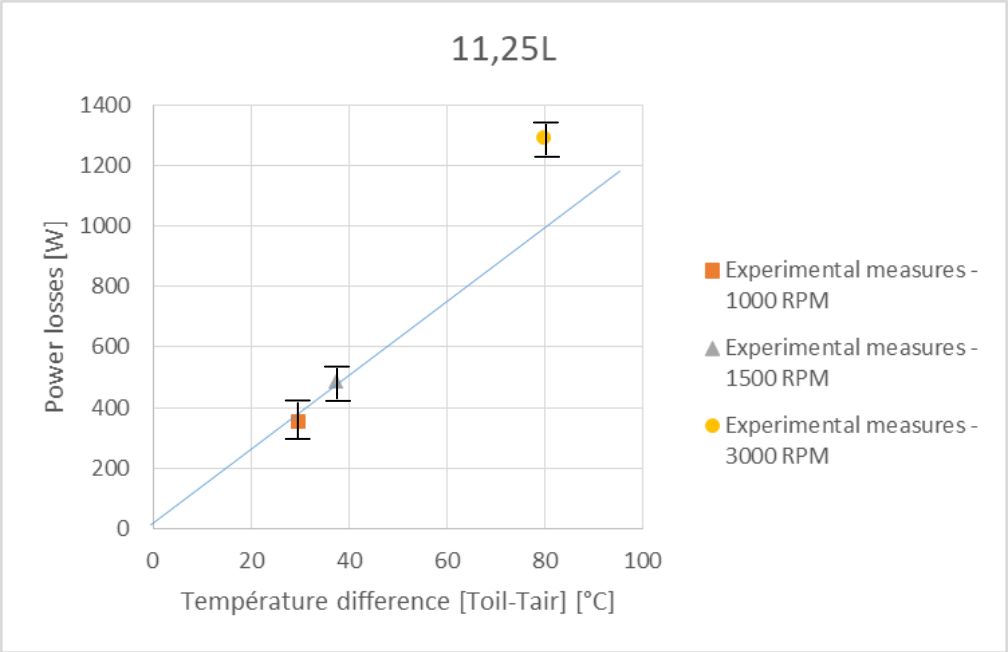

Figure 49: experimental measures of the no-load tests – 11.25L of oil

The f0 bearing parameter for no-load losses value is obtained from catalog given in Schaeffler [3] depending on the bearing type (see Table 8).

Table 8: f0 values [3]

Bearing	f0 value	
	Oil bath	Grease
Ball bearing	2	/
Tapered roller bearing	6	/
Roller bearing	/	2
Spherical roller bearing	/	2.7

Temperatures of bearings (number refers to Figure 7) are in accordance with the experimental measurements as shown on Figure 50, for the 5.75L oil level.

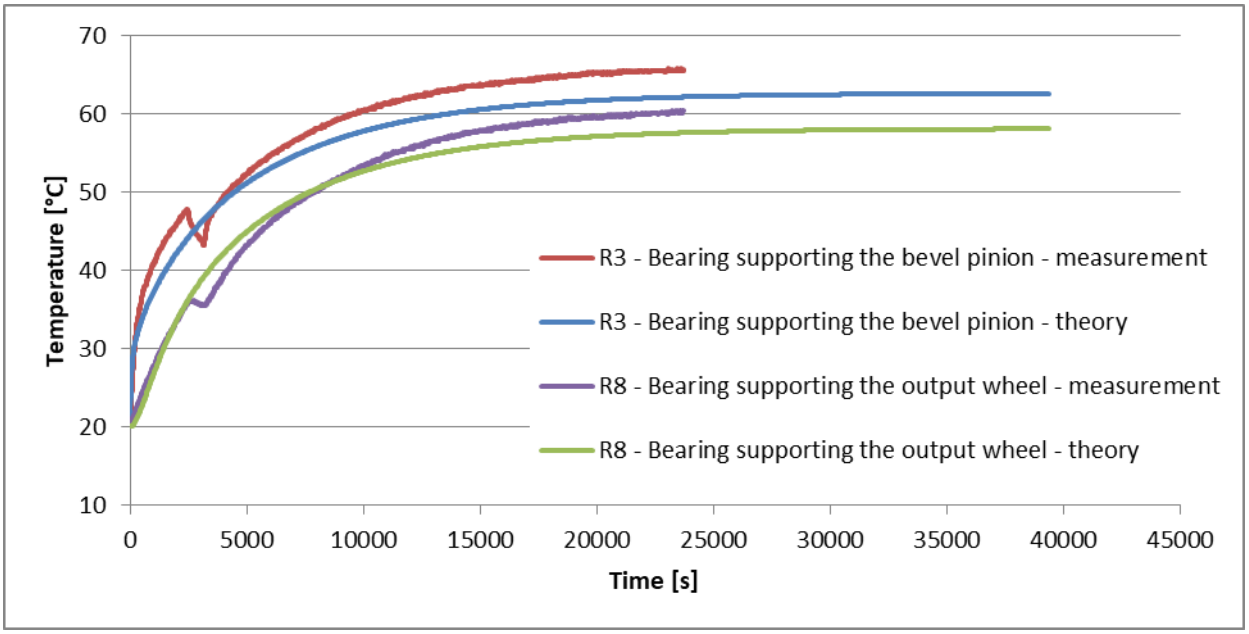

Figure 50: evolution of the bearings temperature – measurements VS theoretical results - 1500 RPM and 5.75L of oil

It is assumed that f0 (equation 40 and 41) changes with the immersion level. Schaeffler proposes a variation between 1 to 3 (Figure 51) as the immersion of the bearing increases from the minimum level –which is located at half the diameter of rolling elements- to the axle level, instead of Harris that proposes a range between 1 and 2. The Harris evolution is considered linear in our study.

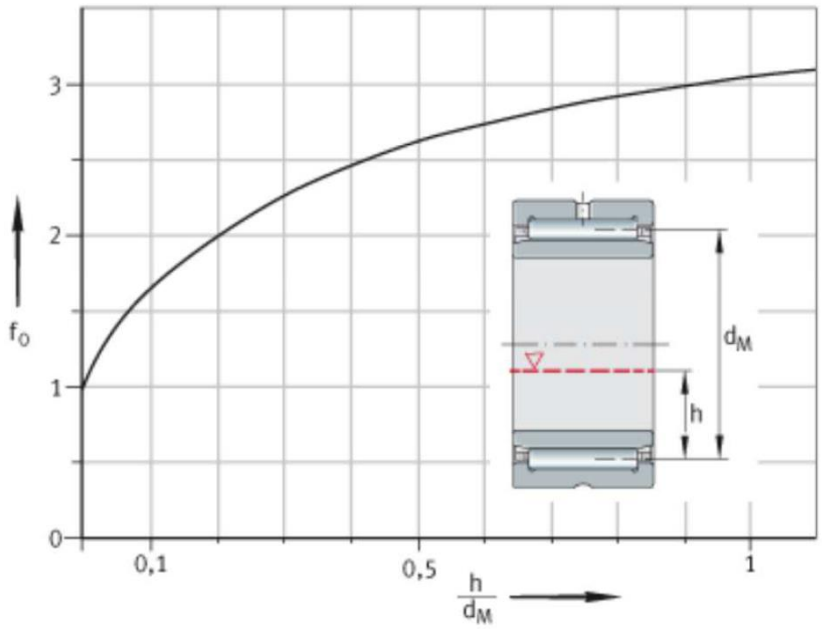

Figure 51: Schaeffler evolution of the f0 [3]

Figure 52 and Figure 53 show the power losses as a function of the temperature difference between oil and air for two kinds of oil volume.

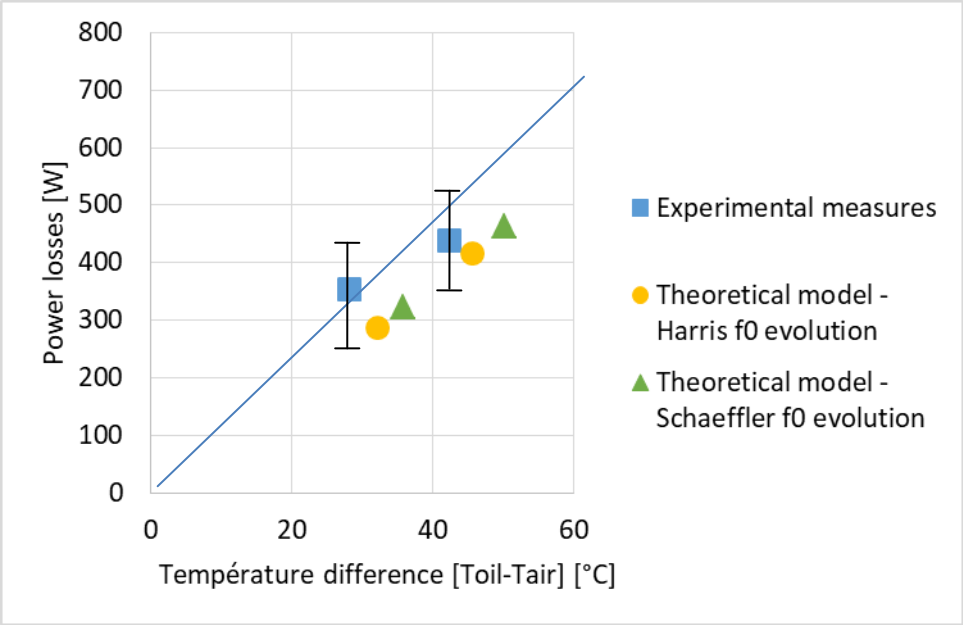

Figure 52: evolution of power losses as a function of temperature difference between oil and air – 5.75L of oil

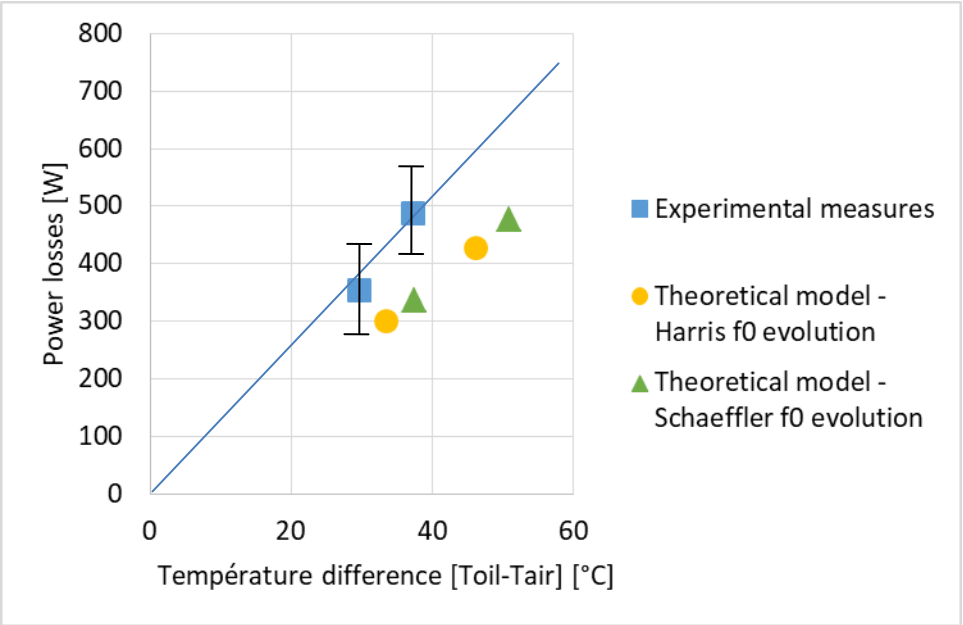

Figure 53: evolution of power losses as a function of temperature difference between oil and air – 11.25L of oil

Considering the tests, the f0 evolution proposed by Harris appears slightly closer than the Schaeffler evolution (Figure 51).

The evolution of the f0 parameter (Harris formula – equation 40 and 41) with the immersion level improves the theoretical results, as shown on Figure 54 and Figure 55.

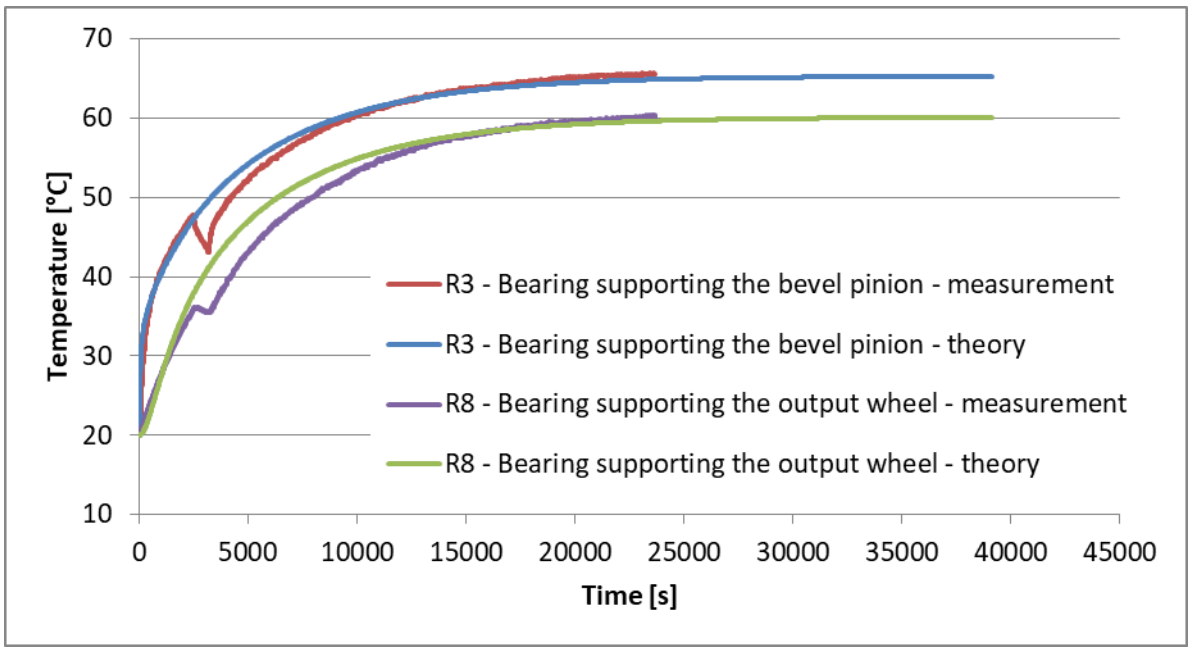

Figure 54: evolution of the bearings temperature considering f0 evolution – measurements VS theoretical results - 1500 RPM and 5.75L of oil

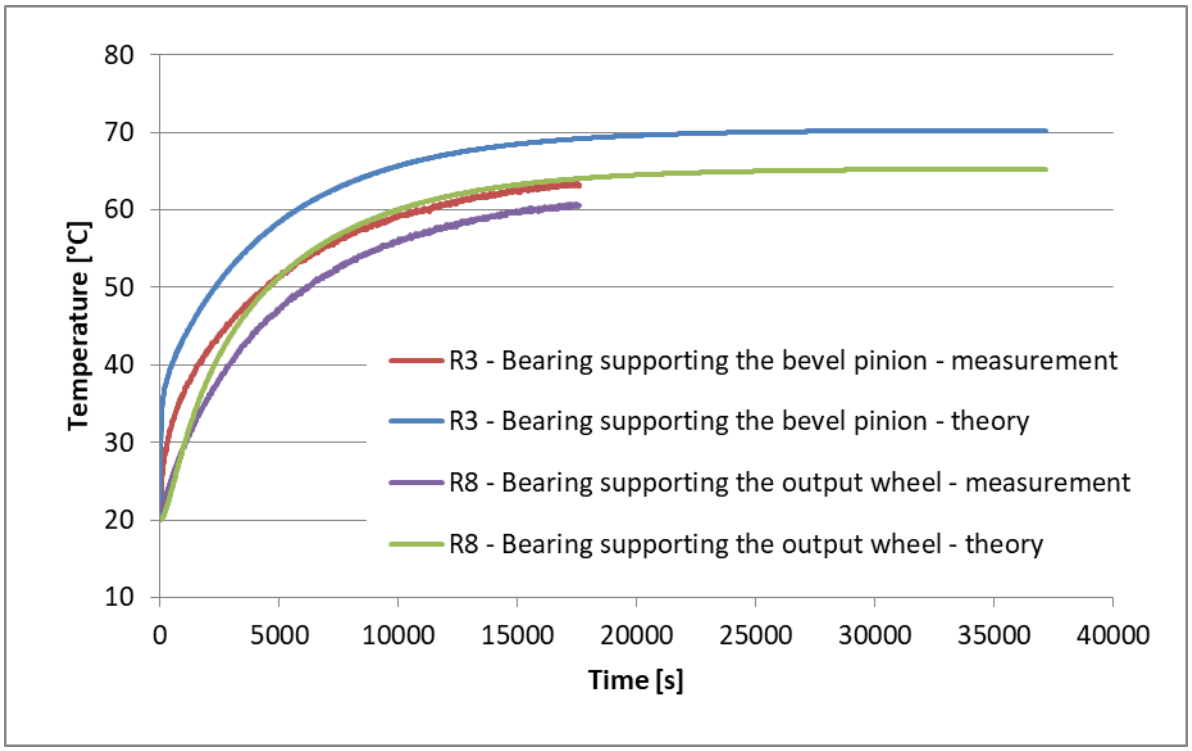

Figure 55: evolution of the bearings temperature considering f0 evolution – measurements VS theoretical results – 1500 RPM and 11.25L of oil

The f0 parameter (equation 40 and 41) level and evolution included in the model allows reproducing the slope of the heat exchange. The no-load parameter f0 accounting for the immersion influence on the behavior of the bearings is validated. The difference between the model and the measures are in a range under 5°C and below the uncertainty range in the estimation of the power losses.

In the following, the f0 evolution and values are retained since the values found in catalog and the Harris evolution of this parameter are consistent with experimental observation. Here the bearings are significantly immersed at low level so the difference between the two levels is not obvious. However the f0 evolution is still considered in the following.

In the following, the results only concern the default oil level which is 5.75 L in the oil bath.

2.4. Preload on the bearings

The load on bearings is computed by the model from the resulting loads exerted on the bearings, for example the model accounts for the preload or meshing efforts exerted on the associated bearings.

The tapered roller bearings supporting the spiral bevel gear are preloaded and this preload leads to extra losses of these bearings. To estimate the impact of the preload on the global behavior of the gear unit, the preload is theoretically studied considering the gear unit under no load operating conditions. In this case, the bearings generate more than 75% of the total losses in the gear unit, and the bearings supporting the spiral bevel gear represent more than 75% of the bearing losses when they are preloaded at 30 kN. The preload of 30 kN is less than 10% of the maximum recommended static load since its static load limit is 335 kN and its dynamic load limit is 264 kN. An example of repartition of the losses between the seals, bearings, gears and churning losses is presented in Figure 56.

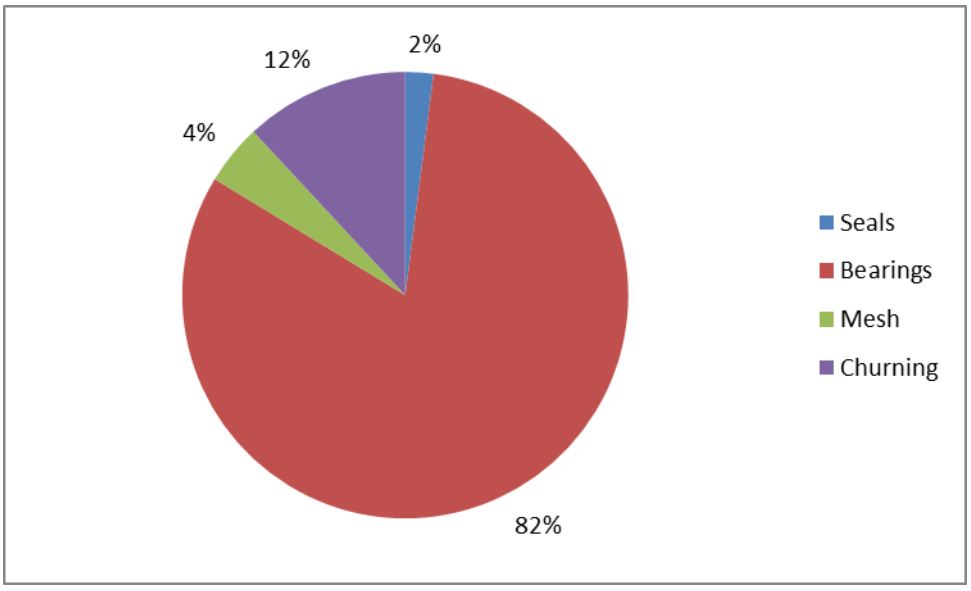

Figure 56: power losses distribution – no load test – 1000 RPM

A variation between 0 and 100kN of the preload is imposed to observe the impact on the temperature evolution and on the power losses. The results are plotted as a relative increase in power losses and temperature compared to the case of no preload exerted on the bearings as shown on Figure 57.

The standard preload is 30kN in our study. It is shown on Figure 57 that under 20kN the impact of the preload does not much influence the temperature and the power losses. Above this value, the power losses and the temperature are much influenced by the preload of the bearings of the spiral bevel pinion. Since the temperature and power losses of the model are in accordance with those obtained through tests, the model is validated. The power loss or temperature distribution is not in accordance with experiments if the preload is changed.

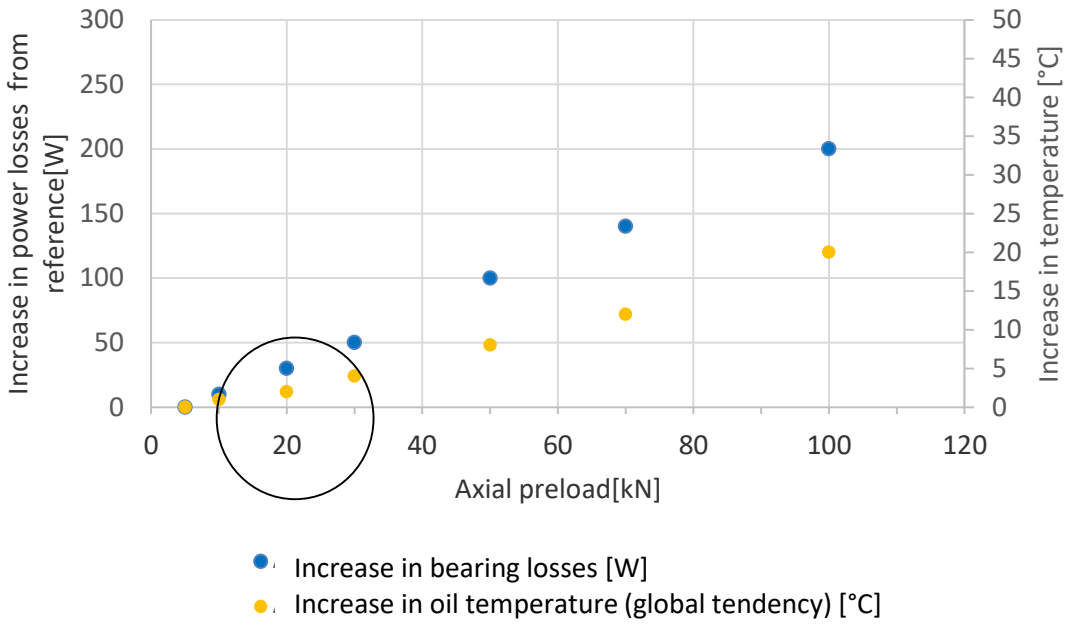

Figure 57: influence of the preload of the bearings supporting the spiral bevel pinion – 1500 RPM – no load test

It appears that reducing this preload is not interesting since it does not lead to any significant reduction in losses or temperature. Preload level was determined primarily to ensure enough stiffness for the spiral bevel mesh. One can notice that the applied preload is therefore located in the optimal area: increasing preload would begin to negatively impact the thermal behavior of the gear unit, while decreasing it would deteriorate the gear mesh, possibly leading to vibrations and even gear scuffing.

3. Loaded tests on the gear unit

Once the no load tests have been compared to theoretical results, the loaded tests are used to validate the behavior under load of the model. The impact of the friction coefficient is tested in this part through the reverse engineering method. If the load level and temperature distribution corresponds to the theoretical values obtained with the model, then the model is validated under this condition.

3.1. Description of the test rig for loaded test

The objective is to load the gear unit under various speeds and load conditions to study its thermal behavior under different operating conditions. The loaded test rig includes an electric motor that is

linked to the gear unit. The gear unit is coupled with a multiplier and an electric generator that allow loading the system. The multiplier allows reducing torque and increasing the rotational speed in order that the electric generator can exert a resisting torque in good conditions. The electrical motor and the electric generator are connected to the electrical network through an electrical cabinet.

Torque meters are placed between the motor and the gear unit and between the gear unit and the multiplier. These two torque meters allow isolating the power losses of the gear unit from the whole system. The system is placed on a metallic plate (Figure 58) and the location of the elements is reproduced on Figure 59. Thermocouples are placed at the same position that the previous tests (see Figure 47).

Operating conditions are given in function of the motor speed and torque.

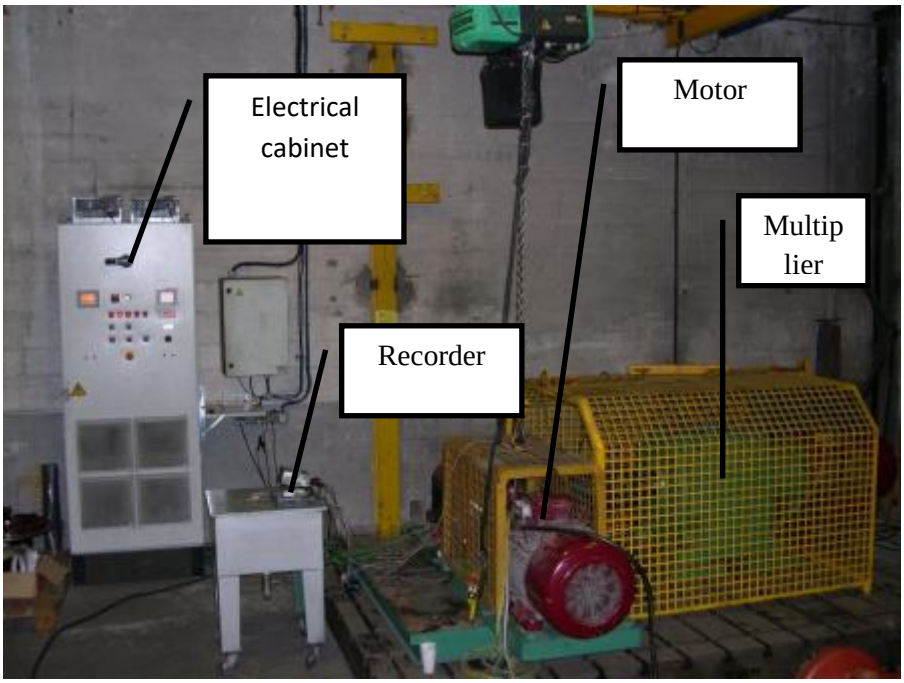

Figure 58: test rig for loaded tests

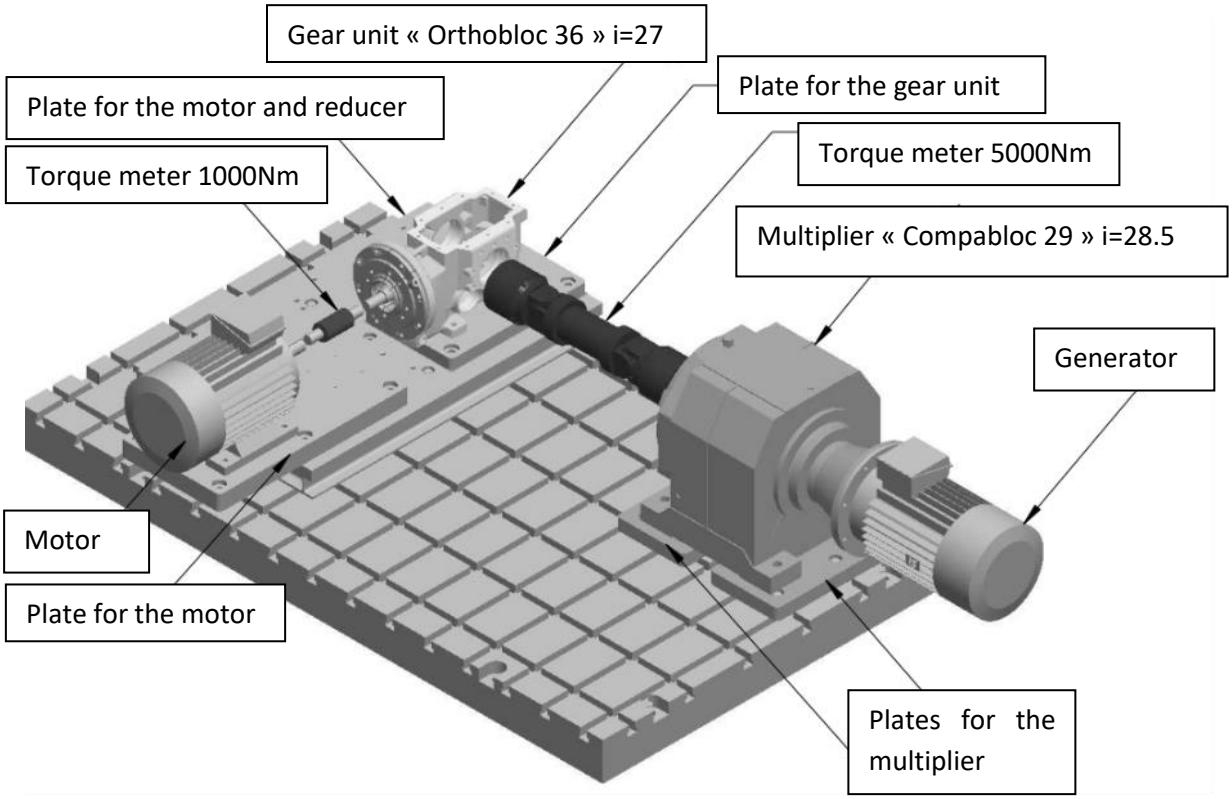

Figure 59: test rig for the loaded tests

The elements are detailed in **Table 9**.

Table 9 : Material in the loaded tests

	N°	Brand	Reference	Accuracy	Range	Comments
Thermocouple			Type T et K	+/-1.5°C over measuring range (0°C to 100°C)		
Recorder	84389	GRAPHTEC	GL450	Thermocouple K ±(0.05 % of reading +1.0 °C)	-100 °C ≦ T ≦ 1370 °C	
				Thermocouple T ±(0.1 % of reading +0.5 °C)	-100 °C ≦ T ≦ 400 °C	
Recorder	84389	GRAPHTEC		0.1% of full scale	20V	5000Nm = 10V
				0.1% of full scale	5V	1000Nm = 5V
Torque meter	133273	SCAIME		0,05% of full scale	+/- 5000Nm	
Torque meter	145078	MEIRI	CR7 DM260	0,1% of full scale	+/- 1000Nm	Calibrated on 22/04/2014 at CETIM
Electrical cabinet	TH29959	DEI	-	-	-	

Materials	Type	HA	Power (nominal)	Voltage	Frequency	
Motor	LSRPM	200	55	360	50	Nominal speed: 1500 RPM
Generator	GLSRPM	225	70	360	50	Nominal speed: 1500 RPM

Materials	Order N°	Type	Size	Reduction ratio		Comments
Multiplier	400118762	CB	29	28,5		
Gear unit		OT	36	28		

3.2. Heat-transfer between housing and environment

The loaded test rig is placed on a metallic plate instead of the configuration of the no load test rig. The influence of this plate is studied on a cool down test.

The thermal network is modified to account for this new heat exchange: a node and a thermal resistance of conduction are added to account for the heat transferred to the metallic plate.

Compared to the initial thermal network, the node 28 is added (see Figure 60) and a conduction heat-transfer between this node and the bottom of the housing is taken into account.

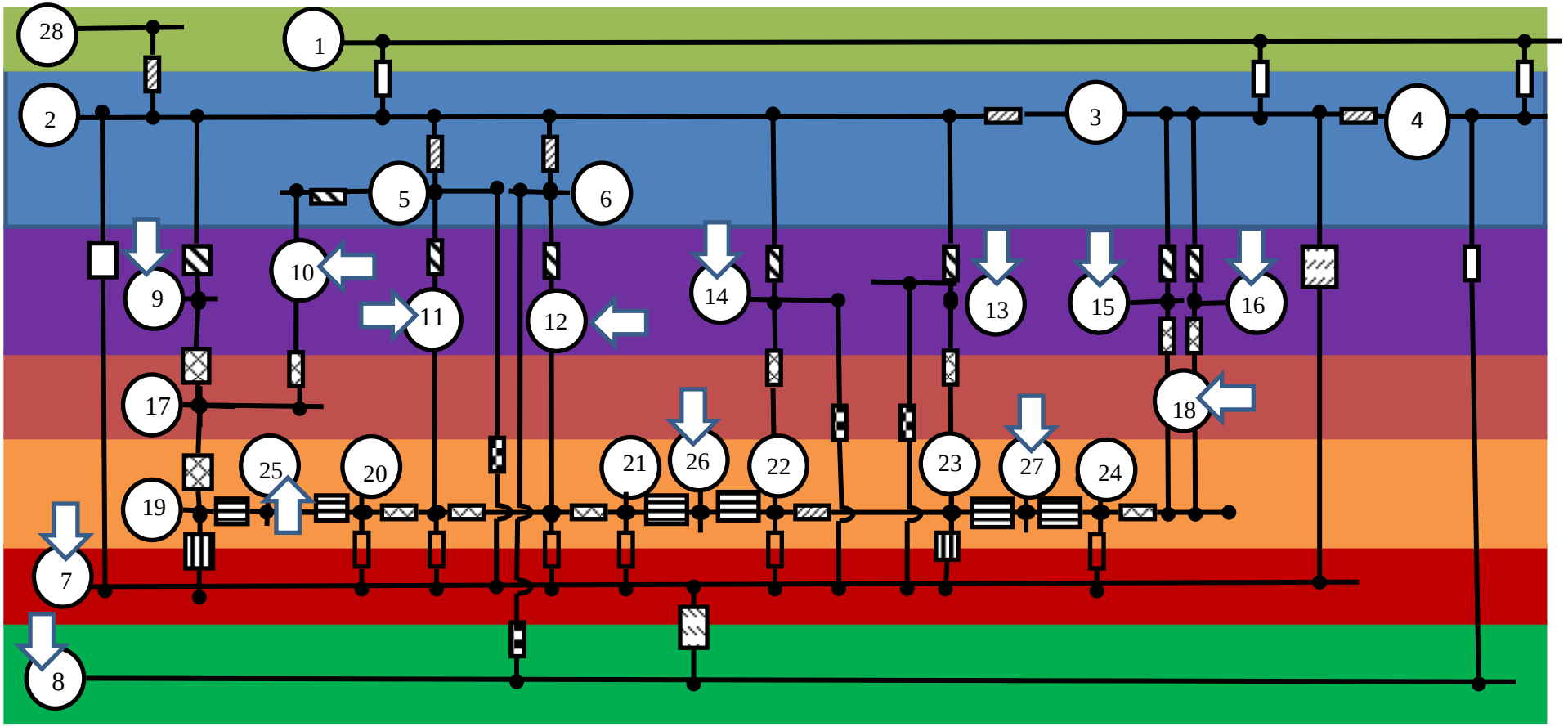

Figure 60: thermal network of the loaded test rig

The symbols are kept the same as the Table 2 given in chapter I. The list of nodes is given in **Table 10**.

Table 10: Nodes of the thermal network – influence of the supporting plate

Nodes	Description
1	Ambient air
2	Bottom of the housing
3	Top of the housing
4	Housing cover
5	Housing – area of the motor side bearing
6	Housing – area of the output side bearing
7	Oil bath
8	Air in the housing
9	Bearing – motor side – first gear
10	Bearing – output side – first gear
11	Bearing – motor side – second and third gears support
12	Bearing – output side – second and third gears support
13	Bearing – conical bevel gear side
14	Bearing – helical output gear side
15	Bearing – motor side – output gear
16	Bearing – output side – output gear
17	Input shaft
18	Output shaft
19	First gear – input side
20	Second gear
21	Third gear
22	Fourth gear

Nodes	Description
23	Fifth gear
24	Sixth gear – output side
25	Input meshing
26	Second meshing
27	Output meshing
28	Test rig plate

From the model, the theoretical behavior of the gear unit is simulated with and without the influence of the supporting plate. Then the theoretical results are compared with experimental measurements and the influence of the supporting plate is observed on Figure 61.

The ambient ventilation of 0.3m/s is retained as the ventilation condition is similar to the one for the no load tests.

The behavior is modified when accounting for the influence of the heat transferred to the supporting plate: the slope of the evolution of the temperature in the cooling down test is steeper when considering the gear unit placed on the metallic plate. The stabilized value of the system is the air temperature since the supporting plate is large enough to have the same temperature that the ambient air far from the gear unit.

From the results, the influence of the supporting plate impacts the thermal behavior of the gear unit, allowing a supplementary heat transfer to the environment (5°C difference in this case). The behavior of the model and the gear unit when considering the heat exchange to the environment is validated: the maximum difference between the theoretical temperatures and measurements is below 3°C.

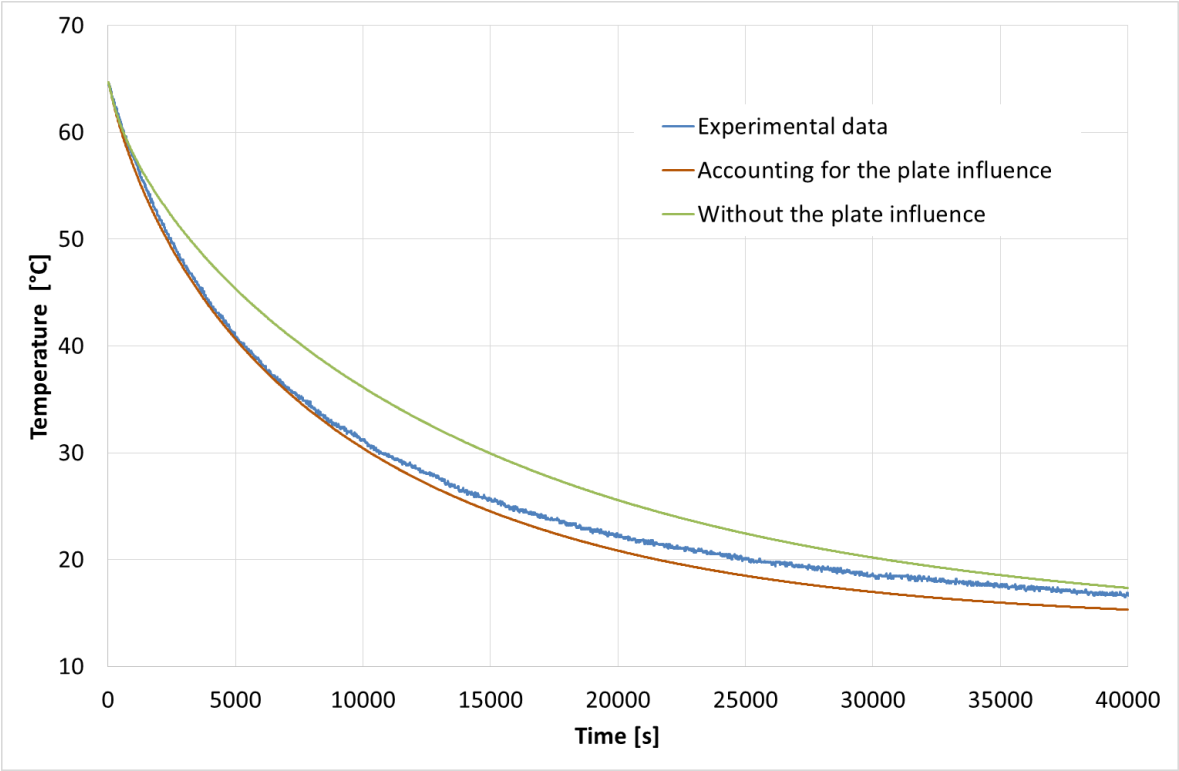

Figure 61: cooling down after a loaded test – temperature of the bearing supporting the bevel pinion

Since the model has been validated in the case of a cooling down test, the model is applied on a loaded test to define the ventilation level for one speed since the motor is equipped with a fan. Because of aerodynamic laws in turbomachines [4], the ventilation level increases linearly as a function of motor speed. The ambient air speed is measured at 1000 RPM and a linear law with the motor speed – the fan is on the motor shaft- is defined from this measure to determine the air speed for the other rotational speed of the motor.

The ventilation is 1m/s at 1000 RPM and the linear relationship with the motor speed is checked with experimental measurements in the environment of the test rig. It results in a linear law with 0.8m/s at 800 RPM, 1m/s at 1000 RPM and 1.5m/s at 1500 RPM. Experimental measures of the ventilation at several motor speeds appear to respect the linear law based on the initial measure of 1m/s at 1000 RPM.

Power losses evaluation of the model is compared with experimental measurements on Figure 62. The values given by the model belong to the uncertainties range of the power loss measuring method. Uncertainties in torque measurement are 1 Nm on output shaft and 0.5 Nm on output shaft. Uncertainties on the recorder lead to 10 Nm of uncertainties on the output torque and 1 Nm on the input torque. The global uncertainties on measurement of power losses vary from 190 W for 800 RPM to 400 W for 1500 RPM. The friction coefficient of the gear mesh is fixed for all gears and all operating conditions.

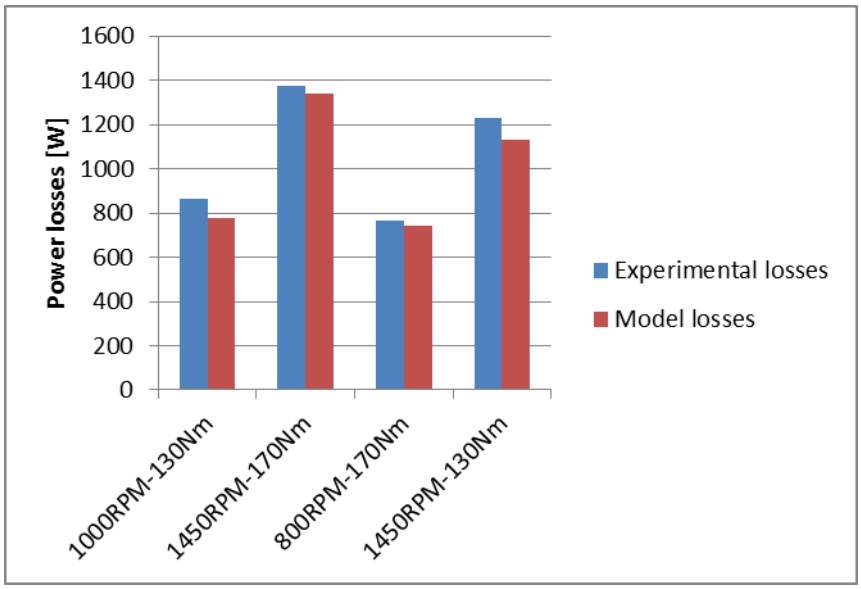

Figure 62: comparison between experimental measures and model power losses

The thermal network needs to be validated both in terms of power losses and temperature level. Temperatures are measured at different points of the gear unit: oil and several bearings on different shafts. The comparison of theoretical and experimental values is shown in Figure 63.

The tests at 1000 RPM and 800 RPM show that the bearing located on the output shaft is always colder than the estimation: the explanation is found in the fact that the convection of the output shaft with the air tends to cool down the surrounding elements, including the bearings. This heat transfer is not taken into account in the thermal network. The same tendency is found on the test at 1450 RPM.

In the case of the test at 1450 RPM and 170Nm, the value of the temperatures appears to overestimate the experimental measures. When the motor is operating at full load, the power electronics is cooled down by a fan that is turned on and off automatically to refresh the electronics: it increases the ventilation level in the test rig area. A test in similar conditions with the ventilation partly obstructed leads to oil temperature above 85°C, which shows the non negligible impact of a change in the ventilation level. In the case of the full load test, the power losses are correctly estimated. However the friction improvement in the tests due to optimal tooth geometry for the full speed and full load operating condition and the punctual extra ventilation of the power electronics leads to reduced experimental temperatures. The model considers constant friction coefficient along the path of action: the friction coefficient can be adapted in the model in function of operating condition to represent the experimental friction evolution.

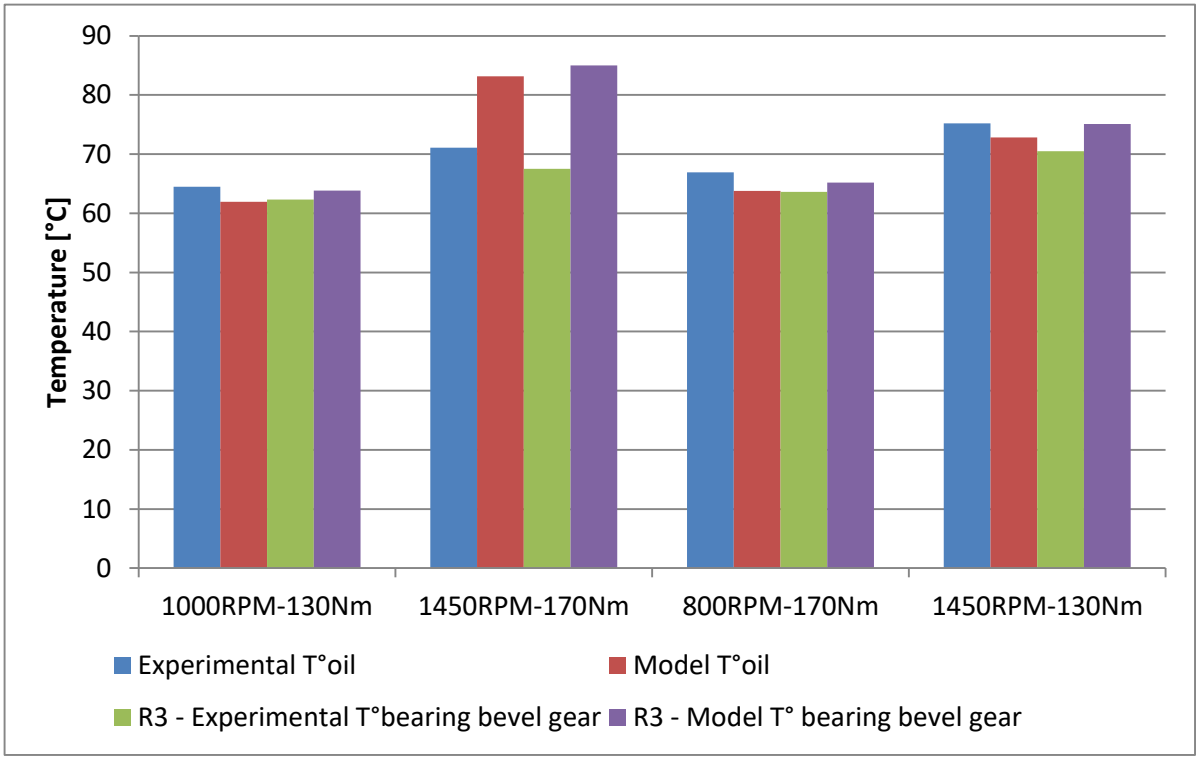

Figure 63: comparison between experimental and model temperature

Based on the loaded test, the validity of the model is evaluated for different operating conditions. Some discrepancies are observed and their sources are identified. The validation criterion is that the power loss estimation is within the uncertainty range (or below 10%) and the temperature discrepancy is below 10°C: it is the case for most of the tests.

Some systematic discrepancy is observed with the experimental results concerning the temperature of the bearing supporting the output wheel (Figure 63). This observation can be explained since the output shaft exchanges with the environment: this exchange is more significant as speed and temperature increase. Considering the exchange of the shaft with the coupling (see appendix A for details) and the ambient air in the case of the 1450 RPM and 130Nm, it results in temperature reduced of 10°C on the bearing of the output wheel (Figure 64) and 30 W of difference on power losses. The behavior of the other elements of the gear unit is much less impacted by adding this exchange (Figure 64).

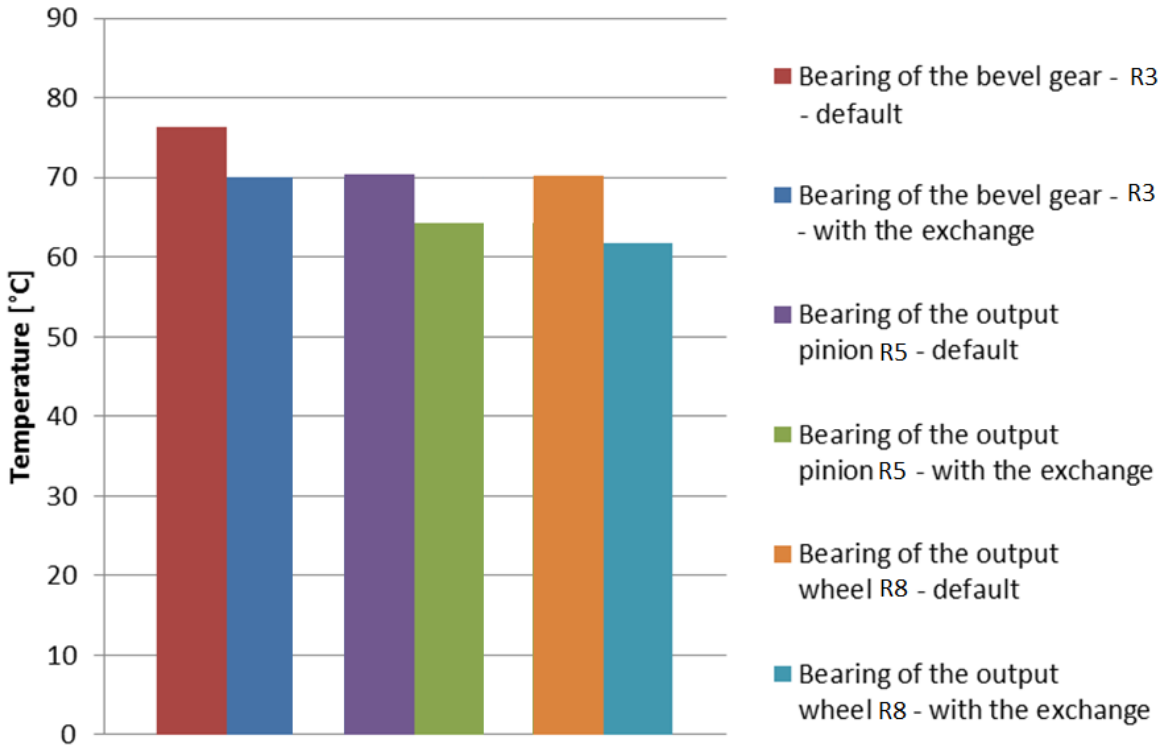

Figure 64: temperature comparison between the model with and without –default case- considering the exchange on the output shaft, for different bearings in the gear unit – 1450 RPM and 130Nm

It is important to note that the heat exchange on the output shaft is significant at high speed and high temperature. At lower speed, the impact of this exchange is only significant on the bearings of the output wheel and is much less influential on the other elements.

Since the heat-transfer is validated in the case of loaded tests, the friction coefficient influence is studied in the next part.

3.3. Influence of the friction coefficient

In the previous part, the model validation has been discussed. This section is focused on the influence of the change in the value of the friction coefficient on the power losses and temperatures of the system.

In case the friction coefficient is fixed to 0.05 for all gear pairs and all operating conditions, the proportion of the meshing losses represents always more than 50% of the total losses in loaded conditions (see Figure 65 – 1000 RPM and 130Nm). The meshing losses are important enough to impact significantly the total power losses; their precise determination is thus critical.

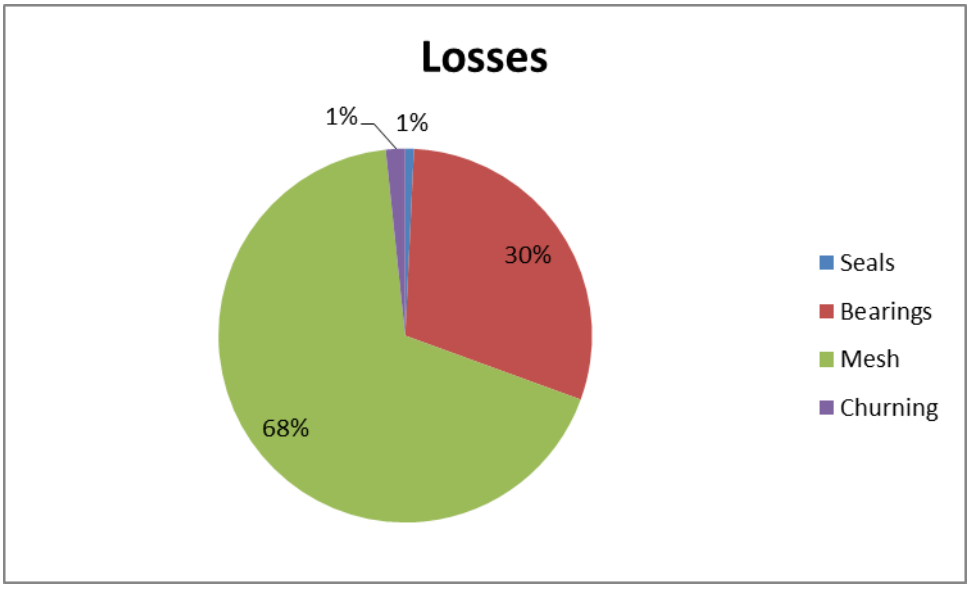

Figure 65: power losses distribution - f=0.05 - 1000 RPM and 130Nm

The friction coefficient is not fixed to a unique value in reality. Each different gear pair has its own friction coefficient. However the relative influence of the different gear pair is not the same. To evaluate the relative influence of the friction coefficient, ISO/TR 14179-2 [2] (equation 38) is used to estimate the friction in cylindrical gears. Then the reverse engineering method is used to determine the friction coefficient of the spiral gear mesh: the power losses and temperature distribution of the model should correspond to experimental measurement to validate the model. The friction coefficient of the spiral bevel gears is fixed at different level to study its influence on the total power loss and the temperature of the elements: the friction coefficient is constant along the path of contact but it is varied in function of operating condition. The friction coefficient of the bevel gear mesh is fixed at different level for each operating condition and the model is used to provide temperatures of the elements and power losses. The input gear friction coefficient is reduced and the output gear one is increased, for all the operating conditions tested, according to ISO/TR 14179-2. The bevel gear friction coefficient is changed to find the adequate value which gives the same power losses and temperatures than measurement. A range of consistent friction coefficient values is obtained accounting for the uncertainties in the power losses and temperatures.

The results for different values of friction coefficient are plotted on Figure 66. Accounting for uncertainties (around +/-100W in this case), the values of the friction coefficient below 0.08 appears to provide a significant value of power loss. Considering all studied cases for this operating condition, the friction coefficient of the input gear is $0.0365<f<0.0373$ and the friction coefficient of the output gear is $0.0893<f<0.0912$, obtained with the model considering equation 38 to compute the friction coefficient.

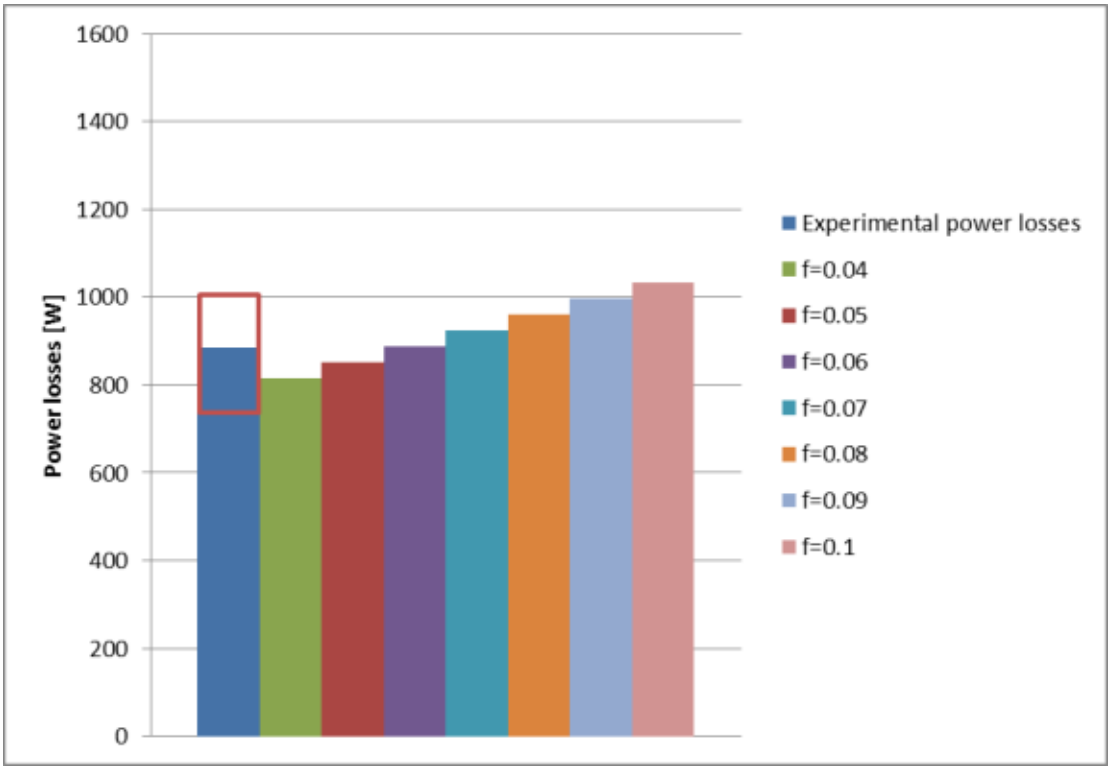

Figure 66: power losses for different friction coefficient of the bevel gear mesh – 1000 RPM and 130Nm

The values of temperature should also be considered: difference in temperatures below 5°C could be retained as valid. Comparisons with the oil temperatures are presented in Figure 67, temperatures of bearings are observed to follow the same trends, and are not reported for sake of clarity. To valid the behavior, values of friction between 0.05 and 0.07 are valid.

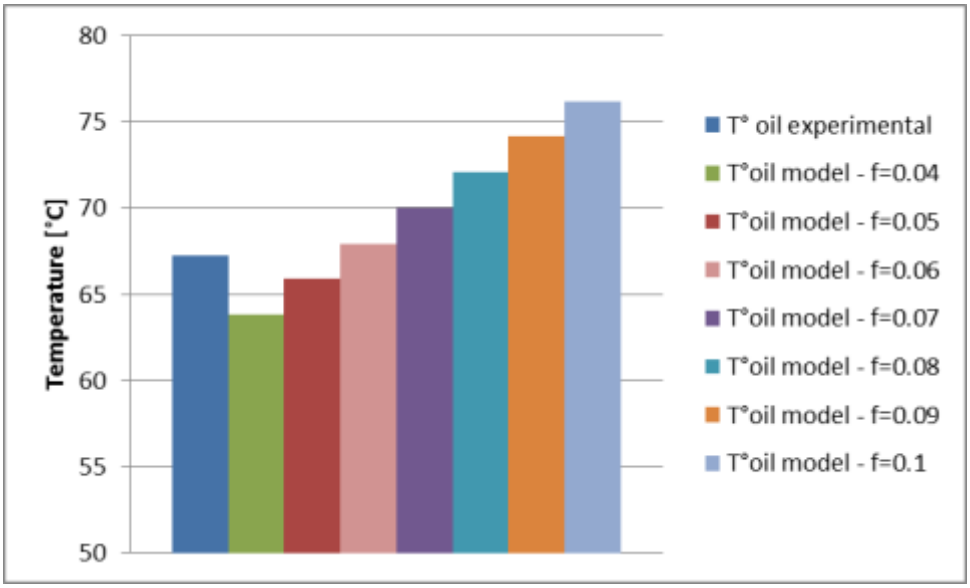

Figure 67: oil temperature for different friction coefficient of the bevel gear mesh – 1000 RPM and 130Nm

In order to valid the hypothesis that the friction coefficient is reduced in the case of full load cases, the same methodology is applied to the case of 1450 RPM and 170Nm of motor torque. The model can account for change in the direction of rotation – clockwise or counterclockwise on the input shaft- and shows changes in thermal behavior of the gear unit. The change in direction is considered through the change in loads direction exerted by the gears on the other elements: the load in the mesh is computed in the model in function of operating conditions, accounting the direction of rotation imposed by the motor. The comparison of the experimental and theoretical power losses is presented on Figure 68. Friction coefficient for the spiral bevel gear between 0.05 and 0.02 are consistent considering uncertainties on the power losses measure, as shown Figure 68 by the red box. Considering the studied cases for this operating condition, the friction coefficient of the input gear is 0.0368<f<0.0374 and the friction coefficient of the output gear is 0.0901<f<0.0916, accounting for the consistent range obtained for the friction coefficient in the spiral gear mesh.

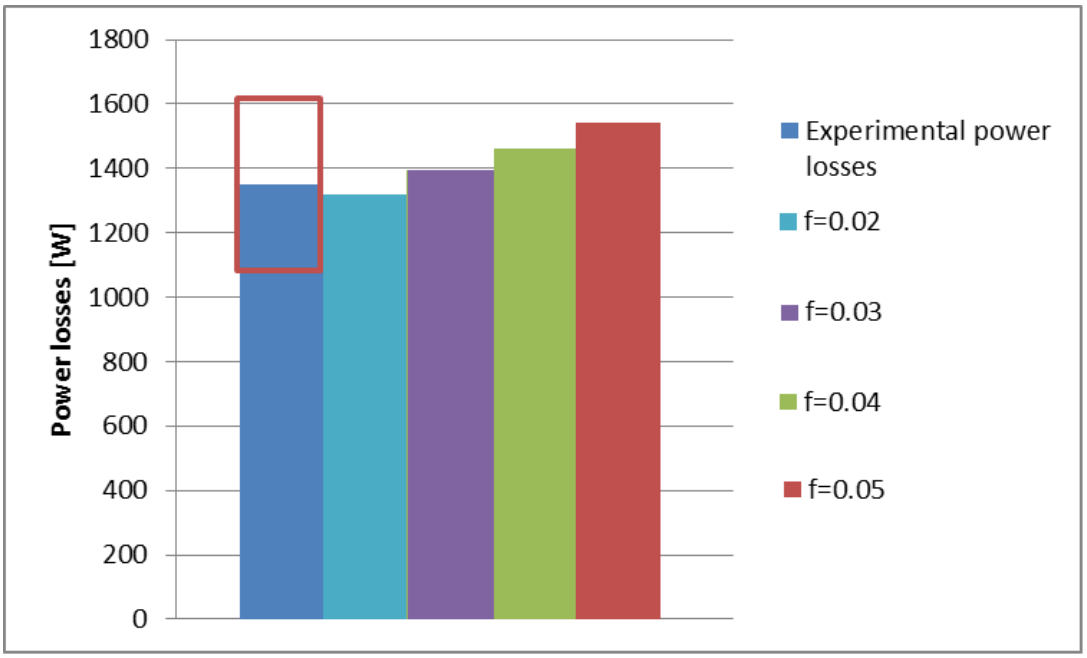

Figure 68: power losses for different friction coefficient of the bevel gear mesh – 1450 RPM and 170Nm – clockwise

The evolution of the power losses distribution as a function of the friction coefficient considered for the bevel gear mesh is shown on Figure 69 and Figure 71. The mesh power loss is reduced of 6% while the total power loss is reduced of 15% between the cases where the spiral bevel gear is considered equal to 0.05 or 0.02. The distribution of power losses is modified by the change in the friction coefficient as shown in Figure 70 and Figure 72.

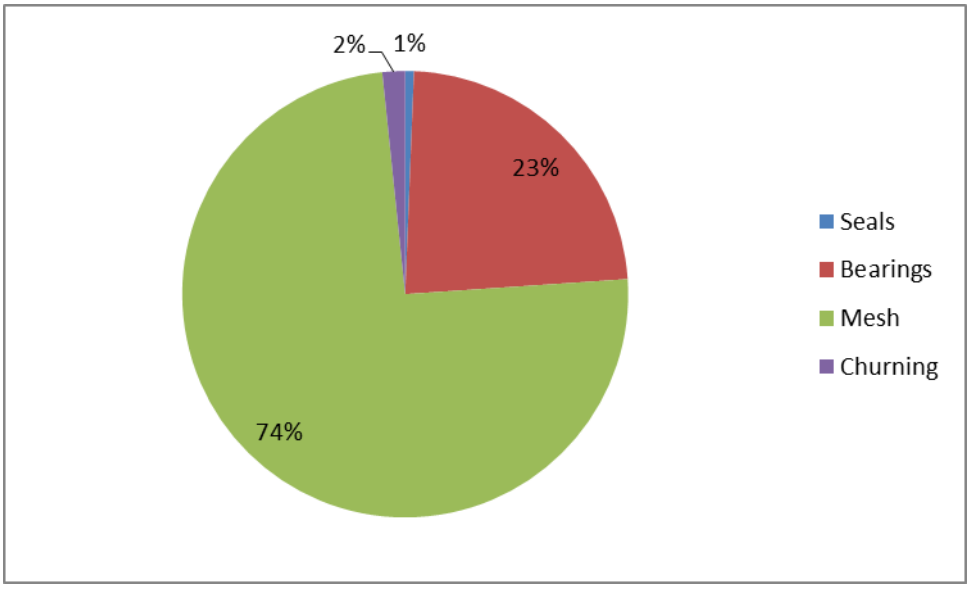

Figure 69: power losses distribution - 1450 RPM and 170Nm - clockwise – f=0.05

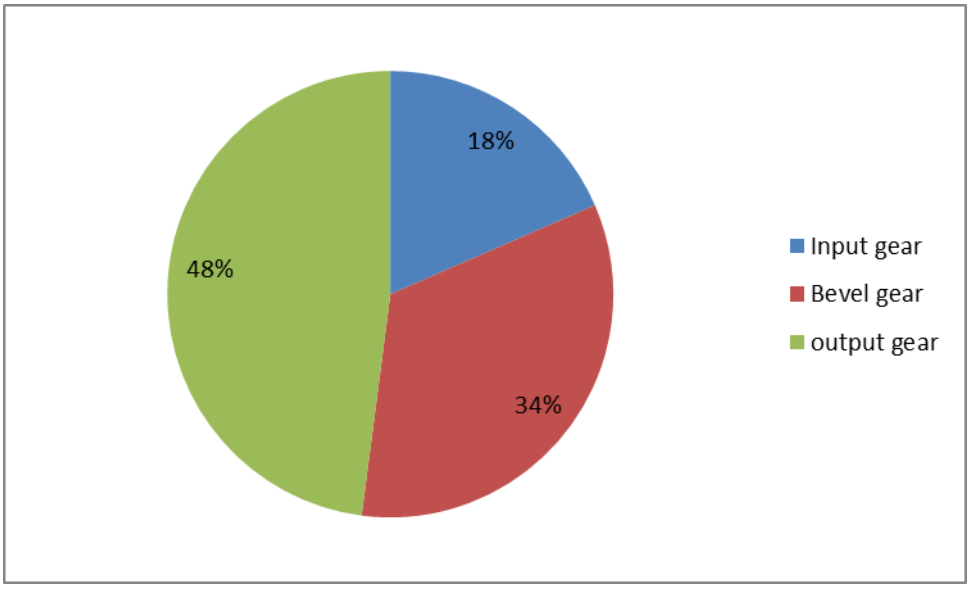

Figure 70: power losses distribution for gears - 1450 RPM and 170Nm - clockwise – f=0.05

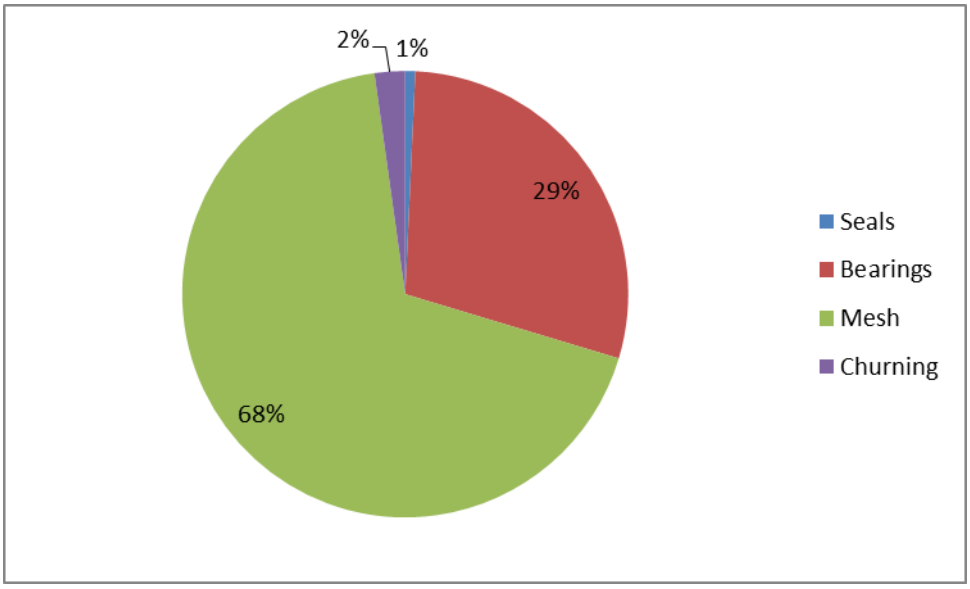

Figure 71: power losses distribution - 1450 RPM and 170Nm - clockwise - f=0.02

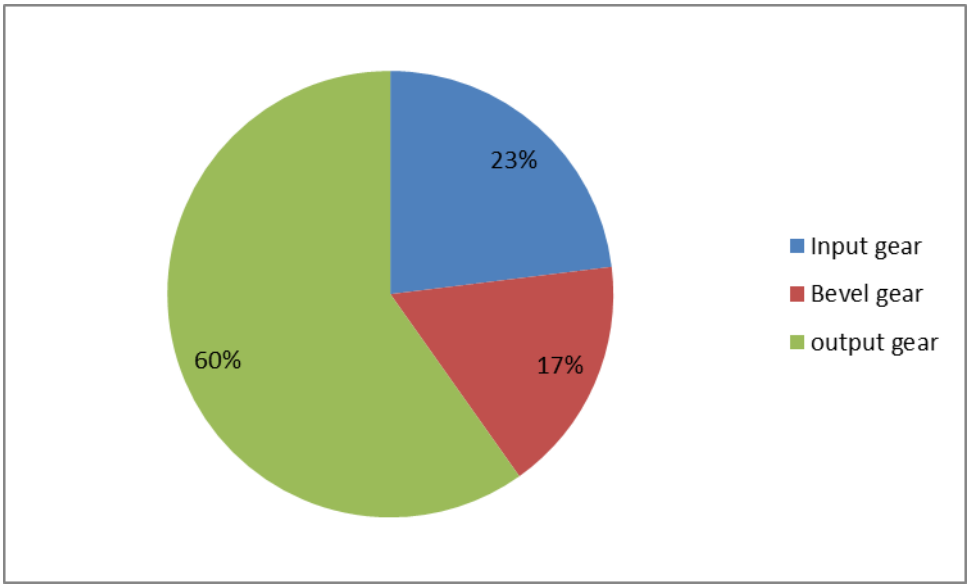

Figure 72: power losses distribution for gears - 1450 RPM and 170Nm - clockwise - f=0.02

Looking at the oil temperature on Figure 73, the values between 0.04 and 0.02 are the one to retain since they both respect the power losses and temperature criteria in the transmission which should remain below 5°C to consider results as consistent. Comparisons with the oil are presented, temperatures of bearings are observed to follow the same trends, and are not reported for sake of clarity.

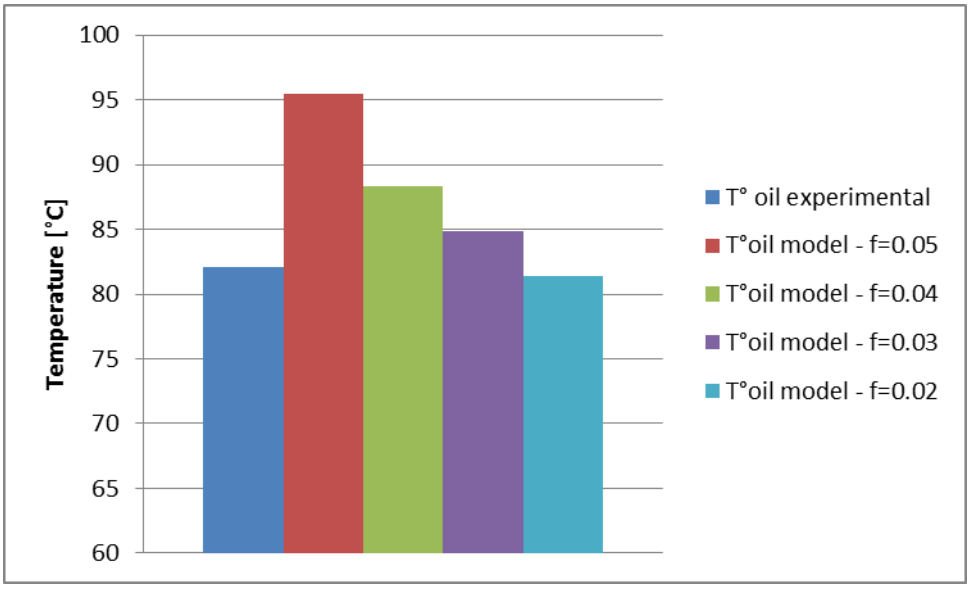

Figure 73: oil temperature for different friction coefficient of the bevel gear mesh – 1450 RPM and 170Nm-clockwise

The distribution of temperatures of bearings (see Figure 74) is observed to be influenced by the modification of the friction coefficient of the bevel gear mesh. The temperatures are globally reduced by the reduction of power losses: the modification is observed to greatly influence the temperatures and power losses.

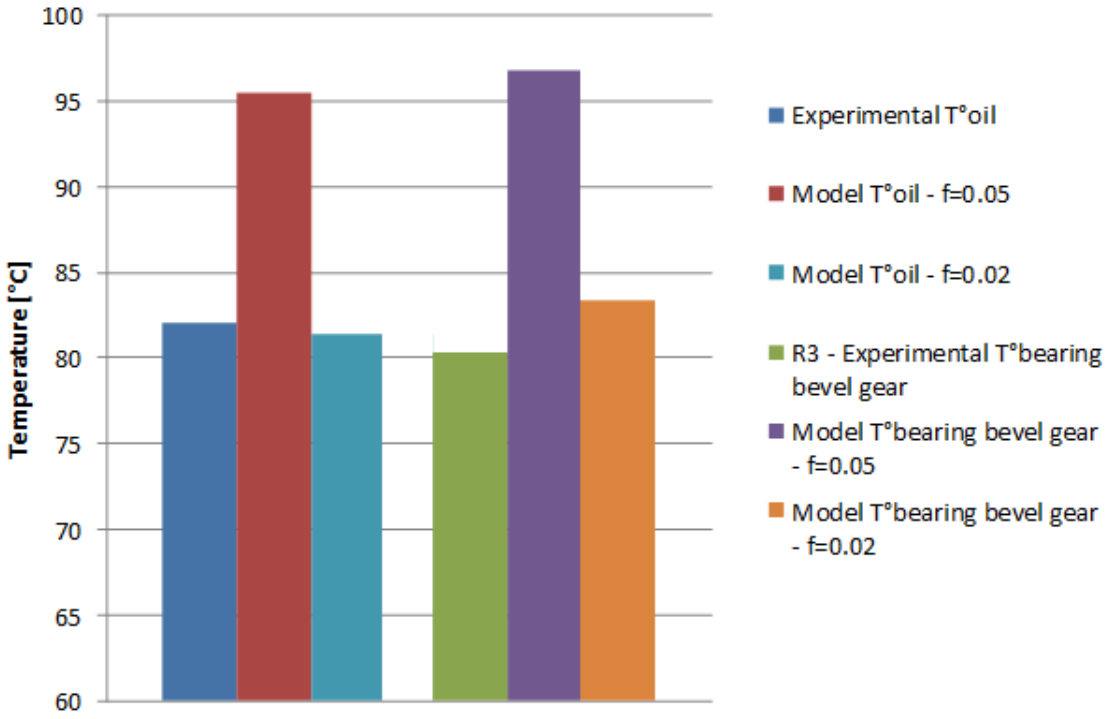

Figure 74: temperature of oil and bearing (number from kinematic scheme) for various friction coefficient of bevel gear mesh

The two examples above show the effect of a change in the friction coefficient on the temperature and power losses. They also point out that the friction coefficient is impacted by the operating conditions imposed to the gear unit. Optimum design of the tooth for the full load operating condition is significant, as shown in the two presented case, with a reduced friction coefficient in the case of the full loaded case. An optimum design of the tooth profile is a balance between the tooth mechanical resistance, the dynamic response of the tooth (tooth vibration for example) and the friction coefficient in the contact area, accounting for cutting process limitation. The optimal design of the tooth profile is focused on the full load and full speed operating conditions in order to reduce power losses where they are the highest over the operating range.

Actually, the tooth profile modification exists on the tested gear unit and is not considered by default in the model. These modifications are optimum in the case of full speed and full load operating conditions, which means that the experimental friction coefficient tends to be reduced when the operating condition are close from full speed and full load ones.

4. Elements influencing the thermal capacity of the gear unit

The previous part is focused on the model comparison and validation with experimental data. Here, the model is used to consider design choice and their influence on the thermal behavior through the simulated thermal behavior.

The objective of this section is quantifying and quantifying the impact of design and environment modifications on the thermal behavior of the gear unit. Only the theoretical model is used in this part.

4.1. Modification of the heat-transfer with the environment

4.1.1. Influence of the foundation

The thermal exchange with the environment is influenced by the metallic plate supporting the housing. The impact of the presence or not of the supporting plate is quantified by a comparison of the cool down test with and without the plate influence, then in the case of loaded tests.

In the case of a loaded test at 1000 RPM and 130Nm, the influence of the supporting plate is significant on the oil and elements temperatures, reducing of around 10°C the maximum temperature as shown on Figure 75 and Figure 76. The supporting plate evacuates 16% of the total heat transferred to the environment when it is considered to exchange with the housing, since the exchange with air is increased through forced convection thanks to the rotating elements. The power losses are not significantly modified, only 20W of difference over 780W between the two cases.

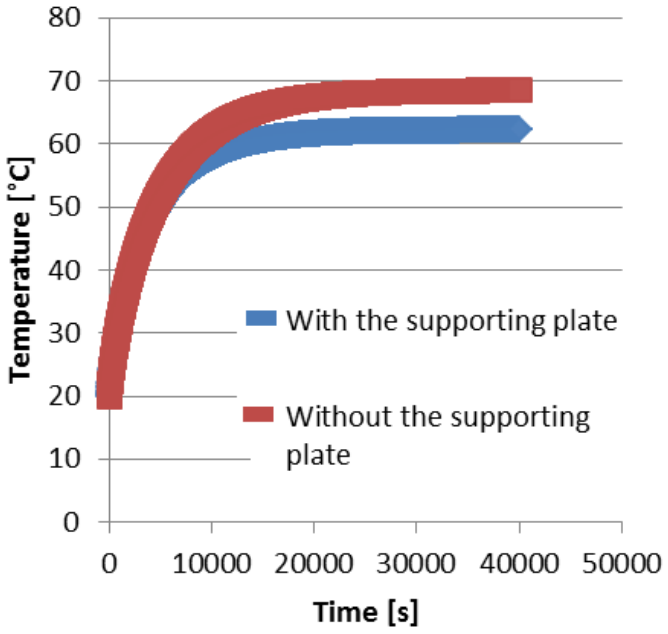

Figure 75: oil temperature evolution – 1000 RPM and 130 Nm

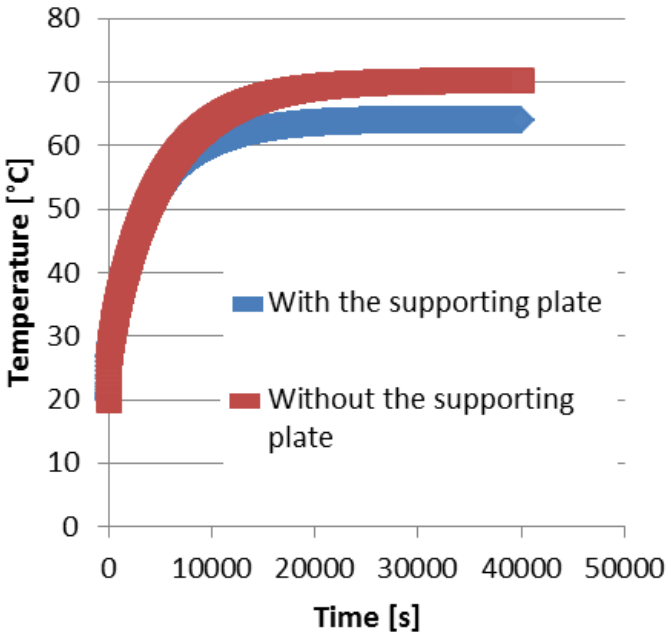

Figure 76: temperature of the bearing supporting the bevel pinion – 1000 RPM and 130 Nm

On the whole, the impact of the presence of the metallic plate is significant on the thermal behavior of the gear unit.

4.1.2. Influence of fins

No fins are used in the design of the existing housing of the gear unit, but fins are used on the motor housing. The thermal model allows testing the improvement of adding fins on the housing on the gear unit.

The exchange between the housing and the environment is modified when fins are added, increasing the capacity of heat exchange with the ambient air. In fact, fins add an additional exchange area to the housing (see appendix A). However their efficiency is reduced when the fins become longer since their temperature is reduced along their length as they transfer heat to the environment.

Fins are added in the model on the housing, separated by a space of 10mm between each. Three cases are considered: 8 fins, 16 fins and 8 fins twice as high as the two previous cases (see Figure 77). Theses cases allow studying two choices: the number of fins and their design.

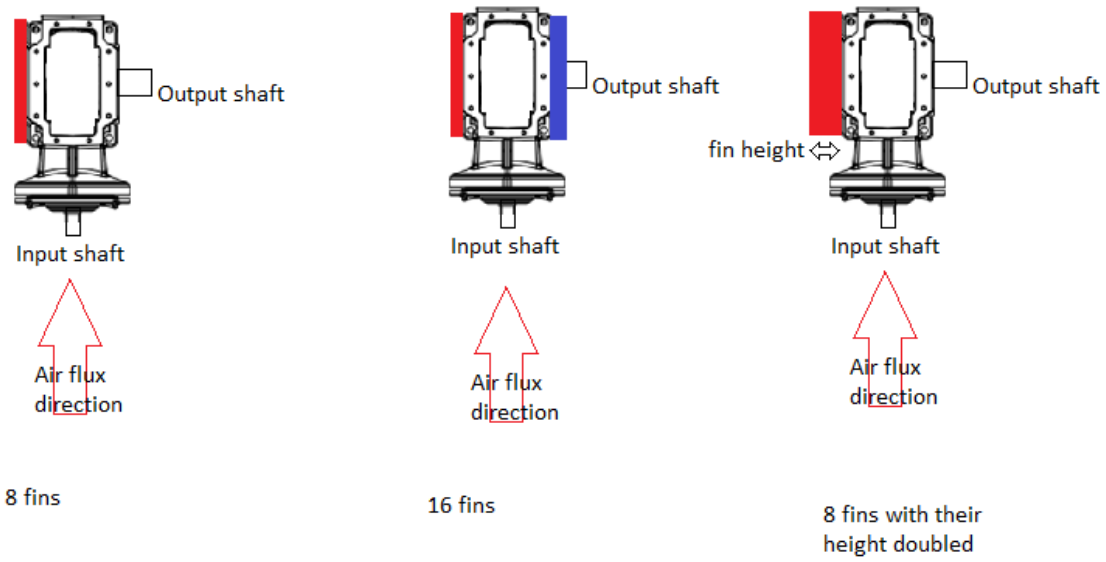

Figure 77: three cases sudied considering fins positions: 8 fins on the red box side or 16 fins on the red and blue boxes sides

On Figure 78, the dimensions of the fins are presented. A section of 10mm (height) by 10mm (width) is considered along the longest side of housing, which is in the direction of the air propelled by the motor. The number of fins is varied from 8 to 16. Then the height is doubled to consider the impact of design choices considering the fins.

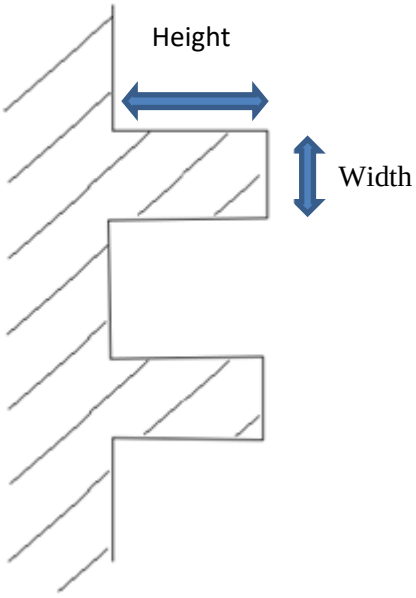

Figure 78: fin dimensions

Figure 79 shows that the power losses are slightly impacted, since the variation observed is caused by the reduced temperatures as shown on Figure 80. The reduced temperatures increase the viscosity of the lubricant which increases the power losses.

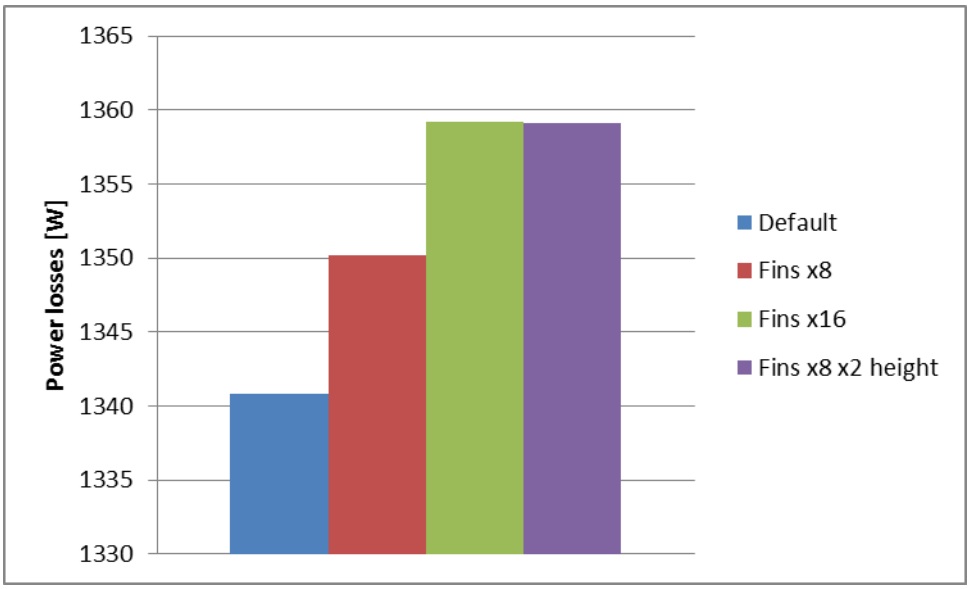

Figure 79: comparison of power losses considering the influence of fins – 1500 RPM and 170Nm

In the presence of fins, some design choices appears equivalent as shown on Figure 80. The cases with 16 and 8 fins with their height doubled give almost the same results since the exchange surface is increased in the same proportion.

If the height of the fins is still increased, the efficiency of the fin is reduced and the difference between the two designs is significant.

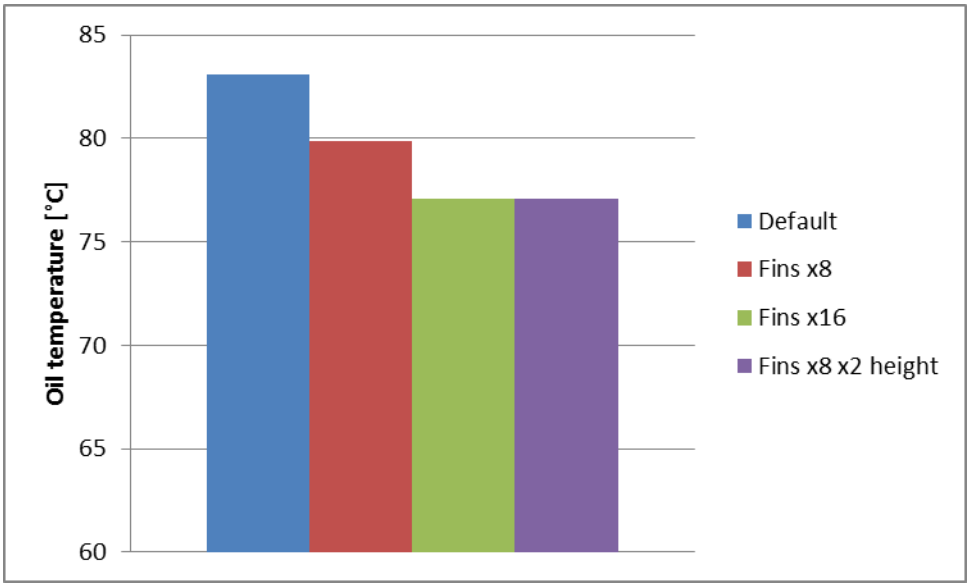

Figure 80: comparison of temperature considering the influence of fins

Fins are a good solution to increase the exchange capacity with the ambient air, with limited modification in the design of the gear unit.

4.1.3. Influence of the convection with ambient air

The fan of the motor provides a ventilation level proportional with its own rotational speed. It is possible to add more ventilation with a fan: the impact of the ventilation level is studied. The ventilation level is varied from 25% above the actual ventilation speed to the level of the room ventilation (0.5 m/s). The default ventilation level with the fan of the motor only is 1.5 m/s since the motor is simulated to run at 1500 RPM.

The power losses increases as the gear unit is colder as observed previously with the fins. The power losses appear to diminish of 5% (around 70W) while the temperature increases of 30% (around 30°C - Figure 81). The ventilation of the motor greatly impacts the temperature of the gear unit but much less the power losses.

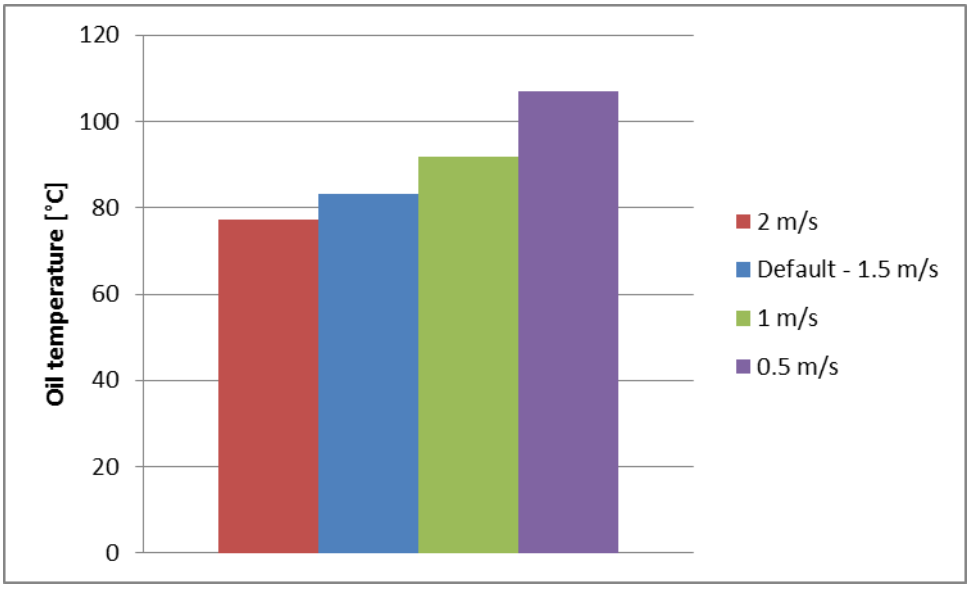

Figure 81: comparison of oil temperature for various level of ambient ventilation

The ventilation speed appears therefore to impact significantly the temperature and power losses.

4.2. Modification inside the gear unit

4.2.1. Influence of tooth profile modification on cylindrical gears

The friction is shown to change in function of operating condition. Since the mesh power losses in the case of loaded conditions represents more than 50% of the total power losses (see Figure 65), it is important to reduce them as much as possible. One way is modifying the tooth profile.

Here the model is used to study the influence of a change in the tooth profile of the cylindrical gears only. In order to do so, the friction coefficient of the spiral bevel gear meesh is fixed at 0.05 and it is discarded of the study in this section only.

The tooth profile modification can improve the behavior of the tooth under load and reduce the friction coefficient. The friction coefficient of the bevel gear mesh is fixed to a value of 0.05. The influence of tooth profile modification is studied on the cylindrical gears geometry: the friction coefficient for cylindrical gear is computed with the technical report ISO/TR 14179-2. The tooth profile modification is computed with the Velex and Ville formula [112] (see Figure 9 and equation 34). The depth P and length T of tooth profile modification are plotted with respect to the power losses. Figure 82 shows their relative influence on the total power losses. The maximum impact of tooth profile modification is shown to reduce by 150W the total power loss (9.5% of the 1550W).

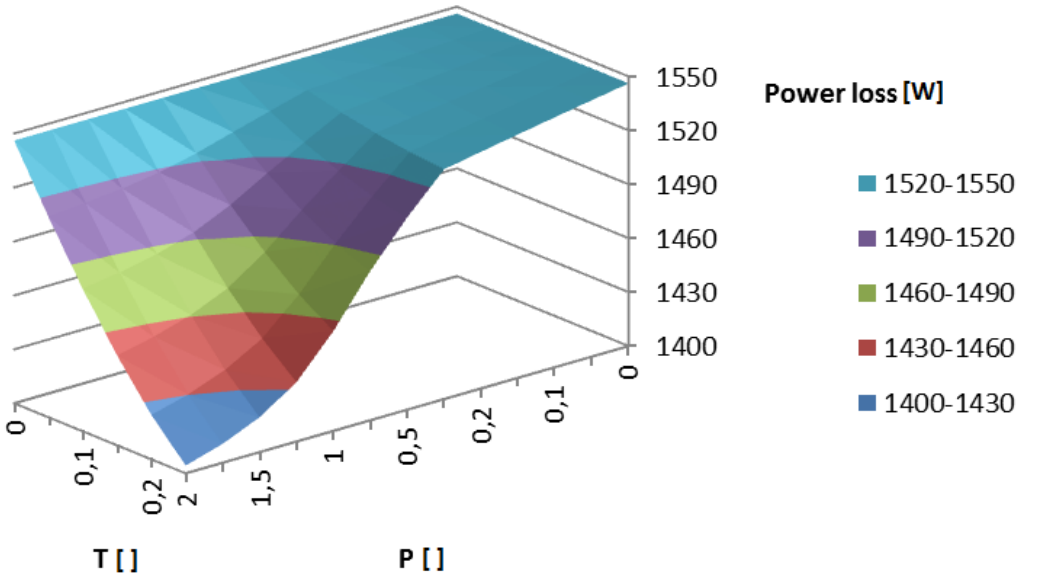

Figure 82: influence of tooth profile modification on power losses – 1500 RPM – 170Nm

The oil bath temperature is also reduced of less than 10°C (11%) at maximum (see Figure 83).

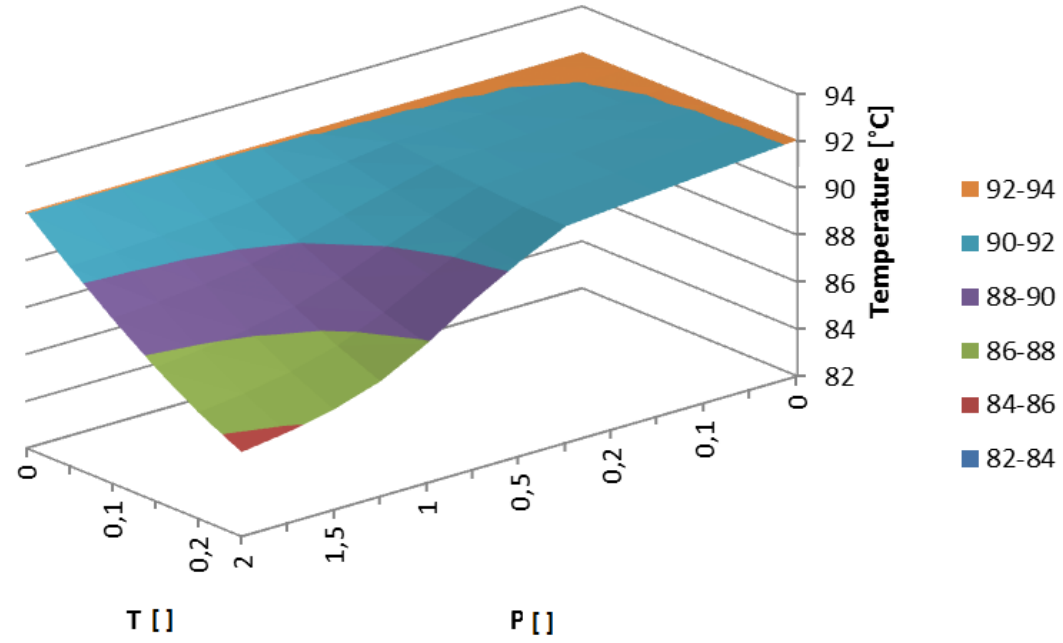

Figure 83: influence of tooth profile modification on oil temperature – 1500 RPM – 170Nm

Considering the test at 1000 RPM and 130Nm as the input torque, the same technical report is used to compute the friction coefficient. The influence of the tooth profile modification is expressed as a function of the length T and depth P of the modification as shown on Figure 84. The maximum reduction of the total power losses is 70W (8.3% of the total losses).

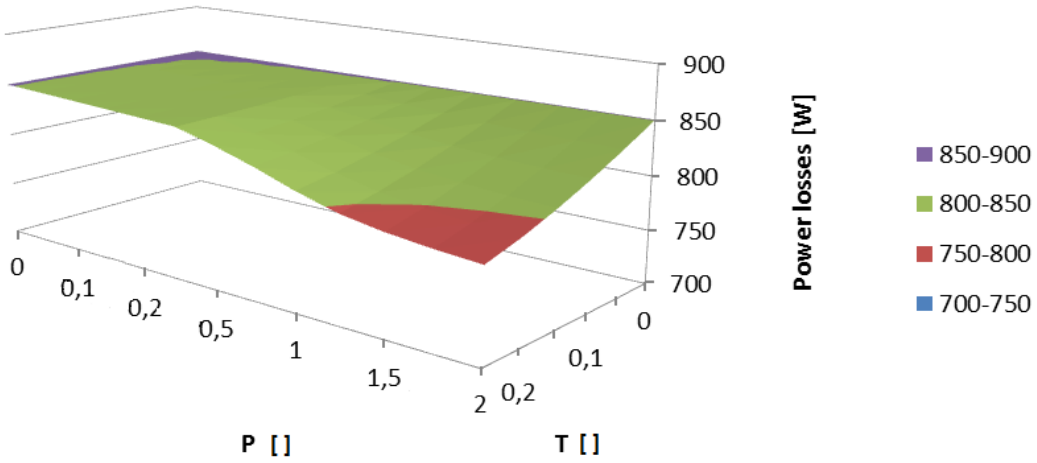

Figure 84: influence of tooth profile modification on power losses – 1000 RPM – 130Nm

The oil bath temperature is reduced of less than 5°C (8%) at maximum (see Figure 85).

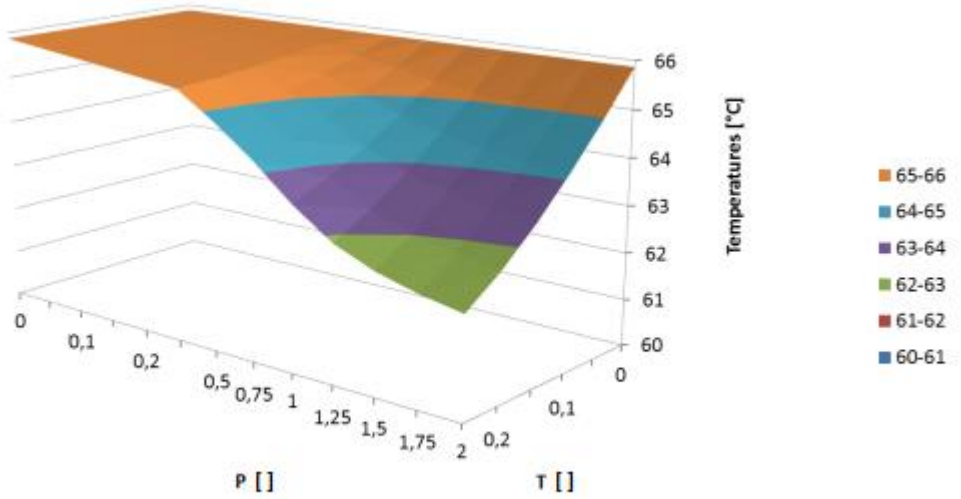

Figure 85: influence of tooth profile modification on oil temperatures – 1000 RPM – 130Nm

The tooth profile modification is shown to reduce the total power losses by around 10% compared to the profile without modification. The temperatures of the oil bath are reduced in the same proportion.

A depression area is observed in the results, which means that different kind of correction can give the same reduction in power losses.

4.2.2. Influence of oil level

The oil level can influence the power losses and the temperature distribution. The default level of the oil bath is fixed at 0.11m from the bottom of the housing of the gear unit. It could be increased or decreased to consider the impact of the oil bath on the thermal behavior of the transmission.

Figure 86 shows that the power loss is reduced as the oil bath level is reduced. The reduction of the immersion of the rotating elements decreases the power losses.

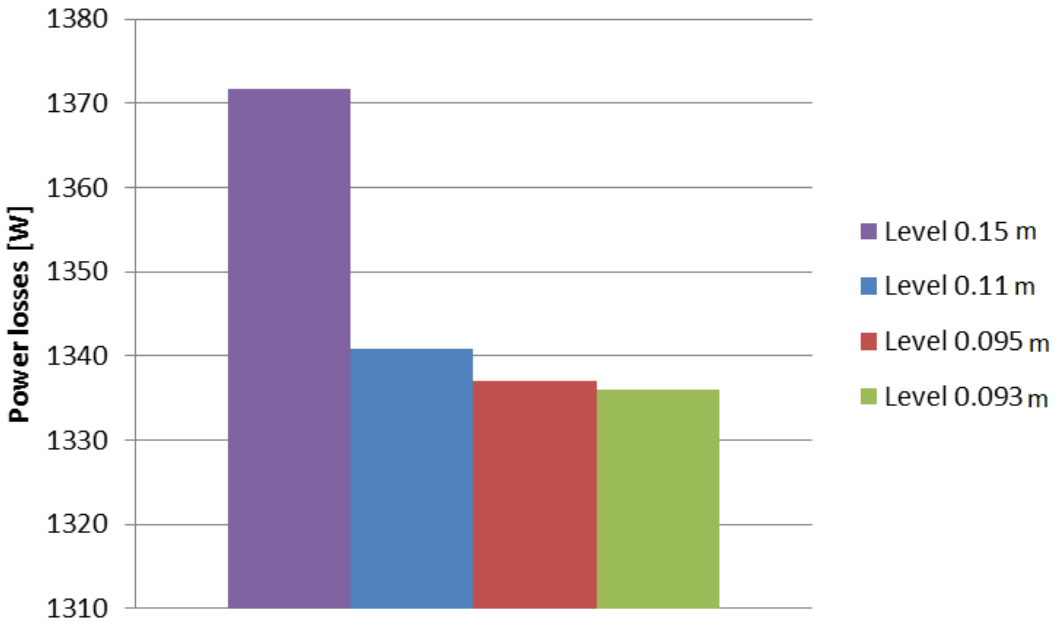

Figure 86: power loss comparison for different oil level

The impact of decreasing the oil level on the temperature is considered on the bearing of the output pinion (Figure 87) and on the bevel pinion (Figure 88). It appears that the temperatures are reduced with the reduced power losses until it raises a minimum level of 0.093 m, where the temperatures increase even if power losses are still reduced. Reducing the oil level under 0.093 m means that the some previously immersed gear are no more immersed (for example the output pinion P5 and the spiral bevel gear P3 are the first one which are no more immersed – refer to figure 7 for kinematic scheme), which leads to the computed behavior. The last observation shows a change in the thermal behavior of the gear unit as the exchange with the oil is much reduced and the surface of exchange tends toward a critical minimum. In this case, the bevel pinion temperature increases even with a slight decrease in the oil level (Figure 88). On the contrary, the bearing supporting the output pinion appears to be impacted as the immersion decrease under a level lower than the critical one for the gear. It derives from the fact that the heat is mainly evacuated by conduction in the bearing, contrary to the gears where oil has a cool down function.

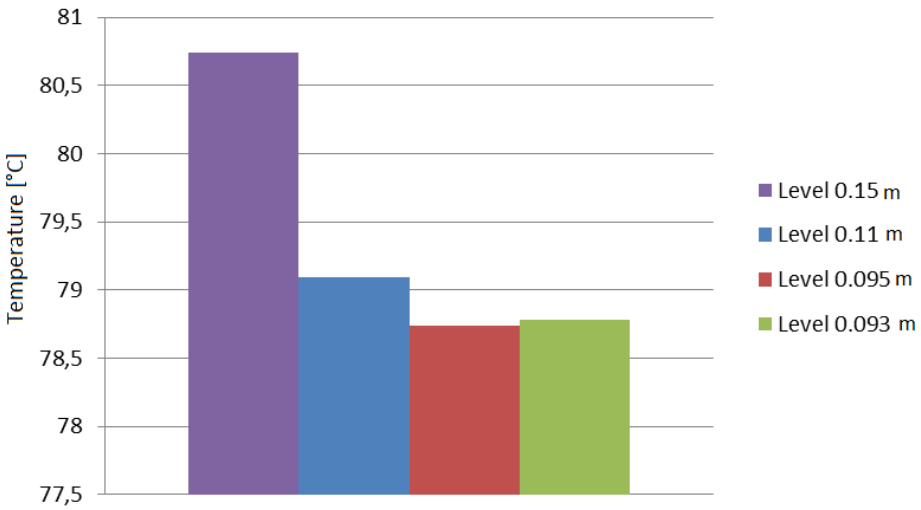

Figure 87: temperature variation of the temperature of the bearing of the output pinion for different oil level

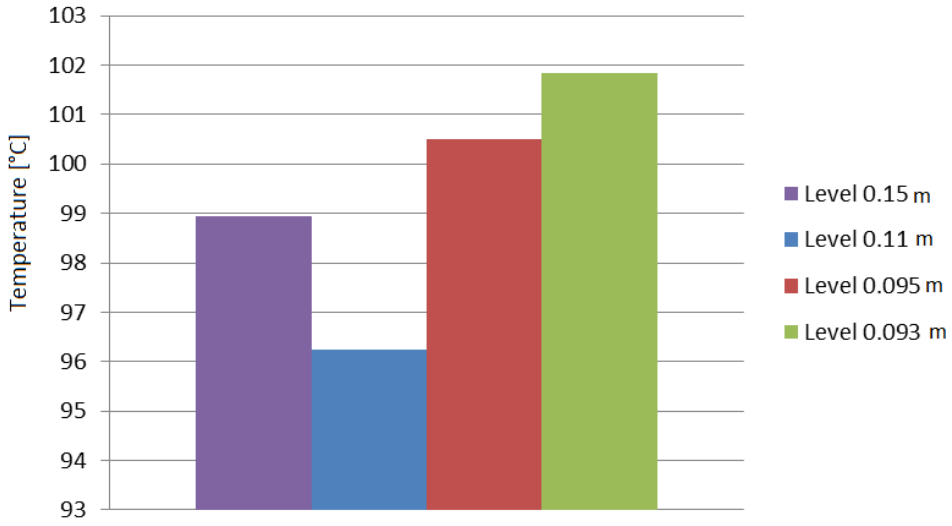

Figure 88: temperature variation of the temperature of the bevel pinion for different oil level

The optimum level of the transmission is shown to be where the power losses are minimum while the temperature are maintained the lowest. It appears that some variation around the optimum level is possible, even if a critical minimum level is identified where all the elements show an increase in temperature, which may result in premature failure. The reference level chosen in the standard design appears at the best choice as shown in theoretical results.

4.3. Influence of a change in lubricant

The choice of the lubricant can impact both viscosity and friction coefficient. Three oils (A, B and D) are chosen to study their impact on power losses and temperatures. The case at 1500 RPM and 170Nm is considered and the friction coefficient is computed thanks to technical report 14179-2 for cylindrical gears and fixed at 0.05 for bevel gears. The more viscous oil is the oil A then oil D and oil B (see Table II.2). Oil A and B are mineral and oil D is synthetic.

It appears that the reduction of viscosity reduces both power losses (Figure 89) and temperatures (Figure 90), as shown when the oil is changed from oil A to oil B, both mineral.

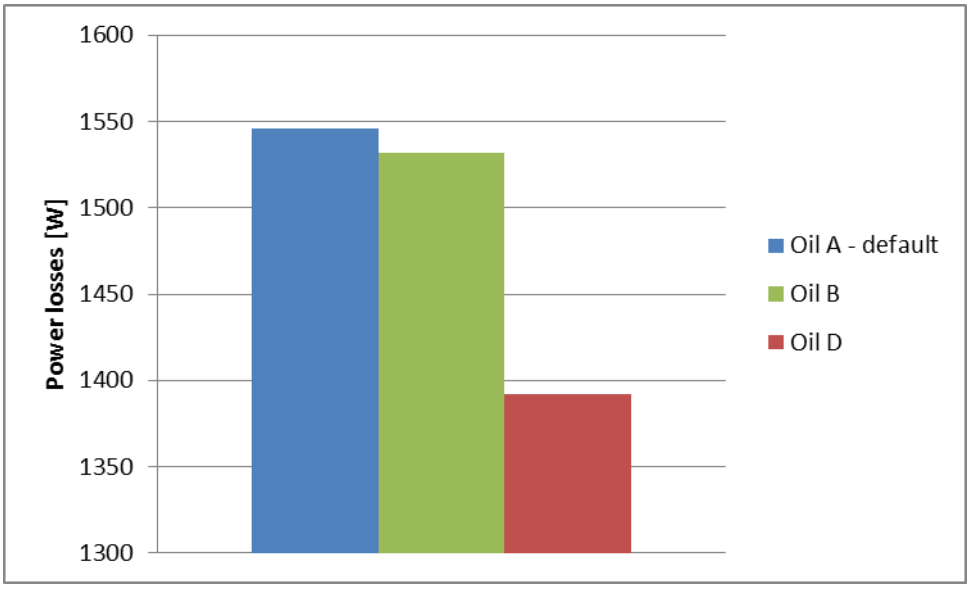

Figure 89: power losses for different oils – 1500 RPM and 170Nm

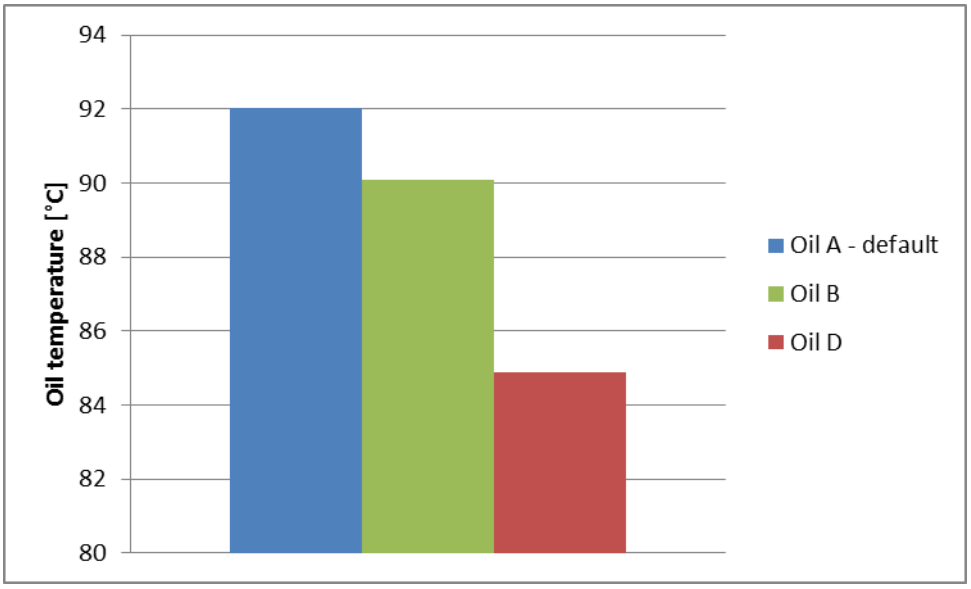

Figure 90: oil temperature for different oils – 1500 RPM and 170Nm

Switching to oil D, which is synthetic, shows a reduction of 10% in power losses and 8°C on the oil bath temperature.

An optimization of the friction in the mesh seems however to be more efficient compared to viscosity lowering. Further tests concerning the impact of a change of lubricant could be the subject of a study with twin-disks measurements [113], since the relation between the oil properties and the friction coefficient is estimated with the technical report formula. This technical report gives only indications on global lubricant behavior, however precise measurement are required to quantify the friction coefficient. Moreover wear problem has to be handled at the same time since a change in lubricant changes the conditions of contact, so a change in lubricant implies work on wear evolution in the contact area.

5. Conclusion

In this chapter, the thermal model of the gear unit is validated. Firstly, the no load behavior is used to define the parameter f0, defining the no load losses of the bearings. The thermal exchange in the case of no load tests is checked thanks to cool down tests. The ambient ventilation level is checked for different tests under no load condition. The impact of the preload of the bearings supporting the spiral bevel pinion is shown to greatly impact the thermal behavior of the transmission in no load tests.

Then the loaded tests are used to check the behavior of the model under loaded conditions. Moreover the influence of the ventilation on the power losses and temperatures appears non negligible, resulting in difference about hundreds of watts on power losses and tens of degrees in temperatures.

The impact of a change in the friction coefficient of the spiral bevel gear is shown very influential on the power losses and temperature. It means that a change in the lubricant may modify the power losses and temperatures not only through its viscosity, but also, through the gear friction coefficient.

The impact of modifications of the exchange with the environment and of internal exchange is studied and shows various levels of influence. It is thus possible to choose between the different solutions in function of their respective influence after evaluating the cost for each of them. This chapter shows the experimental validation of the model and ways to evaluate the impact of different kinds of optimization on the thermal behavior of the gear unit.

From this analysis, some elements are pointed out. First, elements concerning the exchange with the environment are studied. For example, the supporting plate transfers 16% of the heat flux to the environment, helping reducing the temperatures in the gear unit. Adding fins is shown reducing the temperatures of bearings about tens of degrees, while a change in the ambient

ventilation can result in temperature difference about 20°C when increased from ambient ventilation to 2 m/s of forced ventilation.

Then modifications inside the gear unit are studied like tooth profile modifications, which can reduce of a hundred of watt power losses (which leads to a reduction of 5°C in temperatures of the inside elements). The oil level influence is shown to be influential since an optimal level allows good lubrication and cooling down while not much increasing churning losses. Some elements should dip in the oil bath to ensure enough lubrication while not dipping too much elements in the oil unless it increases to much the churning losses.

A change in lubricant is the last parameter analysed. A lubricant change impacts the friction coefficient and the churning losses, resulting in reduction of power losses of a hundred of watts and of ten degrees in temperatures of inner elements. However a great care should be taken when changing the lubricant to avoid wear problems.

Conclusion

1. Conclusion

The objective of this study is developing an efficient and fast program to provide an accurate and reliable description of the thermal behavior of a gear unit. It should give information on the temperature of different parts of the transmission and the power loss level for defined operating conditions. The model should require information available at a design stage to help engineers in design choices.

The first chapter describes the methodology and points out the reason for choosing the thermal network. The use of thermal resistances and nodes to represent the behavior of the gear unit discretized into isothermal elements is detailed. Sources of uncertainties are identified regarding churning losses of spiral bevel gears.

The second chapter focuses on churning losses of spiral bevel gears. Several methods are available and their comparison is not conclusive. The discrepancies between them do not allow considering them equivalent either. Tests are conducted to determine experimentally the power losses associated to spiral bevel gear churning. By means of dimensional analysis, an adapted formula is proposed to represent the behavior observed, since none of the existing formula seems to correlate with test results.

The comparison between theoretical results and experimental measurements on the gear unit is done in the third chapter. The cooling down, no load and loaded sequence measurements constitutes the model validation for different operating condition. Two parameters describing ventilation level and bearings behavior under no load conditions need to be experimentally defined, and are subsequently verified on the remaining validation tests.

The friction coefficient between the spiral bevel gears is determined through measurements of power losses and temperatures (reverse engineering).

This PhD provides a model that could also give information concerning design choices. Several elements influencing the exchange with the environment or the exchange inside the gear unit are considered. Moreover it is also possible to evaluate the influence of a change in lubricant. This study shows the impact of each suggested modification, giving to the design engineer the necessary insight for an optimal cost-performance trade-off.

For example, the environment of the gear unit greatly influences its thermal behavior. The supporting plate is determined to reduce the gear unit temperatures by transferring 16% of the total heat evacuated. Fins may reduce of 10°C the temperature of inner elements like bearings even if few of them are added to the gear unit housing. Moreover adding fans to increase the air flux aroung the gear unit can reduce the temperature of 20°C while the ambient ventilation is increased from 0.5 m/s to 2 m/s.

Then the tooth profile modification influence can be studied through analytical formulas. A reduction of a hundred of watts of the power losses while reducing temperatures of 5°C of the bearings is observed for some tooth profile modification.

The oil level should be kept minimum unless few millimeter of oil level increase results in temperatures about 5°C higher while increasing power losses of 50W. However the oil level should allow enough lubrication while cooling down inner elements of the gear unit: it leads to an optimum oil level that can be theoretically determined thanks to the thermal model.

The thermal model accounts for modification in the lubricant characteristics. A change in lubricant both influences the friction coefficient and churning losses. It results in hundreds of watts of difference in power losses and in ten degrees of difference on bearings temperatures.

2. Suggestions for future work

To improve the present work, some aspects could be developed in future work. Numerous phenomena appear to influence the power loss in the gear unit and the steady state temperatures.

Two elements concerning the power losses could be improved: the bearing preload influence on meshing gear stiffness and the bevel gear mesh representation.

Firstly, bearings preload impacts bearing power losses: the preload must be reduced as much as possible while keeping enough bearing stiffness to ensure a proper gear meshing. Furthermore, bearings preload indirectly impacts the efficiency of the gear pair: this influence is not considered in the present study since this relationship is nonlinear and complex to handle without fine gear geometry definition.

Then, the mesh power losses of spiral bevel gears are studied through Tredgold approximation with equivalent virtual gears. 3D studies represent the behavior of the mesh of spiral bevel gears through detailed analysis like works of Jbili et al. [61] or Teixeira-Alves [108]. It requires much computational time: it could be used in a validation step rather than a design step.

Improvement concerning the temperature reduction in the gear unit can be through reducing friction or increasing the heat transfer to the environment, further work can be done on both of them.

A way to reduce power losses is to lower friction in the gear unit: a change in lubricant is impacting the friction coefficient of all the elements. It is often the low cost and efficient way to reduce friction of a mechanical transmission. The model allows testing a change in viscosity or density, however the introduction of friction laws associated with a couple lubricant – material could

be a further improvement in the existing model. These laws could be determined thanks to experimental measurements with twin disks machine.

Instead of working on power losses to reduce the temperature of the elements of the gear unit, one can foster the thermal exchange with the environment. Setting different standard geometries of fins is interesting for further development of the existing model.

The current model can be further improved by integrating the developments above mentioned.

References

[1] Iso/tr 14179-1 : Gears - thermal capacity ; part 1 : Rating gear drives with thermal equilibrium at 95°c sump temperature. Technical report, 2001. p. 38.

[2] Iso/tr 14179-2 : Gears - thermal capacity ; part 2 : thermal load-carrying capacity. Technical report, 2001. p.42.

[3] Capacité thermique des réducteurs. Technical report, ECAM Lyon and CETIM, 2002.

[4] AIRAP. Présentation des lois aerauliques.

[5] L. Akin, J. Mross, and D. Townsend. Study of lubricant jet flow phenomena in spur gears. *Journal of Lubrication Technology*, 97(2):283–288, 1975.

[6] J. T. Alves, J. Wang, M. Guingand, J.-P. de Vaujany, and P. Velex. Static and dynamic models for spiral bevel gears. *Mechanics & Industry*, 13(5):325–335, 2012.

[7] N. E. Anderson, S. H. loewenthal, and J. D. Black. An analytical method to predict efficiency of aircraft gearboxes. Technical report, NASA, 1984.

[8] Y. Ariura, T. Ueno, T. Sunaga, and S. Sunamoto. The lubricant churning loss in spur gear systems. *Transactions of the Japan Society of Mechanical Engineers*, 38(313):2403–2413, 1972.

[9] J. Ayel. Lubrifiants propriétés et caractéristiques. *Techniques de l'ingénieur Lubrification, base documentaire(b5340)*, 2015.

[10] J.-P. Bardon. *Contribution à l'étude du transfert de chaleur au contact de deux matériaux*. PhD thesis, l'Ecole Nationale supérieure de mécanique et d'aérotechnique, 1965.

[11] J.-P. Bardon and B. Cassagne. Température de surface: Mesure par contact. *Techniques de l'ingénieur. Mesures et contrôle*, (R2730):R2730–1, 1998.

[12] K. M. Becker. Measurements of convective heat transfer from a horizontal cylinder rotating in a tank of water. *International Journal of Heat and Mass Transfer*, 6(12):1053–1062, 1963.

[13] G. H. Benedict and B. W. Kelley. Instantaneous coefficients of gear tooth friction. *ASLE Transactions*, 4:59 – 70, 1961.

[14] H. Blok. Theoretical study of temperature rise at surfaces of actual contact under oiliness lubricating conditions. In *Proceedings of the general discussion on lubrication and lubricants*, volume 2, pages 222–235. London: IMechE, 1937.

[15] H. Blok. Transmission de chaleur par projection centrifuge d'huile. *Société d'Etudes de l'Industrie de l'Engrenage*, 59:14–23, 1970.

[16] R. Boness. Churning losses of discs and gears running partially submerged in oil. In *Proc. ASME Int. Power Trans. Gearing Conf*, volume 1, pages 255–359, 1989.

[17] B. Bourouga, J. M. Briot, and J. P. Bardon. Influence de la vitesse et de la charge sur la conductance thermique de transport entre les bagues d'un roulement à rouleaux. *International Journal of Thermal Sciences*, 40(7):622 – 637, 2001.

[18] E. Buckingham. *Analytical mechanics of gears*. Dover Publications, New York, 1963. 1949.

[19] C. Changenet. *Modélisation du comportement thermique des transmissions par engrenages*. PhD thesis, INSA de Lyon - LaMCoS, 2006. 167 p.

[20] C. Changenet. Eléments en vue de la révision du rapport technique iso/tr 14179-2. Technical report, ECAM LYON, October 2015.

[21] C. Changenet, G. Leprince, F. Ville, and P. Velex. A note on flow regimes and churning loss modeling. *Journal of Mechanical Design, Transactions of the ASME*, 133(12), 2011.

[22] C. Changenet, X. Oviedo-Marlot, and P. Velex. Power loss predictions in geared transmissions using thermal networks-applications to a six-speed manual gearbox. *Journal of Mechanical Design, Transactions of the ASME*, 128(3):618 – 625, 2006.

[23] C. Changenet and P. Velex. A model for the prediction of churning losses in geared transmissions - preliminary results. *Journal of Mechanical Design*, 129 (N°1):128–133, 2007.

[24] S. Churchill and M. Bernstein. A correlating equation for forced convection from gases and liquids to a circular cylinder in crossflow. *Journal of Heat Transfer*, 99(2):300–306, 1977.

[25] E. Cobb and O. Saunders. Heat transfer from a rotating disk. In *Proceedings of the Royal Society of London A: Mathematical, Physical and Engineering Sciences*, volume 236, pages 343–351. The Royal Society, 1956.

[26] H. H. Coe. Predicted and experimental performance of large-bore high-speed ball and roller bearings. 1983.

[27] H. H. Coe. Thermal analysis of a planetary transmission with spherical roller bearings operating after complete loss of oil. *NASA*, page 11, 1984.

[28] H. H. Coe. Comparison of predicted and measured temperatures of uh-60a helicopter transmission. Technical report, DTIC Document, 1989.

[29] F. Concli, C. Gorla, A. Della Torre, and G. Montenegro. Churning power losses of ordinary gears: a new approach based on the internal fluid dynamics simulations. *Lubrication Science*, 27(5):313–326, 2015. LS-14-0016-RA-TT.R1.

[30] F. Concli, A. D. Torre, C. Gorla, and G. Montenegro. A new integrated approach for the prediction of the load independent power losses of gears: Development of a mesh-handling algorithm to reduce the cfd simulation time. *Advances in Tribology*, 2016:8, 2016.

[31] I. F. Concli and I. C. Gorla. Load independent power losses of ordinary gears: Numerical and experimental analysis. 2013.

[32] J. W. Daily and R. E. Nece. Chamber dimension effects on induced flow and frictional resistance of enclosed rotating disks. *Journal of Basic Engineering*, 82 (N°1):217–230, 1960.

[33] P. H. Dawson. Windage loss in larger high-speed gears. *Proc. Inst. Mech. Eng., Part A*, 198A (1):51 – 59, 1984.

[34] B. Deconninck, T. Delvigne, and G. Videx. Air-x, an innovative device for on-line oil aeration measurement in running engines. Technical report, SAE Technical Paper, 2003.

[35] Y. Diab. *Analyse des pertes de puissance dans les transmissions par engrenages à grande vitesse : applications aux réducteurs industriels et aux machines textiles*. PhD thesis, INSA de Lyon - LaMCoS, 2005. 152 p.

[36] Y. Diab, F. Ville, and P. Velex. Prediction of power losses due to tooth friction in gears. *Tribology Transactions*, 49(2):260–270, 2006.

[37] Y. Diab, F. Ville, P. Velex, and C. Changenet. Windage losses in high-speed gears. preliminary theoretical and experimental results. *ASME J. Mech. Des.*, 126 (5):903 – 908, 2004.

[38] J. Durand De Gevigney, C. Changenet, F. Ville, and P. Velex. Thermal modelling of a back-to-back gearbox test machine: Application to the fzg test rig. *Proceedings of the Institution of Mechanical Engineers, Part J: Journal of Engineering Tribology*, 226(6):501 – 515, 2012.

[39] L. E. El-Bayoumy, L. S. Akin, and D. P. Townsend. An investigation of the transient thermal analysis of spur gears. *Journal of mechanisms, transmissions, and automation in design*, 107(4):541–548, 1985.

[40] J. R. Fair. Direct contact gas-liquid heat exchange for energy recovery. *Journal of Solar Energy Engineering*, 112(3):216–222, 1990.

[41] H. Fenech and W. Rohsenow. Prediction of thermal conductance of metallic surfaces in contact. *Journal of Heat Transfer*, 85(1):15–24, 1963.

[42] C. Fernandes, P. Amaro, R. Martins, and J. Seabra. Torque loss in thrust ball bearings lubricated with wind turbine gear oils at constant temperature. *Tribology International*, 66:194–202, 2013.

[43] C. Fernandes, R. Martins, and J. Seabra. Friction torque of cylindrical roller thrust bearings lubricated with wind turbine gear oils. *Tribology International*, 59:121–128, 2013.

[44] C. Fernandes, R. Martins, and J. Seabra. Friction torque of thrust ball bearings lubricated with wind turbine gear oils. *Tribology International*, 58:47–54, 2013.

[45] L. Feuillard and M. Quintanilla Munoz. Etude des pertes de puissance dans les roulements prévues par deux modèles analytiques. Master's thesis, ECAM LYON, 2015-2016.

[46] D. Ghribi. *Optimisation des corrections de forme dans les engrenages droits et hélicodaux: Approches déterministes et probabilistes*. PhD thesis, INSA de Lyon, 2013.

[47] J. Greenwood and J. Tripp. The contact of two nominally flat rough surfaces. *Proceedings of the institution of mechanical engineers*, 185(1):625–633, 1970.

[48] R. Handschuh. Thermal behavior of spiral bevel gears. Technical report, NASA, 1995. 190 p.

[49] R. Handschuh and T. Kicher. A method for thermal analysis of spiral bevel gears. *Journal of Mechanical Design*, 118(4):580–585, 1996.

[50] R. F. Handschuh. *Thermal behavior of spiral bevel gears*. PhD thesis, Case Western Reserve University, 1993.

[51] T. A. Harris. *Rolling bearing analysis*. Woley Interscience, 3rd edition, 1991.

[52] G. Henriot. *Traité théorique et pratique des engrenages*. Number vol. 1 in Traité théorique et pratique des engrenages. Dunod, 1968.

[53] G. Henriot. *Traité théorique et pratique des engrenages*, volume 1. Paris : DUNOD, 6 edition, 1979.

[54] B. Höhn, K. Michaelis, T. Vollmer, and A. G. M. Association. *Thermal Rating of Gear Drives Balance Between Power Loss and Heat Dissipation*. Technical Papers. American Gear Manufacturers Association, 1996.

[55] M. J. Hill, R. F. Kunz, R. W. Noak, L. N. Long, P. J. Morris, and R. Handschuh. Application and validation of unstructured overset cfd technology for rotorcraft gearbox windage aerodynamics simulation. *64th Annual Forum of the American Helicopter Society*, 2008.

[56] J. Holman. *Heat transfer*. Mechanical engineering series. McGraw-Hill, 1989.

[57] R. Howells, J. Sciarra, and G. S. Ng. Thermal and structural analysis of helicopter transmission housings using nastran. 1976.

[58] M. Iritani, H. Aoki, K. Suzuki, and Y. Morita. Prediction technique for the lubricating oil temperature in manual transaxle. *SAE transaction*, 108:337–345, 1999.

[59] D. D. G. J. *Analyse thermo-mécanique d'un réducteur épicycloïdal - application aéronautique*. PhD thesis, LaMCos (INSA LYON), ECAM LYON, Hispano-Suiza, 2013. p.254.

[60] F. Jan and P. Norman. Transferts énergétiques dans une transmission à trains planétaires. *Revue de l'engrenage et des transmissions*, 79:93, 1982.

[61] D. Jbily, M. Guingand, J.-P. de Vaujany, and J. Teixeira-Alves. Simulation sous charge avec usure d'engrenage roue et vis sans fin. In *Journées transmissions mécaniques*, 07 2016.

[62] S. Jeon. *Improving efficiency in drive lines: an experimental study on churning losses in hypoid axle*. PhD thesis, Imperial College London, 2010.

[63] D. Joule, S. Hinduja, and J. Ashton. Thermal analysis of a spur gearbox part 1: steady state finite element analysis. *Proceedings of the Institution of Mechanical Engineers, Part C: Journal of Mechanical Engineering Science*, 202(4):245–256, 1988.

[64] I. Kakavas, A. Olver, and D. Dini. Hypoid gear vehicle axle efficiency. *Tribology International*, 101:314–323, 2016.

[65] B. W. Kelley and A. J. Lemanski. Lubrication of involute gearing. *Proc. Inst. Mech. Eng.*, 182(3A):173–184, 1967.

[66] R. J. Kleckner and G. Dyba. High speed spherical roller-bearing analysis and comparison with experimental performance. *J. Adv. Power Trans. Tech.*, pages 239–252, 1983.

[67] A. S. Kolekar, A. V. Olver, A. E. Sworski, and F. E. Lockwood. The efficiency of a hypoid axle-a thermally coupled lubrication model. *Tribology International*, 59:203 – 209, 2013.

[68] M. Kolivand, S. Li, and A. Kahraman. Prediction of mechanical gear mesh efficiency of hypoid gear pairs. *Mechanism and Machine Theory*, 45(11):1568 – 1582, 2010.

[69] N. Kuzmin. Coefficient of friction in heavily loaded contact. *Vest. Mashinostr*, 34:18–26, 1954.

[70] S. Laruelle, C. Fossier, C. Changenet, F. Ville, and S. Koechlin. Churning power losses of bevel gears. In *STLE*, May 2016.

[71] S. Laruelle, C. Fossier, C. Changenet, F. Ville, and S. Koechlin. Experimental investigations and analysis on churning losses of splash lubricated spiral bevel gears. *Mechanics and Industry*, in press, 2017.

[72] E. Lauster and M. Boos. Zum wärmehaushalt mechanischer schaltgetriebe für nutzfahrzeuge. *VDI-Berichte*, (488):45–55, 1983.

[73] A. O. Lebeck. *Principles and design of mechanical face seals*. John Wiley & Sons, 1991.

[74] G. LePrince, C. Changenet, F. Ville, P. Velex, C. Dufau, and F. Jarnias. Influence of aerated lubricants on gear churning losses–an engineering model. *Tribology Transactions*, 54(6):929–938, 2011.

[75] G. Leprince, C. Changenet, F. Ville, P. Velex, and F. Jarnias. Influence of oil aeration on churning losses. In *JSME 2009 International Motion and Power Transmission Conference*, pages 463–468, 05 2009.

[76] P. Luke and A. V. Olver. A study of churning losses in dip-lubricated spur gears. *Proceedings of the Institution of Mechanical Engineers, Part G: Journal of Aerospace Engineering*, 213(5):337–346, 1999.

[77] L. Manin. *Modèles de comportement multiniveaux pour la Conception Mécanique Assistée par Ordinateur: Application à la prévision du comportement thermique de transmissions de puissance par engrenages*. PhD thesis, Institut National des Sciences Appliquées de Lyon, 1999.

[78] L. Manin and D. Play. Thermal behavior of power gearing transmission, numerical prediction, and influence of design parameters. *ASME Journal of Tribology*, 121:693–702, 1999.

[79] R. W. Mann and C. H. Marston. Friction drag on bladed disks in housings as a function of reynolds number, axial and radial clearance, and blade aspect ratio and solidity. *Journal of Basic Engineering*, 83(4):719–723, 1961.

[80] Y. Marchesse, C. Changenet, F. Ville, and P. Velex. Investigations on cfd simulations for predicting windage power losses in spur gears. *JOURNAL OF MECHANICAL DESIGN*, 133(2), FEB 2011.

[81] P. M. T. Marques, C. M. C. G. Fernandes, R. C. Martins, and J. H. O. Seabra. Power losses at low speed in a gearbox lubricated with wind turbine gear oils with special focus on churning losses. *Tribology International*, 62:186–197, JUN 2013.

[82] R. Martins, J. Seabra, A. Brito, C. Seyfert, R. Luther, and A. Igartua. Friction coefficient in fzg gears lubricated with industrial gear oils: Biodegradable ester vs mineral oil. *Tribology International*, 39(6):512–521, 2006.

[83] S. Matsumoto and K. Morikawa. The new estimation formula of coefficient of friction in rolling-sliding contact surface under mixed lubrication condition for the power loss reduction of power transmission gears. *International Gear Conference, Conference Proceedings*, 2:1078 – 1088, 2014.

[84] W. Mauz. *Hydraulische Verluste von Stirnradgetrieben bei Umfangsgeschwindigkeiten bis 60 m, s*. Berichte des Institutes für Maschinenkonstruktion und Getriebebau. IMK, 1987.

[85] W. H. McAdams. *Transmission de la chaleur*. Dunod, 1964.

[86] H. Merritt. *Gear Engineering*. A Halsted Pr. book. Wiley, 1971.

[87] B. B. Mikic. Thermal contact conductance; theoretical considerations. *International Journal of Heat and Mass Transfer*, 17(2):205–214, 1974.

[88] Y. A. Misharin. Influence of the friction condition on the magnitude of the friction coefficient in the case of rollers with sliding. In *Proceedings of International Conference on Gearing, Mechanical Engineering, London*, pages 159–164, 1958.

[89] T. Misic, M. Najdanovic-Lukic, and L. Nesic. Dimensional analysis in physics and the buckingham theorem. *European Journal of Physics*, 31(4):893, 2010.

[90] T. Moshammer, F. Mayr, K. Kargl, and C. Honeger. Simulation of oil flow in gear box housing. *SAE*, 2032:9, 2006.

[91] G. Niemann and H. Winter. *Maschinenelemente: Band 2: Getriebe allgemein, Zahnradgetriebe - Grundlagen, Stirnradgetriebe*. Springer Berlin Heidelberg, 2013.

[92] J. L. Nikolajsen. Viscosity and density models for aerated oil in fluid-film bearings©. *Tribology transactions*, 42(1):186–191, 1999.

[93] J. O'donoghue and A. Cameron. Friction and temperature in rolling sliding contacts. *ASLE TRANSACTIONS*, 9(2):186–194, 1966.

[94] M. Özisik. *Heat Transfer: A Basic Approach*. Number vol. 1 in Heat Transfer: A Basic Approach. McGraw-Hill, 1985.

[95] S. Pallas, Y. Marchesse, C. Changenet, F. Ville, and P. Velex. A windage power loss model based on cfd study about the volumetric flow rate expelled by spur gears. *MECHANICS & INDUSTRY*, 13(5):317–323, 2012.

[96] N. Patir and H. Cheng. Prediction of the bulk temperature in spur gears based on finite element temperature analysis. *ASLE TRANSACTIONS*, 22(1):25–36, 1979.

[97] S. I. Pinel, H. R. Signer, and E. V. Zaretsky. Comparison between oil-mist and oil-jet lubrication of high-speed, small-bore, angular-contact ball bearings. *Tribology transactions*, 44(3):327–338, 2001.

[98] J. Pirvics. The analysis of thermal effects in rolling element bearing load support systems. *Proceedings of the Royal Society, London*, pages 259–282, 1980.

[99] M. Pleguezuelos, J. I. Pedrero, and M. B. Sanchez. Analytical model of the efficiency of spur gears: study of the influence of the design parameters. In *Proceedings Of The ASME International Design Engineering Technical Conferences And Computers And Information In Engineering Conference, 2011, Vol 8*, pages 557–565, 2012.

[100] F. Pouly. *Modélisation thermo-mécanique d'un roulement à billes grande vitesse*. PhD thesis, INSA de Lyon, 2010. 144 p.

[101] B. Roulet. *Modélisation de l'évolution de la dissipation de puissance et du comportement thermique d'une boîte de vitesse manuelle*. PhD thesis, Université de Paris 6, 1995. 174p.

[102] F. Schuller, S. Pinel, and H. Signer. Operating characteristics of a high-speed, jet-lubricated 35-millimeter-bore ball bearing with a single-outer-land-guided cage. *NASA Technical Paper 1957*, 1980.

[103] S. Seetharaman and A. Kahraman. Load-independent spin power losses of a spur gear pair: Model formulation. *Journal of Tribology-transactions of the ASME*, 131(2), APR 2009.

[104] S. Seetharaman, A. Kahraman, M. D. Moorhead, and T. T. Petry-Johnson. Oil churning power losses of a gear pair: Experiments and model validation. *Journal Of Tribology-transactions Of The ASME*, 131(2), APR 2009.

[105] SIMRIT. *Radialwellendichtringe*. Number 100. Katalog.

[106] SKF. *Rolling bearing*. October 2012.

[107] S. L. Soo and N. J. Princeton. Laminar flow over an enclosed rotating disk. *Transaction of the ASME*, 80:287–296, 1958.

[108] J. Teixeira Alves. *Définition analytique des surfaces de denture et comportement sous charge des engrenages spiro-coniques*. PhD thesis, 2012. Thèse de doctorat dirigée par Vaujany, Jean-Pierre de et Guingand, Michèle Mécanique Lyon, INSA 2012.

[109] Y. Terauchi, K. Nagamura, W. Chang-Lin, and K. Ikejo. On the heat balance of gear equipment: on a method for predicting the bulk temperature rise of gears and temperature rise of oil with dip cooling. *JSME international journal. Ser. 3, Vibration, control engineering, engineering for industry*, 34(1):97–105, 1991.

[110] A. S. Terekhov. Hydraulic losses in gearboxes with oil immersion. *Vestnik Mashinostroeniya*, 55 (5):13 – 17, 1975.

[111] D. P. Townsend and L. S. Akin. Analytical and experimental spur gear tooth temperature as affected by operating variables. *Journal of Mechanical Design*, 103(1):219–226, 1981.

[112] P. Velex and F. Ville. An analytical approach to tooth friction losses in spur and helical gears-influence of profile modifications. *Journal of Mechanical Design, Transactions of the ASME*, 131(10):1010081 – 10100810, 2009.

[113] F. Ville, D. Nélias, G. Tourlonias, L. Flamand, and P. Sainsot. On the two-disc machine: A polyvalent and powerful tool to study fundamental and industrial problems related to elastohydrodynamic lubrication. In *Tribology Research: From Model Experiment to Industrial Problem A Century of Efforts in Mechanics, Materials Science and Physico-Chemistry Proceedings of the 27th Leeds-Lyon Symposium on Tribology*, volume 39 of *Tribology Series*, pages 393 – 402. Elsevier, 2001.

[114] C. Wagner. Heat transfer from a rotating disk to ambient air. *Journal of Applied Physics*, 19(9):837–839, 1948.

[115] H. Winter and K. Michaelis. Fzg gear test rig - description and possibilities. *Coordinate European Council second international symposium on the performance evaluation of automotive fuels and lubricants*, 5-7 June 1985.

[116] H. Winter, K. Michaelis, and G. Funck. Wärmeabführung bei getrieben unter quasistationären betriebsbedingungen. teil ii: Untersuchungen zur wärmeabführung über stahlfundamente und übertragung der prüfstandsergebnisse auf die praxis. *Antriebstechnik*, 26(6):49–55, 1987.

[117] H. Xu and A. Kahraman. Prediction of friction-related power losses of hypoid gear pairs. *Proceedings of the Institution of Mechanical Engineers, Part K: Journal of Multi-body Dynamics*, 221(3):387 – 400, 2007. Gear efficiency;Gear friction;Hypoid gears;Mechanical efficiency losses;.

[118] M. Yazdani and M. Soteriou. A novel approach for modeling the multiscale thermo-fluids of geared systems. *International Journal of Heat and Mass Transfer*, 72:517–530, January 2014.

Appendix A

Thermal resistances

1. Resistances of conduction

1.1. Resistance of axial conduction

The resistance of axial conduction is defined here in the case of conduction through a solid of constant cross section S, as detailed on the Figure 91.

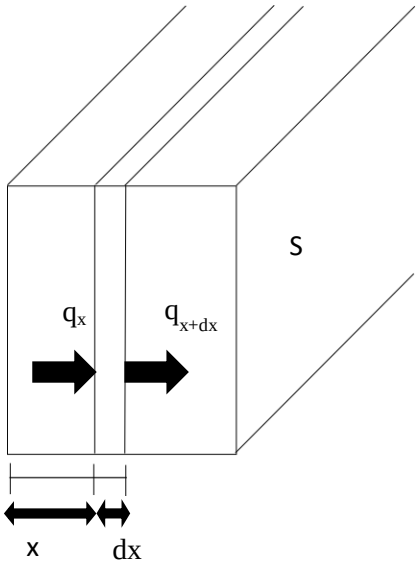

Figure 91: conduction in the case of a solid of constant cross section

Fourier's law defines the heat flux through the cross section S along the x direction as a function of the temperature gradient along the x direction:

$$q_x = -k\frac{dT}{dx}$$

Equation 71

With:

- q_x is the heat flux through the cross section S [W/m²]
- k is the thermal conductivity of the solid [W/m.°C]
- $\frac{dT}{dx}$ is the temperature derivative along the x axis.

If k is assumed to be constant with the temperature (which is the case since k only slightly varies on the 0°C to 100°C domain), the heat conservation between x and x+dx leads to $\frac{d^2T}{dx^2} = 0$ which implies a linear temperature distribution.

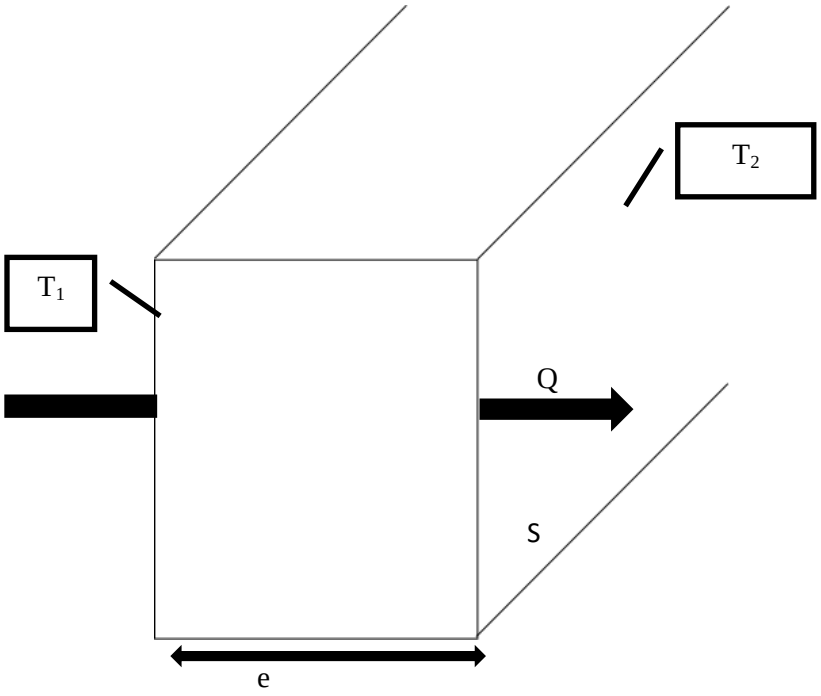

Figure 92: heat flux in case of heat conduction between two surfaces separated by a width e

Considering two isothermal faces of a solid with a thickness e, as illustrated on Figure 92, the heat transferred by conduction between the two faces is:

$$Q = \frac{k.S}{e}(T_1 - T_2)$$

Equation 72

With:

- S is the cross section [m²]
- e is the distance between the two faces of temperature T_1 and T_2 [m]
- T_1 and T_2 are the faces temperatures [°C]

The thermal resistance expresses as follows:

$$R_{th} = \frac{e}{k.S}$$

Equation 73

1.2. Resistance of radial conduction

The radial conduction is encountered in the case of thermal conduction through a solid of cylindrical shape.

Consider a hollow cylinder of inner radius r_{in} , outer radius r_{out} and length e, as the one shown in Figure 93. This cylinder is exposed to a temperature difference T_1-T_2. It is possible to define the thermal resistance in the case of radial heat conduction.

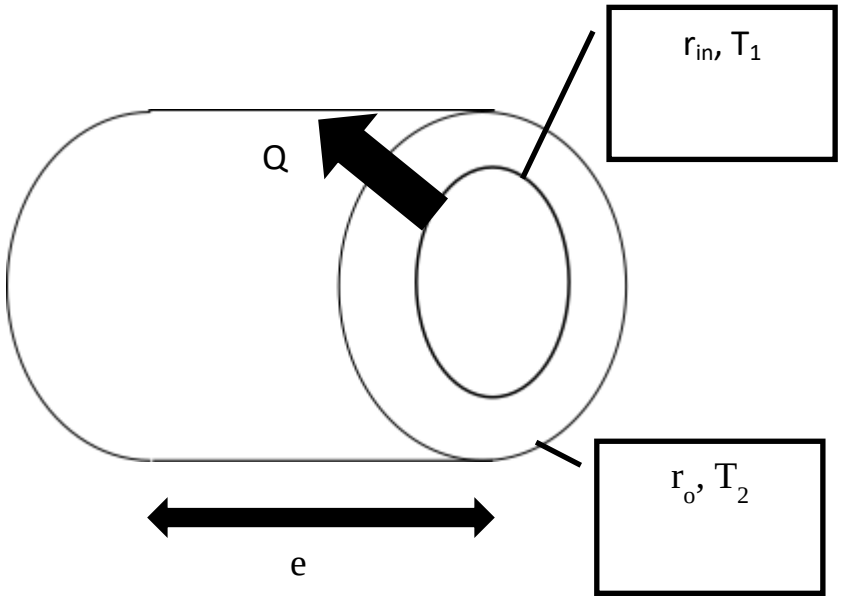

Figure 93: heat conduction in a hollow cylinder

Fourier's law describes the heat transferred at a radius r:

$$Q(r) = -k.2\pi r.e.\frac{dT}{dr}$$

Equation 74

From this expression, the heat conservation between r and r+dr leads to:

$$\frac{d^2T}{dr^2} + \frac{1}{r}\frac{dT}{dr} = 0$$

Equation 75

The solution is a logarithmic distribution [85] as a function of the cylinder radius. The heat transferred equals:

$$Q = \frac{2\pi ke}{\ln\left(\frac{r_o}{r_{in}}\right)}(T_1 - T_2)$$

Equation 76

Where:

- k is the thermal conductivity of the cylinder [W/m.°C]

- e is the cylinder width [m]
- r_o and r_{in} are respectively the outer and inner radius of the hollow cylinder [m]
- T_1 and T_2 are respectively the inner and outer surface temperature [°C]

The thermal resistance finally expresses as follows:

$$R_{th} = \frac{\ln\left(\frac{r_o}{r_{in}}\right)}{2\pi k e}$$

Equation 77

1.3. Resistance between two contacting materials

When two solids are in contact, a drop between the temperature on one side and the other of the contact area is observed. This temperature drop is due to the real geometry of the contacting surfaces: the contact is possible on limited areas. Actually, the remaining areas are separated by the ambient fluid –fluid surrounding the elements when they were put into contact-, since the contact area is not perfectly flat or smooth which means that some ambient fluid is present outer of the contacting points of the two solids.

The study of the heat exchange in the case of contacting solids [10] [41] is complex since it requires high amount of information:

- The fluid width separating the surfaces
- The size of the contacting area
- The number of contacting areas…

Since the topology of the contacts is difficult to acquire over a whole system, the contact resistance is difficult to obtain precisely. However orders of magnitude of this resistance could be found in Holman [56] or Bardon [11] studies in the case of metal-metal contact where the fluid trapped in the contact is air:

$$3.10^{-3} < \bar{k}.S_a.R_{th} < 6.10^{-6}$$

Equation 78

Where:

- $\bar{k}$ is the equivalent thermal conductivity [W/m.°C]

$$\bar{k} = 2\frac{k_1.k_2}{k_1 + k_2}$$

Equation 79

- k_1 and k_2 are the thermal conductivity of the solid 1 and 2 in contact [W/m.°C]
- S_a is the apparent contact area [m²]

2. Resistance of convection with oil

2.1. Exchange with the housing

2.1.1. Forced convection: the gear unit elements are rotating

The housing walls exchange with the oil: both the oil projected on the housing wall and the oil bath participate in the heat exchange.

The housing walls are considered as flat plates: this hypothesis allows considering a mean value of the Nusselt number to represent the exchange with a plate of length L [56]:

- If $Re < 5.10^5$,

$$Nu = 0.664 \times Re^{1/2} \times Pr^{1/3}$$

Equation 80

- If $Re > 5.10^5$

$$Nu = Pr^{\frac{1}{3}} \times (0.037 \times Re^{0.8} - 850)$$

Equation 81

The length L of the plate is the dimension to consider when computing Nu and Re. The speed value to consider in Reynolds number is the speed observed away from the boundary layer, where the viscous forces could be neglected. Two cases are to be considered: in the oil bath and oil runoff on the housing.

As presented in chapter I, it is possible to determine the convection coefficient from the Nusselt number with the following relationship:

$$Nu = \frac{h_{conv} L}{k}$$

Equation 82

From this relationship, the thermal resistance is deduced as follows:

$$R_{th} = \frac{1}{h_{conv} \times S}$$

Equation 83

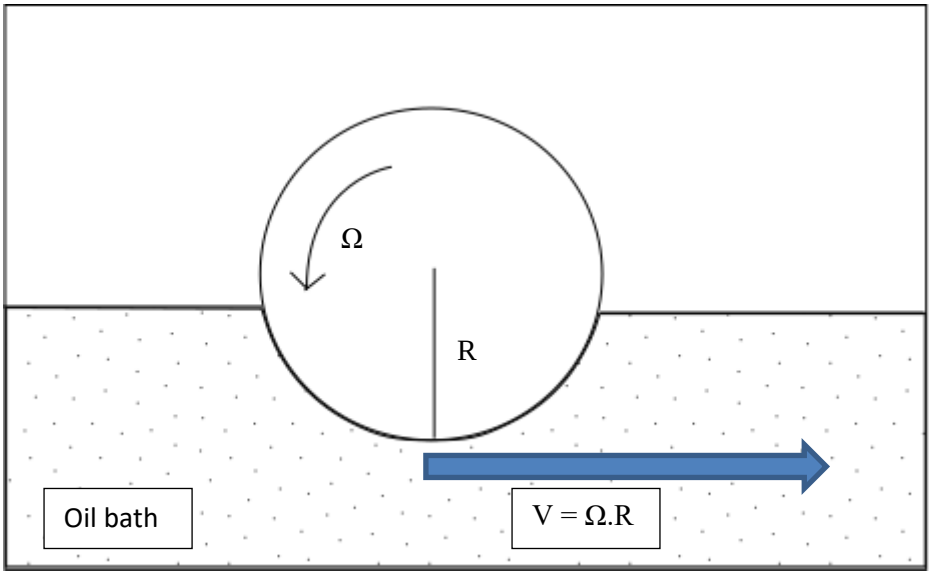

Figure 94: oil bath movement induced by the rotating gear

In the case of the oil bath, the oil is moved by the gear rotation, which means that the tangential speed of the gear is the value to consider when determining the oil movement (see Figure 94).

In the case of the oil runoff along the housing, the gravity is the force that produces the oil flow. Neglecting the drag losses and the viscous forces, the speed of the runoff of the oil equals:

$$V(t) = g.t$$

Equation 84

Then

$$x(t) = \frac{1}{2} g.t^2$$

Equation 85

Where:

- g is the gravitational acceleration [m/s²]
- t is the time [s]

As a mean exchange coefficient value is needed, the mean speed of the flow is retained and computed as follows [19]:

$$V_{mean} = \frac{1}{L}\int_0^L V(x).dx = \frac{1}{L}\int_0^L g.\sqrt{\frac{2x}{g}}dx = \sqrt{\frac{8.g.L}{9}} \approx 2.95\sqrt{L}$$

Equation 86

The dimensions in the case of the runoff of the oil are L the vertical height of the wall and x is the vertical direction of the running off of the oil.

2.1.2. Natural convection: the gear unit elements are not rotating

In the case that the elements of the gear unit are not rotating, the internal part of the housing exchanges either with the internal air for the non-immersed part or with the oil for the immersed part.

Concerning the part submerged in oil, the resistance is computed based on a relationship given in [56] in the case of the upper surface of heated plates:

If $Gr.Pr < 8 \times 10^6$

$$Nu = 0.54 \times (Gr \times Pr)^{0.25}$$

Equation 87

Else

$$Nu = 0.15 \times (Gr \times Pr)^{0.33}$$

Equation 88

Where:

- Gr is the Grashof number []
- Pr is the Prandtl number []

2.2. Exchange with the gears

2.2.1. Forced convection: the gear unit elements are rotating

The gear exchanges with the oil bath when rotating. Two kinds of phenomena could be distinguished: on one hand the gear sides exchange with the oil bath, on the other hand oil located on the teeth is flung off through centrifugal effects.

The first phenomenon is approximated through a mean value of the Nusselt number in the case of a rotating disc [114]:

- If $Re < 2.5 \times 10^5$

$$Nu = 0.4 \times Re^{0.5} \times Pr^{1/3}$$

Equation 89

- If $Re > 3.2 \times 10^5$

$$Nu = 0.238 \times Re^{0.8} \times Pr^{0.6}$$

Equation 90

The peripheral speed of the gears is the speed to consider [38]. The length of reference in Reynolds and Nusselt numbers is the pitch radius of the gear.

The energy evacuated by one tooth per unit width of the tooth is reported on Figure 95 [15].

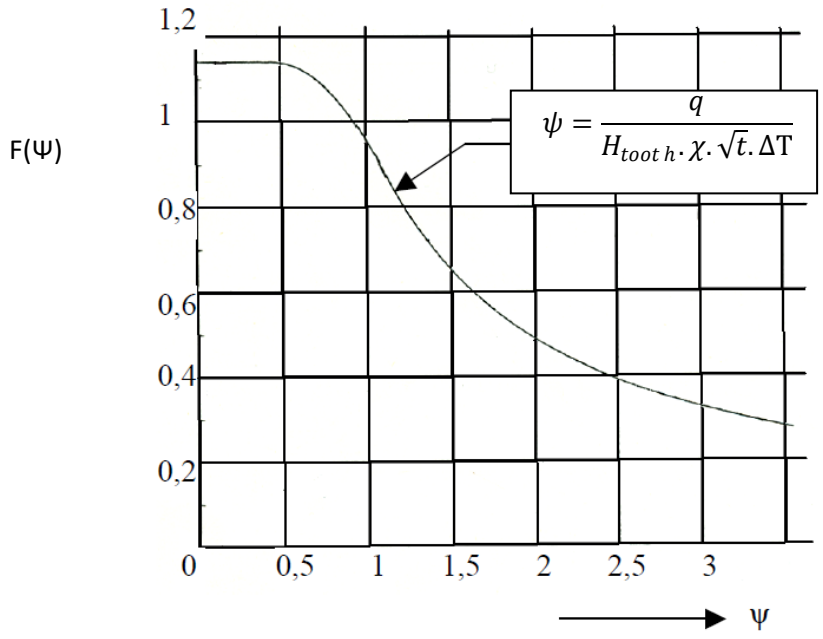

Figure 95: evolution of the energy evacuated by one tooth per unit width of the tooth

The parameter ψ is defined as:

$$\psi = \left(\frac{R_p . a . \theta^2}{\nu . H_{tooth}} \right)^{1/4}$$

Equation 91

Where:

- R_p is the pitch radius [m]
- a is the thermal diffusivity of the oil [m^2/s]
- θ is the centrifugal projection angle [rad]
- ν is the cinematic viscosity of the oil [m^2/s]
- H_{tooth} is the tooth height [m]

From this relationship, the thermal resistance between the gear and the oil in case of flung off through centrifugal effects expresses as follows [19] (see Figure 96 for dimensions):

$$R_{th} = \frac{2\pi}{F(\psi).b.2.Z.H_{tooth}.\chi.\sqrt{\omega.\theta}}$$

Equation 92

The F(Ψ) relationship can be approximated by a linear approximation based on Figure 95:

If $\psi < 0.68$

$$F(\psi) \approx 1.14$$

Equation 93

If $0.68 < \psi < 1.5$

$$F(\psi) \approx 1.55 - 0.6\psi$$

Equation 94

If $1.5 < \psi < 2$

$$F(\psi) \approx 1.16 - 0.32\psi$$

Equation 95

If $2 < \psi < 2.5$

$$F(\psi) \approx 0.84 - 0.18\psi$$

Equation 96

If $2.5 < \psi < 3$

$$F(\psi) \approx 0.74 - 0.14\psi$$

Equation 97

If $3 < \psi < 3.5$

$$F(\psi) \approx 0.62 - 0.1$$

Equation 98

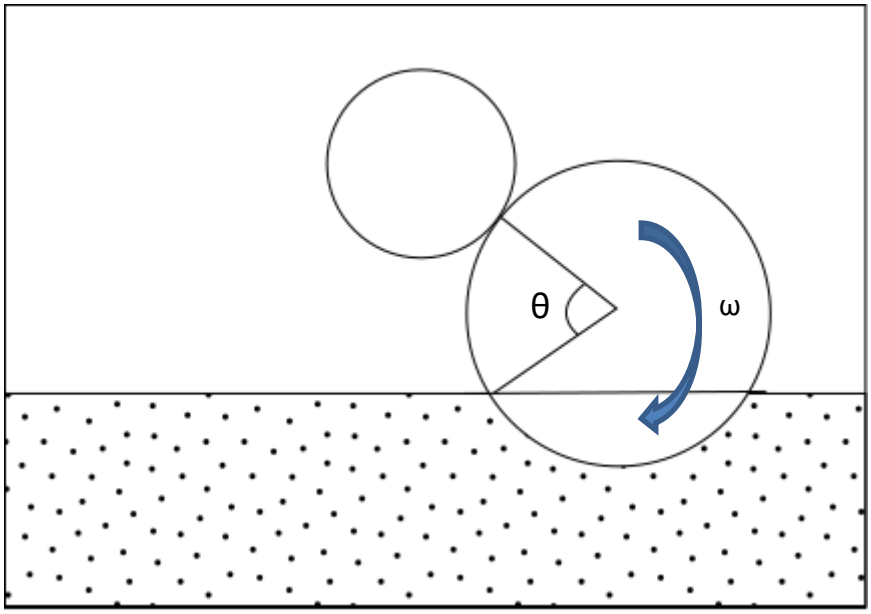

Figure 96: gear churning in the oil bath

2.2.2. Natural convection: the gear unit elements are not rotating

Considering horizontal cylinders dipping in a fluid, Churchill and Chu [56] propose for $10^{-6} < Gr.Pr < 10^{12}$:

$$Nu = \left(0.6 + 0.387 \times \left(\frac{Gr \times Pr}{\left(1 + \left(\frac{0.559}{Pr} \right)^{\frac{9}{16}} \right)^{\frac{16}{9}}} \right)^{\frac{1}{6}} \right)^{2}$$

Equation 99

The thermal resistance is determined from the Nusselt number like previously explained.

2.3. Exchange with the shafts

These elements are approximated by cylinders. Becker [12] gives a relationship to quantify the convection coefficients for cylinders rotating in a fluid for 1 000 < Re < 100 000:

$$Nu = 0.133 \times Re^{2/3} \times Pr^{1/3}$$

Equation 100

This formula is established from tests with water; however Lebeck [73] confirms that it is valid for oil. Reynolds and Nusselt number use the radius of the cylinder as reference length and the speed to consider is the peripheral speed of the cylinder.

In case of motionless shaft, Churchill and Bernstein propose the following relationship [24]:

$$Nu = 0.3 + \frac{0.62 \times Re^{1/2} Pr^{1/3}}{\left[1 + \left(\frac{0.4}{Pr}\right)^{\frac{2}{3}}\right]^{1/4}} \left[1 + \left[\frac{Re}{282\,000}\right]^{5/8}\right]^{4/5}$$

Equation 101

This formula is valid when $100 < Re < 10^7$ and $Re.Pr > 0.2$. Reynolds number considers the cylinder diameter as the reference length in this formula.

3. Resistances of convection and radiation with the environment

3.1. Natural convection

Natural convection appears when the movement of the fluid is only due to difference in density through heated walls.

Two configurations are distinguished: vertical and horizontal walls [19].

a. Vertical walls

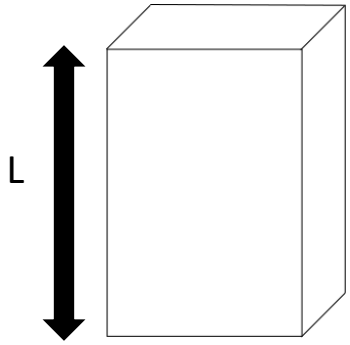

Figure 97: vertical plate

In the case of vertical walls, the Nusselt number defines as follows:

$$Nu = 0.28.(Gr.Pr)^{0.3}$$

Equation 102

Considering properties of ambient air at 293°K their values are included to obtain the convection coefficient value:

$$h_{conv} = 11.06 \times L^{-0.1} \times \left[\frac{T_{wall} - T_{air}}{T_{air}}\right]^{0.3}$$

Equation 103

Where:

- T_{wall} is the mean wall temperature [K]
- L is the reference length of the wall

b. Horizontal walls

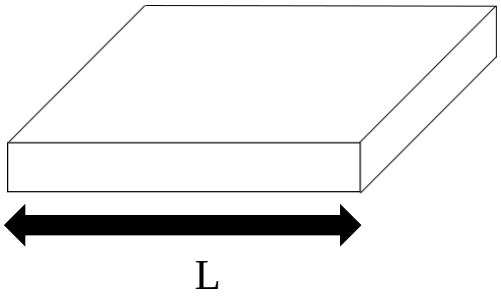

Figure 98: horizontal plate

In the case of horizontal plate, the Nusselt number expresses:

$$Nu = 0.2 \times (Gr.Pr)^{0.32}$$

Equation 104

Considering properties of ambient air at 293°K, their values are included to obtain the convection coefficient value:

$$h_{conv} = 12.87 \times L^{-0.04} \times \left[\frac{T_{wall} - T_{air}}{T_{air}}\right]^{0.32}$$

Equation 105

3.2. Forced convection

Forced convection is encountered in the case of an air flow generated by a fan or by the displacement of the system.

In the case of forced convection, the expressions of the convection coefficient vary in function of the direction of the flow with respect to the wall: tangential or normal flow.

3.2.1. Tangential air flow

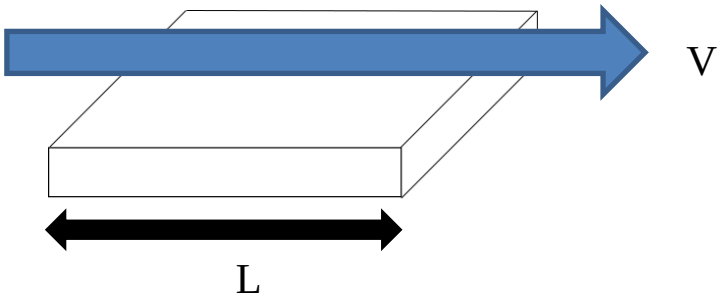

Figure 99: tangential flow

In this case, and by considering properties of ambient air at 20°C, the Nusselt number expresses:

$$Nu = 0.27 \times Re^{0.63}$$

Equation 106

It is possible to neglect the Prandtl number evolution since its value does not much evolves with temperature in the case of air.

Considering properties of ambient air at 20°C, their values are included to obtain the convection coefficient value:

$$h_{conv} = 7.6 \times L^{-0.37} \times V^{0.63}$$

Equation 107

3.2.2. Normal air flow

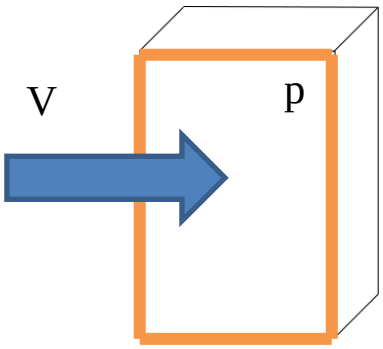

Figure 100: normal flow

In this case and considering properties of ambient air at 20°C, the Nusselt number expresses:

$$Nu = 0.147 \times Re^{0.66}$$

Equation 108

Considering properties of ambient air at 20°C, their values are included to obtain the convection coefficient value:

$$h_{conv} = 5.6 \times \left(\frac{A}{p}\right)^{-0.34} \times V^{0.66}$$

Equation 109

Where:

- A is the frontal area (normal to the flux) [m²]
- p is the perimeter of the frontal area [m]

3.3. Radiative exchange with the environment

The Stephan-Boltzmann law [56] expresses the heat exchange between a wall and the surrounding environment:

$$Q = \varepsilon.\sigma.S.\left(T_{wall}^4 - T_{air}^4\right)$$

Equation 110

Where:

- σ is the Stephan-Boltzmann constant ($\sigma = 5.67 \times 10^{-8}$) [W/m².K⁴]
- S is the exchange area of the wall [m²]
- ε is the material emissivity [ ]

The previous formula is nonlinear with the temperature evolution. The expression is then linearized for simplification needs:

$$Q = \varepsilon.\sigma.S.\left(T_{wall}^2 - T_{air}^2\right)(T_{wall} - T_{air})(T_{wall} - T_{air})$$

Equation 111

From this simplification, the thermal resistance equals:

$$R_{th} = \frac{1}{\varepsilon.\sigma.S.\left(T_{wall}^2 + T_{air}^2\right)(T_{wall} + T_{air})}$$

Equation 112

Radiative exchange is present at the same time that the convection, it means that the two resistances are associated in parallel, as resistances in an electrical network, to obtain the total exchange between air and the wall.

3.4. Heat-transfer through the shafts

When shaft rotates outside the housing (see Figure 101), it exchanges heat with the ambient air.

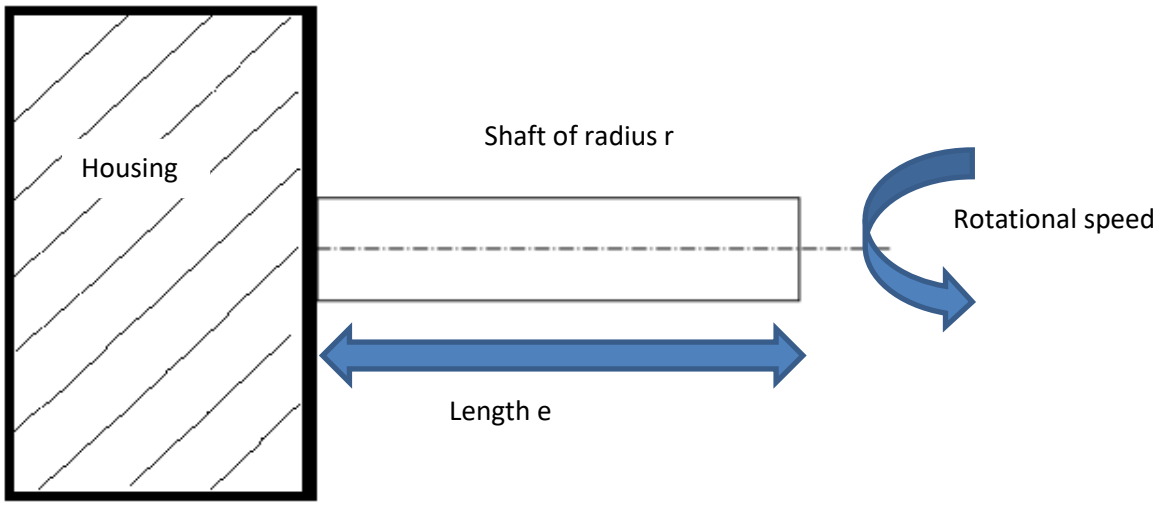

Figure 101: shaft rotating outside the housing

One can express the heat transferred to the air:

$$Q = h_{conv}.A.(T_{shaft} - T_{air})$$

Equation 113

Of course the shaft temperature varies along the length e, so the efficiency of the heat-transfer is considered as follows:

$$\eta = \frac{th\left(\sqrt{\frac{2.h_{conv}}{k.r}}.e\right)}{\left(\sqrt{\frac{2.h_{conv}}{k.r}}.e\right)}$$

Equation 114

Where k is the shaft conductivity.

The exchange area is defined as:

$$A = 2.\pi.r.e.\eta$$

Equation 115

In this case, T_{shaft} is defined as the shaft temperature inside the housing.

The convective exchange coefficient is defined considering a cylinder in rotation in the air [116]:

If $Re < 2500$

$$Nu = 0.4.Gr^{0.25}$$

Equation 116

If $2500 < Re < 15000$

$$Nu = 0.095.(0.5.Re^2 + Gr)^{0.35}$$

Equation 117

If $Re > 15000$

$$Nu = 0.073.Re^{0.7}$$

Equation 118

Nusselt and Reynolds numbers are computed with the ambient air properties, where the characteristic dimension is the shaft radius and the speed is the product of the rotational speed by the radius of the shaft.

The Grashof number is computed as follows:

$$Gr = \frac{g.\beta_f.(T_{mean} - T_{air}).(5.r)^3}{\nu^2}$$

Equation 119

Where T_{mean} is the mean temperature of the part of the shaft located outside the housing.

One can express the temperature of the shaft at the end of the shaft:

$$T_{shaft}(e) - T_{air} = \frac{T_{shaft} - T_{air}}{ch\left(\sqrt{\frac{2.h_{conv}}{k.r}}.e\right)}$$

Equation 120

If T_{mean} is associated to an arithmetic average, then:

$$T_{mean} - T_{air} = \frac{T_{shaft} - T_{air}}{2}\left[1 + \frac{1}{ch\left(\sqrt{\frac{2.h_{conv}}{k.r}}.e\right)}\right]$$

Equation 121

3.5. Resistance in the presence of fins

When fins are added on the housing, the impact on radiation and convection should be evaluated.

The radiative exchange is not much influenced since fin exchanges one with another which does not much impact the radiative heat transfer to the environment. The projected surface should be considered in the radiative exchange estimation.

The convective exchange is much more modified. However, the temperature of the fins varies along the length. Their temperature tends to the ambient temperature as their length increases, which reduces fin efficiency compared to an isothermal fin. The fin efficiency can be found in literature for complex shapes [56] [85] [94].

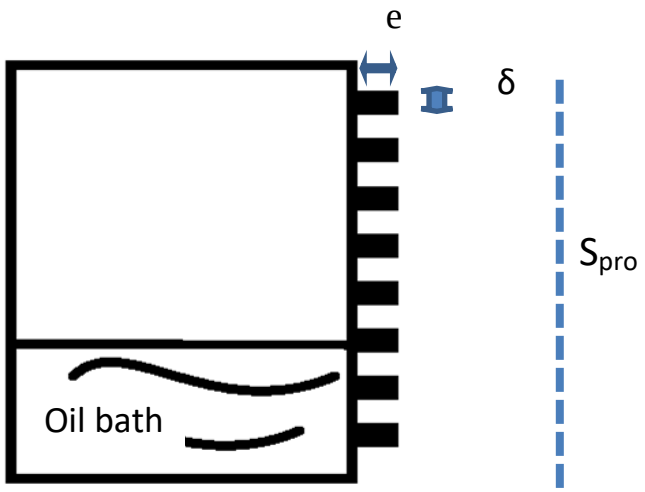

Figure 102: fins on the housing

Only the fin efficiency in the case of parallelepiped shape is reported hereafter [56]:

$$\eta_{fin} = \frac{th\left(\sqrt{\frac{2.h_{conv}}{k.\delta}}.e\right)}{\sqrt{\frac{2.h_{conv}}{k.\delta}}.e}$$

Equation 122

Where:

- k is the thermal conductivity of the material of the fin [W/m.°C]
- h_{conv} is the convective coefficient between the wall and the air [W/m².°C]

In this case, it is possible to obtain the heat transferred by convection by the fin and the housing as follows:

$$Q = h_{conv}\left[S_{pro} + n.\left(\eta_{fin}.S_{fin} - S_{fin\,cross\,section}\right)\right].\Delta T$$

Equation 123

Where:

- n is the number of fins
- S_{fin} is the area of the fin exchanging heat with air [m²]
- $S_{fin\,cross\,section}$ is the cross section (product of the width by the thickness) [m²]
- S_{pro} is the projected area of the housing [m²]
- ΔT is the temperature difference between the housing and the air [°K]

4. Exchange with the internal air

4.1. Natural convection with the gears

The formula 99 is considered with the characteristics of air instead of those of oil.

4.2. Forced convection with the gears

The exchange of air with the rotating gear is expressed through the following Nusselt expressions:

If $Re > 3.2 \times 10^5$, the expression is given by Cobb and Saunders [25]

$$Nu = 0.238 \times Re^{0.8} \times Pr^{0.6}$$

Equation 124

If $Re < 2.5 \times 10^5$, the expression is given by Wagner [114]

$$Nu = 0.4 \times \sqrt{Re} \times Pr^{1/3}$$

Equation 125

Then the thermal resistance expresses:

$$R_{th} = \frac{R_o}{Nu.k.S}$$

Equation 126

Where:

- k is the the thermal conductivity of air [W/m.°C]
- R_o is the external diameter of the gear [m]
- S is the surface of exchange [m^2]

4.3. Exchange with the housing

Formulas 102 to 109 are used in the case of exchange of internal air with the housing, accounting for the appropriate exchange condition.

The reference speed to consider is the peripheral speed of the nearest gear.

4.4. Exchange between oil and internal air

To consider the exchange between the oil and the intern air is represented by the formula from Fair [40]:

$$R_{th} = \frac{1}{h_{Fair}H}$$

Equation 127

Where:

- H is the total height of exchange between oil and air [m]
- h_{Fair} is the exchange coefficient [W/m^3K]

$$h_{Fair} = 2609Q_m$$

Equation 128

- Q_m is the mass flow around the teeth [95] [kg/s]

$$Q_m = \rho_{air} \times 0.0052 \times Zb H_{tooth} \omega$$

Equation 129

Where:

- ρ is the density of air [kg/m^3]
- Z is the number of teeth []
- b is the tooth width [m]
- H_{tooth} is the tooth height [m]
- ω is the rotational speed of the gear [rad/s]

In case all the elements in the gear unit are still, the following formula is used considering a mean value of exchange between air and the wall:

$$R_{th} = \frac{1}{10\,S}$$

Equation 130

Where:

- S is the surface exchange [m^2]

5. Resistances of striction

The mesh power losses are generated at the contact between the teeth in mesh. This contact area is small compared to the gears: the losses generate a temperature elevation which is confined to a thin “thermal skin” on the surface of the mating parts. Blok [14] proposes a relationship between the local temperature and the mean temperature of the gears. The striction resistance is defined from this relationship and allows linking the local temperature elevation with the gear bulk temperature, as explained in [19]:

$$R_{th}(i) = \frac{0.767}{\sqrt{2.l_h}.b.\chi.\sqrt{U_i}}$$

Equation 131

Where:

- $R_{th}(i)$ is the thermal resistance between the gear i and the associated mesh area [°C/W]
- l_h is the half width of the contact between two teeth [m]
- b is the mean length of the contact [m]
- χ is thermal effusivity of the material of the gear I [N/m.s$^{0.5}$.°C]
- U_i is the mean rolling speed of the pinion [m/s]

Appendix B

Lubricant properties

1. Density

Density is generally measured at 15°C. However density evolves with temperature: an analytical formula describes this evolution through a thermal dilatation parameter. This parameter is almost the same for the different kinds of oils: a good approximation is 0.00065. The expression of the evolution of the density is [9]:

$$\rho = \rho_{15°C} - 0.00065(T - 288)$$

Equation 132

2. Viscosity

The kinematic viscosity is really influenced by the temperature evolution. The kinematic viscosity follows a logarithmic law. An analytical formula describes the viscosity evolution based on two temperatures measurements at 40°C and 100°C, giving the A_υ and B_υ parameters [9]:

$$\log(\log(\upsilon \times 10^{-6} + 0.6)) = A_\upsilon \log(T) + B_\upsilon$$

Equation 133

3. Thermal conductivity

The thermal conductivity does not much vary between two oils, it is a little influenced by the temperature. It is expressed as follow:

$$k = -\frac{0.03}{400}(T - 273) + 0.14$$

Equation 134

4. Thermal capacity

The thermal capacity expression in function of the temperature is [9]:

$$C_p = 3.5T(T - 273) + 1800$$

Equation 135

Appendix C
Tredgold approximation for bevel gears

1. Introduction

Buckingham [18] presents a study concerning mechanical behavior of gears from cylindrical shapes to worm gears. Contact geometry, efficiency and mechanical resistance are also presented.

A focus is made on the part concerning spiral bevel gears.

2. Tredgold approximation

A focus is made on relationships defining the meshing contact conditions, especially the spiral bevel gears. The contact and the geometry of spiral bevel gears are possible on a sphere surface, since it allows circumscribing pitch cone. However it is not possible to develop the sphere on a plane: the study of this kind of tooth geometry is then more complex. The objective is to get close enough of the real geometry while developing the geometry on a plane.

A projection of the base circles of the cones is then realized along a plane which is normal to the line tangent to the instantaneous contact line between the two cones, as shown on Figure 103. On the projected geometries, it is then possible to get back to the equivalent geometry of virtual cylindrical gears. This projection is called Tredgold approximation. These equivalent cylindrical gears are used to study contact conditions in an analog way than the real cylindrical gears contact. This method is designed for gears with more than eight teeth, however the approximation should be considered with great care.

One more approximation is made on the tooth profile: it is considered as a circle involute but it is an octoid tooth.

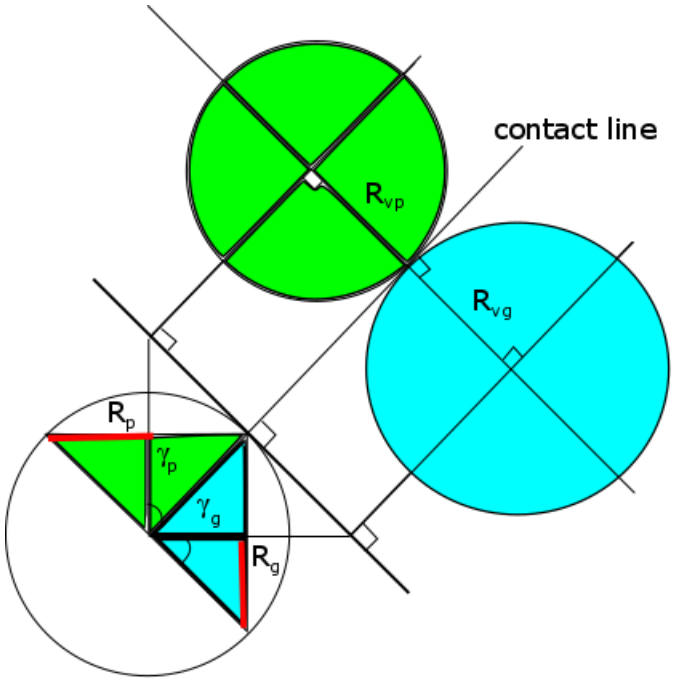

Figure 103: Tredgold approximation scheme

3. Geometric relationships – virtual gears

The Tredgold approximation leads to geometrical relationships which defines the virtual gears.

The half angle of the pitch cones are linked as follow:

$$\Sigma = \gamma_p + \gamma_g$$

Equation 136

The link between the half angle of the pinion and the sum of half angles of the pinion and the wheel expresses as follow:

$$tan(\gamma_p) = \frac{\sin(\Sigma)}{\left(N_g/N_p\right) + \cos(\Sigma)}$$

Equation 137

If ∑=90°, the half angle of the pinion equals the simplified expression:

$$tan(\gamma_p) = \frac{N_p}{N_g}$$

Equation 138

The half angle of the wheel is then:

$$\tan(\gamma_g) = \frac{N_g}{N_p}$$

Equation 139

The radius of the sphere circumscribing the two cones is expressed as follow:

$$A = \frac{R_p}{\sin(\gamma_p)} = \frac{R_g}{\sin(\gamma_g)}$$

Equation 140

The radius and number of teeth of the virtual cylindrical gears are obtained when projecting the cones. It is detailed in the following equations. The virtual radius of the equivalent pinion is then:

$$R_{vp} = \frac{R_p}{\cos(\gamma_p)} = A \times \tan(\gamma_p)$$

Equation 141

The virtual radius of the equivalent wheel is:

$$R_{vg} = \frac{R_g}{\cos(\gamma_g)} = A \times \tan(\gamma_g)$$

Equation 142

The virtual number of teeth of the equivalent cylindrical pinion is expressed as:

$$N_{vp} = \frac{N_p}{\cos(\gamma_p)}$$

Equation 143

The virtual number of teeth of the equivalent cylindrical wheel is:

$$N_{vg} = \frac{N_g}{\cos(\gamma_g)}$$

Equation 144

The design of the conical gears is as follow: the geometry is defined on the equivalent cylindrical gear, and then it is represented on the real conical gear geometry.

3.1. Design of teeth geometry on the gears with crossing axes

Tooth profile is defined on the equivalent virtual cylindrical gear. Then this tooth profile is associated with the real conical gear thanks to the following relationships which link the virtual and the real geometries.

The addendum and dedendum angles are respectively:

$$\tan \alpha = \frac{a}{A}$$

Equation 145

With a the addendum

$$\tan \delta = \frac{b}{A} \, avec \; b : dedendum$$

Equation 146

With b the dedendum

The top and root angles are respectively defined as follow:

$$\tan(\gamma_0) = \gamma + \alpha$$

Equation 147

$$\tan(\gamma_r) = \gamma - \alpha$$

Equation 148

The spiral angle formula is:

$$arc(\beta) = \frac{(t/2) + b \times \tan(\Phi_c)}{A}$$

Equation 149

With:

- t: tooth width at the pitch cone
- Φ_c: pressure angle of the generating hob

3.2. Design of special teeth in case of crossing axle gears

The modification of the pressure angle is possible through the generation angle and operating angle. This is equivalent to a modification of the gear center distance when considering cylindrical gears. Tredgold method is then used to work on the equivalent virtual cylindrical gear and compute the real geometry based on these results.

4. Spiral bevel gear with octoid teeth

4.1. Logarithmic spiral

The logarithmic spiral allows keeping a constant spiral angle along the tooth and should be preferred. However cutting methods tend to provide circular arc, like Gleason methodology.

4.2. Contact curvature

Since the cutting is made thanks to a circular rack, the tooth profile is made from circular arcs. The concave and convex profiles of the tooth have different spiral angle: the spiral angle is slightly lower on the convex part of the tooth.

N.B.: the variation of the spiral angle between the concave and convex profiles is always lower than the distance between two teeth.

From this variation of spiral angle, the load tends to be placed on the internal part of the tooth for low loads and to expend to the external part for higher loads as shown on Figure 104.

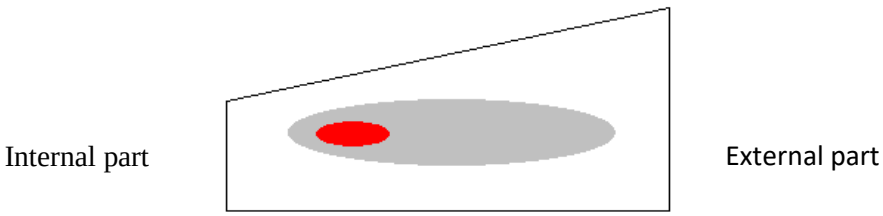

Figure 104: load repartition of the tooth: red area for lighter loads to grey area for higher loads

5. Shape of the circular rack

The circular rack used by Gleason has a conical shape, not a plane, which induces slight error from the ideal profile. However the error is much lower than cutting errors.

6. Operating limitation of the meshing teeth

Three factors are limiting the load capacity of gears:

- Excessive temperature
- Tooth rupture
- Excessive wear

Moreover excessive noise can also be a limit, even if none of the previous factors is involved. Noise is always present, but excessive noise level represents operating conditions outer of an adapted range. Solutions exist in tooth shape modifications, improvement in the manufacturing or assembly quality, or change in the lubricant.

7. Efficiency of gears

Buckingham proposes several formulas to compute efficiency of different kinds of gear pairs from the analysis of the transmitted power and the estimation of a friction coefficient. Only the efficiency formulas are reported, the intermediate developments are not detailed.

7.1. Hypothesis

The following hypotheses are used to establish the efficiency formulas presented in this part:

- The tooth follow an involute shape without error and equally distant
- The pressure is constant, normal to the surface, all along the mesh between two teeth
- When two teeth or more share the load, the pressure is equally distributed between them

7.2. Efficiency of spur gears

The following formula is the efficiency in the case of spur gears:

$$\eta = 1 - \left[\frac{1+\left(\frac{1}{m}\right)}{\beta a1 + \beta r1}\right]\left(\frac{fa}{2}\beta a1^2 + \frac{fr}{2}\beta r1^2\right)$$

Equation 150

With:

- fa and fr are friction coefficients in approach and recess path of contact
- $m = \frac{N_2}{N_1}$ is the reduction ratio
- Arc of approach:

$$\beta a = \frac{\sqrt{Ro2^2 - Rb2^2} - R2 \times \sin(\Phi)}{Rb1}$$

Equation 151

- Arc of recess:

$$\beta r = \frac{\sqrt{Ro1^2 - Rb1^2} - R1 \times \sin(\Phi)}{Rb1}$$

Equation 152

N.B.: The friction coefficients are based on the experimental tests realized by ASME Research Publication in 1931 in “dynamic loads on gar teeth”.

7.3. Efficiency of helical gears

The helix modifies the efficiency of helical gears with respect to spur gear. It expresses as follow:

$$\eta = 1 - \left(\frac{\cos(\Phi)}{\cos(\Phi n)\cos(\psi)}\right)\left[\frac{1 + \left(\frac{1}{m}\right)}{\beta a1 + \beta r1}\right]\left(\frac{fa}{2}\beta a1^2 + \frac{fr}{2}\beta r1^2\right)$$

Equation 153

With:

- ψ is the helix angle at the pitch radius
- Φ is the pressure angle in the plane of the rotation
- Φn is the normal pressure angle
- $N1$ and $N2$ are the number of teeth of the pinion and the wheel
- m is the reduction ratio

7.4. Efficiency of spiral bevel gears

The spiral angle is taken into account in the following formula proposed by Buckingham:

$$\eta = 1 - \left(\frac{\cos(\Phi)}{\cos(\Phi n)\cos(\psi)}\right)\left[\frac{1+\left(\frac{1}{m}\right)}{(\beta a1 + \beta r1)\cos(\psi)}\right]\left(\frac{fa}{2}\beta a1^2 + \frac{fr}{2}\beta r1^2\right)$$

Equation 154

With:

- m is the reduction ratio
- Arc of approach:

$$\beta a = \frac{\sqrt{Rog^2 - Rbg^2} - Rvg \times \sin(\Phi)}{Rbp}$$

Equation 155

- Arc of recess:

$$\beta r = \frac{\sqrt{Rop^2 - Rbp^2} - Rvp \times \sin(\Phi)}{Rbp}$$

Equation 156

- Rvp and Rvg are the virtual radii of the pinion and the wheel
- Rog and Rop are the outer radii of the wheel and the pinion respectively

$$Ro = Rv + a_i$$

Equation 157

- Rb is the equivalent base radius

$$Rb = Rv \times \cos(\Phi)$$

Equation 158

- a_i is the addendum of the associated gear
- ϕ is the pressure angle

7.5. Efficiency of spiral bevel gears

The efficiency of hypoid gears is a combination of the spiral gears and the worm gears:

$$\eta = \frac{1}{1 + A + B}$$

Equation 159

With:

- A is the power losses of the spiral bevel gear:

$$A = \frac{power\ losses}{power\ transmitted}$$

Equation 160

$$A = \left(\frac{\cos(\Phi)}{\cos(\Phi n)\cos(\psi)}\right)\left[\frac{1 + \left(\frac{1}{m}\right)}{(\beta a1 + \beta r1)\cos(\psi)}\right]\left(\frac{fa}{2}\beta a1^2 + \frac{fr}{2}\beta r1^2\right)$$

Equation 161

- B is the power losses of the worm gear

$$B = \frac{pertes}{puissance} = \left(\frac{2\mathrm{f}}{\cos(\Phi n)\sin(2\gamma p) + 2f}\right)$$

Equation 162

With:

- γp is the generating angle of the pinion
- Φn is the normal pressure angle in the middle of the face
- f is the mean friction coefficient

7.6. Generalized expression of the efficiency formulas

From Velex and Ville study [112], the efficiency expression could be rewritten when considering fa=fr=f:

$$\eta = 1 - f(1+u)\frac{\pi}{Z_1}\frac{1}{\cos(\beta_b)}\varepsilon_\alpha \Lambda$$

Equation 163

With:

- Λ is a power loss factor
- f is the friction coefficient
- u is the reduction ratio

$$u = \frac{Z_1}{Z_2}$$

Equation 164

- β_b is the base helix angle
- Zi is the number of teeth of i gear
- ε_α is the contact ratio

7.6.1. Spur and helical gears

For the spur and helical gears, the power losses factor is:

$$\Lambda = 2\kappa_0^2 - 2\kappa_0 + 1$$

Equation 165

With:

$$\kappa_0 = \frac{Z_1}{2\pi}\frac{1}{\varepsilon_\alpha u}\left[\sqrt{\left(\frac{R_{a2}}{R_{p2}cos(\alpha_p)}\right)^2 - 1} - \tan(\alpha_p)\right] = \frac{Z_1}{2\pi}\frac{1}{\varepsilon_\alpha}\beta_a$$

Equation 166

7.6.2. Spiral bevel gears

The general expression is conserved for spiral bevel gears and the power loss factor is written as:

$$\Lambda = \frac{2\kappa_0^2 - 2\kappa_0 + 1}{\cos(\beta)}$$

Equation 167

Appendix D

Formulas for the determination of the immersed area in case of gears

1. Sm formula in the case of spur and helical gears

From the work of Changenet et al. concerning churning of cylindrical gears in the case of a gearbox [22], the immersed area Sm formula is the sum of the sides and the teeth areas:

$$S_{sides} = R_p^2(2\theta - \sin(2\theta))$$

Equation 168

$$S_{teeth} = D_p b\theta + \frac{2Z\theta H_{tooth} b}{\pi \times \cos(\alpha)}$$

Equation 169

$$S_m = S_{sides} + S_{teeth}$$

Equation 170

With:

- Rp, Dp: respectively the pitch radius and pitch diameter [m]
- θ is the angle defined in Figure 105

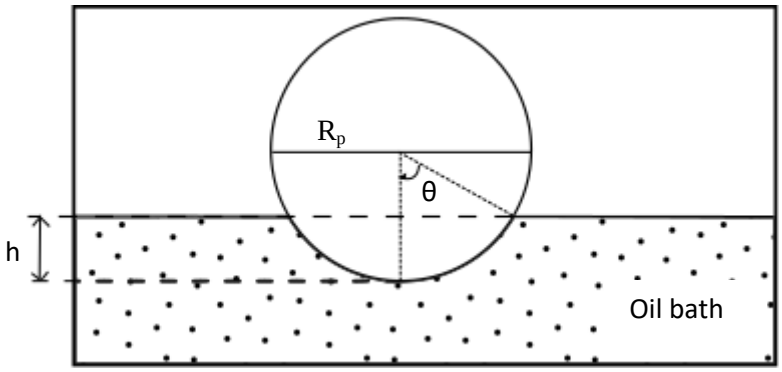

Figure 105: pinion immersed in an oil bath

- b is the gear width [m]
- Z is the number of teeth
- H_{tooth} is the tooth height [m]
- α is the pressure angle [rad]

2. Sm formula in the case of bevel gears

The immersed areas of a bevel gear are identified in Figure 106.

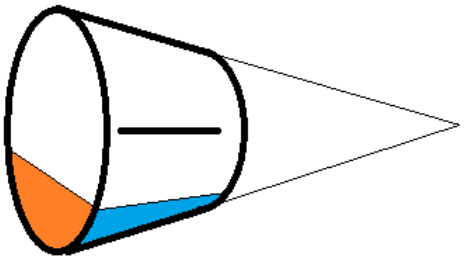

Figure 106: scheme from the back side of the pinion (tooth not represented), with the cone angle

To simplify the problem, two areas are isolated: the front and back areas {a}, the peripheral area {b}.

a. the front and back areas (orange areas in Figure 106)

The areas are computed as follows for the front and back side of the gear:

- h^* is defined as a constant value computed from the back end of the gear:

$$h^* = R - h$$

Equation 171

- Then, the orange area for the back side is:

$$A1 = \frac{1}{2}R^2\left(2\,\mathrm{acos}\left(\frac{h^*}{R}\right) - \sin\left(2\,acos\left(\frac{h^*}{R}\right)\right)\right)$$

Equation 172

For the front side, it is:

$$A2 = \frac{1}{2}e_o^2\left(2\,\mathrm{acos}\left(\frac{h^*}{e_o}\right) - \sin\left(2\,acos\left(\frac{h^*}{e_o}\right)\right)\right)$$

Equation 173

e_o represents the radius of the front side of the truncated cone associated to the cone of base radius R.

b. the peripheral area

It represents the area of the side face of the truncated cone which is immersed in the lubricant sump. It is colored in blue on Figure 106. A function shown in Figure 107 is defined which represents the slope of the external surface.

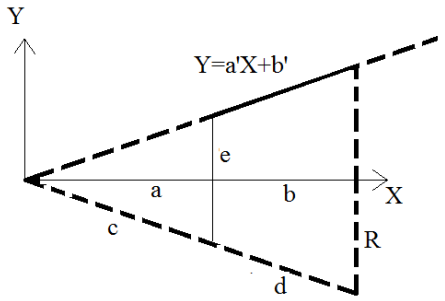

Figure 107: function representing the slope of external surface

b' is equal to zero so a' is defined. Θ_{max} is set as:

$$\theta_{max} = \text{acos}\left(\frac{h^*}{R}\right)$$

Equation 174

From the Figure 107 and these notations, the area of the external surface of the cone of radius R is expressed as:

$$A3 = \int_a^{a+b} 2\theta(x)r(x)\,dx$$

Equation 175

Finally the area is equal to:

$$A3 = \left[(a+b)\left(a'(a+b)\,\text{acos}\left(\frac{h^*}{a'(a+b)}\right) - H\sqrt{1-\frac{h^{*2}}{a'^2(a+b)}}\right)\right] - \left[a\left(a'a\,\text{acos}\left(\frac{h^*}{a'a}\right) - H\sqrt{1-\frac{h^{*2}}{a'^2a^2}}\right)\right]$$

Equation 176

Appendix E

Churning tests

1. List of the churning tests

1.1. List of churning tests – oil A

Rotational speed [RPM]	Oil temperature [°C]	Immersion ratio h/R [ ]	Gear tested	Measured power losses [W]
997	42	0.49	Gear 1	38.7
1491	42	0.49	Gear 1	78.6
1013	70	0.49	Gear 1	26.4
1496	70	0.49	Gear 1	54.0
1997	70	0.49	Gear 1	90.9
800	20	0.49	Gear 1	48.5
800	40	0.49	Gear 1	25.5
800	55	0.49	Gear 1	20.2
800	70	0.49	Gear 1	17.8
1000	20	0.49	Gear 1	67.5
1000	40	0.49	Gear 1	39.5
1000	55	0.49	Gear 1	30.4
1000	70	0.49	Gear 1	26.5
1500	20	0.49	Gear 1	133.4
1500	40	0.49	Gear 1	76.4
1500	55	0.49	Gear 1	61.2
1500	70	0.49	Gear 1	57.1
2000	20	0.49	Gear 1	203.6
2000	40	0.49	Gear 1	117.7
2000	55	0.49	Gear 1	106.7
2000	70	0.49	Gear 1	96.7

800	20	0.38	Gear 2	22.0
800	40	0.38	Gear 2	12.2
800	55	0.38	Gear 2	8.6
800	70	0.38	Gear 2	5.5
1000	20	0.38	Gear 2	31.4
1000	40	0.38	Gear 2	17.8
1000	55	0.38	Gear 2	11.6
1000	70	0.38	Gear 2	8.8
1500	20	0.38	Gear 2	55.8
1500	40	0.38	Gear 2	31.0
1500	55	0.38	Gear 2	21.5
1500	70	0.38	Gear 2	16.7
2000	20	0.38	Gear 2	80.5
2000	40	0.38	Gear 2	44.5
2000	55	0.38	Gear 2	30.6
2000	70	0.38	Gear 2	25.2
977	41	0.57	Gear 3	69.6
1426	42	0.57	Gear 3	145.4
1016	70	0.57	Gear 3	67.5
1500	70	0.57	Gear 3	147.1
1011	70	0.48	Gear 4	26.8

1501	70	0.48	Gear 4	56.9
2005	70	0.48	Gear 4	97.3

1.2. List of churning tests – oil B

Rotational speed [RPM]	Oil temperature [°C]	Immersion ratio h/R [ ]	Gear tested	Measured power losses [W]
976	70	0.36	Gear 1	10.8
1506	70	0.36	Gear 1	22.6
2006	70	0.36	Gear 1	35.7
980	50	0.36	Gear 1	10.6
1508	50	0.36	Gear 1	21.5
2010	50	0.36	Gear 1	31.5
978	30	0.36	Gear 1	10.8
1502	30	0.36	Gear 1	20.5
2012	30	0.36	Gear 1	31.0
959	32	0.49	Gear 1	22.1
1491	32	0.49	Gear 1	50.3
2009	32	0.49	Gear 1	89.9
2513	32	0.49	Gear 1	120.3
3009	32	0.49	Gear 1	115.4
945	50	0.49	Gear 1	17.9
1485	50	0.49	Gear 1	41.6
1997	50	0.49	Gear 1	71.7

2509	50	0.49	Gear 1	99.5
3001	50	0.49	Gear 1	104.5
951	70	0.49	Gear 1	14.9
1489	70	0.49	Gear 1	34.7
1995	70	0.49	Gear 1	59.6
2514	70	0.49	Gear 1	84.3
3005	70	0.49	Gear 1	86.4
943	70	0.49	Gear 1	16.1
1487	70	0.49	Gear 1	38.9
1999	70	0.49	Gear 1	68.3
943	50	0.49	Gear 1	19.3
1487	50	0.49	Gear 1	45.7
2001	50	0.49	Gear 1	78.7
933	32	0.49	Gear 1	21.4
1485	32	0.49	Gear 1	50.3
1997	32	0.49	Gear 1	88.7
981	70	0.38	Gear 2	5.7
1517	70	0.38	Gear 2	11.8
2015	70	0.38	Gear 2	18.6
981	50	0.38	Gear 2	7.4
1505	50	0.38	Gear 2	15.5
2013	50	0.38	Gear 2	24.6
989	30	0.38	Gear 2	7.9
1503	30	0.38	Gear 2	15.1

2013	30	0.38	Gear 2	23.6
929	60	0.47	Gear 3	31.7
1481	61	0.47	Gear 3	83.9
931	69	0.47	Gear 3	32.2
1475	70	0.47	Gear 3	85.1
901	30	0.47	Gear 3	42.9
1473	30	0.47	Gear 3	107.7
931	50	0.47	Gear 3	35.6
1475	50	0.47	Gear 3	91.7
847	22	0.47	Gear 3	50.5
1467	22	0.47	Gear 3	133.7
829	31	0.47	Gear 3	47.5
1455	31	0.47	Gear 3	121.6
1007	50	0.47	Gear 3	54.9
1457	50	0.47	Gear 3	111.0
1015	69	0.47	Gear 3	52.3
1463	69	0.47	Gear 3	100.1
968	70	0.48	Gear 4	16.3
1499	70	0.48	Gear 4	37.2
2011	70	0.48	Gear 4	63.4
967	50	0.48	Gear 4	19.7
1497	50	0.48	Gear 4	45.0

2009	50	0.48	Gear 4	76.1
963	31	0.48	Gear 4	20.9
1495	31	0.48	Gear 4	47.7
2007	31	0.48	Gear 4	82.9

1.3. List of churning tests – oil C

Rotational speed [RPM]	Oil temperature [°C]	Immersion ratio h/R [ ]	Gear tested	Measured power losses [W]
1000	40	0.40	Gear 1	11.8
1500	40	0.40	Gear 1	23.8
2000	40	0.40	Gear 1	38.8
1000	40	0.49	Gear 1	22.9
1500	40	0.49	Gear 1	45.3
2000	40	0.49	Gear 1	78.3
1000	40	0.49	Gear 1	26.5
1500	40	0.49	Gear 1	59.5
2000	40	0.49	Gear 1	100.2
1000	40	0.38	Gear 2	6.6
1500	40	0.38	Gear 2	13.1
2000	40	0.38	Gear 2	21.2
1000	40	0.46	Gear 2	10.0
1500	40	0.46	Gear 2	20.3
2000	40	0.46	Gear 2	34.4
1000	40	0.54	Gear 2	13.2

1500	40	0.54	Gear 2	28.2
2000	40	0.54	Gear 2	48.5
1000	40	0.41	Gear 3	27.8
1500	40	0.41	Gear 3	59.9
2000	40	0.41	Gear 3	106.0
1000	40	0.50	Gear 3	51.9
1500	40	0.50	Gear 3	102.9
2000	40	0.50	Gear 3	160.0
1000	40	0.57	Gear 3	63.2
1500	40	0.57	Gear 3	132.2
2000	40	0.57	Gear 3	220.8
1000	40	0.40	Gear 4	15.7
1500	40	0.40	Gear 4	21.4
2000	40	0.40	Gear 4	31.6
1000	40	0.48	Gear 4	21.4
1500	40	0.48	Gear 4	48.3
2000	40	0.48	Gear 4	75.6
1000	40	0.60	Gear 4	26.3
1500	40	0.60	Gear 4	59.6
2000	40	0.60	Gear 4	91.4

1.4. List of churning tests – oil D

Rotational speed [RPM]	Oil temperature [°C]	Immersion ratio h/R [ ]	Gear tested	Measured power losses [W]
1000	39	0.62	Gear 1	39.0
1252	40	0.62	Gear 1	56.8
1497	41	0.62	Gear 1	79.1
1761	41	0.62	Gear 1	100.5
1989	41	0.62	Gear 1	118.8
2495	41	0.62	Gear 1	154.4
997	40	0.49	Gear 1	28,3
1245	40	0.49	Gear 1	41,8
1497	40	0.49	Gear 1	53,8
1759	40	0.49	Gear 1	71,6
2007	40	0.49	Gear 1	82,5
2495	40	0.49	Gear 1	110,1
995	40	0.40	Gear 1	16,8
1253	40	0.40	Gear 1	24,1
1503	40	0.40	Gear 1	28,2
1747	40	0.40	Gear 1	35,8
2017	40	0.40	Gear 1	44,1
2501	40	0.40	Gear 1	50,7
984	80	0,46	Gear 2	8,26
1240	80	0,46	Gear 2	12,08
1508	80	0,46	Gear 2	16,63

1764	80	0,46	Gear 2	22,05
2012	80	0,46	Gear 2	27,17
980	79	0,46	Gear 2	8,35
1240	79	0,46	Gear 2	12,21
1514	79	0,46	Gear 2	16,72
1766	79	0,46	Gear 2	22,52
2012	79	0,46	Gear 2	26,92
978	78	0,45	Gear 2	8,28
1236	78	0,45	Gear 2	12,06
1512	78	0,45	Gear 2	16,71
1760	78	0,45	Gear 2	21,95
2010	78	0,45	Gear 2	27,30
978	77	0,45	Gear 2	8,19
1240	77	0,45	Gear 2	12,16
1514	77	0,45	Gear 2	16,80
1762	77	0,45	Gear 2	22,25
2010	77	0,45	Gear 2	26,45
984	76	0,45	Gear 2	8,25
1240	76	0,45	Gear 2	12,13
1514	76	0,45	Gear 2	16,81
1766	76	0,45	Gear 2	21,93
2008	76	0,45	Gear 2	27,28
982	75	0,45	Gear 2	8,44
1238	75	0,45	Gear 2	12,07
1510	75	0,45	Gear 2	16,83
1764	75	0,45	Gear 2	22,11

2012	75	0,45	Gear 2	27,01
988	74	0,45	Gear 2	8,40
1244	74	0,45	Gear 2	12,21
1514	74	0,45	Gear 2	16,64
1764	74	0,45	Gear 2	21,98
2012	74	0,45	Gear 2	27,09
978	73	0,44	Gear 2	8,45
1244	73	0,44	Gear 2	12,25
1515	73	0,44	Gear 2	16,67
1762	73	0,44	Gear 2	22,09
2012	73	0,44	Gear 2	26,91
984	72	0,44	Gear 2	8,28
1240	72	0,44	Gear 2	12,13
1516	72	0,44	Gear 2	16,46
1764	72	0,44	Gear 2	21,86
2010	72	0,44	Gear 2	26,74
982	71	0,44	Gear 2	8,41
1240	71	0,44	Gear 2	12,02
1510	71	0,44	Gear 2	16,21
1764	71	0,44	Gear 2	21,85
2012	71	0,44	Gear 2	26,09
986	70	0,44	Gear 2	8,49
1244	70	0,44	Gear 2	11,98
1512	70	0,44	Gear 2	16,48
1762	70	0,44	Gear 2	21,47
2012	70	0,44	Gear 2	26,23

982	69	0,44	Gear 2	8,49
1240	69	0,44	Gear 2	12,24
1512	69	0,44	Gear 2	16,58
1762	69	0,44	Gear 2	21,34
2014	69	0,44	Gear 2	26,62
984	68	0,44	Gear 2	8,28
1240	68	0,44	Gear 2	11,97
1510	68	0,44	Gear 2	16,43
1766	68	0,44	Gear 2	21,79
2014	68	0,44	Gear 2	26,55
980	67	0,44	Gear 2	8,32
1238	67	0,44	Gear 2	11,90
1510	67	0,44	Gear 2	16,41
1764	67	0,44	Gear 2	21,65
2012	67	0,44	Gear 2	26,74
986	66	0,44	Gear 2	8,33
1240	66	0,44	Gear 2	12,29
1508	66	0,44	Gear 2	16,31
1766	66	0,44	Gear 2	21,74
2016	66	0,44	Gear 2	26,54
986	65	0,44	Gear 2	8,54
1244	65	0,44	Gear 2	12,08
1506	65	0,44	Gear 2	16,43
1762	65	0,44	Gear 2	22,22
2012	65	0,44	Gear 2	26,55
986	64	0,43	Gear 2	8,50

1240	64	0,43	Gear 2	12,05
1512	64	0,43	Gear 2	16,38
1766	64	0,43	Gear 2	21,71
2020	64	0,43	Gear 2	26,40
988	63	0,43	Gear 2	8,46
1242	63	0,43	Gear 2	12,18
1508	63	0,43	Gear 2	16,66
1760	63	0,43	Gear 2	21,46
2016	63	0,43	Gear 2	26,51
978	62	0,43	Gear 2	8,32
1240	62	0,43	Gear 2	12,16
1510	62	0,43	Gear 2	16,59
1764	62	0,43	Gear 2	21,33
2010	62	0,43	Gear 2	26,32
986	61	0,43	Gear 2	8,64
1244	61	0,43	Gear 2	12,33
1508	61	0,43	Gear 2	16,36
1764	61	0,43	Gear 2	21,94
2014	61	0,43	Gear 2	25,49
982	60	0,43	Gear 2	8,64
1242	60	0,43	Gear 2	12,44
1510	60	0,43	Gear 2	16,27
1770	60	0,43	Gear 2	21,59
2012	60	0,43	Gear 2	26,37
990	59	0,42	Gear 2	8,50
1240	59	0,42	Gear 2	12,24

1514	59	0,42	Gear 2	16,63
1764	59	0,42	Gear 2	22,13
2012	59	0,42	Gear 2	26,85
976	58	0,42	Gear 2	8,67
1240	58	0,42	Gear 2	12,44
1506	58	0,42	Gear 2	16,31
1764	58	0,42	Gear 2	22,04
2012	58	0,42	Gear 2	26,99
988	57	0,42	Gear 2	8,59
1244	57	0,42	Gear 2	12,60
1514	57	0,42	Gear 2	16,75
1760	57	0,42	Gear 2	21,71
2016	57	0,42	Gear 2	27,46
980	56	0,42	Gear 2	8,80
1240	56	0,42	Gear 2	12,55
1508	56	0,42	Gear 2	16,55
1762	56	0,42	Gear 2	21,60
2014	56	0,42	Gear 2	26,48
986	55	0,42	Gear 2	8,75
1238	55	0,42	Gear 2	12,65
1514	55	0,42	Gear 2	16,95
1759	55	0,42	Gear 2	21,40
2018	55	0,42	Gear 2	26,49
988	54	0,42	Gear 2	8,73
1244	54	0,42	Gear 2	12,81
1512	54	0,42	Gear 2	16,80

1766	54	0,42	Gear 2	21,54
2014	54	0,42	Gear 2	26,68
982	53	0,42	Gear 2	8,75
1238	53	0,42	Gear 2	12,82
1506	53	0,42	Gear 2	16,84
1762	53	0,42	Gear 2	21,70
2016	53	0,42	Gear 2	26,03
982	52	0,42	Gear 2	8,88
1238	52	0,42	Gear 2	12,55
1516	52	0,42	Gear 2	16,72
1770	52	0,42	Gear 2	21,62
2010	52	0,42	Gear 2	25,45
980	51	0,42	Gear 2	9,01
1236	51	0,42	Gear 2	12,73
1508	51	0,42	Gear 2	16,30
1758	51	0,42	Gear 2	21,02
2012	51	0,42	Gear 2	24,89
984	50	0,42	Gear 2	8,90
1244	50	0,42	Gear 2	12,88
1508	50	0,42	Gear 2	16,67
1758	50	0,42	Gear 2	21,60
2014	50	0,42	Gear 2	25,30
984	49	0,42	Gear 2	9,14
1240	49	0,42	Gear 2	12,85
1508	49	0,42	Gear 2	16,72
1760	49	0,42	Gear 2	20,76

2014	49	0,42	Gear 2	25,72
984	48	0,42	Gear 2	9,10
1242	48	0,42	Gear 2	12,94
1508	48	0,42	Gear 2	17,22
1760	48	0,42	Gear 2	21,24
2010	48	0,42	Gear 2	25,58
984	47	0,42	Gear 2	9,26
1236	47	0,42	Gear 2	13,17
1512	47	0,42	Gear 2	17,67
1760	47	0,42	Gear 2	21,04
2014	47	0,42	Gear 2	25,32
988	46	0,42	Gear 2	9,46
1236	46	0,42	Gear 2	12,95
1510	46	0,42	Gear 2	17,28
1766	46	0,42	Gear 2	21,62
2014	46	0,42	Gear 2	24,98
988	45	0,42	Gear 2	9,66
1236	45	0,42	Gear 2	13,44
1512	45	0,42	Gear 2	17,52
1760	45	0,42	Gear 2	21,19
2012	45	0,42	Gear 2	25,42
980	44	0,41	Gear 2	9,60
1236	44	0,41	Gear 2	13,53
1510	44	0,41	Gear 2	17,76
1762	44	0,41	Gear 2	21,49
2014	44	0,41	Gear 2	25,43

978	43	0,41	Gear 2	9,68
1234	43	0,41	Gear 2	13,79
1510	43	0,41	Gear 2	17,48
1760	43	0,41	Gear 2	21,44
2014	43	0,41	Gear 2	25,00
980	42	0,41	Gear 2	9,94
1234	42	0,41	Gear 2	14,04
1506	42	0,41	Gear 2	17,89
1760	42	0,41	Gear 2	21,34
2012	42	0,41	Gear 2	25,69
980	41	0,41	Gear 2	9,99
1230	41	0,41	Gear 2	13,93
1508	41	0,41	Gear 2	17,96
1760	41	0,41	Gear 2	21,43
2014	41	0,41	Gear 2	25,02
982	40	0,41	Gear 2	10,21
1234	40	0,41	Gear 2	14,35
1512	40	0,41	Gear 2	18,51
1760	40	0,41	Gear 2	21,48
2014	40	0,41	Gear 2	25,28
982	39	0,40	Gear 2	10,48
1234	39	0,40	Gear 2	14,65
1506	39	0,40	Gear 2	18,73
1762	39	0,40	Gear 2	22,05
2010	39	0,40	Gear 2	25,23
984	38	0,40	Gear 2	10,54

1236	38	0,40	Gear 2	14,86
1506	38	0,40	Gear 2	18,66
1760	38	0,40	Gear 2	22,35
2012	39	0,40	Gear 2	25,80
978	37	0,40	Gear 2	10,75
1239	37	0,40	Gear 2	15,17
1510	37	0,40	Gear 2	18,76
1762	37	0,40	Gear 2	22,80
2012	38	0,40	Gear 2	25,38
978	36	0,40	Gear 2	10,98
1234	36	0,40	Gear 2	15,54
1506	36	0,40	Gear 2	19,15
1758	36	0,40	Gear 2	23,53
2014	37	0,40	Gear 2	25,56
978	35	0,40	Gear 2	11,10
1234	35	0,40	Gear 2	15,59
1508	35	0,40	Gear 2	19,52
1758	36	0,40	Gear 2	22,88
2012	36	0,40	Gear 2	26,47
978	34	0,40	Gear 2	11,43
1232	34	0,40	Gear 2	16,12
1504	34	0,40	Gear 2	20,28
1764	34	0,40	Gear 2	23,89
2012	35	0,40	Gear 2	26,17
978	33	0,40	Gear 2	11,43
1238	33	0,40	Gear 2	16,27

1506	33	0,40	Gear 2	20,61
1762	34	0,40	Gear 2	23,83
2010	34	0,40	Gear 2	27,48
976	32	0,39	Gear 2	11,66
1240	32	0,39	Gear 2	16,74
1506	33	0,39	Gear 2	20,42
1762	33	0,39	Gear 2	24,47
2010	33	0,39	Gear 2	27,10
980	31	0,39	Gear 2	12,01
1230	31	0,39	Gear 2	16,76
1504	31	0,39	Gear 2	21,02
1762	32	0,39	Gear 2	24,18
2010	32	0,39	Gear 2	27,81
976	30	0,38	Gear 2	11,99
1246	30	0,38	Gear 2	17,15
1502	31	0,38	Gear 2	21,38
1762	31	0,38	Gear 2	25,03
2012	31	0,38	Gear 2	27,67
972	29	0,38	Gear 2	12,20
1236	29	0,38	Gear 2	17,30
1502	30	0,38	Gear 2	21,74
1766	30	0,38	Gear 2	25,38
2008	30	0,38	Gear 2	28,18
974	28	0,38	Gear 2	12,46
1234	28	0,38	Gear 2	17,66
1508	28	0,38	Gear 2	21,75

1764	28	0,38	Gear 2	25,72
2008	29	0,38	Gear 2	27,84
974	27	0,38	Gear 2	12,67
1238	27	0,38	Gear 2	18,10
1502	28	0,38	Gear 2	22,21
1764	28	0,38	Gear 2	26,28
2010	28	0,38	Gear 2	27,93
976	26	0,38	Gear 2	12,80
1234	26	0,38	Gear 2	18,22
1510	26	0,38	Gear 2	22,64
1762	26	0,38	Gear 2	26,39
2014	26	0,38	Gear 2	29,15
976	25	0,38	Gear 2	12,98
1238	25	0,38	Gear 2	18,45
1510	26	0,38	Gear 2	23,12
1760	26	0,38	Gear 2	26,65
2012	26	0,38	Gear 2	28,98
970	80	0,384615	Gear 2	5,77
1226	80	0,384615	Gear 2	8,46
1496	80	0,384615	Gear 2	11,24
1758	80	0,384615	Gear 2	14,07
2004	80	0,384615	Gear 2	16,65

970	79	0,384615	Gear 2	5,73
1236	79	0,384615	Gear 2	8,70
1506	79	0,384615	Gear 2	11,24
1754	79	0,384615	Gear 2	14,09
2004	79	0,384615	Gear 2	16,18
970	78	0,384615	Gear 2	5,72
1234	78	0,384615	Gear 2	8,53
1500	78	0,384615	Gear 2	11,03
1752	78	0,384615	Gear 2	13,97
2006	78	0,384615	Gear 2	16,57
968	77	0,384615	Gear 2	5,78
1234	77	0,384615	Gear 2	8,46
1502	77	0,384615	Gear 2	11,09
1754	77	0,384615	Gear 2	13,90
2002	77	0,384615	Gear 2	16,65
970	76	0,384615	Gear 2	5,77
1230	76	0,384615	Gear 2	8,56
1500	76	0,384615	Gear 2	11,23
1756	76	0,384615	Gear 2	14,22
2002	76	0,384615	Gear 2	16,22
964	75	0,384615	Gear 2	5,72
1230	75	0,384615	Gear 2	8,62
1504	75	0,384615	Gear 2	11,56
1754	75	0,384615	Gear 2	14,30
1998	75	0,384615	Gear 2	16,43
970	74	0,384615	Gear 2	6,94

1228	74	0,384615	Gear 2	9,74
1498	74	0,384615	Gear 2	11,25
1752	74	0,384615	Gear 2	14,22
2012	74	0,384615	Gear 2	16,66
964	73	0,384615	Gear 2	6,80
1230	73	0,384615	Gear 2	10,10
1502	73	0,384615	Gear 2	13,38
1758	73	0,384615	Gear 2	17,10
2014	73	0,384615	Gear 2	21,03
970	72	0,384615	Gear 2	6,96
1230	72	0,384615	Gear 2	10,04
1501	72	0,384615	Gear 2	13,39
1756	72	0,384615	Gear 2	17,37
2010	72	0,384615	Gear 2	20,17
968	71	0,384615	Gear 2	7,02
1228	71	0,384615	Gear 2	10,29
1502	71	0,384615	Gear 2	13,63
1752	71	0,384615	Gear 2	17,23
2012	71	0,384615	Gear 2	20,98
968	70	0,384615	Gear 2	6,95
1228	70	0,384615	Gear 2	9,92
1504	70	0,384615	Gear 2	13,44
1750	70	0,384615	Gear 2	16,88
2014	70	0,384615	Gear 2	20,88
966	69	0,384615	Gear 2	7,07
1234	69	0,384615	Gear 2	10,28

1500	69	0,384615	Gear 2	13,26
1760	69	0,384615	Gear 2	17,35
2010	69	0,384615	Gear 2	20,50
968	68	0,384615	Gear 2	7,01
1236	68	0,384615	Gear 2	10,04
1504	68	0,384615	Gear 2	13,49
1774	68	0,384615	Gear 2	17,66
2022	68	0,384615	Gear 2	20,63
972	67	0,384615	Gear 2	7,03
1236	67	0,384615	Gear 2	10,05
1502	67	0,384615	Gear 2	13,45
1770	67	0,384615	Gear 2	17,18
2018	67	0,384615	Gear 2	20,66
974	66	0,384615	Gear 2	7,12
1250	66	0,384615	Gear 2	10,40
1512	66	0,384615	Gear 2	13,38
1756	66	0,384615	Gear 2	16,85
2014	66	0,384615	Gear 2	20,91
974	65	0,384615	Gear 2	7,08
1236	65	0,384615	Gear 2	10,25
1510	65	0,384615	Gear 2	13,49
1756	65	0,384615	Gear 2	17,18
2026	65	0,384615	Gear 2	21,29
974	64	0,384615	Gear 2	7,26
1236	64	0,384615	Gear 2	10,50
1506	64	0,384615	Gear 2	13,56

1764	64	0,384615	Gear 2	17,58
2020	64	0,384615	Gear 2	21,59
970	63	0,384615	Gear 2	7,27
1238	63	0,384615	Gear 2	10,31
1501	63	0,384615	Gear 2	13,45
1753	63	0,384615	Gear 2	17,26
2008	63	0,384615	Gear 2	21,91
966	62	0,384615	Gear 2	7,49
1228	62	0,384615	Gear 2	10,47
1500	62	0,384615	Gear 2	13,41
1760	62	0,384615	Gear 2	17,40
2010	62	0,384615	Gear 2	21,42
970	61	0,384615	Gear 2	7,59
1224	61	0,384615	Gear 2	10,58
1496	61	0,384615	Gear 2	13,53
1754	61	0,384615	Gear 2	17,48
2010	61	0,384615	Gear 2	20,68
966	60	0,384615	Gear 2	7,38
1226	60	0,384615	Gear 2	10,44
1506	60	0,384615	Gear 2	13,70
1752	60	0,384615	Gear 2	17,52
2008	60	0,384615	Gear 2	20,82
962	59	0,384615	Gear 2	7,62
1230	59	0,384615	Gear 2	10,58
1498	59	0,384615	Gear 2	13,79
1758	59	0,384615	Gear 2	17,32

2004	59	0,384615	Gear 2	20,62
962	58	0,384615	Gear 2	7,47
1234	58	0,384615	Gear 2	10,59
1506	58	0,384615	Gear 2	13,75
1764	58	0,384615	Gear 2	17,28
2006	58	0,384615	Gear 2	21,00
970	57	0,384615	Gear 2	7,69
1232	57	0,384615	Gear 2	10,96
1508	57	0,384615	Gear 2	13,91
1756	57	0,384615	Gear 2	17,26
2016	57	0,384615	Gear 2	20,32
972	56	0,384615	Gear 2	7,78
1230	56	0,384615	Gear 2	10,89
1502	56	0,384615	Gear 2	14,11
1768	56	0,384615	Gear 2	17,68
2024	56	0,384615	Gear 2	20,66
972	55	0,384615	Gear 2	7,78
1228	55	0,384615	Gear 2	10,83
1494	55	0,384615	Gear 2	13,86
1764	55	0,384615	Gear 2	17,42
2008	55	0,384615	Gear 2	20,83
984	54	0,384615	Gear 2	7,96
1226	54	0,384615	Gear 2	11,01
1494	54	0,384615	Gear 2	13,80
1770	54	0,384615	Gear 2	17,86
2028	54	0,384615	Gear 2	21,48

972	53	0,384615	Gear 2	7,89
1230	53	0,384615	Gear 2	11,11
1502	53	0,384615	Gear 2	14,35
1760	53	0,384615	Gear 2	18,08
2000	53	0,384615	Gear 2	20,92
968	52	0,384615	Gear 2	8,13
1224	52	0,384615	Gear 2	11,02
1504	52	0,384615	Gear 2	14,17
1760	52	0,384615	Gear 2	18,09
2008	52	0,384615	Gear 2	21,25
966	51	0,384615	Gear 2	7,95
1230	51	0,384615	Gear 2	11,28
1500	51	0,384615	Gear 2	14,15
1772	51	0,384615	Gear 2	18,28
2014	51	0,384615	Gear 2	21,34
970	50	0,384615	Gear 2	7,88
1224	50	0,384615	Gear 2	11,43
1500	50	0,384615	Gear 2	14,34
1760	50	0,384615	Gear 2	18,21
2008	50	0,384615	Gear 2	21,55
956	49	0,384615	Gear 2	7,81
1228	49	0,384615	Gear 2	11,37
1500	49	0,384615	Gear 2	14,78
1758	49	0,384615	Gear 2	17,93
2012	49	0,384615	Gear 2	22,01
974	48	0,384615	Gear 2	8,44

1232	48	0,384615	Gear 2	11,63
1506	48	0,384615	Gear 2	14,74
1758	48	0,384615	Gear 2	18,43
2008	48	0,384615	Gear 2	22,05
962	47	0,384615	Gear 2	8,54
1224	47	0,384615	Gear 2	11,59
1504	47	0,384615	Gear 2	15,15
1756	47	0,384615	Gear 2	18,59
2010	47	0,384615	Gear 2	22,22
966	46	0,384615	Gear 2	9,29
1228	46	0,384615	Gear 2	13,31
1502	46	0,384615	Gear 2	17,30
1769	46	0,384615	Gear 2	21,59
2002	46	0,384615	Gear 2	25,55
964	45	0,384615	Gear 2	9,60
1220	45	0,384615	Gear 2	13,32
1496	45	0,384615	Gear 2	17,40
1758	45	0,384615	Gear 2	21,79
2010	45	0,384615	Gear 2	25,21
968	44	0,384615	Gear 2	9,68
1222	44	0,384615	Gear 2	13,59
1506	44	0,384615	Gear 2	18,03
1752	45	0,384615	Gear 2	21,65
2016	44	0,384615	Gear 2	25,48
962	43	0,384615	Gear 2	9,73
1224	43	0,384615	Gear 2	13,96

1506	43	0,384615	Gear 2	18,24
1772	43	0,384615	Gear 2	22,33
2024	43	0,384615	Gear 2	26,88
960	42	0,384615	Gear 2	9,81
1220	42	0,384615	Gear 2	13,95
1502	42	0,384615	Gear 2	18,13
1768	42	0,384615	Gear 2	22,31
2020	43	0,384615	Gear 2	26,42
962	41	0,384615	Gear 2	10,06
1222	41	0,384615	Gear 2	14,08
1504	41	0,384615	Gear 2	18,71
1754	41	0,384615	Gear 2	21,93
2010	41	0,384615	Gear 2	26,39
962	40	0,384615	Gear 2	9,98
1224	40	0,384615	Gear 2	14,43
1498	40	0,384615	Gear 2	18,41
1758	40	0,384615	Gear 2	22,42
2012	41	0,384615	Gear 2	25,92
966	39	0,384615	Gear 2	10,17
1228	39	0,384615	Gear 2	14,49
1496	39	0,384615	Gear 2	18,73
1766	39	0,384615	Gear 2	22,85
2006	39	0,384615	Gear 2	26,30
966	38	0,384615	Gear 2	10,47
1222	38	0,384615	Gear 2	14,82
1498	38	0,384615	Gear 2	18,96

1752	39	0,384615	Gear 2	22,39
2014	39	0,384615	Gear 2	25,97
964	37	0,384615	Gear 2	10,47
1218	37	0,384615	Gear 2	14,86
1508	37	0,384615	Gear 2	19,58
1762	37	0,384615	Gear 2	23,13
2010	38	0,384615	Gear 2	26,51
960	36	0,384615	Gear 2	10,67
1232	36	0,384615	Gear 2	15,57
1498	36	0,384615	Gear 2	19,60
1758	37	0,384615	Gear 2	23,40
2006	37	0,384615	Gear 2	26,10
958	35	0,384615	Gear 2	10,89
1220	35	0,384615	Gear 2	15,66
1498	36	0,384615	Gear 2	19,80
1752	36	0,384615	Gear 2	23,50
2006	36	0,384615	Gear 2	27,00
960	34	0,384615	Gear 2	11,05
1223	34	0,384615	Gear 2	16,01
1498	34	0,384615	Gear 2	20,44
1752	34	0,384615	Gear 2	24,47
2010	35	0,384615	Gear 2	27,27
964	33	0,384615	Gear 2	11,23
1218	33	0,384615	Gear 2	16,17
1494	33	0,384615	Gear 2	20,36
1756	34	0,384615	Gear 2	24,64

2010	34	0,384615	Gear 2	27,27
960	32	0,384615	Gear 2	11,39
1220	32	0,384615	Gear 2	16,41
1498	32	0,384615	Gear 2	20,51
1752	33	0,384615	Gear 2	24,75
2006	33	0,384615	Gear 2	27,98
962	31	0,384615	Gear 2	11,71
1222	31	0,384615	Gear 2	16,70
1494	32	0,384615	Gear 2	21,04
1750	32	0,384615	Gear 2	25,16
2002	32	0,384615	Gear 2	28,13
960	30	0,384615	Gear 2	12,20
1222	30	0,384615	Gear 2	17,94
1500	30	0,384615	Gear 2	22,70
1756	31	0,384615	Gear 2	26,90
2012	31	0,384615	Gear 2	29,19
956	29	0,384615	Gear 2	12,40
1222	29	0,384615	Gear 2	18,02
1498	30	0,384615	Gear 2	23,23
1754	30	0,384615	Gear 2	27,23
2004	30	0,384615	Gear 2	30,54
956	28	0,384615	Gear 2	12,70
1226	28	0,384615	Gear 2	18,40
1504	28	0,384615	Gear 2	23,29
1754	28	0,384615	Gear 2	28,09
2008	29	0,384615	Gear 2	30,71

954	27	0,384615	Gear 2	12,75
1224	27	0,384615	Gear 2	18,40
1492	28	0,384615	Gear 2	23,84
1750	28	0,384615	Gear 2	28,11
2006	28	0,384615	Gear 2	31,19
954	27	0,384615	Gear 2	12,56
1230	27	0,384615	Gear 2	18,61
1502	27	0,384615	Gear 2	23,37
1754	27	0,384615	Gear 2	28,33
2010	27	0,384615	Gear 2	31,62
997	40	0.54	Gear 2	16.3
1245	40	0.54	Gear 2	24.6
1501	40	0.54	Gear 2	34.8
1759	40	0.54	Gear 2	46.2
1993	40	0.54	Gear 2	55.5
2505	40	0.54	Gear 2	77.3
995	40	0.46	Gear 2	12.3
1236	40	0.46	Gear 2	18.3
1495	40	0.46	Gear 2	24.4
1761	40	0.46	Gear 2	29.3
1997	40	0.46	Gear 2	35.2
2501	40	0.46	Gear 2	42.0
1001	40	0.38	Gear 2	9.0
1269	40	0.38	Gear 2	12.5

1497	40	0.38	Gear 2	15.5
1751	40	0.38	Gear 2	16.9
1997	40	0.38	Gear 2	19.2
2499	40	0.38	Gear 2	24.0
996	21,477851	0,574468	Gear 3	83,9547999
996	21,498664	0,574468	Gear 3	82,6061896
994	21,529037	0,574468	Gear 3	82,8537649
994	21,546901	0,574468	Gear 3	83,9050884
1004	25,639941	0,574468	Gear 3	84,5016025
1022	25,672821	0,574468	Gear 3	88,7587299
1012	25,699431	0,574468	Gear 3	86,5101186
1012	25,759328	0,574468	Gear 3	87,9756661
1002	25,829496	0,574468	Gear 3	83,535391
1006	30,772622	0,574468	Gear 3	80,023977
1014	30,789469	0,574468	Gear 3	80,0881151
1006	30,800045	0,574468	Gear 3	78,8479764
1020	30,801435	0,574468	Gear 3	81,2597193
1018	30,817129	0,574468	Gear 3	79,399615
1014	35,253756	0,574468	Gear 3	76,7179892
1018	35,279552	0,574468	Gear 3	78,7767236
1016	35,301416	0,574468	Gear 3	77,0411351
1030	35,376872	0,574468	Gear 3	77,8983283
1020	35,481378	0,574468	Gear 3	77,1004831
1012	35,491988	0,574468	Gear 3	75,3831273

1018	35,48948	0,574468	Gear 3	77,3237014
1002	35,492361	0,574468	Gear 3	75,2426269
1002	40,519383	0,574468	Gear 3	71,8933919
1002	40,515892	0,574468	Gear 3	71,190786
1002	40,523993	0,574468	Gear 3	70,4657253
1006	40,519655	0,574468	Gear 3	72,2812096
982	40,068307	0,574468	Gear 3	69,4256242
986	40,098917	0,574468	Gear 3	71,3567587
986	40,121221	0,574468	Gear 3	70,8060036
982	40,237287	0,574468	Gear 3	70,3777716
1004	40,404097	0,574468	Gear 3	72,6707725
1008	40,414233	0,574468	Gear 3	72,9001297
1004	40,423724	0,574468	Gear 3	72,9149044
1020	40,437283	0,574468	Gear 3	73,5269089
1002	45,455492	0,574468	Gear 3	67,2431399
1008	45,442001	0,574468	Gear 3	67,8965981
1000	45,443865	0,574468	Gear 3	65,6221109
1002	45,443119	0,574468	Gear 3	66,8937257
1016	50,165605	0,574468	Gear 3	62,580209
1006	50,172554	0,574468	Gear 3	61,5288585
1010	50,168249	0,574468	Gear 3	62,8672421
1014	50,155978	0,574468	Gear 3	62,8985403
1010	50,126894	0,574468	Gear 3	60,2672788
998	55,010867	0,574468	Gear 3	59,2102148
998	55,125814	0,574468	Gear 3	57,1542879
1002	55,151746	0,574468	Gear 3	59,2470106

996	55,188322	0,574468	Gear 3	56,0098834
1006	60,205581	0,574468	Gear 3	52,3314449
1004	60,192768	0,574468	Gear 3	50,5490782
1004	60,190327	0,574468	Gear 3	50,8381043
1012	60,167718	0,574468	Gear 3	50,7984059
1016	65,045149	0,574468	Gear 3	47,5282572
1012	65,015929	0,574468	Gear 3	47,5885929
1024	65,127656	0,574468	Gear 3	47,7680252
1018	65,122843	0,574468	Gear 3	46,9923159
1018	65,141351	0,574468	Gear 3	46,8970113
1010	70,183017	0,574468	Gear 3	46,4108561
1008	70,183966	0,574468	Gear 3	45,3685136
1002	70,182508	0,574468	Gear 3	45,5464057
1002	70,165627	0,574468	Gear 3	44,67308
998	70,157864	0,574468	Gear 3	45,9933177
1022	75,052279	0,574468	Gear 3	47,5634237
1016	75,073295	0,574468	Gear 3	47,4494183
1022	75,093532	0,574468	Gear 3	47,9691502
1020	75,12343	0,574468	Gear 3	48,0462865
1012	75,178141	0,574468	Gear 3	47,0787405
1012	80,149503	0,574468	Gear 3	46,8902085
1010	80,171062	0,574468	Gear 3	44,7016622
1006	80,178858	0,574468	Gear 3	44,1552755
1010	80,18018	0,574468	Gear 3	44,5944145
1008	80,191265	0,574468	Gear 3	45,5513392

844,005634	40,33976	0,468085	Gear 3	39,714124
842,005621	40,329794	0,468085	Gear 3	38,7395912
1446,00965	40,377962	0,468085	Gear 3	107,995299
1460,00835	40,403725	0,468085	Gear 3	110,264392
1000,00668	40,148204	0,468085	Gear 3	51,9716898
986,005642	40,134882	0,468085	Gear 3	51,8784352
990,006609	40,124543	0,468085	Gear 3	50,13242
1498	40,183763	0,468085	Gear 3	115,478895
1500	40,197593	0,468085	Gear 3	114,674258
1498	40,208949	0,468085	Gear 3	113,873956
1754,03346	40,36159	0,468085	Gear 3	157,028202
1770,03376	40,380233	0,468085	Gear 3	162,3483
1776,03388	40,406301	0,468085	Gear 3	164,136926
1756,03349	40,511587	0,468085	Gear 3	160,781918
1772,0338	40,527587	0,468085	Gear 3	164,994032
1760,03357	40,587416	0,468085	Gear 3	165,783382
1510,0288	40,928053	0,468085	Gear 3	118,282547
1496,02853	40,935002	0,468085	Gear 3	115,018289
1498,02857	40,941036	0,468085	Gear 3	116,00976
980,018692	40,844869	0,468085	Gear 3	50,8974378
980,019627	40,830021	0,468085	Gear 3	51,5148895
986,018807	40,77809	0,468085	Gear 3	51,5514501
1030,01965	78,287098	0,468085	Gear 3	37,6212793
1028,01961	78,343572	0,468085	Gear 3	36,9234048
1502,02865	78,667192	0,468085	Gear 3	79,9929277
1502,02865	78,724818	0,468085	Gear 3	81,1633381

1994,03803	79,251622	0,468085	Gear 3	134,047162
1994,03803	79,385416	0,468085	Gear 3	135,687405
2312,01323	80,024251	0,468085	Gear 3	159,255342
2312,01543	80,210756	0,468085	Gear 3	160,288574
2308,01541	80,277738	0,468085	Gear 3	159,588051
2310,01322	80,307127	0,468085	Gear 3	163,457578
1992,0114	80,356007	0,468085	Gear 3	133,303457
1990,01139	80,355262	0,468085	Gear 3	133,759581
1470,00981	80,248281	0,468085	Gear 3	76,9530095
1466,00979	80,16974	0,468085	Gear 3	76,9448787
1466,00979	80,113402	0,468085	Gear 3	76,9384308
1030,00688	79,917745	0,468085	Gear 3	37,5681165
1032,00689	79,873305	0,468085	Gear 3	37,627015
1028	79,681003	0,468085	Gear 3	37,0003915
1019,98055	100,00024	0,468085	Gear 3	32,4509812
1023,98047	100,010545	0,468085	Gear 3	32,4761563
1501,96992	100,027968	0,468085	Gear 3	71,1286345
1503,97131	100,04512	0,468085	Gear 3	70,5127869
2001,95991	100,041765	0,468085	Gear 3	121,512908
2001,96182	100,02068	0,468085	Gear 3	119,642557
2525,95182	99,912852	0,468085	Gear 3	154,455658
2525,95182	99,95797	0,468085	Gear 3	151,396783
3006,0774	99,969563	0,468085	Gear 3	175,738563
3012,07469	99,984139	0,468085	Gear 3	147,90956
3526,09079	100,057866	0,468085	Gear 3	135,286988
3522,09069	100,012409	0,468085	Gear 3	137,563384

3514,09049	100,009155	0,468085	Gear 3	121,380413
3538,0911	100,037222	0,468085	Gear 3	124,187554
3016,07766	100,135051	0,468085	Gear 3	149,715316
3018,07771	100,149627	0,468085	Gear 3	138,521413
2518,06484	100,179389	0,468085	Gear 3	154,123177
2514,06474	100,165355	0,468085	Gear 3	151,141102
2006,05165	100,027934	0,468085	Gear 3	118,224847
2004,0516	99,995155	0,468085	Gear 3	119,902151
1502,03868	99,776888	0,468085	Gear 3	70,0919618
1504	99,723906	0,468085	Gear 3	70,0383282
1020	99,507978	0,468085	Gear 3	34,5145359
1022	99,494012	0,468085	Gear 3	32,03505
1013,98743	100,02224	0,468085	Gear 3	34,751053
1017,98738	100,030782	0,468085	Gear 3	34,9361097
1011,98649	100,035527	0,468085	Gear 3	34,8434569
1017,98738	100,024206	0,468085	Gear 3	34,9600955
1501,98138	100,27593	0,468085	Gear 3	70,5882036
1495,98003	100,290912	0,468085	Gear 3	70,9160394
1501,97135	100,323285	0,468085	Gear 3	70,8285926
1497,97143	100,368911	0,468085	Gear 3	71,4699518
2003,96178	100,701582	0,468085	Gear 3	107,774988
1997,96189	100,709548	0,468085	Gear 3	106,872752
2001,95991	100,693616	0,468085	Gear 3	106,909054
2001,96182	100,689718	0,468085	Gear 3	106,255679
1999,96185	100,624228	0,468085	Gear 3	105,621542
2516,08158	100,198338	0,468085	Gear 3	118,355749

2518,08165	100,215999	0,468085	Gear 3	114,500766
2510,079	100,242608	0,468085	Gear 3	115,528977
2516,07918	100,29498	0,468085	Gear 3	120,831083
3012,09767	100,315217	0,468085	Gear 3	104,949712
3014,09773	100,292811	0,468085	Gear 3	105,306943
3130,10149	100,281285	0,468085	Gear 3	109,396238
3196,10363	100,248269	0,468085	Gear 3	104,867156
3500,11349	100,184406	0,468085	Gear 3	98,902177
3494,10996	100,179491	0,468085	Gear 3	107,607543
3526,11097	100,175932	0,468085	Gear 3	105,7439
3506,11369	100,191457	0,468085	Gear 3	95,1482561
3950,12432	100,287794	0,468085	Gear 3	108,004622
4074,1321	100,308404	0,468085	Gear 3	111,271838
3996,12957	100,323115	0,468085	Gear 3	102,858103
3926,1273	100,343454	0,468085	Gear 3	111,665865
1016	45,393764	0,361702	Gear 3	22,422165
1016	45,378171	0,361702	Gear 3	23,0731977
1012	45,373087	0,361702	Gear 3	22,5280375
1014	45,372171	0,361702	Gear 3	23,9488339
1010	45,359833	0,361702	Gear 3	23,5959725
1504	45,328647	0,361702	Gear 3	38,8052708
1508	45,331833	0,361702	Gear 3	39,3072177
1502	45,329291	0,361702	Gear 3	38,8480415
1502	45,335494	0,361702	Gear 3	39,4883653

1498	45,332104	0,361702	Gear 3	39,2984933
1996	45,396205	0,361702	Gear 3	58,4628615
2000	45,396781	0,361702	Gear 3	56,1140808
2000	45,39929	0,361702	Gear 3	58,4497502
1998	45,411933	0,361702	Gear 3	59,9312338
1994	45,423255	0,361702	Gear 3	55,868896
996	50,307534	0,361702	Gear 3	22,929296
1018	50,290077	0,361702	Gear 3	22,8951739
996	50,273874	0,361702	Gear 3	21,231382
1016	50,232146	0,361702	Gear 3	22,7450747
992	50,207095	0,361702	Gear 3	19,984507
994	50,196655	0,361702	Gear 3	21,61136
1500	50,009947	0,361702	Gear 3	41,1856514
1500	50,070861	0,361702	Gear 3	40,725251
1502	50,089606	0,361702	Gear 3	40,9560296
1502	50,114962	0,361702	Gear 3	41,5328087
1500	50,218282	0,361702	Gear 3	40,5890629
2002	50,359194	0,361702	Gear 3	60,0103347
1998	50,387702	0,361702	Gear 3	57,123157
1996	50,389905	0,361702	Gear 3	59,2930915
2000	50,386007	0,361702	Gear 3	59,7327766
2000	50,388482	0,361702	Gear 3	56,875184
1016	55,35503	0,361702	Gear 3	21,0444527
1016	55,338149	0,361702	Gear 3	21,2039392
1016	55,334861	0,361702	Gear 3	20,8244272
1014	55,318828	0,361702	Gear 3	20,9389965

1018	55,311913	0,361702	Gear 3	21,5095259
1504	54,976868	0,361702	Gear 3	36,8981213
1506	55,067341	0,361702	Gear 3	38,1236893
1504	55,087374	0,361702	Gear 3	36,4799628
1502	55,155543	0,361702	Gear 3	37,6183555
1508	55,179339	0,361702	Gear 3	37,4144199
2000	55,332658	0,361702	Gear 3	51,5068304
2000	55,337844	0,361702	Gear 3	50,4328246
2006	55,336861	0,361702	Gear 3	49,8135943
2000	55,330421	0,361702	Gear 3	52,1221637
2004	55,34059	0,361702	Gear 3	51,5095318
1018	60,262326	0,361702	Gear 3	21,0757513
1018	60,277207	0,361702	Gear 3	20,4723686
1000	60,258224	0,361702	Gear 3	19,4808066
1020	60,247072	0,361702	Gear 3	20,6164128
1008	60,208496	0,361702	Gear 3	20,1543071
1508	60,167209	0,361702	Gear 3	37,2531862
1504	60,180971	0,361702	Gear 3	36,8515018
1506	60,175344	0,361702	Gear 3	37,2208113
1502	60,20192	0,361702	Gear 3	38,0381601
1504	60,235682	0,361702	Gear 3	37,9829711
2000	60,135311	0,361702	Gear 3	47,3310255
2004	60,135311	0,361702	Gear 3	47,3963074
2002	60,134125	0,361702	Gear 3	45,3592275
2002	60,127617	0,361702	Gear 3	48,733737
2004	60,126295	0,361702	Gear 3	46,4811149

1000	65,058505	0,361702	Gear 3	19,1537668
1022	65,138978	0,361702	Gear 3	20,2308832
1012	65,206638	0,361702	Gear 3	19,1344615
1020	65,22179	0,361702	Gear 3	19,6172732
1016	65,22257	0,361702	Gear 3	19,1723215
1502	65,141995	0,361702	Gear 3	34,587867
1510	65,105656	0,361702	Gear 3	34,4297454
1500	65,073827	0,361702	Gear 3	34,5441674
1504	65,057725	0,361702	Gear 3	34,3557804
1506	65,049352	0,361702	Gear 3	34,5512888
2000	64,862373	0,361702	Gear 3	45,0095979
2000	64,884915	0,361702	Gear 3	42,7991734
1998	64,931423	0,361702	Gear 3	45,4757374
2016	65,013624	0,361702	Gear 3	45,9208961
2000	65,050946	0,361702	Gear 3	44,1967632
1018	70,147221	0,361702	Gear 3	19,293747
1008	70,185084	0,361702	Gear 3	18,6920189
998	70,180847	0,361702	Gear 3	16,8102752
996	70,198508	0,361702	Gear 3	18,6615128
1014	70,192915	0,361702	Gear 3	19,4275474
1502	70,100815	0,361702	Gear 3	31,7796279
1506	70,154644	0,361702	Gear 3	31,5198265
1504	70,170915	0,361702	Gear 3	31,2618796
1504	70,204575	0,361702	Gear 3	31,3483463
1506	70,23166	0,361702	Gear 3	32,1692679
2004	70,183017	0,361702	Gear 3	41,4780909

2000	70,165152	0,361702	Gear 3	40,4310408
2002	70,161119	0,361702	Gear 3	41,294344
2004	70,149254	0,361702	Gear 3	42,6627415
2002	70,143966	0,361702	Gear 3	40,7433865
996	75,116922	0,361702	Gear 3	17,0046933
998	75,110583	0,361702	Gear 3	17,5109124
998	75,133532	0,361702	Gear 3	16,8523929
998	75,123905	0,361702	Gear 3	17,2474419
994	75,09021	0,361702	Gear 3	16,8181575
1506	75,007364	0,361702	Gear 3	33,3397763
1502	75,040923	0,361702	Gear 3	31,6868273
1506	75,05177	0,361702	Gear 3	32,2629464
1502	75,056177	0,361702	Gear 3	31,4230536
1506	75,06655	0,361702	Gear 3	31,8361887
2006	75,044449	0,361702	Gear 3	43,9485005
2000	75,053533	0,361702	Gear 3	42,3583032
2002	75,03011	0,361702	Gear 3	43,4346501
2000	75,014042	0,361702	Gear 3	41,6455805
2004	75,006687	0,361702	Gear 3	42,4375635
1000	80,062183	0,361702	Gear 3	18,768817
1008	80,041607	0,361702	Gear 3	17,296443
1006	80,046149	0,361702	Gear 3	16,940497
996	80,031776	0,361702	Gear 3	16,4378181
996	80,020149	0,361702	Gear 3	17,7300016
1504	80,126215	0,361702	Gear 3	33,5656103
1504	80,129198	0,361702	Gear 3	32,6900761

1504	80,116215	0,361702	Gear 3	31,9156559
1502	80,109741	0,361702	Gear 3	32,8123879
1506	80,108521	0,361702	Gear 3	32,8963015
2004	80,025065	0,361702	Gear 3	44,2257668
1998	80,036929	0,361702	Gear 3	44,2511138
2000	80,04581	0,361702	Gear 3	45,0240493
2002	80,061471	0,361702	Gear 3	46,0028497
1996	80,10147	0,361702	Gear 3	43,8941235

2. Comparison of experimental Cm VS theoretical Cm

2.1. Experimental Cm VS theoretical Cm – oil C

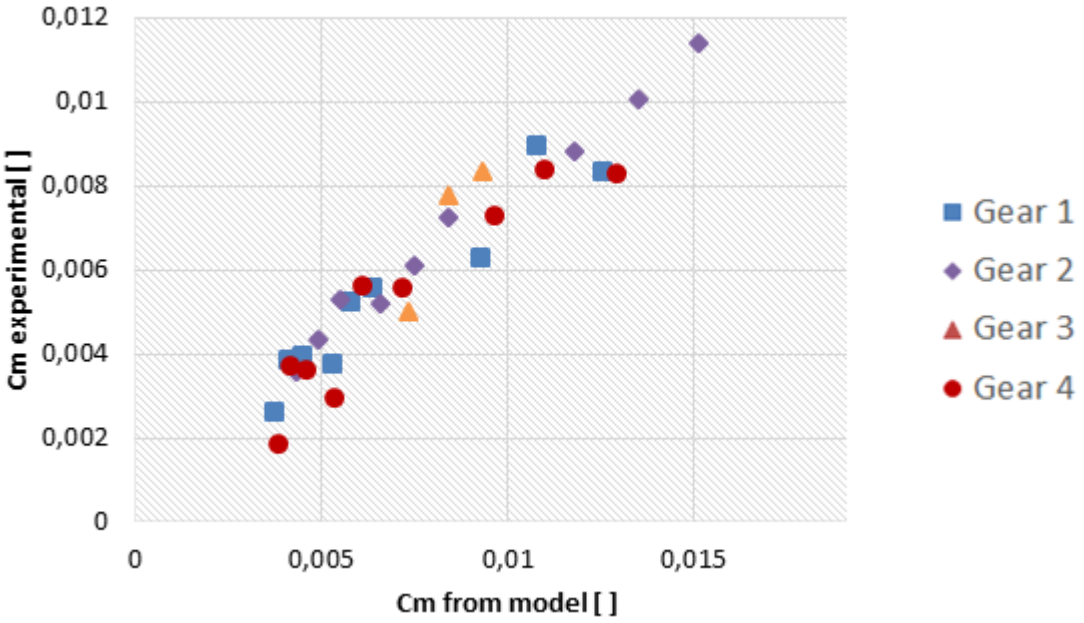

Figure 108: experimental Cm VS theoretical Cm – oil C

2.2. Experimental Cm VS theoretical Cm – oil D

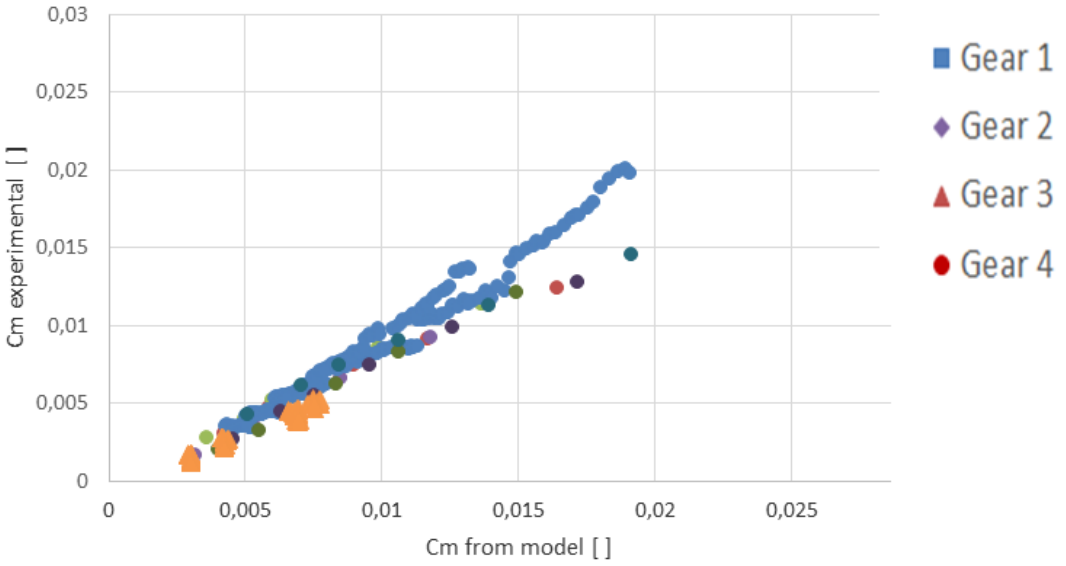

Figure 109: experimental Cm VS theoretical Cm – oil D

Appendix F

Bearing losses: SKF formula

1. Sliding friction torque parameters

f_{sl} is the sliding friction coefficient: it is associated to the parameter φ_{bl} which define the lubrication regime in the contact. This parameter defines the relative influence of the boundary lubrication regime f_{bl} and the full film regime f_{EHL}: it is a balance between the lubricated and dry contact area in function of operating conditions.

$$f_{sl} = \varphi_{bl} \times f_{bl} + (1 - \varphi_{bl}) \times f_{EHL}$$

Equation 177

$$\varphi_{bl} = \frac{1}{e^{2{,}6.10^{-8} \nu N^{1.4} d_m}}$$

Equation 178

2. Rolling friction torque parameters

The rolling friction torque impact on the total torque losses is corrected thanks to two parameters:

- In the contact entrance, oil is trapped and it results in shearing the oil, which increases the oil temperature. SKF takes this phenomenon into account with:

$$\varphi_{ish} = \frac{1}{1 + 1.84 \times 10^{-9} (N \times d_m \times 10^3)^{1.28} (\nu \times 10^6)^{0.64}}$$

Equation 179

- The rolling elements eject the lubricant because of the centrifugal effect. The contact is less lubricated and the draining of the contact may appear, which is taken into account through the φ_{rs} parameter:

$$\varphi_{rs} = \frac{1}{e^{K_{rs} (\nu \times 10^6) N (d+D) \times 10^3 \sqrt{\frac{K_Z}{2(d+D) \times 10^3}}}}$$

Equation 180

With:

- K_{rs} is function of the lubrication type
- K_Z is function of the bearing type

- D is the external diameter [m]
- d is the internal diameter [m]

These two parameters are greatly influenced by the rotational speed of the bearing. When the viscosity is high, the product νN is high, which means that these two parameters impact the start of the system and when the system is cold, since the viscosity increases with decreasing temperature.

Appendix G

Churning formulas

1. Changenet et al. formula

A model of Changenet et al. [23] [21] gives good results for a wide range of cylindrical gears, lubricants and rotational speed. The churning torque is defined as:

$$T_{churning} = \frac{\rho \omega^2 S_m R_p^3 C_m}{2}$$

Equation 181

With:

- ρ is the lubricant density [kg/m^3]
- ω is the rotational speed of the pinion [rad/s]
- S_m is the immersed area of the pinion [m²]
- R_p is the pitch diameter of the pinion [m]
- C_m is a dimensionless torque associated with dimensionless analysis on the experiments

The immersed area of the pinion is the sum of the immersed side areas and the teeth immersed area. The details of the computation of the immersed areas are explained in annex D.

The dimensionless torque depends on the flow regimes: four regimes are distinguished thanks to two parameters [21]. The first parameter is similar to a centrifugal acceleration:

$$\gamma = \omega^2 (R_p B m)^{1/3}$$

Equation 182

With:

- m is the pinion modulus [m]
- B is the pinion width [m]

The second parameter is a critical Reynolds number dependent on the pitch radius and the tooth width.

$$Re_c = \frac{\omega R_p B}{\upsilon}$$

Equation 183

The dimensionless torque is expressed as follow:

If $\gamma < 750 m/s^2$ and $Re_c < 4000$

$$C_m = 1.366 \left(\frac{h}{D_p}\right)^{0.45} \left(\frac{V_0}{{D_p}^3}\right)^{0.1} Fr^{-0.6} Re_c^{-0.21} \left(\frac{B}{R_p}\right)^{0.21}$$

Equation 184

With the Froude number Fr equals to:

$$Fr = \frac{\omega^2 R_p}{g}$$

Equation 185

If $\gamma < 750 m/s^2$ and $Re_c > 4000$

$$C_m = 0.239 \left(\frac{h}{D_p}\right)^{0.45} \left(\frac{V_0}{{D_p}^3}\right)^{0.1} Fr^{-0.6} \left(\frac{B}{R_p}\right)^{0.21}$$

Equation 186

If $\gamma > 1250 m/s^2$ and $Re_c < 4000$

$$C_m = 20.797 \left(\frac{h}{D_p}\right)^{0.1} \left(\frac{V_0}{{D_p}^3}\right)^{-0.35} Fr^{-0.88} Re_c^{-0.21} \left(\frac{B}{R_p}\right)^{0.85}$$

Equation 187

If $\gamma > 1250 m/s^2$ and $Re_c > 4000$

$$C_m = 3.644 \left(\frac{h}{D_p}\right)^{0.1} \left(\frac{V_0}{{D_p}^3}\right)^{-0.35} Fr^{-0.88} \left(\frac{B}{R_p}\right)^{0.85}$$

Equation 188

With:

- h is the oil level above the lowest immersed point of the pinion [m] (refer to Figure 105)
- V_0 is the oil volume in the carter [m^3]

2. ISO/TR 14179-1

Gear windage and churning losses encompass three types of loss [1] . For those losses associated with a smooth outside diameter, such as the outside diameter of a shaft, use P_{diam} formula. For those losses associated with the smooth sides of a disc, such as the faces of a gear, use P_{sides} formula. It should be pointed out that P_{sides} formula includes both sides of the gear, so do not double the value. For those losses associated with the tooth surfaces, such as the outside diameter of a gear or pinion, refer to P_{tooth} formula.

For smooth sides of discs:

$$P_{sides} = \frac{1.474.f_g.\nu.n^3.D^{5.7}}{A_g.10^{26}}$$

Equation 189

For tooth surfaces:

$$P_{tooth} = \frac{7.37.f_g.\nu.n^3.D^{4.7}.F.\left(\frac{\kappa_f}{\sqrt{\tan(\beta)}}\right)}{A_g.10^{26}}$$

Equation 190

With the roughness factor:

$$R_f = 7.93 - \frac{4.648}{m_t}$$

Equation 191

Where:

- P_{GWi} is the power loss for each individual element [kW]
- f_g is the gear dip factor ($0 \leq f_g \leq 1$)
- R_f is the roughness factor
- m_t is the transverse tooth module
- D is the outside diameter of the element [mm]
- A_g is the arrangement constant
- F is the total face width [mm]
- L is the length of the element [mm]

- β is the generated helix angle [°] (if $\beta < 10°$ then consider $\beta = 10°$)
- n is the rotational speed [RPM]

3. ISO/TR 14179-2

The churning loss expresses [2]:

$$P = T_H . \omega$$

Equation 192

$$T_H = C_{sp} . C_1 . e^{C_2 \left(\frac{v_t}{v_{to}}\right)}$$

Equation 193

Where:

- ω is the rotational speed [rad/s]
- T_H is the churning torque [Nm]
- C_{sp} is the splash oil factor

$$C_{sp} = \left(\frac{4.h_{e\,max}}{3.h_c}\right)^{1.5} \frac{2.h_c}{l_h}$$

Equation 194

$$C_1 = 0.063 \left(\frac{h_{e1}+h_{e2}}{h_{e0}}\right) + 0.0128 \left(\frac{b}{b_o}\right)^3$$

Equation 195

$$C_2 = \frac{h_{e1}+h_{e2}}{80.h_{e0}} + 0.2$$

Equation 196

Where:

- h_{e1} and h_{e2} are the tip circle immersion depth with oil level stationary [mm]
- h_{e0} is the reference value of immersion depth [mm]
- h_c is the height of point of contact above the lowest point of the immersing gear [mm]
- l_h is the hydraulic length [m]

- b is the tooth width [m]

With: $h_{e0} = 10$mm ; $b_0 = 10$mm ; $v_{t0} = 10$m/s

The hydraulic length expresses as follows:

$$l_h = 4.\frac{A_G}{U_M}$$

Equation 197

Where:

- A_G is the enclosure surface [m²]
- U_M is the enclosure peripheral length [m]

4. Jeon PhD work

The churning loss formula is [62]:

$$P = \frac{1}{2}\rho_{lub}.\omega^3.R_p^2.b.S_m.C_m$$

Equation 198

and

$$C_m = 2.18599\left(\frac{h_{lub}}{R_p}\right)^{0.14772}\left(\frac{V_{lub}}{R_p^s}\right)^{-0.1988}Re^{-0.25015}Fr^{-0.52985}$$

Equation 199

Where:

- ρ_{lub} is the lubricant density [kg/m^3]
- ω is the rotational speed [rad/s]
- R_p is the pitch radius [m]
- b is the gear width [m]
- S_m is the submerged surface of the gear [m²]

- C_m is the dimensionless parameter accounting for specific gear geometry
- h_{lub} is the immersion height [m]
- V_{lub} is the oil volume [m^3]
- Re is the Reynolds number
- Fr is the Froude number

FOLIO ADMINISTRATIF

THESE DE L'UNIVERSITE DE LYON OPEREE AU SEIN DE L'INSA LYON

NOM : LARUELLE DATE de SOUTENANCE : 29/09/2017

Prénoms : Sandrine Nicole Marie

TITRE : Etude du comportement thermique d'un motoréducteur

NATURE : Doctorat Numéro d'ordre : 2017LYSEI061

Ecole doctorale : MEGA (Mécanique, Energétique, Génie Civil, Acoustique)

Spécialité : Mécanique

RESUME :

La diminution de l'impact environnemental des moteurs électriques conduit à des améliorations du rendement et de la compacité. Puisque la taille de la transmission est réduite, des problèmes d'échauffements peuvent apparaître car la surface d'échange avec l'environnement est fortement réduite, diminuant les possibilités de refroidissement. L'ensemble du système doit être caractérisé en termes de pertes de puissance et de capacité de transfert thermique pour déterminer si la température maximale en fonctionnement correspond aux exigences de fiabilité tout au long de la durée de vie du système.

Cette thèse propose un modèle thermique d'une transmission avec des engrenages spiraux coniques, lubrifiée par bain d'huile. Le modèle thermique utilise la méthode des réseaux thermiques. Par conséquent, une estimation précise des pertes et des transferts thermiques entre les différents éléments est nécessaire. Une revue des méthodes existantes est présentée, indiquant que les pertes par barbotage des engrenages spiraux coniques ne sont pas totalement maîtrisées, entraînant la conduite d'une série d'essais sur un banc d'essai dédié. Cette étude se conclue sur l'application du modèle à la transmission ainsi que la proposition de points d'améliorations.

MOTS-CLÉS : méthode des réseaux thermiques, engrenages spiraux coniques, barbotage, pertes, transfert thermique

Laboratoire (s) de recherche :

Laboratoire de Mécanique des Contacts et des Structures (LaMCoS)
UMR CNRS-INSA n°5259

Directeur de thèse : Fabrice VILLE, Christophe CHANGENET

Président de jury :

Composition du jury :

Bouyer, Jean ; Changenet, Christophe ; Fabre, Agnès ; Koechlin, Samuel ; Maré, Jean-Charles ; Ville, Fabrice